

# **Novel bacterial degradation pathways for organosulfonates**

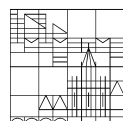
**Dissertation zur Erlangung des  
akademischen Grades eines Doktors der  
(Dr.rer.nat.)**

vorgelegt von

Anna Georga Burrichter

an der

Universität  
Konstanz



Mathematisch-Naturwissenschaftliche Sektion  
Fachbereich Biologie

Konstanz, 2020

Tag der mündlichen Prüfung: 22.05.2020

1. Referent/Referentin: Prof. Dr. David Schleheck
2. Referent/Referentin: Prof. Dr. Bernhard Schink
3. Referent/Referentin: Prof. Dr. Dieter Spiteller

## Danksagung

Ich bedanke mich zuallererst bei Prof. Dr. David Schleheck für den Vorschlag dieses faszinierenden Themas und die Möglichkeit, es in seinem Labor zu bearbeiten. Ich bedanke mich für die lehrreichen Jahre, die Unterstützung, die Ideen und die Motivation.

Des weiteren bedanke ich mich bei Prof. Dr. Bernhard Schink und Prof. Dr. Valentin Wittmann für die Mitbetreuung im Rahmen des *thesis committee* und die hilfreichen Diskussionen. Innerhalb der Universität Konstanz möchte ich mich noch bei folgenden Personen im Besonderen bedanken: Prof. Dr. Dieter Spitteler für die stetige Hilfsbereitschaft im Bereich der Massenspektroskopie, Dr. Thomas Huhn für die Synthese verschiedener Ausgangsmaterialien und die tatkräftige Hilfe bei eigenen Synthesversuchen, Dr. Andreas Marquardt, Dr. Anna Sladeswka-Marquardt und Silke Müller am Proteomics Centre und Dr. Michael Laumann und Paavo Bergmann am Electron Microscopy Centre. Ich bedanke mich bei der Konstanz Research School Chemical Biology für die Finanzierung, die interessanten Weiterbildungsmöglichkeiten sowie die Möglichkeit, mich mit meinen Mitdoktorand\*innen aus verschiedensten Richtungen der Biochemie zu vernetzen.

Persönlich bedanke ich mich im Speziellen bei Karin Denger für die Hilfe in allen Laborlagen und bei Alexander Fiedler für die jahrelange gute Labornachbarschaft und den Spaß beim Reparieren und Erfinden von Dingen. Des weiteren danke ich natürlich der ganzen AG Schink/Schleheck und der AG Spitteler dafür, dass die letzten vier Jahre nicht nur wissenschaftlich erfolgreich sondern auch so voll Spaß, Feiern, Süßigkeiten, Unterstützung und genau der richtigen Menge Chaos waren. Auf der wissenschaftlichen Seite bedanke ich mich besonders bei Anja Keller und Nick Müller für das gemeinsame Sortieren der Gedanken sowie bei den von mir betreuten Studierenden Nail Özmen, Alexander Fiedler, Stefanie Dörr, Alina Kindinger, Anne Van Humbeeck und Sebastian Haiß für die Mitarbeit und Hilfe, die Gelegenheit an meiner Lehrfähigkeit zu arbeiten und die angenehme gemeinsame Zeit.

Ich bedanke mich bei meiner ganzen Familie für das Interesse daran, was ich gerade so mache, im Besonderen meiner Mutter für die vielen guten Gespräche über die Universität an sich, sowie meinem Vater für die andauernde Unterstützung und die innovativen Vorschläge zur Methodenentwicklung. Ich danke Arne für die vielen selbstgekochten Mittagessen und liefere hiermit den endgültigen Beweis, dass die letzten vier Jahre entgegen seines Verdachts nicht nur aus Kaffeepausen bestanden.

## **Table of Contents**

Summary.....	1
Zusammenfassung.....	3
Chapter 1: General introduction.....	5
Biogeochemical sulfur cycle.....	5
Sulfate reduction.....	6
Organosulfonates .....	7
Microbial organosulfonate metabolism.....	9
The human microbiome, H <sub>2</sub> S formation and its role in health and disease.....	12
Aims of the thesis .....	14
Chapter 2: Anaerobic degradation of the plant sugar sulfoquinovose concomitant with H <sub>2</sub> S production: <i>Escherichia coli</i> K-12 and <i>Desulfovibrio</i> sp. strain DF1 as co-culture model .....	15
Abstract .....	16
Introduction.....	16
Materials and methods .....	20
Results and discussion .....	28
General conclusion .....	45
Author contributions.....	47
Acknowledgments .....	47
Supplementary material.....	48
Chapter 3: A glycyl radical enzyme enables hydrogen sulfide production by the human intestinal bacterium <i>Bilophila wadsworthia</i> .....	50
Abstract .....	51
Significance .....	51
Introduction.....	52
Results .....	55
Discussion .....	61
Materials and methods .....	64
Acknowledgments .....	65
Author contributions.....	65
Supplementary material.....	66

Chapter 4: Bacterial microcompartments as part of taurine metabolism in <i>Bilophila wadsworthia</i> .....	93
Abstract .....	93
Introduction.....	94
Results .....	98
Discussion .....	106
Materials and methods .....	109
Acknowledgments .....	115
Author contributions.....	115
Supplementary Material.....	116
Chapter 5: General Discussion and Outlook.....	119
List of abbreviations .....	126
Additional material.....	130
Record of achievement and list of publications .....	135
References.....	136

## Summary

Organosulfonates are a class of organosulfur compounds that are widespread in nature and produced by many different organisms. Their microbial degradation under oxic conditions has been rather well investigated in recent years, however, their degradation under anoxic conditions, which occur for example in sediments or in the gastrointestinal tracts of humans and animals, has not. The organosulfonate-bound sulfur can be transformed into hydrogen sulfide ( $H_2S$ ) by microbes in these environments, a substance that due to its corrosiveness and toxicity is of interest in fields ranging from industry to human health, since microbial  $H_2S$  production in the human gut has been linked to the development of various diseases. Furthermore, anaerobic mineralization of organosulfonates to  $H_2S$  is a link in the biogeochemical sulfur cycle that has not been explored in depth so far. In this thesis, the first detailed description of the mineralization of a sulfonated C<sub>6</sub>-sugar, sulfoquinovose, by an anaerobic two-member bacterial consortium is presented, as well as a complete degradation pathway for taurine in the anaerobic human gut bacterium *Bilophila wadsworthia*.

Sulfoquinovose (6-deoxy-6-sulfoglucose) is produced by plants as a lipid headgroup on a gigatonne scale per year. Previously, two aerobic bacterial degradation pathways for sulfoquinovose were discovered. In this work, it was demonstrated that sulfoquinovose can be degraded also anaerobically in a two-step process, using a model bacterial consortium consisting of *Escherichia coli* K-12 and *Desulfovibrio* sp. DF1: *E. coli* ferments sulfoquinovose to dihydroxypropanesulfonate (DHPS), acetate and formate, employing a novel combination of the known sulfo-Embden-Meyerhof-Parnas and mixed acid fermentation pathways; the DHPS is then degraded to  $H_2S$  by *Desulfovibrio* sp. DF1, which was isolated specifically for this ability. Based on differential proteomic analysis, a hypothetical pathway for DHPS degradation was proposed and confirmed by *in vitro* reconstruction using recombinant enzymes. DHPS is first oxidized to sulfolactate *via* sulfolactaldehyde by two newly discovered enzymes, NAD<sup>+</sup>-dependent DHPS dehydrogenase (DhpA) and sulfolactaldehyde dehydrogenase (SlaB); the sulfolactate is then cleaved to pyruvate and sulfite by sulfolactate sulfite-lyase (SuyAB), which was previously known only from aerobic bacteria. The sulfite is then utilized as electron acceptor for sulfite respiration and reduced to  $H_2S$ .

Taurine (2-aminoethanesulfonate) is a compound produced by the human body for many different purposes; it can also be part of the human diet as a component of meat and energy drinks. It has been known for a long time that *B. wadsworthia* can utilize taurine, *i.e.*, the sulfite released from taurine as electron acceptor for sulfite respiration, requiring an

additional electron donor such as lactate, formate or hydrogen. The complete taurine pathway revealed in this work proceeds *via* isethionate (2-hydroxyethanesulfonate) through a known taurine:pyruvate aminotransferase (Tpa) and a newly identified NAD<sup>+</sup>-dependent sulfoacetaldehyde reductase (SarD). The isethionate is then desulfonated by a newly discovered glycyl radical enzyme (GRE), isethionate sulfite-lyase (IslAB): in a radical-mediated reaction, IslAB cleaves isethionate into sulfite and acetaldehyde. The sulfite is then reduced to H<sub>2</sub>S as respiratory electron acceptor and the acetaldehyde is oxidized to acetyl-CoA and, ultimately, converted to acetate, yielding one ATP. The key enzyme IslAB represents a new class of carbon-sulfur bond-cleaving GREs. Additionally, it could be shown that the IslAB reaction in *B. wadsworthia* and most likely the following acetaldehyde conversion are contained within a bacterial microcompartment (BMC), a subcompartment within the cells that confines the toxic intermediate acetaldehyde. The taurine-dependent formation of these BMCs in *B. wadsworthia* as well as the enzyme activities associated to them could be demonstrated by electron microscopy and proteomic analysis, and, thus, a new subclass of BMCs for organosulfonate metabolism could be identified. Thus, the taurine degradation pathway in *B. wadsworthia* could be elucidated in detail, revealing potential novel targets for control of intestinal H<sub>2</sub>S production.

Overall, the demonstration of the existence of these metabolic routes to H<sub>2</sub>S formation and the identification of the relevant pathways and enzymes revealed the fundamental understanding on which these processes can be investigated further, for example in the human gut in respect to their biomedical relevance.

## Zusammenfassung

Organosulfonate sind eine Untergruppe der Organoschwefelverbindungen, die in der Natur weitverbreitet sind und von vielen verschiedenen Lebewesen gebildet werden. Der Abbau dieser Substanzen unter oxischen Bedingungen wurde in den letzten Jahren eingehend untersucht, der Abbau unter Sauerstoffausschluss wie z.B. in Sedimenten oder im Gastrointestinaltrakt jedoch nicht. Der in Organosulfonaten gebundene Schwefel kann von Mikroorganismen unter diesen Bedingungen zu Schwefelwasserstoff ( $H_2S$ ) umgesetzt werden, einer Substanz, die aufgrund ihrer Giftigkeit und chemischen Aggressivität in vielen Bereichen von Interesse ist, so zum Beispiel in der Industrie oder in der medizinischen Forschung, die mikrobiell produziertes  $H_2S$  im Darm mit der Entstehung verschiedener Krankheiten in Verbindung bringt. Abgesehen davon ist die Mineralisierung des Schwefels aus Organosulfonaten unter anoxischen Bedingungen ein bisher nicht ausreichend erforschter Teil des biogeochemischen Schwefelkreislaufes. In dieser Arbeit stelle ich die erste detaillierte Beschreibung der Mineralisierung des sulfonierten C<sub>6</sub>-Zuckers Sulfoquinovose durch ein anaerobes Konsortium vor sowie einen vollständigen Abbauweg für Taurin in *Bilophila wadsworthia*, einem Darmbakterium des Menschen.

Sulfoquinovose (6-Desoxy-6-sulfoglukose) wird von Pflanzen als Kopfgruppe von Lipiden im Maßstab von Gigatonnen pro Jahr produziert. Bisher waren zwei aerobe Abbauwege für Sulfoquinovose bekannt. In dieser Arbeit wurde gezeigt, dass Sulfoquinovose unter anoxischen Bedingungen von einem Modellkonsortium aus *Escherichia coli* K-12 und *Desulfovibrio* sp. DF1 in einem zweistufigen Prozess abgebaut wird. Es konnte nachgewiesen werden, dass *E. coli* Sulfoquinovose unter anoxischen Bedingungen über einen neuartigen Stoffwechselweg zu Dihydroxypropansulfonat (DHPS), Acetat und Formiat vergärt, der den bereits bekannten Sulfo-Embden-Meyerhof-Parnas-Weg mit einzelnen Zweigen der gemischten Säuregärung kombiniert. Auf Grundlage von differenzieller Proteomanalyse wurde ein detaillierter Abbauweg für DHPS postuliert und bewiesen, indem die einzelnen Schritte des Abbauwegs mit heterolog exprimierten Enzymen bestätigt wurden. So wurde nachgewiesen, dass DHPS von zwei neu entdeckten Enzymen, einer NAD<sup>+</sup>-abhängigen DHPS-Dehydrogenase (DhpA) und Sulfolaktaldehyd-Dehydrogenase (SlaB) zu Sulfolaktat oxidiert wird, welches dann von einer Sulfolaktat-Sulfatlyase (SuyAB) in Pyruvat und Sulfat gespalten wird. SuyAB war bisher nur aus aeroben Bakterien bekannt. Das Sulfat wird schließlich als Elektronenakzeptor verwendet und zu  $H_2S$  reduziert.

Taurin (2-Aminoethansulfonat) wird vom menschlichen Körper für verschiedene Zwecke produziert, kann aber auch als Bestandteil von Fleisch und ‚Energydrinks‘ Teil der menschlichen Ernährung sein. Es ist seit einiger Zeit bekannt, dass *B. wadsworthia* Taurin

bzw. das daraus freigesetzte Sulfit als Elektronenakzeptor in einer Organosulfonatatmung verwenden kann, wenn ein zusätzlicher Elektronendonator wie Laktat, Formiat oder Wasserstoff vorhanden ist. Der in dieser Arbeit vollständig aufgeklärte Taurinabbauweg verläuft über Isethionat (2-Hydroxyethansulfonat): Eine bereits bekannte Taurin:Pyruvat-Aminotransferase (Tpa) deaminiert Taurin zu Sulfoacetaldehyd, welches dann von einer erstmals charakterisierten Sulfoacetaldehydreduktase (SarD) zum entsprechenden Alkohol Isethionat reduziert wird. Isethionat wiederum wird durch das neuartige Glycylradikalenzym (GRE) Isethionat-Sulfitlyase (IslAB) weiter verstoffwechselt, indem in einer radikalischen Reaktion Isethionat zu Sulfit und Acetaldehyd gespalten wird. Das Sulfit wird zu H<sub>2</sub>S reduziert während das Acetaldehyd zu Acetyl-CoA oxidiert und schließlich zum Endprodukt Acetat umgesetzt wird, wobei ein ATP gewonnen wird. Das Schlüsselenzym IslAB stellt eine neue Klasse der GRES dar, die Kohlenstoff-Schwefel-Bindungen spaltet. Weiterhin konnte beobachtet werden, dass die Reaktion von IslAB und die folgende Oxidation des Acetaldehyds wahrscheinlich in einem bakteriellen Mikrokompartiment vom Rest des Cytosols isoliert stattfinden. In diesem separaten Reaktionsraum in der Zelle wird das giftige Zwischenprodukt Acetaldehyd vom Rest der Zelle abgetrennt. Die Taurin-abhängige Bildung dieser Mikrokompartimente konnte sowohl elektronenmikroskopisch als auch auf Proteinebene beobachtet werden und die mit ihnen assoziierten Enzymaktivitäten wurden beschrieben. Somit konnte eine neue Klasse der bakteriellen Mikrokompartimente vorgeschlagen werden. Der Taurinabbauweg in *B. wadsworthia* wurde somit detailliert beschrieben, was neue Ansatzpunkte für eine Kontrolle der H<sub>2</sub>S-Produktion im Darm aufzeigen könnte.

Insgesamt konnten in dieser Dissertation neuartige H<sub>2</sub>S-bildende bakterielle Stoffwechselwege inklusive der beteiligten Enzyme detailliert beschrieben werden. Auf dieser Grundlage können diese mikrobiellen Prozesse nun zum Beispiel im menschlichen Darm hinsichtlich ihrer biomedizinischen Relevanz untersucht werden.

## **Chapter 1: General introduction**

### **Biogeochemical sulfur cycle**

Sulfur, like other major elements such as carbon and nitrogen, is not distributed statically across the earth but instead is transported, transformed and recycled in its own biogeochemical cycle. In nature, sulfur species are present in many different oxidation states: -II, such as in hydrogen sulfide, inorganic FeS and organic sulfides; -I, such as in organic disulfides and formally in polysulfides and pyrite; 0, as in elemental sulfur and partially in polysulfides; +II, such as in thiosulfuric acid, thiosulfates and organic sulfones; +IV, such as in sulfurous acid and sulfites, sulfur dioxide and organic sulfonates; and +VI, such as in sulfuric acid, sulfates and sulfur trioxide. This variety of oxidation states and forms of sulfur species make the global sulfur cycle a very complex network of inorganic and organic transformations in the atmo-, hydro-, litho- and biosphere.

Inorganic sulfur species enter the sulfur cycle mostly as sulfates and sulfides dissolved from soil, rocks and the oceanic crust, hydrogen sulfide ( $H_2S$ ) from hydrothermal deep sea vents or as sulfur dioxide from volcanic eruptions or fossil fuel combustion (Canfield and Farquhar 2012). The largest sulfur sink in the cycle is the burial of mineral sulfides, mostly pyrite (Canfield and Farquhar 2012). While the oxidation and reduction of sulfur species can happen as a purely chemical, abiotic process, it is often mediated by biological processes. Plants, bacteria and archaea assimilate inorganic sulfur such as  $H_2S$  or sulfate and form organosulfur compounds that are central to life on earth: sulfur-containing amino acids (cysteine, methionine), cofactors (biotin, thiamine), intracellular antioxidants such as glutathione, iron-sulfur clusters in proteins and many more. Additionally to this assimilation of sulfur and conversion to cell components, bacteria and archaea are also able to use sulfur species as electron acceptors and/or donors in dissimilatory sulfur metabolism. Sulfate, zero-valent sulfur, sulfite, thiosulfate and organosulfonates can all be used as electron acceptors in anaerobic respirations. Of these processes, sulfate reduction (see below) *via* sulfite to  $H_2S$  is the most closely studied and is also thought to be the most common one in anoxic habitats, especially in marine sediments where sulfate is present in high concentrations (Thompson, Lang *et al.* 1927; Morris and Riley 1966). In low-sulfate environments, organically bound sulfur has recently been appreciated as a major contributor to sulfur fluxes, both in current freshwater ecosystems (Fakhraee, Li *et al.* 2017) and in the low-sulfate oceans of the early earth where it is suggested by Fakhraee and Katsev to be the main

source of H<sub>2</sub>S and pyrite (Fakhraee and Katsev 2019). H<sub>2</sub>S, zero-valent sulfur, sulfite and thiosulfate can in turn be used as electron donors with oxygen or nitrate as electron acceptors by chemolithotrophic bacteria or, under anoxic conditions, by green sulfur bacteria, purple bacteria and Chloroflexi performing anoxygenic photosynthesis (Muyzer and Stams 2008). Additionally, sulfur species of intermediate oxidation levels such as sulfite, thiosulfate or elemental sulfur, can be disproportionated (Finster 2008). Sulfate-reducing organisms are typically diverse in their metabolism and can use alternative electron acceptors such as nitrate (Keith and Herbert 1983; Dalsgaard and Bak 1994), nitrite (Moura, Bursakov *et al.* 1997) and oxidized iron (Fe(III)) (Lovley, Roden *et al.* 1993; Park, Lin *et al.* 2008), they can often ferment substrates such as pyruvate and some species specialize on inorganic sulfur species such as tetrathionate, but these processes will not be further discussed here.

The utilization of sulfur compounds as electron donors and acceptors closely links the sulfur and carbon cycles: for example, under anoxic conditions, sulfate-reducing microorganisms can use a vast range of organic substrates as electron donors and/or carbon sources, including fermentation products such as short-chain fatty acids and alcohols, and oxidize these further, either incompletely to acetate or completely to CO<sub>2</sub>. Sulfate respiration alone can contribute a significant amount to total carbon oxidation in sediments (Canfield, Jørgensen *et al.* 1993). Sulfate-reducing bacteria and archaea are found across several different phylogenetic lines but most account to the classes Deltaproteobacteria and Clostridia (Muyzer and Stams 2008).

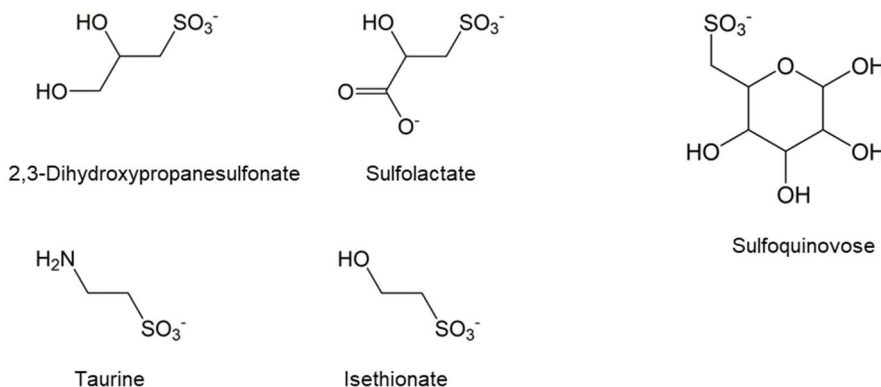
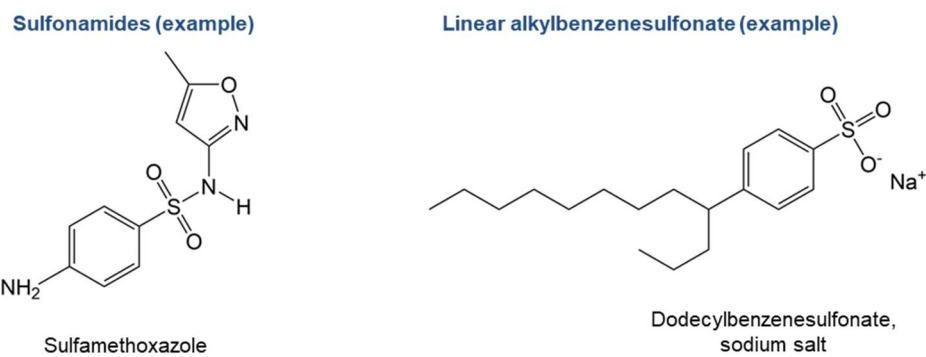
## **Sulfate reduction**

Reduction of sulfate to sulfite is the first step in both dissimilatory and assimilatory sulfate reduction. This reduction step cannot be carried out directly because the redox potential of the sulfate/sulfite redox couple ( $E^{\circ}$ ) of -516 mV (Muyzer and Stams 2008) is too negative to be reduced by intracellular redox carriers such as NADH ( $E^{\circ} = -320$  mV, -280 mV under physiological conditions) or ferredoxin ( $E^{\circ} = -420$  mV, down to -500 mV under physiological conditions)(Buckel and Thauer 2013). Sulfate reducers therefore have to activate sulfate first to adenosine-5'-phosphosulfate (APS), which requires an energy investment equivalent of two ATP. This activation is catalyzed by sulfate adenylyltransferase (Sat). The APS/sulfite redox couple has a potential (-60 mV) at which it can be reduced by (dissimilatory) APS reductase (AprAB) using reduced ferredoxin, transferring two electrons (sulfur oxidation state +VI to +IV). The AMP is released and, in dissimilatory sulfate reduction, the sulfite is reduced further to sulfide by the dissimilatory sulfite reductase (Dsr) complex. These reduction steps are coupled to energy conservation *via* electron transport phosphorylations (Badziong and

Thauer 1978; Muyzer and Stams 2008) at various membrane complexes, which supply electrons to the Dsr complex from the oxidation of, e.g., H<sub>2</sub> or lactate as the electron donors (Fuchs, Eitinger *et al.* 2014).

## **Organosulfonates**

Organosulfonates contain an oxidized form of organically bound sulfur with the general formula R<sub>3</sub>C-SO<sub>3</sub><sup>-</sup>. The term organosulfonates is used throughout this work exclusively for C-sulfonates with a direct carbon-sulfur bond; sulfate esters (R-O-SO<sub>3</sub><sup>-</sup>) and sulfonamides (R-N-SO<sub>3</sub><sup>-</sup>) are sometimes called O- and N-sulfonates respectively in literature but this terminology is not used here. The formal oxidation state of the sulfur atom in organosulfonates is usually given as +IV (Clayden, Greeves *et al.* 2012), although X-ray absorption near-edge structure measurements place it at +V (Frank, Hedman *et al.* 1987; Waldo, Carlson *et al.* 1991; Vairavamurthy, Manowitz *et al.* 1993). Organosulfonates are present in the environment in considerable amounts, both from natural sources (Harwood and Nicholls 1979; Durham, Sharma *et al.* 2015) and as xenobiotics (for an overview of chemical structures refer to Figure 1.1): artificial organosulfonates are produced on a large scale, for example as surfactants, most commonly in the form of alkylbenzenesulfonates with approx. 5 million metric tons per year (Kronberg, Holmberg *et al.* 2014), which are one of the main components of today's biodegradable laundry detergents (Sawyer and Ryckman 1957; Schleheck 2003). Sulfonamides are used in pharmacology as antibacterial agents as they interfere with bacterial folate synthesis (Fuchs, Eitinger *et al.* 2014).

**Naturally occurring organosulfonates****Artificially synthesized organosulfonates****Figure 1.1. An overview of organosulfonates occurring in the environment**

Natural organosulfonates can be found in all lifeforms, for example isethionate (2-hydroxyethanesulfonate) in places as diverse as squid axons (Koechlin 1954), red algae (Holst, Nielsen *et al.* 1994), the heart tissue of dogs (Welty, Read *et al.* 1962), human urine (Jacobsen, Collins *et al.* 1967) and spider webs (Vollrath, Fairbrother *et al.* 1990); sulfolactate in bacterial endospores (Bonsen, Spudich *et al.* 1969), archaeal biosynthesis pathways (Graham, Xu *et al.* 2002) and plant leaves (Lee and Benson 1972); or taurine in most animal lifeforms (see below). Their physiological functions are often only partially understood, or not at all. This is all the more surprising considering their wide occurrence throughout life on earth. Additionally, organosulfonates can make up 20–40% of the total organically bound sulfur in soils and sediments (Autry and Fitzgerald 1990; Vairavamurthy, Zhou *et al.* 1994), meaning they form a major part of the sulfur reservoir in soils (Anderson and Pratt 1995; Werne and Hollander 2004; Zhu, Chen *et al.* 2016).

Prominent naturally occurring organosulfonates that are the subject of this thesis are sulfoquinovose (6-deoxy-6-sulfoglucose, SQ), 2,3-dihydroxypropanesulfonate (DHPS) and

taurine (2-aminoethanesulfonate) (see Figure 1.1). SQ is a sugar produced by plants (Benson, Daniel *et al.* 1959; Benson 1963; Anderson, Kates *et al.* 1978; Harwood and Nicholls 1979), mosses, ferns, algae and cyanobacteria, where it is usually found in the photosynthetic membranes as the polar headgroup of a so-called sulfolipid. The annual production of SQ in the biosphere is estimated to be on the scale of gigatonnes (Harwood and Nicholls 1979), making it a major sulfur compound in the biosphere. DHPS, a degradation product of SQ (see below), is similarly ubiquitous: while it was first identified as an excretion product of diatoms only a few years after the identification of SQ (Busby 1966), it has recently been found to be an important component of the microbial foodweb in seawater, linking the oceanic carbon and sulfur cycle (Durham, Sharma *et al.* 2015). DHPS of yet unknown origin was even found in hydrothermal vent fluid (Longnecker, Sievert *et al.* 2018). Both SQ and DHPS likely are so far overlooked, but major carbon and sulfur “currencies” in food webs in marine and freshwater habitats and their sediments, although their pool sizes and turnover rates are still not clearly defined.

In contrast to these plant-derived organosulfonates, taurine is a metabolite with various functions produced by animals (Huxtable 1992; Ripps and Shen 2012). In the human body, taurine is found as a component of bile salts in the digestive tract, in muscle tissue in the  $\mu\text{mol/g}$  range, and in the nervous system (Huxtable 1992). It is thought to be involved in osmoregulation as well as in the control of  $\text{Ca}^{2+}$  fluxes and balance. Not all of its functions are clear yet but just as the plant-derived and microbially produced organosulfonates, it is present in large amounts in the environment including in humans and other animals.

The microbial degradation of these organosulfonates and mineralization of the sulfur they contain thus is an important and relevant link between the organic and inorganic parts of the biogeochemical sulfur cycle, as well as of direct interest to understanding the processes within human bodies, as described below.

## **Microbial organosulfonate metabolism**

Unlike in sulfate esters and sulfonamides, the sulfur atom in organosulfonates is directly bound to a carbon atom. This covalent bond, similar in bond strength to a C-C bond (Clayden, Greeves *et al.* 2012), requires specific enzymes other than hydrolases to cleave and not all life forms can catalyze such desulfonation reactions: so far, only bacteria and fungi are known to harbor enzymes that can cleave the C-S bond (Huxtable 1992). Animals cannot enzymatically cleave sulfonates but can only indirectly split reduced sulfur-containing compounds such as cysteine by transforming it to cysteine sulfonate and then  $\beta$ -sulfinyl

pyruvate, which decomposes spontaneously into pyruvate and sulfur dioxide/sulfite (Huxtable 1992).

The dissimilatory aerobic microbial degradation of SQ as carbon and energy source has been uncovered in our group several years ago. It was shown that SQ is metabolized by two different sulfoglycolytic pathways in bacteria: the SQ-Embden-Meyerhof-Parnas (sulfo-EMP) pathway, e.g. in *Escherichia coli* (Denger, Weiss *et al.* 2014), or the sulfo-Entner-Doudoroff pathway, e.g. in *Pseudomonas putida* (Felux, Spiteller *et al.* 2015). Both of these pathways run analogous to the classic glycolytic pathways, respectively the EMP and Entner-Doudoroff pathways for glucose, but have specific enzymes that are encoded in separate gene clusters. In the meantime, a third aerobic degradation pathway has been uncovered in our research group, the transaldolase pathway, which will be more closely discussed in Chapter 5. In all of these bacteria, the sulfonate moiety itself is not cleaved off the carbon moiety, but excreted in form of a C<sub>3</sub>-organosulfonate, either DHPS or sulfolactate. These in turn can be degraded completely by other aerobic bacteria containing one of various desulfonating enzymes (van der Ploeg, Weiss *et al.* 1996; Eichhorn, van der Ploeg *et al.* 1997; Eichhorn, van der Ploeg *et al.* 1999; Denger, Ruff *et al.* 2001; Ruff, Denger *et al.* 2003; Rein, Gueta *et al.* 2005; Denger, Smits *et al.* 2006; Denger, Mayer *et al.* 2009; Mayer, Huhn *et al.* 2010; Denger, Huhn *et al.* 2012), as shown in Figure 1.2. The gene clusters encoding for the enzymes of these pathways are widely spread throughout different bacterial groups, suggesting that the utilization of organosulfonates as carbon and energy source may be an old nutrition strategy in respect to evolutionary history. Notably, it has been observed that organosulfonates can serve also as sole sulfur sources to some bacterial species for their assimilatory metabolism, either under oxic (Seitz, Leadbetter *et al.* 1993; Uria-Nickelsen, Leadbetter *et al.* 1994) or anoxic (Chien, Leadbetter *et al.* 1995; Denger, Kertesz *et al.* 1996; Denger and Cook 1997) conditions; this nutrition strategy is not relevant for the present doctoral thesis and therefore is not further discussed here.

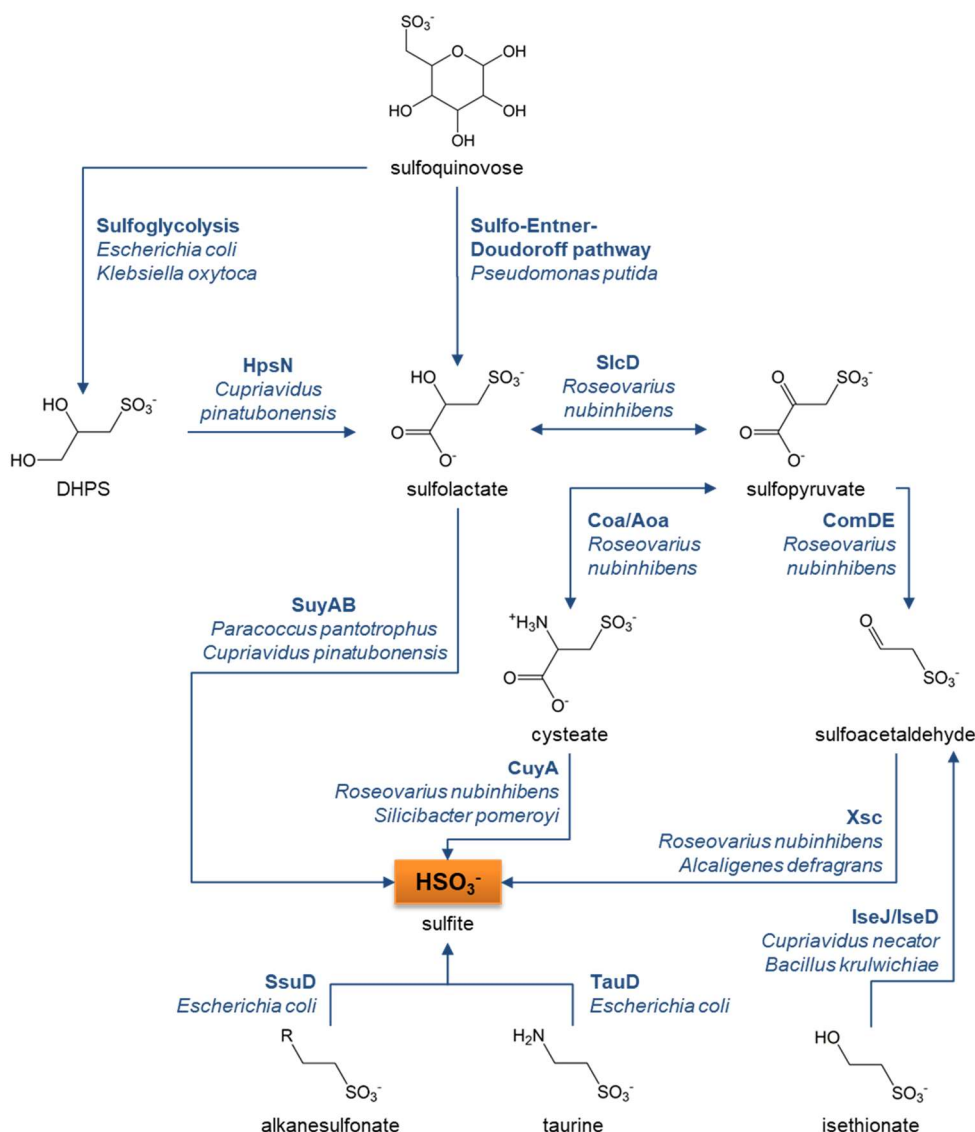


**Figure 1.2. Known pathways for organosulfonate degradation, including desulfonation.** SQ can be degraded by two different aerobic pathways, with the sulfonate moiety excreted as a C<sub>3</sub>-organosulfonate, DHPS or sulfolactate. There are five desulfonating enzymes known so far: sulfolactate sulfite-lyase (SuyAB) (Rein, Gueta *et al.* 2005; Denger and Cook 2010) that desulfonates sulfolactate to pyruvate and sulfite, L-cysteate sulfite-lyase (CuyA) (Cook, Denger *et al.* 2006; Denger, Smits *et al.* 2006) that cleaves cysteate to sulfite, pyruvate and ammonium; sulfoacetaldehyde acetyltransferase (Xsc) (Cook and Denger 2002; Ruff, Denger *et al.* 2003; Denger, Mayer *et al.* 2009) that forms sulfite and acetyl phosphate from sulfoacetaldehyde.  $\alpha$ -Ketoglutarate-dependent taurine dioxygenase (TauD) (van der Ploeg, Weiss *et al.* 1996; Eichhorn, van der Ploeg *et al.* 1997), and SsuD, an alkanesulfonate monooxygenase (Eichhorn, van der Ploeg *et al.* 1999), are strictly oxygen dependent enzymes from *E. coli* that can split sulfite from taurine (TauD) or various alkanesulfonates (SsuD), resulting in the respective aldehydes. Isethionate can be oxidized to sulfoacetaldehyde by isethionate dehydrogenases such as IseJ in *Cupriavidus necator* (Weinitschke, Sharma *et al.* 2010) or IseD in *Bacillus kruwlichiae* (Tong, Wei *et al.* 2019). DHPS can be converted to sulfolactate by DHPS dehydrogenase (HpsN) (Mayer, Huhn *et al.* 2010). Sulfolactate and cysteate can be interconverted via sulfopyruvate by sulfolactate dehydrogenase (SlcD) and a cysteate aminotransferase (Coa)/aspartate:2-oxoglutarate aminotransferase (Aoa). Sulfopyruvate can also be decarboxylated to sulfoacetaldehyde by sulfopyruvate decarboxylase (ComDE)(Denger, Mayer *et al.* 2009). The sulfite released from these organosulfonates is usually oxidized to nontoxic sulfate and then excreted, but can occasionally also be exported directly as sulfite, for example by *Silicibacter pomeroyi* (Denger, Smits *et al.* 2006).

The anaerobic dissimilatory metabolism of organosulfonates on the other hand has been studied much less intensively, since thus far most anaerobic sulfur metabolism research focused mainly on the reduction of inorganic sulfur species such as sulfate or elemental sulfur. While aerobic bacteria cleave the sulfonate group, oxidize it and excrete sulfate as the end product, anaerobic bacteria may use the oxidized sulfur as an electron acceptor. Indeed, production of sulfide (Lie, Pitta *et al.* 1996; Laue, Denger *et al.* 1997; Lie, Godchaux *et al.* 1999), sulfate (Denger, Laue *et al.* 1997a), or thiosulfate (Denger, Laue *et al.* 1997b) from organosulfonates under anoxic conditions has been described before but no complete pathways have yet been uncovered.

## **The human microbiome, H<sub>2</sub>S formation and its role in health and disease**

Research interest in the human microbiome has increased vastly in the last decade. Among the many different consortia colonizing different parts of the human body, the gut microbiome in the small and large intestine has been studied especially intensively. Changes in the gut flora have been associated with various health concerns, such as inflammatory bowel diseases (see below), cardiovascular diseases (Gregory, Buffa *et al.* 2015; Jie, Xia *et al.* 2017), obesity (Turnbaugh, Ley *et al.* 2006; Vrieze, Van Nood *et al.* 2012; Kootte, Levin *et al.* 2017) and even neurological and psychiatric disorders (Rogers, Keating *et al.* 2016; Bastiaanssen, Cowan *et al.* 2018) such as depression (Naseribafrouei, Hestad *et al.* 2014; Jiang, Ling *et al.* 2015), bipolar disorder (Evans, Bassis *et al.* 2017) or Parkinson's disease (Sampson, Debelius *et al.* 2016; Hertel, Harms *et al.* 2019). To gain further insight into these connections, not only the involved microbial communities, but also the chemical intermediates and biochemical pathways have to be studied much more intensively. Importantly, only the identification of the enzymes and genes that are involved in these pathways allows for a further evaluation of their significance and abundance, especially by DNA-based approaches, such as metagenome or metatranscriptome sequencing (see also Chapter 5).

H<sub>2</sub>S produced by microbes in the gut has been proposed as the mediating compound in the development of certain diseases (Carbonero, Benefiel *et al.* 2012; Guo, Yu *et al.* 2016). H<sub>2</sub>S has been shown to have anti-inflammatory and vasorelaxing properties (Hosoki, Matsuki *et al.* 1997; Zhao, Zhang *et al.* 2001; Wallace 2010; Kimura 2011; Kabil, Vitvitsky *et al.* 2014), but a lot of recent research has focused on its more detrimental role in disease development in the gut. There, H<sub>2</sub>S has been implicated in the development of ulcerative colitis and

irritable bowel syndrome (Gibson, Cummings *et al.* 1991; Roediger, Moore *et al.* 1997; Levine, Ellis *et al.* 1998; Devkota, Wang *et al.* 2012) and even bowel cancer (Ramasamy, Singh *et al.* 2006). Different effects on cancer cells and colorectal tumors have been reported, with H<sub>2</sub>S both promoting the growth of cancer cells (Cai, Wang *et al.* 2010; Szabo, Coletta *et al.* 2013) and inhibiting apoptosis (Sen, Paul *et al.* 2012) as well as inhibiting cell proliferation in some studies (Cao, Zhang *et al.* 2010; Wu, Wang *et al.* 2012).

Mechanistically, a weakening of the mucus layer in the colon due to H<sub>2</sub>S breaking disulfide bonds has been proposed as a cause for this effect (Ijssennagger, Belzer *et al.* 2015; Ijssennagger, van der Meer *et al.* 2016), as well as the fact that H<sub>2</sub>S is directly genotoxic (Attene-Ramos, Wagner *et al.* 2006; Attene-Ramos, Wagner *et al.* 2007; Attene-Ramos, Nava *et al.* 2010). Furthermore, H<sub>2</sub>S production may be a defense mechanism of bacteria against antibiotics (Shatalin, Shatalina *et al.* 2011).

The H<sub>2</sub>S content in the gut is dependent on many factors: the presence of sulfate, organosulfonates and other sulfur compounds in the diet (Magee, Richardson *et al.* 2000), increased endogenous production of sulfonated compounds such as taurine-conjugated bile acids (taurocholate) (Ridlon, Wolf *et al.* 2016) or H<sub>2</sub>S directly (Kabil, Vitvitsky *et al.* 2014), and the distribution of all of these compounds between cells of the digestive tract (Dawson and Karpen 2015) that detoxify H<sub>2</sub>S (Suarez, Furne *et al.* 1998; Furne, Springfield *et al.* 2001), and the bowel lumen, where these substances may be substrates for the gut flora. A stunningly clear connection was made by Devkota *et al.* in mice (Devkota, Wang *et al.* 2012): a diet rich in taurine, or even a diet rich in saturated fat that stimulates the production of bile salts, led to a bloom of the H<sub>2</sub>S-producing (sulfidogenic) organosulfonate degrader *Bilophila wadsworthia* and subsequently to an increase in colitis incidence in these animals. The pathways of anaerobic organosulfonate degradation and the consecutive production of H<sub>2</sub>S are therefore of direct interest to human health and disease.

## **Aims of the thesis**

In this thesis, it was planned to elucidate bacterial pathways, enzymes and genes for anaerobic degradation of the organosulfonates SQ, taurine and DHPS. Therefore, different bacterial strains served as model systems, when being cultivated with the organosulfonates as substrate either alone or in defined co-culture. The model species were *Escherichia coli* K-12, a facultative anaerobe that was known to degrade SQ aerobically to DHPS, and *Desulfovibrio* sp. strain DF1, a strain isolated in our lab specifically for its ability to ferment DHPS (Chapter 2); and *B. wadsworthia* 3.1.6, a reference strain from the Human Microbiome Project, which is known for its association with various diseases (Baron, Summanen *et al.* 1989; Baron 1997). *B. wadsworthia* utilizes taurine as electron acceptor but the desulfonation pathway had so far remained unknown (Chapter 3). Both *E. coli* and *B. wadsworthia* are typical members of the human gut flora. The enzymes involved in the degradation pathways were first identified by proteomic analysis and this identification was reinforced by *in vitro* reconstruction of the pathway reactions using recombinant enzymes. In the course of this work, it was discovered that *B. wadsworthia* employs a novel type of glycyl radical enzyme (GRE) to cleave carbon-sulfur bonds (Chapter 3) and that this reaction is probably sequestered in a bacterial microcompartment (BMC), which isolates it from the main cytosol. The examination of these BMCs contributed an additional chapter to my thesis (Chapter 4).

## Chapter 2: Anaerobic degradation of the plant sugar sulfoquinovose concomitant with H<sub>2</sub>S production: Escherichia coli K-12 and Desulfovibrio sp. strain DF1 as co-culture model

**Short title:** A bacterial consortium ferments sulfoquinovose to acetate and sulfide

Anna Burrichter<sup>1,3</sup>, Karin Denger<sup>1</sup>, Paolo Franchini<sup>1</sup>, Thomas Huhn<sup>2,3</sup>, Nicolai Müller<sup>1</sup>, Dieter Spitteler<sup>1,3</sup> and David Schleheck<sup>1,3\*</sup>

### **Affiliations:**

<sup>1</sup> Department of Biology, University of Konstanz, D-78457 Konstanz, Germany

<sup>2</sup> Department of Chemistry, University of Konstanz, D-78457 Konstanz, Germany

<sup>3</sup> The Konstanz Research School Chemical Biology, University of Konstanz,  
D-78457 Konstanz, Germany

### **Corresponding author:**

**David Schleheck**

Department of Biology and Konstanz Research School Chemical Biology, University of  
Konstanz, D-78457 Konstanz, Germany

Tel.: +49-7531-88-4247

Email: david.schleheck@uni-konstanz.de

This chapter was published in Frontiers in Microbiology (2018):

<https://doi.org/10.3389/fmicb.2018.02792>

### **Keywords:**

anaerobic bacterial metabolism; sulfidogenesis; hydrogen sulfide production;  
organosulfonate respiration; sulfoquinovosyldiacylglycerol; plant sulfolipid;  
biogeochemical carbon and sulfur cycle; gut microbiome, human health and disease

## **Abstract**

Sulfoquinovose (SQ, 6-deoxy-6-sulfoglucose) is produced by plants and other phototrophs and its biodegradation is a relevant component of the biogeochemical carbon and sulfur cycles. SQ is known to be degraded by aerobic bacterial consortia in two tiers *via C<sub>3</sub>-organosulfonates* as transient intermediates to CO<sub>2</sub>, water and sulfate.

In this study, we present a first laboratory model for anaerobic degradation of SQ by bacterial consortia in two tiers to acetate and hydrogen sulfide (H<sub>2</sub>S). For the first tier, SQ-degrading *Escherichia coli* K-12 was used. It catalyzes the fermentation of SQ to 2,3-dihydroxypropane-1-sulfonate (DHPS), succinate, acetate and formate, thus, a novel type of mixed-acid fermentation. It employs the characterized SQ-Embden-Meyerhof-Parnas pathway, as confirmed by mutational and proteomic analyses. For the second tier, a DHPS-degrading *Desulfovibrio* sp. isolate from anoxic sewage sludge was used, strain DF1. It catalyzes another novel fermentation, of the DHPS to acetate and H<sub>2</sub>S. Its DHPS desulfonation pathway was identified by differential proteomics and demonstrated by heterologously produced enzymes: DHPS is oxidized *via* 3-sulfolactaldehyde to 3-sulfolactate by two NAD<sup>+</sup>-dependent dehydrogenases (DhpA, SlaB); the sulfolactate is cleaved by a sulfolactate sulfite-lyase known from aerobic bacteria (SuyAB) to pyruvate and sulfite. The pyruvate is oxidized to acetate, while the sulfite is used as electron acceptor in respiration and reduced to H<sub>2</sub>S.

In conclusion, anaerobic sulfidogenic SQ degradation was demonstrated as a novel link in the biogeochemical sulfur cycle. SQ is also a constituent of the green-vegetable diet of herbivores and omnivores and H<sub>2</sub>S production in the intestinal microbiome has many recognized and potential contributions to human health and disease. Hence, it is important to examine bacterial SQ degradation also in the human intestinal microbiome, in relation to H<sub>2</sub>S production, dietary conditions and human health.

## **Introduction**

SQ is the polar headgroup of plant sulfolipids (sulfoquinovosyl diacylglycerols; SQDGs) in the photosynthetic (thylakoid) membranes of, essentially, all higher plants, ferns, mosses, algae as well as most phototrophic bacteria (Benson, Daniel *et al.* 1959; Benson 1963); SQ is also a component of the cell wall of archaea (Palmieri, Balestrieri *et al.* 2013). SQ is one of the most abundant organosulfur species in the biosphere, with an estimated annual production of 10 billion tonnes and in a scale comparable with the amino acids cysteine and methionine (Harwood and Nicholls 1979). Thus, SQ is an important component of the biogeochemical

sulfur cycle and an understanding of its complete biodegradation, i.e., including recycling of the organosulfur in form of inorganic sulfur species such as sulfate, is of importance.

Two bacterial pathways for degradation of SQ have been discovered in the recent years. The first is analogous to the Embden-Meyerhof-Parnas pathway of glycolysis and was found in *Escherichia coli* K-12 (Denger, Weiss *et al.* 2014) (Figure 2.1A).

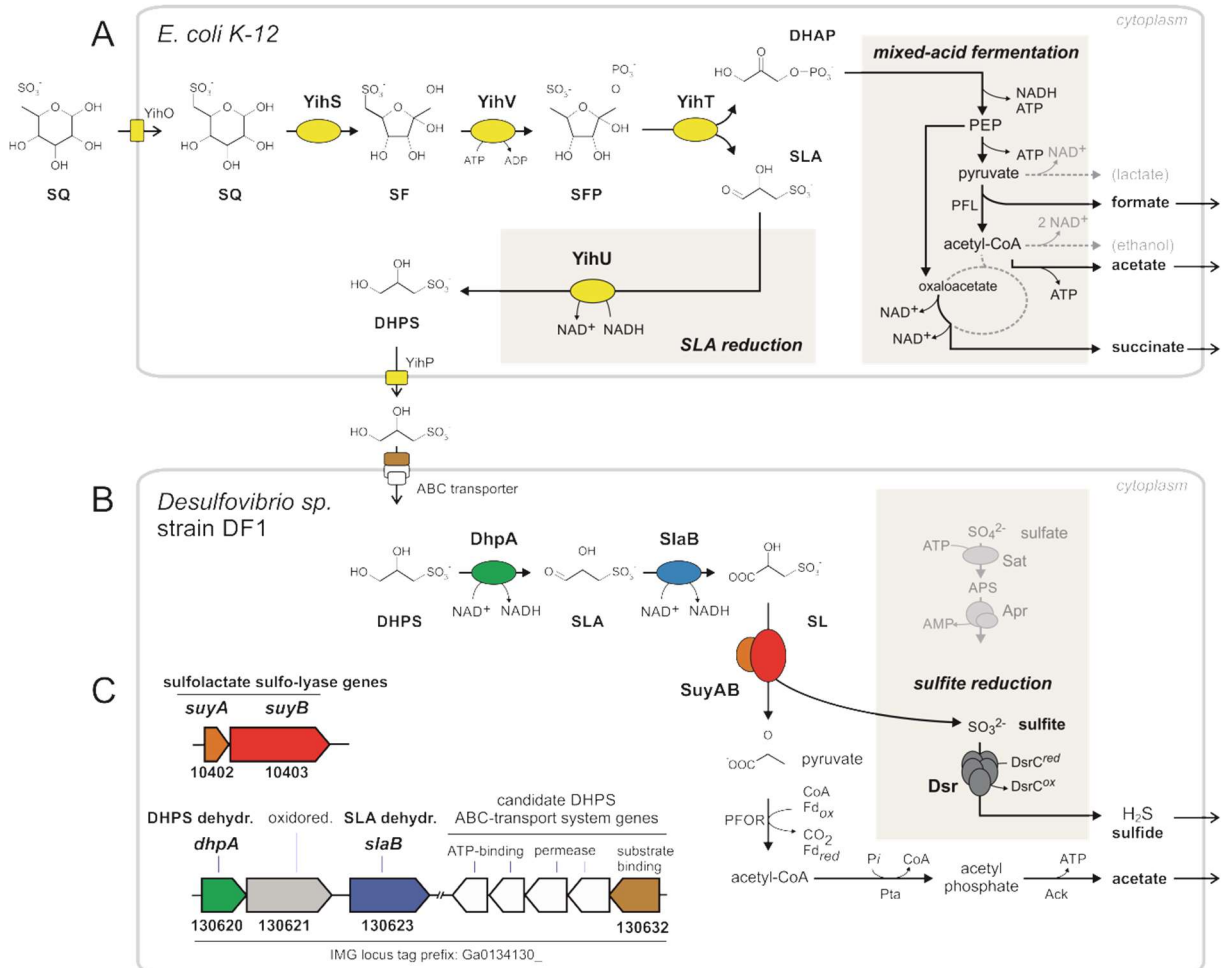


**Figure 2.1. Anaerobic two-step degradation of SQ to H<sub>2</sub>S, as demonstrated in this study using a defined two-member bacterial co-culture. (A)** Fermentation of sulfoquinovose (SQ) to 2,3 dihydroxypropane-1-sulfonate (DHPS), formate, acetate and succinate by *E. coli* K-12. SQ is metabolized and cleaved into dihydroxyacetone phosphate (DHAP) and 3-sulfolactaldehyde (SLA) by a reaction sequence (enzymes YihS, V and T) analogous to the Embden-Meyerhof-Parnas pathway, as demonstrated previously for aerobic growth of *E. coli* (Denger, Weiss *et al.* 2014). The C<sub>3</sub>-organosulfonate DHPS is excreted and available as substrate to other bacteria. Under anoxic growth conditions, *E. coli* funnels most of the DHAP-carbon into mixed-acid fermentation (see schematic in the gray inset on the right) to succinate, formate and acetate as fermentation products. In addition, the reduction of sulfolactaldehyde to DHPS, as catalyzed by the previously characterized NADH-dependent SLA reductase YihU (Denger, Weiss *et al.* 2014), serves as additional fermentation step (gray inset in the middle). **(B)** Fermentation of the DHPS to acetate and H<sub>2</sub>S by *Desulfovibrio* sp. strain DF1. As revealed in this study, DHPS is oxidized to 3-sulfolactate (SL) by two subsequent dehydrogenase reactions and the SL is cleaved into pyruvate and (bi)sulfite (HSO<sup>3-</sup>). The pyruvate is utilized for ATP generation concomitant with acetate excretion (and as carbon source for biomass formation, not shown). The sulfite is utilized as electron acceptor for sulfite respiration, as catalyzed by

dissimilatory sulfite reductase (Dsr), and reduced to H<sub>2</sub>S (gray inset; for comparison, the ATP-consuming activation of sulfate is also shown). **(C)** The genes for DHPS-degradative enzymes identified by differential proteomics in *Desulfovibrio* sp. strain DF1 cells are indicated by the color coding (B, C) and/or by their IMG locus tag numbers; they are located on different contigs of the draft genome sequence. In addition to the DHPS-desulfonation pathway genes, a candidate DHPS-transporter gene was identified by differential proteomics, *i.e.*, for the soluble substrate binding protein (indicated in brown), which is co-encoded with candidate ABC-transporter permease and ATP-binding component genes (indicated in white) and a candidate aldehyde:ferredoxin oxidoreductase gene (oxidored.; IMG locus tag no. 130621) (see text). Other abbreviations used: SF, 6 deoxy 6 sulfofructose; SFP, 6 deoxy 6 sulfofructose phosphate; PEP, phosphoenolpyruvate; YihO, SQ importer; YihP, DHPS exporter; PFL, pyruvate formate-lyase; PFOR, pyruvate:ferredoxin oxidoreductase; Pta, phosphotransacetylase; Ack, acetate kinase; Sat, ATP sulfurylase; Apr, adenylylsulfate reductase.

SQ is transported into the cell by YihO, converted to 6-deoxy-6-sulfofructose (SF) by SQ isomerase YihS, phosphorylated to 6-deoxy-6-sulfofructose-1-phosphate (SFP) by kinase YihV and the SFP is cleaved by aldolase YihT. This results in one molecule of dihydroxyacetonephosphate (DHAP), which is used for energy generation and growth, and one molecule of 3-sulfolactaldehyde (SLA), which is not further degraded (not desulfonated) but reduced to 2,3-dihydroxypropane-1-sulfonate (DHPS) by NADH-dependent reductase YihU. The DHPS is then transported out of the cell most likely by YihP. All genes in *E. coli* required for this pathway are encoded in one gene cluster, which is a core feature of commensal and pathogenic *E. coli* species (Denger, Weiss *et al.* 2014), together with an α-glucosidase gene (*yihQ*) for a hydrolysis of the SQ-glycoside (Speciale, Jin *et al.* 2016), an aldose epimerase gene (*yihR*) for an interconversion of the SQ epimers (Abayakoon, Lingford *et al.* 2017) and an SQ-responsive DoeR-family repressor gene (*yihW/csqR*) (Shimada, Yamamoto *et al.* 2018). This SQ-Embden-Meyerhof-Parnas (SQ-EMP) pathway has been identified for aerobic growth of *E. coli* K-12 (Denger, Weiss *et al.* 2014), but the potential of *E. coli* to utilize SQ also for anaerobic, fermentative growth has not yet been explored. This was the subject of the present study (see below). The second known pathway for a primary degradation of SQ (which is not a topic of this study) proceeds analogous to the Entner-Doudoroff pathway for glucose degradation and was studied in aerobic *Pseudomonas putida* (Felux, Spiteller *et al.* 2015). Here, also SLA is produced and not further degraded (not desulfonated), but the SLA is oxidized by an NAD<sup>+</sup>-dependent dehydrogenase to sulfolactate (SL), rather than reduced to DHPS as with *E. coli* K-12, prior to excretion of the SL.

The two C<sub>3</sub>-organosulfonate intermediates DHPS or SL produced by primary degradation of SQ can be degraded completely by aerobic bacteria (Rein, Gueta *et al.* 2005; Denger, Smits *et al.* 2006; Denger, Mayer *et al.* 2009; Mayer, Huhn *et al.* 2010; Denger, Huhn *et al.* 2012) and were shown to play an important ecological role in ocean plankton (Durham, Sharma *et al.* 2015; Landa, Burns *et al.* 2017). For a typical soil bacterium, *Cupriavidus pinatubonensis*

JMP134, the first desulfonation pathway for DHPS has been described by Mayer et al. (Mayer, Huhn et al. 2010). In the first steps, DHPS is oxidized via SLA to SL (Figure 2.1B) by DHPS dehydrogenase (HpsN). The SL is then cleaved by SL sulfite-lyase (SuyAB) (EC 4.4.1.24) (Rein, Gueta et al. 2005) into sulfite, which is excreted as sulfate (see below), and pyruvate, which is used for energy conservation and growth. Further, there are two other pathways for heterotrophic growth with SL known in aerobic bacteria. *Silicibacter pomeroyi* oxidizes SL to 3-sulfopyruvate by SL dehydrogenase (SlcD), followed by transamination of the 3-sulfopyruvate to cysteate (3-sulfoalanine) and desulfonation by deaminating cysteate sulfite-lyase (CuyA) (EC 4.4.1.25), yielding pyruvate, sulfite and ammonium (Denger, Smits et al. 2006). In *Roseovarius nubinhibens*, SL is oxidized also to 3-sulfopyruvate, but then decarboxyled to sulfoacetaldehyde and desulfonated by sulfoacetaldehyde acetyltransferase (Xsc) (EC 2.3.3.15), yielding acetyl phosphate and sulfite (Denger, Mayer et al. 2009). Notably, these DHPS- or SL-utilizing aerobic bacteria (with exception of *S. pomeroyi*) employ sulfite dehydrogenases and, hence, oxidize the sulfite generated by the desulfonation reactions to sulfate.

All detailed examinations on the degradation of SQ have been performed under oxic conditions with aerobic bacteria. In contrast, degradation of SQ under anoxic conditions by anaerobic bacteria and its potential role as a novel substrate for hydrogen sulfide ( $H_2S$ ) production (sulfidogenesis), has not been explored. Clearly, SQ is available as a substrate also in anoxic habitats, for example from decomposition of plant matter in water-saturated soils and of macro- and microalgae in marine and freshwater sediments, inside of photosynthetic microbial mats, but also in the gastrointestinal tracts of herbivorous and omnivorous animals and humans, for which SQ is part of their green-vegetable diet: the sulfolipid is found in significant amounts in many green vegetables, for example in spinach with up to 36% of the total lipid content (Kuriyama, Musumi et al. 2005).

Here, we demonstrate that anaerobic degradation of SQ concomitant with sulfide production is performed by a defined two-member consortium of laboratory model organisms: SQ-degrading *E. coli* K-12 and a DHPS-degrading *Desulfovibrio* sp. strain newly isolated from an anaerobic enrichment culture inoculated with sewage sludge. For the first degradation step, we established the growth physiology and a novel type of mixed-acid fermentation of *E. coli* and confirmed the involvement of the SQ-EMP pathway (Figure 2.1A). For the second degradation step, we established the growth physiology of isolate *Desulfovibrio* sp. strain DF1 and a novel type of sulfidogenic organosulfonate fermentation for DHPS (Figure 2.1B). Further, the key genes for the DHPS desulfonation pathway (Figure 2.1C) in the

*Desulfovibrio* sp. strain were, firstly, identified by genome sequencing and proteomics and, secondly, confirmed in their functions using recombinant enzymes.

## **Materials and methods**

### Chemicals

Racemic (*R,S*)-DHPS and (*R,S*)-SL were synthesized as described elsewhere (Wood 1971; Roy, Hewlins *et al.* 2003; Mayer, Huhn *et al.* 2010). SQ was provided by MCAT GmbH (Donaueschingen, Germany). Routine chemicals were from Merck, Roth or Sigma-Aldrich. NAD<sup>+</sup> was purchased from Roche, IPTG from VWR and NADH from Biomol. PCR supplies were from New England BioLabs (PCR for cloning) and Genaxxon biosciences (colony PCR).

### Bacterial strains

*Desulfovibrio* sp. strain DF1, which was enriched and isolated from anoxic sewage sludge in this study, was deposited at the Leibniz Institute DSMZ-German Collection of Microorganism and Cell Cultures (<https://www.dsmz.de>) under the reference number DSM 107641. Its annotated draft genome can be accessed *via* IMG (<https://img.jgi.doe.gov>) under IMG project ID Gp0153975 (GOLD ID Ga0134130). *E. coli* K-12 substrain MG1655 was available in the lab (Denger, Weiss *et al.* 2014), as were the knockouts strains obtained previously from the *E. coli* Keio Knockout Collection (Baba, Ara *et al.* 2006).

### Growth conditions

*Desulfovibrio* sp. strain DF1 and *E. coli* were grown anaerobically in a carbonate-buffered minimal medium reduced with 1 mM titanuim(III)nitriloacetate (Ti(III)-NTA) [basal medium, (Widdel and Pfennig 1981); trace elements solution, (Widdel, Kohring *et al.* 1983); Ti(III)NTA solution, (Moench and Zeikus 1983); selenium-tungstate solution, (Tschech and Pfennig 1984); vitamin solution, (Pfennig 1978)] and 12 mM SQ or 6 mM glucose (*E. coli*) or 10 mM DHPS (*Desulfovibrio* sp.). For sulfate-respiring growth conditions, *Desulfovibrio* sp. DF1 was grown with 10 mM lactate as the carbon source and electron donor and 20 mM sulfate as the terminal electron acceptor. The gas phase was 20% CO<sub>2</sub> and 80% N<sub>2</sub>. All cultures were incubated at 30°C. Cultures for proteomic analysis, 2D-PAGE and enzyme assays in cell-free extracts were harvested in late exponential phase at an optical density (OD<sub>580</sub>) of about 0.4.

The cells were resuspended in 50 mM Tris-HCl buffer, pH 8.0, containing 5 mM MgCl<sub>2</sub>, 1.7 µg/ml DNase I and 1x Halt™ protease inhibitor (ThermoFisher Scientific) and disrupted in a cooled French pressure cell.

*E. coli* for cloning and overexpression was grown in LB medium with, if necessary, 30 µg/ml kanamycin, 100 µg/ml ampicillin or 35 µg/ml chloramphenicol, aerobically on an orbital shaker at 37°C or 15°C. For details on the cloning, see below.

#### Enrichments and isolation

Enrichment cultures (20 ml) were set up in 50 ml serum bottles with butyl rubber stoppers and N<sub>2</sub>/CO<sub>2</sub> gas, and incubated at 30°C in the dark. The anoxic Ti(III)NTA-reduced medium described above was used, containing either 5 mM SQ as sole source of carbon and energy for fermentative growth or 5 mM SQ plus 20 mM sulfate as electron acceptor; 10 mM DHPS as sole substrate was provided later in the process of isolating *Desulfovibrio* sp. strain DF1. Initial inoculation was performed with 1 ml of anoxic material from a sewage plant, a biogas plant, garden compost or sulfidic sediment of Lake Constance, Germany. When growth of bacteria was detected by turbidity formation in the supernatant of the cultures and by microscopy (after 3 days to 2 weeks), about 10% (v/v) of the culture was transferred to fresh medium. After 4–5 transfers, pure cultures were obtained by repeated application of the agar shake dilution method (Pfennig 1978).

#### Draft-genome sequencing of *Desulfovibrio* sp. DF1, assembly and sequence analysis

Genomic DNA was extracted from an overnight culture (LB medium) using JGI's Bacterial Genomic DNA isolation protocol (JGI Bacterial DNA isolation CTAB-2012; <https://jgi.doe.gov/user-program-info/pmo-overview/protocols-sample-preparation-information/>). The whole-genome shotgun sequencing was performed by GATC Biotech (Konstanz, Germany) using the Illumina HiSeq2000 platform and a 125-bp paired-end library, which resulted in 15,158,760 reads (3.78 x 10<sup>9</sup> total bases).

The trimming, mapping, as well as the *de novo* assembly of the raw reads, was performed at the Genomics Center of the University of Konstanz. The remaining adapters were removed and reads were trimmed by quality in CLC Genomics Workbench v6.5 (CLC bio, Aarhus, Denmark). To estimate the mapping rate against different *Desulfovibrio* genomes, the program Bowtie v2.2.3 (Langmead and Salzberg 2012) was used to align the filtered reads against the genomes of *D. alcoholivorans* DSM 5433 (NCBI genome ID 32104), *D. desulfuricans* DSM 642 (ID 15717), *D. fairfieldensis* (ID 42991) and *D. fructosivorans* JJ (ID

2656). The highest mapping (62%) was against the genome of *D. alcoholivorans* and this genome was later used in the reference-guided scaffolding approach (see below). The reads were then assembled *de novo* using the program SOAPdenovo v2.04 (Luo, Liu *et al.* 2012) with a *k*-mer size of 67 and setting the minimum contig length at 200 bp. The scaffolding step of SOAPdenovo produced a final assembly including 340 sequences (N50: 141 Kb). The *de novo* assembled sequences were then scaffolded by the reference-guided algorithm implemented in Ragout 2.0b (Kolmogorov, Raney *et al.* 2014) using the genome of *D. alcoholivorans* as reference. The final assembly included 315 sequences (N50: 332 Mb). This assembly was uploaded to the DoE-JGI Integrated Microbial Genomes (IMG) annotation pipeline (<http://img.jgi.doe.gov/>). The size of the draft genome is 4.9 Mb with 4,333,987 DNA coding bases. The average G+C content is 64.68%. Analysis of genomes for orthologous gene clusters was done *via* the Gene Cassette Search and Neighborhood Regions Search options of the IMG/ER and IMG Human Microbiome Project (IMG/HMP) platforms.

### Gene cloning

Each gene for heterologous expression was first amplified from genomic DNA by PCR using primers targeting the start codon or downstream of the stop codon, respectively, and that contained restriction sites for NdeI (CATATG) in front of the start codon or XhoI (CTCGAG) at the end of the reverse primer (followed each by three random base pairs needed for restriction efficiency). Primers were designed using DNASTar PrimerSelect, and SerialCloner for virtual PCR and ligation as a control tool. Primers were synthesised by Microsynth AG (Balgach, Switzerland). The primer sequences are provided in the Supplemental Information file, Table S2.2.

The PCR product was first cloned by blunt end cloning into a pJet suicide vector using the CloneJet PCR cloning kit (ThermoFisher Scientific). The plasmid was transformed into chemically competent *E. coli* NovaBlue cells, which were streaked onto selective LB plates containing ampicillin; *E. coli* NovaBlue were chosen for improved transformation efficiency and plasmid stability. The resulting colonies were tested by colony PCR using the insert primers. Positive colonies were cultured in 5 ml LB with ampicillin and the plasmids were extracted using the Zippy Plasmid Miniprep kit (Zymo Research). The plasmids were digested with NdeI and XhoI (New England BioLabs Inc.) simultaneously in CutSmart buffer for 2h at 37°C. The digest was loaded onto an agarose gel, the insert bands were excised and extracted using the Gel extraction Mini Spin Column kit (Genaxxon biosciences).

As an expression vector, we chose the pET 28a(+) vector (Novagen) that results in an N-terminally His-tagged protein, and which has restriction sites for NdeI and XbaI. The vector is designed for high expression levels from a T7 system under control of a lac repressor and carries a kanamycin resistance cassette. The empty vector was digested and gel-purified from as described above. The NdeI and XbaI-digested, purified inserts were then ligated into the vector using T4 ligase; the resulting plasmid was again transformed into *E. coli* NovaBlue and streaked on selective plates containing kanamycin. Positive clones identified by colony PCR were picked into 5 ml LB medium with kanamycin, and after overnight growth, the plasmids were extracted and sequenced; primers for the T7 expression region were used for sequencing, as provided by GATC (Konstanz, Germany). GATCViewer and SerialCloner were used to confirm the correct insert sequences.

#### Heterologous expression and protein purification

For overexpression, the pET28 plasmid constructs were transformed into chemically competent *E. coli* Rosetta 2 DE3 cells; this strain enables expression under control of a T7 promoter and contains a rare codon usage plasmid (pRARE2), which also bears a chloramphenicol resistance. The transformed cells were cultured overnight in 5 or 10 ml of liquid LB medium containing kanamycin and chloramphenicol. For expression, 100 ml of LB with kanamycin and chloramphenicol were inoculated (2.5–5%) with the overnight culture and incubated shaking at 37°C until they reached an OD<sub>580</sub> of about 0.5. Expression was induced by addition of 1 mM isopropyl-β-D-thiogalactopyranoside (IPTG). The cultures were incubated further either for 5–6 h at 37°C (for DHPS dehydrogenase) or at 15°C overnight in order to aid with folding and solubility (for SLA dehydrogenase, SuyA and SuyB).

Cells were harvested by centrifugation at 13,000 × g for 15 min and washed twice in 20 mM phosphate buffer, pH 7.2, containing 500 mM NaCl, 2.5 mM MgCl<sub>2</sub>, 10 U/ml DNaseI, 1x Halt™ protease inhibitor (ThermoFisher Scientific) and 20 mM imidazole. Cells were disrupted by 4 passages through a French pressure cell, or by incubation with 5 mg/ml lysozyme for 1 h at 37°C followed by a freeze-thaw cycle and 5 minutes in an ultrasound bath. Cell debris was then removed by centrifugation at 17,000 × g for 10 min and the His-tagged protein was purified over a Ni-NTA column (His SpinTrap™ kit, GE Healthcare) with wash steps at 20, 40 and 60 mM imidazole and elution at 500 mM imidazole. To remove the imidazole, the buffer was then exchanged to 50 mM Tris-HCl, pH 9.0, using Illustra™ Nap™-5 columns (GE Healthcare).

For anaerobic expression of the aldehyde:ferredoxin oxidoreductase gene, *E. coli* Rosetta 2 DE3 was grown anaerobically in the minimal medium described above containing also 0.4% glucose, 5 mM sodium nitrate, 0.1% yeast extract and the required antibiotics. IPTG was added anoxically to a final concentration of 1 mM when the cultures had reached an optical density of about 0.5. The cells were harvested by centrifugation in the culture flasks at 1,200 × g for 30 min. The pellet was resuspended, transferred into a vial flushed with N<sub>2</sub> gas and disrupted in a French pressure cell flushed with N<sub>2</sub>. The purification and buffer exchange were performed in an anoxic tent with an atmosphere of 95% N<sub>2</sub> and 5% H<sub>2</sub>. All buffers were degassed under vacuum, flushed with N<sub>2</sub>, and additionally contained 3 mM of dithiothreitol (DTT).

### Enzyme assays

Enzyme assays were conducted in 50 mM Tris-HCl buffer, pH 9.0. Assays with purified DHPS and SLA dehydrogenases, or with cell-free extracts, contained 5 mM DHPS and 10 mM NAD<sup>+</sup>. Typically, 0.8–1.0 µg/ml purified DHPS dehydrogenase and 16.5 µg/ml purified SLA dehydrogenase were used in an assay. Assays with cell-free extract were performed with 5 µl of extract per ml reaction (31.5 µg/ml total protein). Enzymes were heat inactivated at 100°C for 10 min in a heating block for negative control reactions.

The enzyme assay for the recombinant aldehyde:ferredoxin oxidoreductase was conducted in anoxic 50 mM Tris-HCl buffer, pH 7.4, under an atmosphere of 80% N<sub>2</sub> and 20% CO<sub>2</sub>. The assay typically contained 5 µg of purified enzyme, 1 mM benzylviologen and/or NAD<sup>+</sup> as electron acceptor and 0.5 mM lactaldehyde or acetaldehyde as substrate. SLA as substrate was produced under these anoxic conditions from 2 mM DHPS in the presence of 4 mM NAD<sup>+</sup> and 1 mg of DHPS dehydrogenase. The reduction of benzylviologen was observed photometrically by measuring the absorption at 578 nm for 1 min after addition of the aldehyde substrate, and the reduction of NAD<sup>+</sup> at 365 nm.

For the recombinant SuyAB enzyme, both subunits were expressed and purified separately. For the SL desulfonation assay, 0.15 mg/ml of SuyA and 0.6 mg/ml of SuyB were typically used (meaning equimolar amounts, with SuyB having approximately four times the mass of SuyA). The enzyme was first reconstituted from both subunits overnight at -20°C in 0.1 M MOPS buffer with 1 mM FeCl<sub>2</sub> and 10% (v/v) glycerol. To prevent oxidation of Fe<sup>2+</sup>, the mixture was degassed under vacuum and saturated with 80% N<sub>2</sub> and 20% CO<sub>2</sub> gas before freezing. The reaction was started by addition of 2.5 mM (final concentration) SL. Samples for quantification of sulfite and pyruvate were taken discontinuously.

### Analytical methods

For quantification of glucose, SQ, SL, DHPS, pyruvate, NADH and NAD<sup>+</sup> a Shimadzu HPLC system, a hydrophilic interaction liquid chromatography column (Merck ZIC-HILIC, 5µm, 200 Å, 150 x 2.1 mm) and a UV/Vis-DAD detector (Shimadzu SPD-M20A) and evaporative light scattering detector (ELSD) (Schambeck SFD ZAM3000) were used. The total eluent flow was 0.3 ml/min with acetonitrile as the eluent A and 0.1 M ammonium acetate plus 10% acetonitrile as eluent B. HPLC conditions were as follows: gradient from 90% to 75% A for 20 min; gradient from 75% to 65% for ten min; isocratic at 65% A for 10 min; to 20% A within 1 min; wash step at 20% for 9 min; back to 90% A in 1 min; equilibration at 90% A for 19 min. Under these conditions, DHPS eluted at 13.5 min, glucose at 17.6 min, sulfolactate at 20.5 min, and SQ at 26.7 min (as detected by ELSD). Pyruvate eluted at 6.6 min, NADH at 26.6 min, and NAD<sup>+</sup> at 28.6 min (as detected at 350 nm).

For qualitative detection of DHPS, SLA, and SL the same column and conditions were used on an Agilent 1100 HPLC system coupled to a LCQ ion trap mass spectrometer (ThermoFisher Scientific) for electrospray ionization tandem mass spectrometry (ESI-MS/MS) operated in the negative mode. The compounds were detected using ion trace search of the [M-H]<sup>-</sup> ions:  $m/z$  = 155 for DHPS,  $m/z$  = 153 for SLA,  $m/z$  = 169 for SL.

Short chain fatty acids and alcohols against authentic standards were analyzed on a Shimadzu HPLC system with an Aminex column (Aminex HPX-87H, BioRad) and a refractive index detector (RID; Shimadzu RID-10A) at 60°C. The eluent was 5 mM H<sub>2</sub>SO<sub>4</sub> at an isocratic flow of 0.6 ml/min. Under these conditions, the fermentation products succinate eluted at 11.7 min, formate at 14.0 min, acetate at 15.2 min and ethanol at 22.0 min; lactate eluted at 13.0 min and pyruvate at 20.0 min. This Aminex HPLC-RID method generally separates and detects carbohydrates, carboxylic acids, short-chain fatty acids, alcohols, ketones and other metabolites; no other products (peaks) than the ones stated in the Results section were detected in any growth experiment (*E. coli* K-12 and *Desulfovibrio* sp. DF1).

Hydrogen production was tested with a Peak Performer 1 (Peak Laboratories) trace gas analyzing gas chromatography system with a reducing compound photometer detector; N<sub>2</sub> was used as the carrier gas.

Sulfide in culture media was routinely measured using an adapted methylene blue assay with Na<sub>2</sub>S as standard (Cline 1969). Therefore, 10 µl of sample was added immediately to 100 µl 0.1 M zinc acetate solution and the sample was stored at -20°C. For analysis, the solution was brought to 895 µl total volume by addition of MilliQ water and 100 µl of a 10 mM solution

of *N,N*-dimethyl-*p*-phenylenediamine sulfate in 20% sulfuric acid was added. The reaction was started by addition of 5 µl of a solution of 5 g NH<sub>4</sub>Fe(SO<sub>4</sub>)<sub>2</sub> in 2% sulfuric acid. After 45 min, the absorption was measured at 670 nm.

Total protein content of cell pellets was determined by a modified Lowry assay as described in (Kennedy and Fewson 1968), scaled to 1 ml total reaction volume. Protein concentration in solutions was determined by the Bradford assay in 1-ml scale (Bradford 1976).

Sulfite was measured after derivatisation with *N*-(9-Aridinyl)maleimide (NAM) (Akasaka, Matsuda *et al.* 1990). Briefly, 50 µl of fresh sample were added to 150 µl borate buffer (0.3 M boric acid, 0.3 M potassium chloride, adjusted to pH 9.3 with a solution of 0.3 M sodium carbonate and 0.02 M EDTA). 50 µl of a solution of 10 mM NAM dissolved in acetone were added and the derivatisation reaction was incubated at 50°C for 30 min. The samples were then frozen to precipitate protein and centrifuged for 1 minute at 14,500 × g. NAM-Sulfite was quantified using a Phenomenex Luna Omega column (5 µm PS C<sub>18</sub> 100 Å, 150 × 3.0 mm) with a Phenomenex SecurityGuard guard cartridge kit and an UV detector under the following conditions: solvent A, Milli-Q water with 0.1% (v/v) formic acid; solvent B, acetonitrile; total flow, 0.5 ml/min; column temperature, 30°C; detection wavelength, 254 nm. Gradient: 10% B for 3 min; gradient to 80% B in 10 min; reequilibration at 10% B for 7 min. The NAM-sulfite signal was split into two peaks at 3.4 and 4.0 min respectively, and the peak areas were added up for quantification. A fresh solution of sodium sulfite was used as the standard.

Pyruvate from SuyAB enzyme assays was measured also as a 2,4-dinitrophenylhydrazine (DNPH) derivate. 50 µl of fresh sample were added to 50 µl of a solution of 0.5 mg/ml DNPH in acetonitrile with 0.1% phosphoric acid (Koivusalmi, Haatainen *et al.* 1999; Frey, Schneider *et al.* 2018). The reaction was incubated for 2 h at room temperature. The samples were then frozen to precipitate protein and centrifuged for 1 minute at 14,500 × g. NAM-Sulfite was quantified on a Phenomenex Luna Omega column (5 µm PS C<sub>18</sub> 100 Å, 150 × 3.0 mm) with a Phenomenex SecurityGuard guard cartridge kit and an UV detector under the following conditions. Solvent A, Milli-Q water with 0.1% (v/v) formic acid; solvent B, acetonitrile; total flow, 0.75 ml/min; column temperature, 40°C; detection wavelength, 360 nm. Gradient: 25% B for 4.5 min; to 70% B in 15 min; reequilibration at 25% B for 10.5 min. Pyruvate-DNPH eluted as a single peak at 12.3 min retention time and was quantified against freshly prepared standards using a freshly prepared sodium pyruvate stock solution.

## Proteomics

Cells were grown, harvested and disrupted by 4 passages through a French pressure cell as described above. Intact cells and cell debris was removed by centrifugation at  $12,000 \times g$  for 5 min,  $4^{\circ}\text{C}$ . The protein concentration in these cell-free extracts was determined by Bradford assay. The total protein was purified when samples of 200  $\mu\text{g}$  of total protein were mixed with SDS-PAGE loading dye (Roti-Load 1, Carl Roth) and denatured at  $100^{\circ}\text{C}$  for 10 minutes. The samples were then loaded on an SDS gel (12% resolving gel, 6% stacking gel) and run at 30 mA for 1 h until the proteins had entered the stacking gel (without any separation). The gel was stained with Coomassie Blue (Meyer and Lamberts 1965) and each total-protein band was excised and submitted to the Proteomics Facility at the University of Konstanz for identification by peptide fingerprinting-mass spectrometry (see below). For analyzing only the soluble proteins in cell-free extract directly (without any SDS-PAGE purification), the membrane fragments were removed first from the extract by ultracentrifugation at  $104,000 \times g$  for 35 min at  $4^{\circ}\text{C}$ , and then samples of the soluble protein were submitted to peptide fingerprinting-mass spectrometry.

The protein extracts, and the protein band or spots excised from SDS-PAGE gels, were subjected to peptide fingerprinting-mass spectrometry (PF-MS) at the Proteomics Facility of the University of Konstanz ([www.proteomics-facility.uni-konstanz.de](http://www.proteomics-facility.uni-konstanz.de)) as described previously (Schmidt, Müller *et al.* 2013; Denger, Weiss *et al.* 2014; Felux, Spiteller *et al.* 2015) with the exception that each sample was analyzed twice on a Orbitrap Fusion with EASY-nLC 1200 (Thermo Fisher Scientific), and that Tandem mass spectra were searched against an appropriate protein database (retrieved from IMG) using Mascot (Matrix Science) and Proteom Discoverer V1.3 (Thermo Fisher Scientific) with “Trypsin” enzyme cleavage, static cysteine alkylation by chloroacetamide, and variable methionine oxidation.

## Protein gel electrophoresis

To evaluate the purity of recombinant proteins, aliquots of the protein preparations corresponding to 15  $\mu\text{g}$  of total protein (Bradford assay) were mixed with 4x SDS-PAGE loading dye (Roti-Load 1, Carl Roth) and denatured at  $100^{\circ}\text{C}$  for 10 min. The samples were then loaded onto an SDS gel (12% acrylamide for the resolving gel, 4% for the stacking gel) and run at a constant voltage of 100 V; the gels were stained with Coomassie Blue.

For differential two-dimensional PAGE and identification of proteins spots by peptide fingerprinting-mass spectrometry (Denger, Weiss *et al.* 2014; Felux, Spiteller *et al.* 2015), *Desulfovibrio* sp. DF1 was grown with 10 mM DHPS or with 15 mM lactate plus 30 mM of

sulfate. The cells were grown and harvested as described above and resuspended in 50 mM Tris-HCl buffer, pH 8.1, containing 2.5 mM MgCl<sub>2</sub>, 10 U/ml DNaseI and 1x Halt protease inhibitor (ThermoFisher Scientific). The cells were disrupted by four passages through a French pressure cell, centrifuged for 5 min at 12,000 × g to remove cell debris and then for 30 min at 104,000 × g to obtain the soluble protein fraction. An amount corresponding to 500 µg of total protein was precipitated by adding 5 volumes of acetone followed by incubation overnight at -20°C. Acetone was removed after centrifugation at 9,000 × g for 20 min, the protein pellets were dried under air, and then resuspended in 8 M urea, 2 M thiourea, 3% CHAPS (3-[(3-Cholamidopropyl)dimethylammonio]-1-propanesulfonate), 60 mM DTT and 0.2% Bio-Lyte 3/10 ampholytes (Bio-Rad); the solution was incubated for 30 min in a cooled ultrasonic bath, followed by two hours of shaking at room temperature. The samples were then loaded each onto an IPG Bio-Rad ReadyStrip pH gradient strip (pH range 5–8) and incubated overnight to rehydrate the IPG strip. The isoelectric focusing was performed with a voltage ramp to 10,000 V in 3 h, and a total focusing of 40,000 Vh. Thereafter, the strip was equilibrated in equilibration buffer (6 M urea, 0.375 M Tris, 2% SDS, 20% glycerol 2% (w/v) DTT) for 10 min on an orbital shaker and then washed with the same buffer containing additionally 2.5% (w/v) iodoacetamide. The strip was then placed onto a 12% SDS PAGE gel and mounted with SDS gel buffer containing 0.5% agarose. The gel was run overnight at 40 mA and stained with Coomassie Blue. Protein spots of interest were excised and analyzed at the Proteomics Facility of University of Konstanz (see above).

## Results and discussion

### E. coli K-12 employs the SQ-EMP pathway for a mixed-acid fermentation of SQ

We cultivated *E. coli* K-12 MG1655 routinely under fermentative conditions with SQ in a carbonate-buffered mineral salts medium in the presence of Ti(III)NTA as reducing agent instead of Na<sub>2</sub>S, in order to allow for a co-cultivation of *Desulfovibrio* sp. and for a quantification of H<sub>2</sub>S production during DHPS degradation (see below). For the physiological growth experiments with *E. coli* K-12 in pure culture, we used mixed-acid fermentation of glucose, as well as its aerobic growth with SQ or glucose (Denger, Weiss *et al.* 2014), as references.

At first, we confirmed the involvement of the SQ-EMP pathway in *E. coli* K-12 during fermentative growth with SQ. The knockout mutants used previously (Denger, Weiss *et al.* 2014) with deleted SQ importer gene ( $\Delta yihO$ ), sulfosugar-metabolic genes ( $\Delta yihS$ ,  $\Delta yihV$  and  $\Delta yihT$ ), or 3-sulfolactate reductase gene ( $\Delta yihU$ ), each failed to grow with SQ under

fermentative conditions while these mutants grew by glucose fermentation (data not shown). In addition, differential proteomics confirmed proteins YihS, YihV, YihT, YihU and YihQ to be highly induced during SQ fermentation but not during glucose fermentation (Figure 2.2), as was observed previously for its aerobic growth with SQ (Denger, Weiss *et al.* 2014).

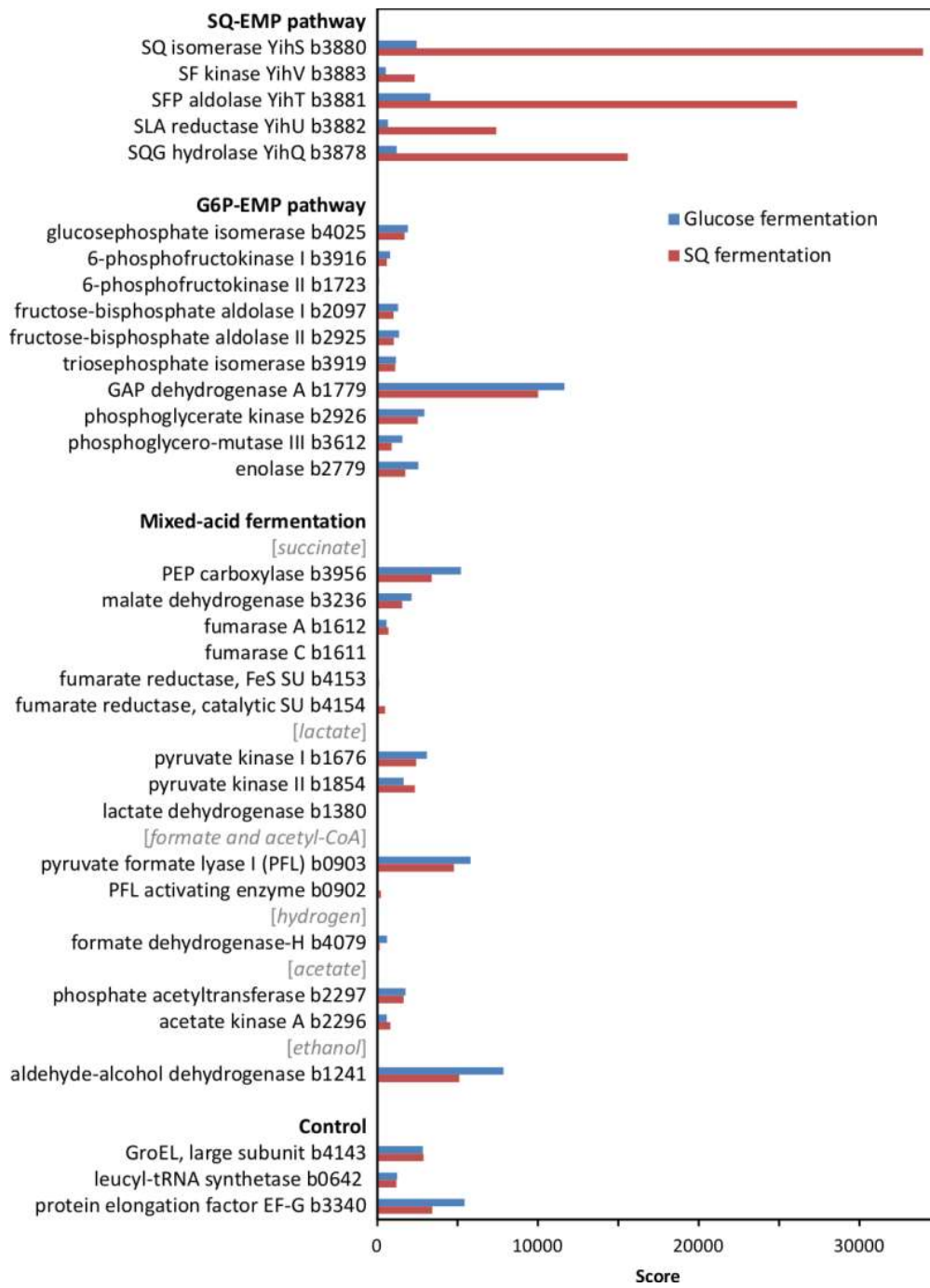


**Figure 2.2. Total proteomic analysis comparing abundant soluble proteins in cell-free extracts of SQ- and glucose-fermenting *E. coli* cells.** Shown are metabolic enzymes grouped according to the SQ-EMP pathway, the EMP pathway for glucose (G6P-EMP pathway) and to mixed-acid fermentation. Constitutively expressed proteins are shown for comparison (control). IMG locus tag numbers are given for each protein. Shown is data of a proteomic analysis replicated once. A higher score represents a more abundant protein.

Notably, no significant differences in the abundance of the EMP pathway enzymes for glucose (G6P-EMP pathway/gluconeogenesis) and of key enzymes involved in mixed-acid fermentation, such as aldehyde-alcohol dehydrogenase, were detected by proteomics (Figure 2.2).

For the aerobic growth of *E. coli* with SQ (Denger, Weiss *et al.* 2014), the molar growth yield is approximately 50% of that for glucose, which reflects that only half of the SQ-carbon can be made available for energy conservation (aerobic respiration) and biomass growth (assimilation) through the SQ-EMP pathway (*via* DHAP/GAP), whereas the sulfonated C<sub>3</sub>-half is excreted (as DHPS). Therefore, we routinely supplied equivalent amounts of accessible substrate-carbon to our cultures for comparative growth experiments, *i.e.*, 12 mM SQ and 6 mM glucose, respectively, for which a growth experiment sampled in great detail is shown in Figure 2.3.

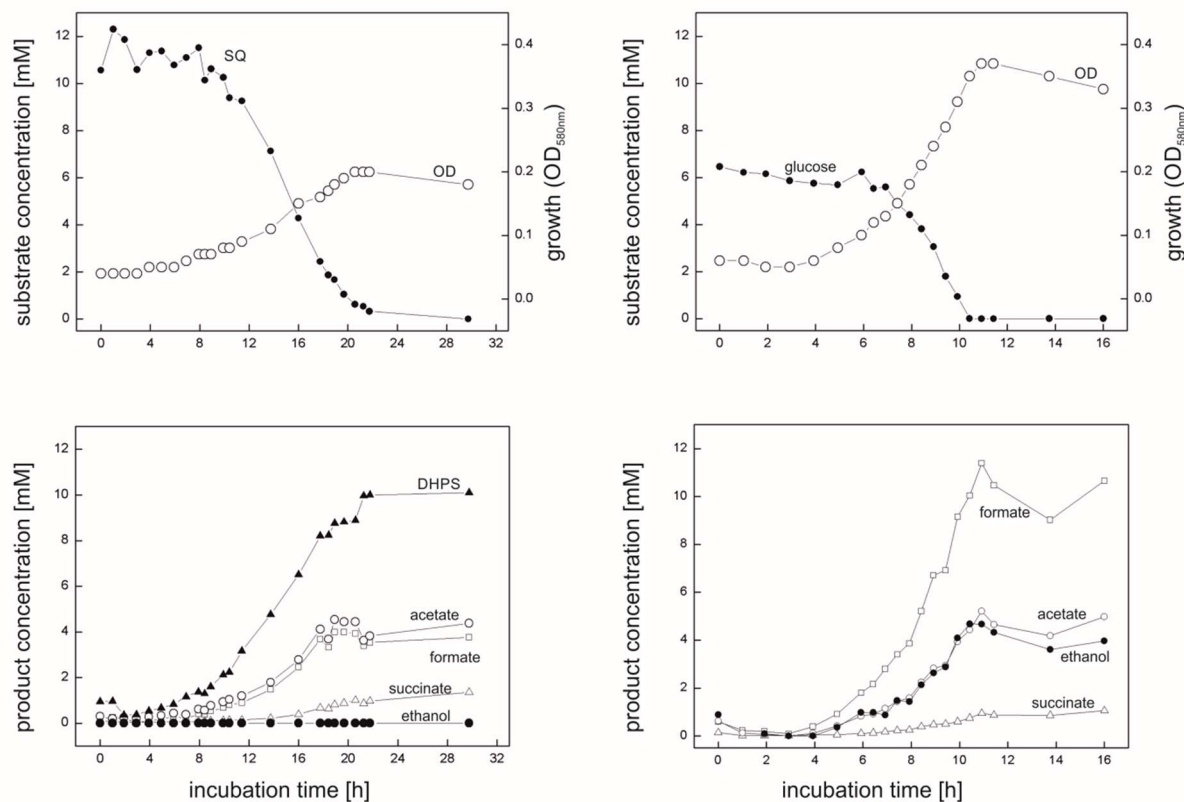


**Figure 2.3. *E. coli* K-12 growing in pure culture under fermentative conditions with SQ (A, C) and glucose (B, D).** For the growth experiment shown, 12 mM SQ or 6 mM glucose was used, so that both cultures had access to the same amount of C<sub>3</sub>-carbon (DHAP/GAP) for growth through the SQ-EMP and G6P-EMP pathways, respectively (*i.e.*, 1 mol DHAP per mol of SQ, compared to 2 mol DHAP/GAP per mol of glucose; see Figure 2.1). **(A, B)** biomass formation shown here as optical density (OD<sub>580nm</sub>), open circles; SQ or glucose disappearance, solid circles. **(C, D)** product formation (mM); formate, open square; acetate, open circle; ethanol, solid circle; succinate, open triangle; DHPS, solid triangle. For both cultures, lactate and H<sub>2</sub> production was not detectable and therefore this data was omitted in this illustration. The cultures were incubated in 60 ml serum flasks with rubber

stoppers containing, initially, 25 ml culture fluid and 35 ml N<sub>2</sub>/CO<sub>2</sub> gas in the headspace. At each time interval, 1.0 ml of sample was removed with a syringe. The growth experiment was replicated once when sampled in such detail, and at least three times in smaller scale when evaluating only the outgrown cultures ( $t_{end}$ ) (see Figure 2.4 and Table S2.1).

Strain K-12 exhibited a lower growth rate during SQ fermentation ( $\mu = 0.1 \text{ h}^{-1}$ ) in comparison to glucose fermentation ( $\mu = 0.27 \text{ h}^{-1}$ ) (Figure 2.3AB); a lower growth rate with SQ compared to glucose was also observed for its aerobic growth ( $\mu = 0.13$  and  $0.5 \text{ h}^{-1}$ , respectively (Denger, Weiss et al. 2014). Further, in comparison to aerobic respiration, only approximately 10–15% of total biomass (estimated as total protein content) was formed with SQ and glucose under fermentative conditions, which reflects that during fermentations the vast majority of the substrate-carbon is allocated to the production of electron acceptors. The molar growth yield for carbon determined for SQ fermentation in comparison to glucose fermentation however was consistently less than 50% (approximately 35–40% as estimated by total protein) and, thus, not equal when growth with equivalent amounts of accessible substrate-carbon was compared (12 mM SQ and 6 mM glucose), which is illustrated in Figure 2.3AC by the different final optical densities observed. The replicate growth experiments in smaller scale (10 ml), which were sampled only after the growth ( $t_{end}$ ), confirmed this pattern, including the fermentation products formed (see below) (Figure 2.4 and Table S2.1 in the Supplementary Material); these results were independent of the addition of Ti(III)NTA as reducing agent.

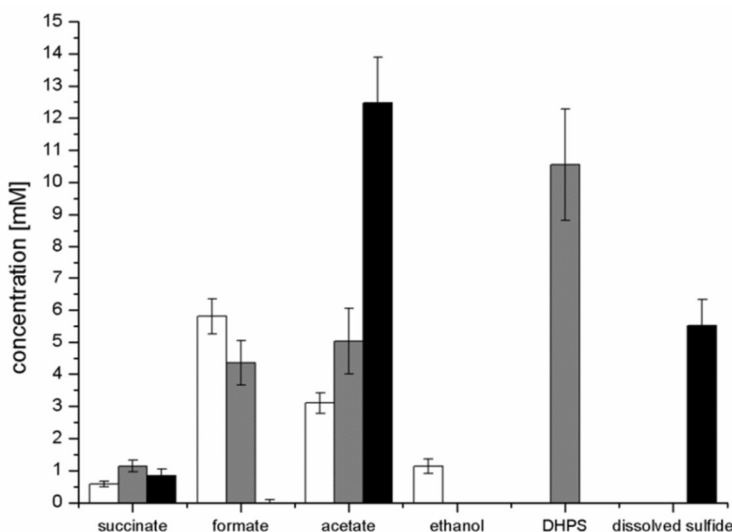


**Figure 2.4. Concentration of products detected after growth of *E. coli* in pure culture with glucose (white bars) or SQ (gray bars) and after growth with SQ in co-culture with a DHPS-degrading *Desulfovibrio* sp. strain (black bars).** The cultures were incubated in 25 ml culture tubes containing 10 ml culture fluid containing 12 mM SQ or 6 mM glucose and 15 ml N<sub>2</sub>/CO<sub>2</sub> gas in the headspace; samples were collected when the cultures had entered stationary phase ( $t_{end}$ ). For a calculation of the carbon and electron recoveries for mixed-acid fermentation of SQ and glucose by *E. coli* in pure culture, see Table S2.1 in the Supplementary Material. The data represents the mean of at least three growth experiments; the standard deviations is indicated.

Mixed-acid fermentation of glucose under our cultivation conditions yielded formate, acetate, ethanol and succinate as products (Figure 2.3D and Figure 2.4, Table S2.1), as detected by HPLC. There was no lactate or any other fermentation product detectable (see Materials section) in the culture fluid, and there was no H<sub>2</sub> in the headspace in relevant amounts, as determined by the gas chromatography (detection limit 4 µM). The SQ fermentation (Figure 2.3D and Figure 2.4, Table S2.1) yielded quantitative amounts of DHPS, but no ethanol, more acetate and less formate as well as more succinate, when compared to glucose fermentation (see Figure 2.3CD and Figure 2.4), as illustrated also by the dissimilation equation calculated for SQ fermentation in comparison to glucose fermentation under our growth conditions (see Table S2.1). There was no other fermentation product detectable in the culture fluid and no H<sub>2</sub> in the headspace. From this data (Figure 2.4, Table S2.1), a carbon recovery of 82% and an electron recovery of 85% was calculated for SQ fermentation.

In conclusion, we demonstrated that *E. coli* K-12 is capable of utilizing SQ as sole substrate also for anaerobic growth through mixed-acid fermentation *via* the SQ-EMP pathway, for which the majority of the acquired C<sub>3</sub>-carbon is allocated to fermentation products, as in the case of mixed-acid fermentation of glucose. With the SQ-EMP pathway however, *E. coli* employs the metabolite 3-SLA as an additional electron acceptor for NAD<sup>+</sup> regeneration, using the NADH-dependent reductase YihU (Figure 2.1A). This is reflected by the different ratio of fermentation products observed for SQ fermentation in comparison to glucose fermentation (Figure 2.3 and Figure 2.4): the different ratio of formate/succinate suggests that with SLA as additional electron acceptor, more of the phosphoenolpyruvate (PEP) is funneled to fumarate reduction for NAD<sup>+</sup> regeneration (and proton pumping), rather than to acetyl-CoA and formate. The different ratio of acetate/ethanol however suggests that this acetyl-CoA is then fed only into the acetate-arm of the pathway for ATP conservation (see Figure 2.1A) while the ethanol-arm for NAD<sup>+</sup> regeneration (aldehyde-alcohol dehydrogenase) is inactive. The observation that the molar growth yield for SQ fermentation is only approx. 35–40% of that for glucose is reflected by the carbon balance determined (see Table S2.1), which suggests that a higher proportion of the accessible carbon was invested into dissimilation during growth with SQ in comparison to glucose (as indicated by the lower molar growth yield for dissimilated substrate, see Table S2.1). While it appeared that SQ-fermentative growth yields less energy than initially expected, the exact reason remains unclear. It might point at an interesting tradeoff between metabolic yield (or metabolic rate) relative to the investment cost for enzyme production (protein synthesis) [e.g., (Stettner and Segre 2013);(Flamholz, Noor *et al.* 2013)], given the observed high expression of the SQ-EMP pathway enzymes in fermenting cells (see Figure 2.2) as well as in aerobically respiring

cells (as seen previously on 2D-gels (Denger, Weiss *et al.* 2014). For example, a higher investment of resources into protein synthesis for maintaining the SQ-EMP pathway flux relative to the G6P-EMP pathway flux (which yields twice the amount of DHAP/GAP per flux) might weight higher during fermentative substrate-level phosphorylation (with its low ATP yield) in comparison to oxidative phosphorylation under oxic conditions (high ATP yield). Unfortunately, we are as yet unable to conduct kinetic experiments with the key SQ-EMP pathway enzymes in comparison to the G6P-EMP pathway enzymes, because the appropriate substrates (SF, SFP, SLA) are not available.

Enrichments and isolation of an SQ-fermenting *Citrobacter* sp. strain and a DHPS-fermenting *Desulfovibrio* sp. strain

In order to initially examine the occurrence of anaerobic SQ- and DHPS-degrading bacteria and when aiming at isolating new SQ- and/or DHPS-metabolizing strains, we set up enrichment cultures with inocula from different anoxic environmental habitats: from a sewage treatment plant, a biogas plant, garden compost and Lake Constance sediment. All enrichment cultures, and the subcultures thereof, grew and degraded SQ completely and in some cultures transient DHPS formation was detected by HPLC (data not shown). H<sub>2</sub>S production, as detected by its smell, was confirmed for all enrichments. The fastest growing enrichments (sewage sludge and compost) were purified *via* agar dilution series using SQ as substrate and colony picking. In these agar shakes, we observed two colony types: light beige colonies and dark beige colonies. One representative light beige colony (enriched from compost) was purified further using SQ-containing agar dilution and colony picking into SQ-containing liquid medium. The isolate degraded SQ completely and produced DHPS. It was identified by 16S rRNA gene sequencing as a *Citrobacter* sp. strain (99% identity with *C. freundii*). Thus, it represented another anaerobic SQ-degrading, DHPS-producing enterobacterium, such as *E. coli* K-12. In the genomes of other *Citrobacter* species, the SQ-EMP pathway is encoded (as examined *via* the JGI-IMG platform). Hence, because the isolate most likely employed also the SQ-EMP pathway, it was not further examined.

The other, dark beige colonies however never grew when transferred into SQ-containing liquid medium, but grew in DHPS-containing liquid medium. The DHPS was completely degraded and H<sub>2</sub>S was formed, even when sulfate as additional electron acceptor had been omitted in these cultures (see below). One representative colony enriched from sewage sludge was purified further *via* DHPS-containing agar dilution and colony picking into DHPS-containing liquid media without additional sulfate. The isolate was identified by 16S rRNA gene sequencing as a *Desulfovibrio* sp. strain (99% identity with *D. alcoholivorans*).

The DHPS-degrading *Desulfovibrio* sp. isolate was termed strain DF1 ('DHPS-fermenting isolate no. 1'), was draft-genome sequenced and its growth with DHPS as sole substrate in the absence of sulfate as electron acceptor was characterized in detail. As illustrated by a linearized growth plot in Figure 2.5, DHPS disappeared concomitant with biomass formation and nearly quantitative amounts of acetate were formed.

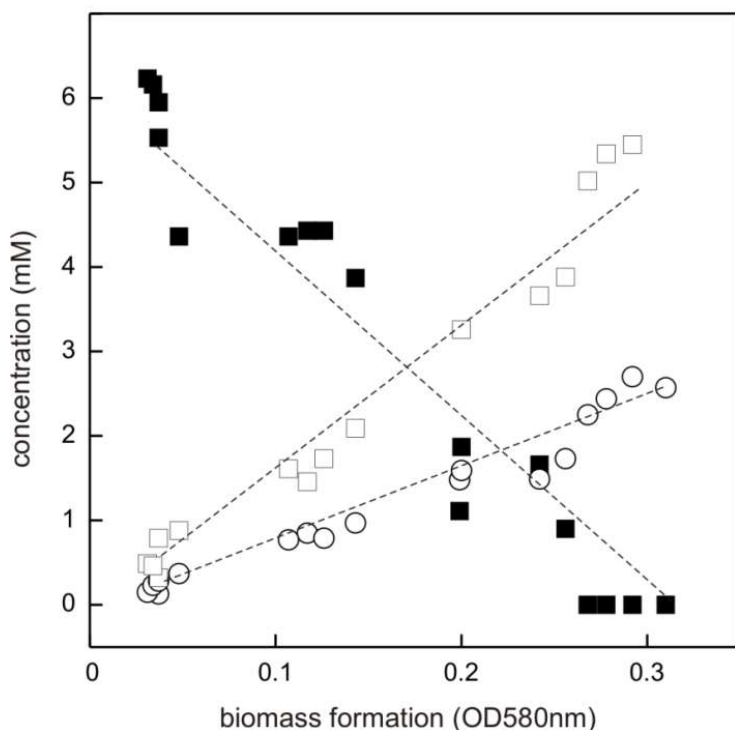
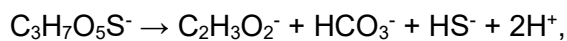


**Figure 2.5. Linearized growth plot illustrating substrate disappearance and formation of acetate and sulfide during growth of *Desulfovibrio* sp. strain DF1 with DHPS.** Concentrations of DHPS (solid square), acetate (open square) and of dissolved sulfide/bisulfide in the culture fluid (open circle) were determined and the values plotted against biomass formation (OD580nm). Note that we did not determine the fraction of H<sub>2</sub>S dissolved in the gas phase of the culture vessel, which is thus missing in the overall sulfur quantitation. No sulfate or sulfite were detectable in the culture at any time during growth (not shown). This growth experiment was conducted once when sampled in such detail; the substrate disappearance, biomass and product formation was confirmed in smaller scale when evaluating only the outgrown cultures ( $t_{end}$ ) (see Figure 2.4).

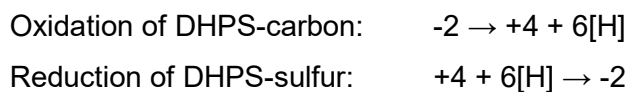
Further, there was sulfide produced during growth, as detected by the dissolved sulfide/bisulfide in samples of culture fluid, though not in quantitative amounts relative to substrate disappearance and acetate formation (Figure 2.5). This is because of the partitioning of the sulfide between the liquid phase of the culture and its gas phase (as H<sub>2</sub>S gas, some of which is also lost during the sampling). Notably, the nearly quantitative conversion of DHPS to acetate, and the absence of any other product in the culture fluid (as determined by Aminex HPLC; see Materials section), implied that no other (sulfonated) degradation product of DHPS was formed. The growth rate of *Desulfovibrio* sp. strain DF1 with DHPS was approx.  $\mu = 0.01 \text{ h}^{-1}$ .

In conclusion, *Desulfovibrio* sp. strain DF1 produced sulfide during DHPS utilization in the absence of added sulfate as electron acceptor. This implied that strain DF1 utilizes the carbon-moiety of DHPS as a source of carbon and electrons and its sulfonate-moiety as electron acceptor, hence, by a metabolism in analogy to the described respiration with taurine (2-aminoethanesulfonate) by *Bilophila wadsworthia* (Laue, Denger *et al.* 1997) or isethionate (2-hydroxyethanesulfonate) by *Desulfovibrio* spp. (Lie, Pitta *et al.* 1996): the sulfite released by a desulfonation of an organosulfonate substrate, such as taurine, isethionate or DHPS, is utilized as electron acceptor in respiration and reduced to sulfide by dissimilatory sulfite reductase (Dsr), as illustrated in Figure 2.1B for DHPS. Compared to sulfate-reducing bacteria (Muyzer and Stams 2008), such ‘organosulfonate respiration’ confers the ability to occupy distinct metabolic niches and there is no expenditure of ATP necessary for generating sulfite from sulfate as electron acceptor (see Figure 2.1B).

For *Desulfovibrio* sp. strain DF1 and DHPS as substrate (Figure 2.1B), the respiratory energy metabolism is represented by the following equation,



which through the following redox half-reactions represents a fermentation of DHPS,



Conversion of SQ via DHPS to sulfide by a co-culture of *E. coli* K-12 and *Desulfovibrio* sp. DF1

The co-culture consisting of *E. coli* K-12 and *Desulfovibrio* sp. strain DF1 growing with SQ released reduced inorganic sulfur, i.e., sulfide, as shown in Figure 2.6.

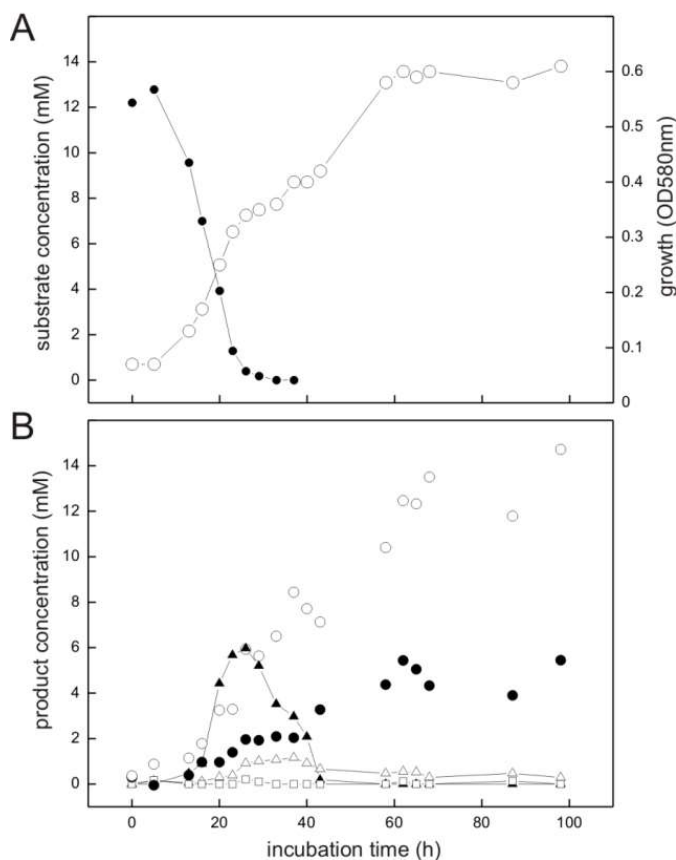


**Figure 2.6. Co-culture of *E. coli* K-12 and *Desulfovibrio* sp. strain DF1 growing with SQ under fermentative conditions.** The culture was incubated in a 60 ml serum flask containing, initially, 25 ml culture fluid and 35 ml N<sub>2</sub>/CO<sub>2</sub> gas in the headspace; at each time interval, 1.0 ml of sample was removed with a syringe. **(A)** biomass formation as monitored by optical density (OD580nm), open circles; disappearance of SQ, solid circles. **(B)** degradation products as detected in the culture supernatant; DHPS, solid triangles; acetate, open circles; dissolved sulfide, solid circles; succinate, open triangles; formate, open squares. The growth experiment was replicated once when sampled in such detail; substrate disappearance, biomass and product formation was confirmed in smaller scale when evaluating only the outgrown co-cultures ( $t_{end}$ ) (see Figure 2.4).

Strains K-12 and DF1 were co-inoculated into culture medium containing 12 mM SQ and the growth of the culture was monitored. A two-phasic growth was observed, as illustrated by the overall optical-density readings obtained (Figure 2.6A). After the first growth phase (after approx. 25 h incubation time), SQ (12.2 mM) had disappeared completely (Figure 2.6A) and DHPS was formed, though not in quantitative amounts (approx. 6 mM DHPS) (Figure 2.6B). Furthermore, acetate and succinate was produced but no formate was detectable (Figure 2.6B) in comparison to growth of *E. coli* with SQ in pure culture (see Figure 2.3 and Figure

2.4).

In addition, sulfide formation (up to approx. 2 mM) was observed already in the first growth phase (Figure 2.6B). After the following growth phase (after approx. 60 h incubation time; Figure 2.6A), DHPS had disappeared completely from the culture fluid and additional sulfide and acetate were formed; some of the succinate had also disappeared (Figure 2.6A; see also Figure 2.4). Overall, these observations reflect the growth of SQ-degrading, DHPS-excreting *E. coli* predominantly in the first growth phase and of DHPS-utilizing, sulfide-producing *Desulfovibrio* sp. strain DF1 predominantly in the second growth phase. The absence of formate in the co-culture, as produced by *E. coli* during SQ-fermentation in pure culture (see Figure 2.4), can be explained by its utilization as an additional electron donor by *Desulfovibrio* sp. strain DF1.

#### Identification of the DHPS desulfonation pathway in *Desulfovibrio* sp. strain DF1

We next studied the DHPS-desulfonation pathway in *Desulfovibrio* sp. strain DF1. Firstly, cell-free extracts of *Desulfovibrio* sp. strain DF1 grown with DHPS in comparison to lactate/sulfate as electron donor/acceptor were examined in respect to detectable enzyme activities. With DHPS as substrate, a high NAD<sup>+</sup>-dependent dehydrogenase activity (up to 225 mU per mg protein at its pH optimum, pH 10.5) was detected in the soluble protein fraction. The product of the reaction was identified as SLA by HPLC-MS. No activity was observed in extracts of lactate/sulfate-grown cells, thus, the DHPS dehydrogenase was specifically and highly induced during growth with DHPS. Furthermore, sulfite was formed after addition of SL as substrate to the soluble protein fraction of DHPS-grown cells (up to 38 mU/mg), but not after addition of DHPS. There was no sulfite formation after addition of SL to cell-free extracts of lactate/sulfate-grown cells. Hence, a DHPS dehydrogenase and a sulfolactate-desulfonating enzyme were found to be specifically induced during growth with DHPS in *Desulfovibrio* sp. strain DF1.

We then proceeded with differential proteomics in order to identify these inducible enzymes (Denger, Weiss *et al.* 2014),(Felux, Spiteller *et al.* 2015). An annotated draft-genome sequence of strain DF1 was generated for proteomics using Illumina HiSeq sequencing and JGI's Integrated Microbial Genomes (IMG) annotation pipeline (Felux, Spiteller *et al.* 2015); the annotation is publicly available under IMG Project ID Gp0153975. 2D-gel-based proteomics (Figure 2.7A) as well as total proteomics (Figure 2.7B) were performed for strain DF1 cells grown with DHPS in comparison to cells grown with lactate/sulfate.

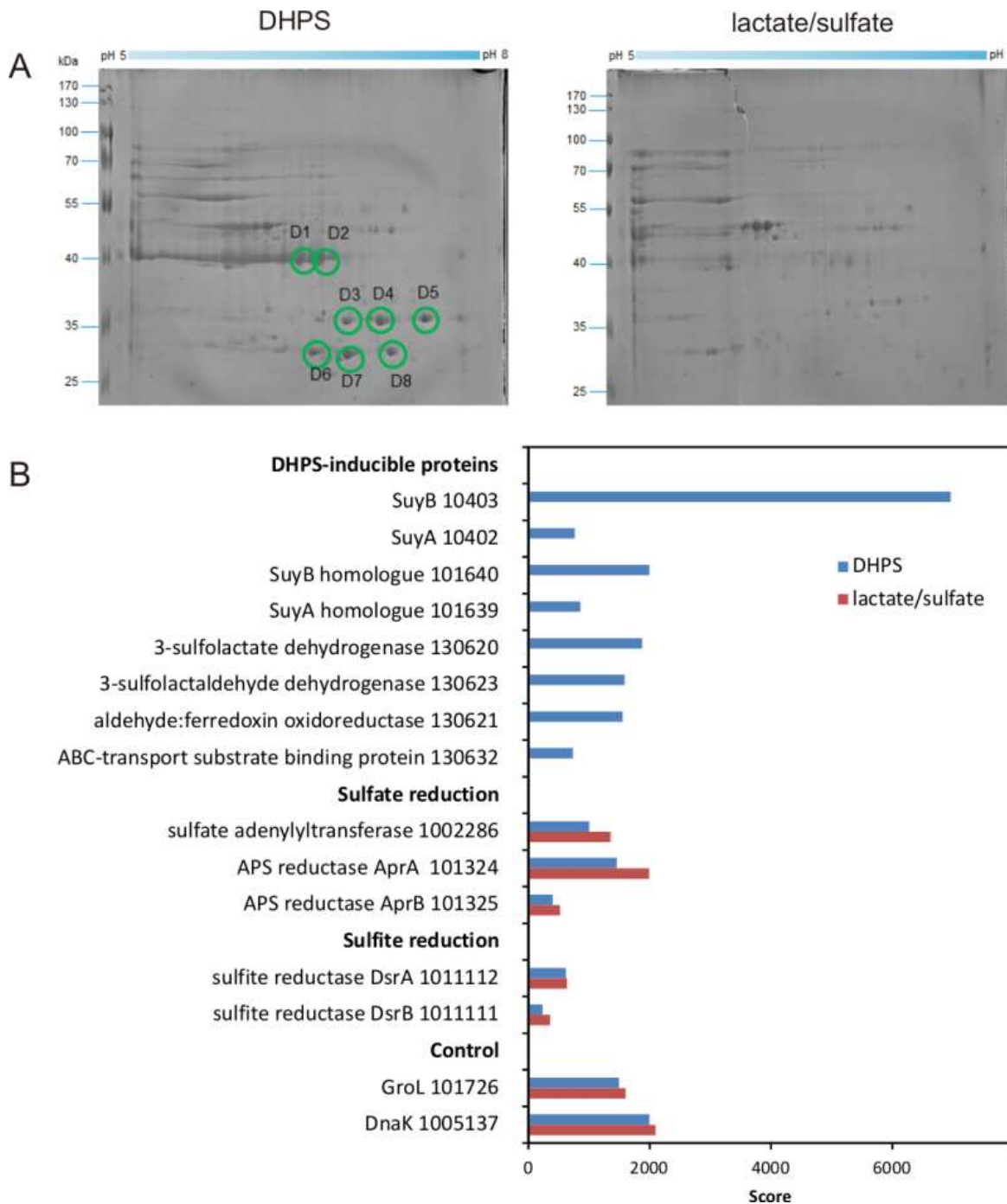


**Figure 2.7. Proteomic identification of DHPS-inducible proteins in cell-free extracts of DHPS-grown *Desulfovibrio* sp. strain DF1 in comparison to lactate/sulfate-grown cells.** (A) Two-dimensional PAGE gels. All prominent protein spots (labelled D1 – D8) that were found exclusively on the gel for DHPS-grown cells were excised and identified by peptide fingerprinting mass spectrometry. Their identities are described in the main text. The identification of the protein spots was done once. (B) Total-proteomics results. Shown are proteins which were highly abundant exclusively in DHPS-grown cell extracts in comparison to constitutively expressed proteins for sulfate reduction, sulfite reduction and other cellular functions (control). IMG locus tag numbers are given for each protein. The results were replicated once when starting from an independent growth experiment.

For the 2D-gels (Figure 2.7A), major protein spots visible only for DHPS-grown cells indicated abundant proteins specifically induced during growth with DHPS. These were identified by peptide-fingerprinting mass spectrometry.

The most prominent spots on the 2D-gel for DHPS-grown cells, spots D1 and D2 (Figure 2.7A), exhibited about the same molecular weight but were resolved at different isoelectric points. The two protein spots identified a gene (IMG locus tag Ga0134130\_10403) (in the following, the IMG locus tag prefix Ga0134130\_ is omitted) annotated to encode a large, catalytic subunit (SuyB) of the desulfonating enzyme (SuyAB). Hence, protein 10403 was the prime candidate for the inducible sulfolactate-desulfonating enzyme observed in cell-free extracts of *Desulfovibrio* sp. strain DF1 (see above). The total proteomics data (Figure 2.7B) confirmed and expanded on these results. The prominent SuyB-component 10403 was detected as the highest scoring protein specifically in DHPS-grown cells, but not in lactate/sulfate grown cells, as well as an homologous *suyB* gene (87.6% identity) encoded elsewhere in the genome (with lower score, IMG locus tag number 101640; see Figure 2.7B). In addition, the SuyA component gene 10402 encoded directly upstream of the SuyB gene was also identified (and its parologue 101639; 73.4% identity) specifically in DHPS-grown cells (Figure 2.7B).

Two other prominent spots, D7 and D8 (Figure 2.7A) observed at about the same molecular weight but different isoelectric points, were identified as protein 130620, annotated as NAD<sup>+</sup>-dependent β-hydroxyacid/3-hydroxyisobutyrate dehydrogenase: it belongs to the same group of orthologues (Clusters of Orthologous Group COG2084) as the characterized oxidoreductase catalyzing the reverse reaction in *E. coli* K-12, that is, sulfolactaldehyde reductase YihU; their overall sequence identity however is low (27%). Thus, protein 130620 (termed DhpA) was a prime candidate for the enzyme converting DHPS to sulfolactaldehyde in strain DF1. DhpA was confirmed to be a highly abundant, DHPS-inducible protein by total proteomics (Figure 2.7B).

Spots D3 – D6 identified gene 130632, coding for a substrate-binding protein of a predicted organosulfonate ABC-type transport system (SsuA/TauT family), thus, a candidate for DHPS transport. It is encoded together with each two candidate genes for ATP-binding and permease components on the same contig as the candidate DHPS dehydrogenase (DhpA) (Figure 2.1C). This soluble substrate-binding protein was also detected in DHPS-grown cells by total proteomics (Figure 2.7B).

Another protein, 130623, annotated as succinate semialdehyde dehydrogenase and co-encoded with the DhpA gene, appeared to be highly abundant in DHPS-grown cells by

total proteomics (Figure 2.7B). This protein belongs to the same COG and is 61% identical to the characterized NAD<sup>+</sup>-dependent sulfolactaldehyde dehydrogenase of the SQ-pathway of *Pseudomonas putida* SQ1 (locus tag PpSQ1\_00088) (Felux, Spiteller *et al.* 2015). Hence, protein 130623 encodes for the prime candidate for a dehydrogenase converting SLA to SL (and was termed SlaB; Figure 2.1B). In addition, another DHPS-inducible protein co-encoded with the genes for DhpA and SlaB was detected by total proteomics (protein 130621; Figure 2.7B), predicted as aldehyde:ferredoxin oxidoreductase (COG2414) (gene labelled as oxidored. in Figure 2.1C); it may represent a second candidate for an oxidation of SLA to SL.

In conclusion, the strongly DHPS-inducible proteins identified by proteomics and their annotation in accordance to the activities of DHPS-inducible enzymes detected in cell-free extracts, suggested a desulfonation pathway for DHPS in *Desulfovibrio* sp. strain DF1 (see Figure 2.1B) in analogy to the pathway described for the aerobic *Cupriavidus pinatubonensis* JMP134 (Mayer, Huhn *et al.* 2010): DHPS is transported into the cells and oxidized in two steps via SLA to SL by two NAD<sup>+</sup>-dependent dehydrogenases in strain DF1 (DhpA and SlaB; proteins 130620 and 130623, respectively); the oxidation of SLA may involve also a ferredoxin-coupled aldehyde dehydrogenase (protein 130621). Then, SL is desulfonated by SuyAB (proteins 10402 and 10403) yielding pyruvate as a carbon and energy source and sulfite as the terminal electron acceptor.

#### Reconstruction of a DHPS-desulfonation pathway by three recombinant enzymes overexpressed in *E. coli*

The gene for the candidate DHPS dehydrogenase DhpA (annotated as 3-hydroxyisobutyrate dehydrogenase) was cloned and heterologously overexpressed, and the protein was purified by His-Tag affinity chromatography. The purified protein produced a single band on a SDS gel at around 33 kDa (calculated mass: 33.25 kDa including the His-tag) (Figure S2.1). No activity was observed with 3-hydroxyisobutyrate as substrate, but the enzyme oxidized DHPS with NAD<sup>+</sup> but not with NADP<sup>+</sup> as cosubstrate. The product of the reaction was confirmed as SLA by HPLC-MS using SLA as standard that had been generated by SLA reductase YihU of *E. coli* catalyzing the reverse reaction with DHPS (Denger, Weiss *et al.* 2014). The K<sub>m</sub><sup>app</sup> for DHPS was observed at 36 ± 4 µM (V<sub>max</sub> 4.75 ± 0.10 U/mg protein) at pH 9.5 (Figure 2.8) and at 1.54 ± 0.33 mM (V<sub>max</sub> 3.15 ± 0.38 U/mg) at pH 7.5. Hence, we demonstrated that DhpA is a NAD<sup>+</sup>-dependent SLA-producing DHPS dehydrogenase.

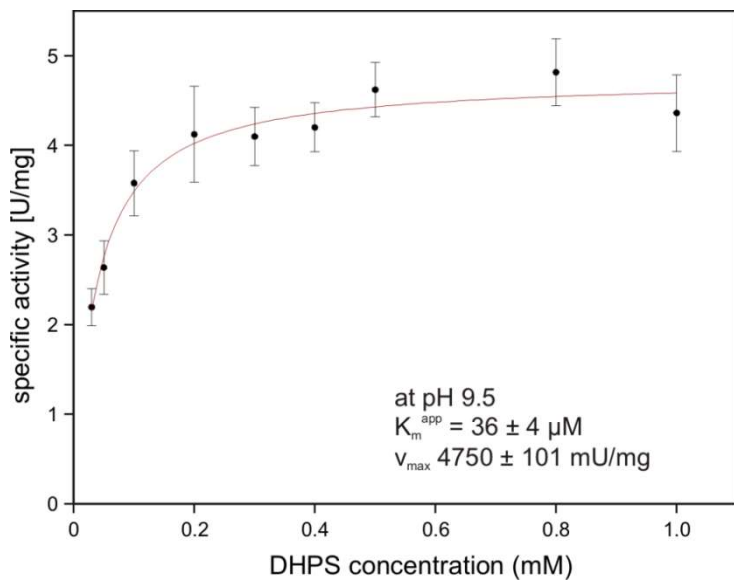


**Figure 2.8. NAD<sup>+</sup>-dependent DHPS oxidation by recombinant dehydrogenase DhpA.** The reactions contained 0.85 µg/ml DhpA in 50 mM Tris-HCl buffer at pH 9.5. The DHPS concentration was varied in the presence of 10 mM NAD<sup>+</sup> and the initial rates of NADH formation were determined spectrophotometrically as increase of absorbance at 340 nm. The data shown represents the mean ± standard deviation of three technical replicates.

Recombinant candidate SLA dehydrogenase SlaB (annotated as succinate semialdehyde dehydrogenase) on an SDS gel produced a single band as expected at around 55 kDa (calculated mass: 54.9 kDa including the His-tag) (Figure S2.1). Because the substrate SLA is not commercially available, the candidate SLA dehydrogenase was tested in reactions coupled with SLA-producing DhpA and DHPS as substrate (Figure 2.9). Hence, we could not determine the kinetic parameters of the SLA dehydrogenase.

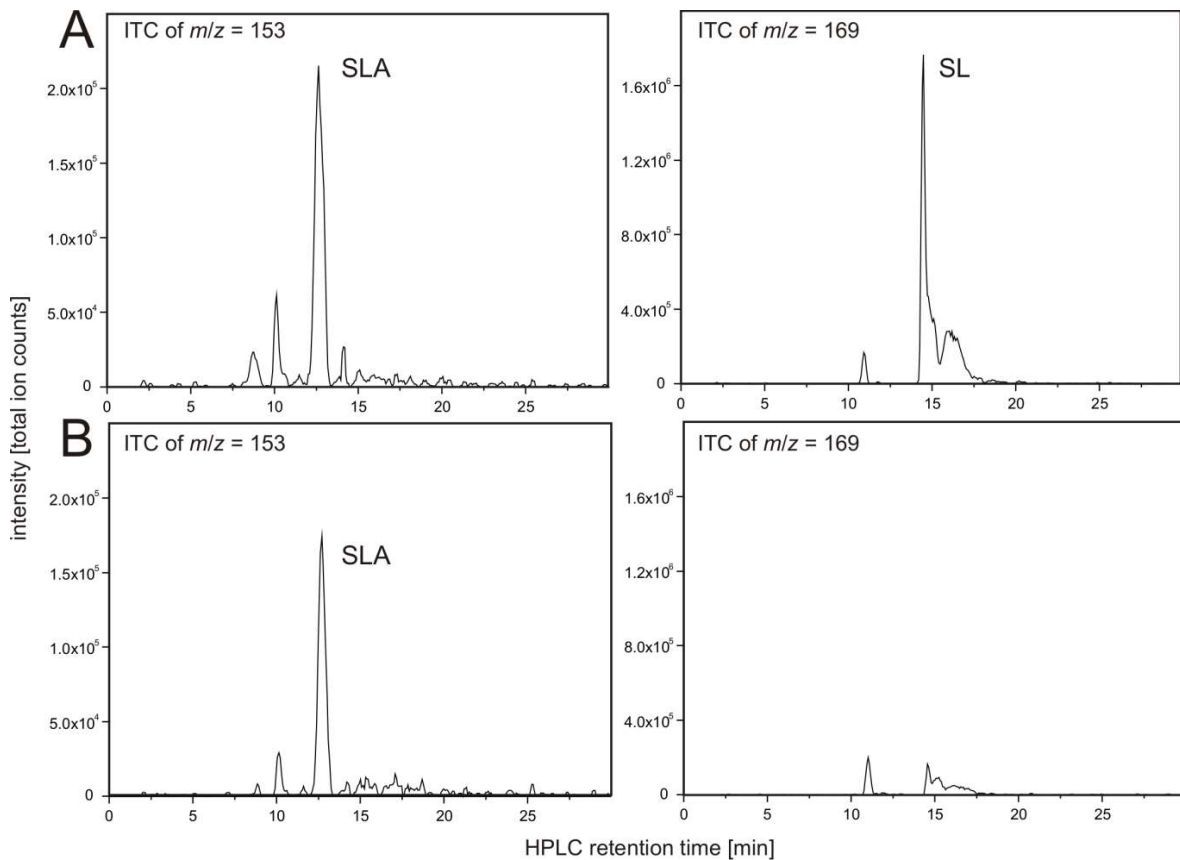


**Figure 2.9. NAD<sup>+</sup>-dependent SLA oxidation to SL by recombinant dehydrogenase SlaB.** Substrate sulfolactaldehyde for candidate sulfolactaldehyde dehydrogenase SlaB was generated from DHPS by coupling of the DhpA reaction. The reactions contained 5 µg/mL DhpA, 16.5 µg/mL protein SlaB, 5 mM DHPS and 10 mM NAD<sup>+</sup> in 50 mM Tris-HCl buffer at pH 9.0. Shown are HPLC-MS ion trace chromatograms of samples taken after the reactions when screening for the quasimolecular ions of SLA (left panel) and SL (right panel). (**A**) Ion trace chromatograms demonstrating formation of SLA and SL in a reaction containing both enzymes, SlaB and DhpA. (**B**) Ion trace chromatograms of control reaction containing active DhpA and heat-inactivated SlaB. The results (A, B) were replicated once with independently prepared enzyme preparations. No quantitative measurements were possible for SLA due to the lack of an analytical standard.

As illustrated in Figure 2.9A, the combination of DhpA and SlaB produced SL from DHPS with NAD<sup>+</sup> as co-substrate, compared to, an assay for which heat-inactivated SlaB of *Desulfovibrio* was used. Hence, we confirmed that SlaB is a NAD<sup>+</sup>-dependent, SL-producing SLA dehydrogenase. Furthermore, we confirmed that the NAD<sup>+</sup>-dependent DHPS dehydrogenase DhpA produces SLA but does not catalyze its oxidation to SL. The identified aldehyde:ferredoxin oxidoreductase (locus tag Ga0134130\_130621) was also produced recombinantly, purified, and tested as candidate SLA dehydrogenase under anoxic conditions with benzylviologen (replacing ferredoxin) as the electron acceptor and with SLA as substrate generated from DHPS by dehydrogenase 130620 in the presence of NAD<sup>+</sup>. We could not detect benzylviologen-reducing activity in the spectrophotometrical assays when the SLA was formed through DHPS dehydrogenase 130620, and we detected no SL

formation by HPLC, under the conditions we used. The enzyme showed also no activity with lactaldehyde or acetaldehyde as substrates. Hence, the role of this inducible protein in *Desulfovibrio* sp. strain DF1 remained unclear.

Finally, SuyA and SuyB were separately expressed and purified. The proteins on an SDS gel produced bands as expected at around 15 kDa and 46 kDa (calculated mass: 14.5 and 45.9 kDa including the His-tags), respectively (Figure S2.1). Desulfonation reactions with SL as substrate were followed by formation of sulfite and pyruvate, as determined each by HPLC in samples that were taken at intervals from the reactions, derivatized and analyzed (Figure 2.10): the cleavage of SL to sulfite and pyruvate was detected after addition of both subunits, SuyA and B, and a lower but significant activity after addition of the SuyB subunit only; no activity was detectable when only the SuyA subunit was added.

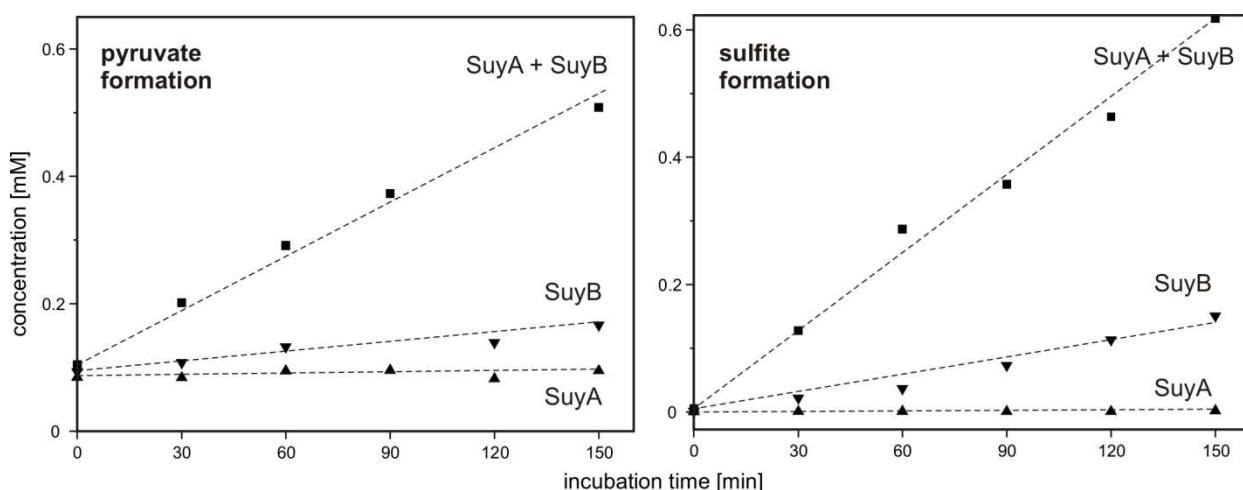


**Figure 2.10. Cleavage of sulfolactate into pyruvate and sulfite by recombinant SuyAB proteins.** The reactions contained 150 µg/mL SuyA and/or 600 µg/mL SuyB and 2.5 mM SL in 100 mM anoxic MOPS buffer at pH 7.0, containing 10% glycerol and 1 mM FeCl<sub>2</sub>. Formation of pyruvate and sulfite was detected by HPLC-DAD in samples taken discontinuously and after derivatization with DNPH and NAM, respectively (see Methods section). Left panel: pyruvate formation. Right panel: sulfite formation. Upward triangles, reaction containing SuyA; downward triangles, reaction containing SuyB; squares, reactions containing both subunits, SuyA and B. The results were replicated once with an independently prepared enzyme preparation.

Hence, we confirmed that SuyAB is a SL sulfite-lyase, with SuyB being the catalytically active subunit. For reactions with the holoenzyme (SuyAB) a specific activity of 4.5 mU/mg (271 mkat/kg) was determined, and for SuyB alone, a specific activity of 1.9 mU/mg (115 mkat/kg).

### Phylogenetic distribution of SuyB among sulfate/sulfite-reducing bacteria

A search for putative genes for SuyB in microbial genomes retrieved 397 hits in the NCBI non-redundant protein database with >70% amino acid identity to the *Desulfovibrio* sp. strain DF1 sequence (Figure 2.11).

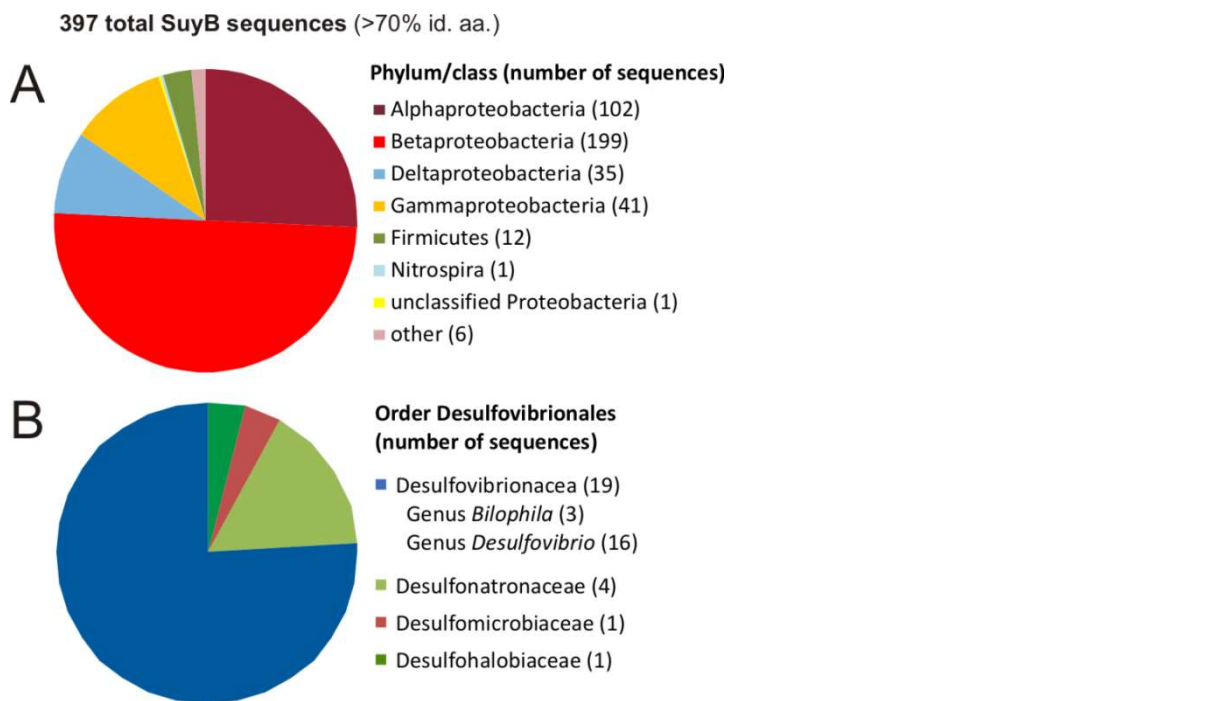


**Figure 2.11. Distribution of SuyB in bacterial genomes.** Pie charts illustrating the distribution of 397 BLAST hits retrieved from the non-redundant database when searching for SuyB homologs with a threshold of >70% on the phylum/class level (**A**) and in the order Desulfovibrionales (**B**).

Most of these sequences were found in genomes of Betaproteobacteria (199 genomes), Alphaproteobacteria (102 genomes) and Gammaproteobacteria (41 genomes), hence, in organisms that most likely employ SuyAB in aerobic and facultatively anaerobic catabolism of DHPS and/or cysteate or SL (see Introduction) as carbon and energy source(s), while the sulfite may be oxidized to sulfate, such as in aerobic *Cupriavidus pinatubonensis* JMP134 (Mayer, Huhn *et al.* 2010) and *Paracoccus pantotrophus* NKNCYSA (Rein, Gueta *et al.* 2005).

Furthermore, 35 genomes of Deltaproteobacteria and 12 genomes of Firmicutes contained *suyB* (as well as *suyA*) genes. For the largest group of sulfate/sulfite-reducing bacteria among the Deltaproteobacteria, *suyB* (and *suyA*) genes were found in the sulfate/sulfite-reducing bacteria of the human gut microbiota and Human Microbiome Project (HMP) reference strains *Desulfovibrio* sp. 3.1.syn3 and 6.1.46AFFAA, in *D. fairfieldensis* CCUG45958, and in all three available *Bilophila wadsworthia* strains. Furthermore, candidate

genes were found, for example, in *Desulfovibrio desulfuricans desulfuricans* DSM 642, *Desulfovibrio litoralis* DSM 11393, *Desulfonatronum lacustre* DSM 10312, *Desulfomicrobium baculum* DSM 4028, *Desulfobulbus oralis* 041 and *Desulfomonile tiedjei* DSM 6799. For the second largest group of sulfate-reducing bacteria among the Firmicutes, candidate genes were found, for example, in *Desulfotomaculum ruminis* DSM 2154, *Desulfotomaculum arcticum* DSM 17038, *Desulfitobacterium hafniense* DSM 12704 and *Desulfosporosinus acidiphilus* DSM 22704. Hence, these sulfate/sulfite-reducing bacterial strains likely employ SuyAB also for a desulfonation of SL and organosulfonate respiration, when utilizing DHPS, SL and/or cysteate or yet unknown organosulfonates that may be metabolized via SL and SuyAB. Notably, our preliminary tests with *Bilophila wadsworthia* (at the time unpublished results, see Chapters 3 and 4 of this thesis) revealed its ability to utilize SL as electron acceptor with lactate as electron donor, and our preliminary proteomic analysis confirmed a strong induction of SuyAB.

## **General conclusion**

Aerobic bacterial degradation of SQ has been reported almost 60 years ago (Benson and Shibuya 1961) and the formation of DHPS or SL during its primary degradation 15 years ago (Roy, Hewlins *et al.* 2003). The latter observation implied an involvement of two-tier bacterial consortia for closing the sulfur cycle for SQ, as has been demonstrated in 2012 (Denger, Huhn *et al.* 2012). Further, the pathways for degradation of DHPS and/or SL to sulfate [e.g. (Denger and Cook 2010; Mayer, Huhn *et al.* 2010)] as well as for primary degradation of SQ to DHPS or SL (Denger, Weiss *et al.* 2014; Felux, Spiteller *et al.* 2015) have been demonstrated each for aerobically respiring model bacteria. Our present knowledge on degradation of SQ, DHPS and SL has been recapitulated in a recent review (Goddard-Borger and Williams 2017), however, the anaerobic bacterial degradation of SQ, potentially producing harmful H<sub>2</sub>S instead of sulfate, has never been addressed. Using a laboratory model community, we demonstrated for the first time bacteria and pathways for anaerobic bacterial SQ degradation concomitant with H<sub>2</sub>S production, which represents another novel, important link in the biogeochemical sulfur cycle.

We demonstrated also two novel types of energy metabolism in anaerobic bacteria. Firstly, *E. coli* K-12 catalyzes the fermentation of SQ to DHPS, succinate, acetate and formate, thus, a novel type of mixed-acid fermentation, for which the SQ-EMP pathway is employed (Figure 2.1A). The option to utilize SQ as carbon and energy (electron) source for both mixed-acid fermentation (e.g., Figure 2.3AD) and aerobic respiration (Denger, Weiss *et al.* 2014) is another example of the adaptations of *E. coli* to its commensal lifestyle in the intestinal tract

[e.g., (Conway and Cohen 2015)] as well as for its survival in extra-intestinal environments [e.g., (van Elsas, Semenov *et al.* 2011)]. Secondly, *Desulfovibrio* sp. strain DF1 catalyzes a fermentation of DHPS to acetate and sulfide which involves energy conservation through sulfite respiration: the sulfite generated by the DHPS desulfonation pathway is utilized as terminal sink for the electrons derived from the oxidation of the DHPS-carbon (Figure 2.1B). Hence, DHPS was identified as a fourth organic sulfite-donor for anaerobic respiration, in addition to taurine (Laue, Denger *et al.* 1997), isethionate and cysteate (Lie, Pitta *et al.* 1996). We believe that sulfidogenic organosulfonate respiration is more widespread and abundant in microbiomes than initially was realized. For example, it might be employed also by archaea (Lin, Handley *et al.* 2015). The organosulfonate substrates are at least abundant in the environment, for example in soils and in sediments (Autry and Fitzgerald 1990), (Vairavamurthy, Zhou *et al.* 1994) and in gut microbiomes (see below). Clearly, a microbiomic examination of organosulfonate respiring microorganisms is needed to fully reveal their diversity, ecological niches, and significance in the sulfur cycle, for which the description of sulfur-metabolizing biochemical pathways and their enzymes and genes in laboratory model bacteria, as achieved in this study, is an essential prerequisite (Wasmund, Mussmann *et al.* 2017).

SQ is a relevant constituent of the vegetable diet of herbivores and omnivores, and sulfide production in the intestinal microbiome has many recognized and potential contributions to human health and disease [e.g., (Carbonero, Benefiel *et al.* 2012),(Singh and Lin 2015)]: sulfide is a potent genotoxin and may contribute to the onset of colorectal cancer (Attene-Ramos, Nava *et al.* 2010); it can reduce disulfide bonds in the mucus layer of the gut epithelium, disrupting its barrier function and potentially playing a role in inflammatory bowel disease (IBD) (Ijssennagger, van der Meer *et al.* 2016); and it can induce antibiotic resistance, so that sulfide production by the gut microbiota may trigger blooms of opportunistic bacteria during antibiotic treatment (Shatalin, Shatalina *et al.* 2011). The occurrence of the genes for a DHPS/SL desulfonation pathway *via* SuyAB also in typical anaerobic sulfate/sulfite-reducing bacteria of the human gut microbiota may highlight an important role for respiration with DHPS and/or sulfolactate-sulfite also in this microbial habitat, e.g., in dependence on the dietary conditions of the host: a sulfidogenic metabolism driven by substrates derived of green-vegetable diet (SQ, DHPS, SL) would contrast the already recognized sulfidogenic taurine metabolism (e.g. by the opportunistic pathogen *Bilophila wadsworthia*) in dependence on the consumption of a high-fat (high taurocholate) diet (Devkota, Wang *et al.* 2012) and/or high-meat (high taurine) diet (Denger, Weiss *et al.* 2014). Notably, most recently microbial SL desulfonation has been associated with altered sulfur metabolism in the microbiome of pediatric IBD patients (Zhang, Deeke *et al.* 2018).

Hence, it is important to examine in future also in the human intestinal microbiome the pathways and bacterial consortia involved in sulfidogenic SQ degradation, in relation to H<sub>2</sub>S production, dietary conditions and human health. This will not only enable efforts to understand the biological roles of this metabolic activity in the human body, but may also open the door to new approaches to control intestinal H<sub>2</sub>S production.

### **Author contributions**

A.B., K.D. and D.Sch conceived and designed the experiments. A.B. and K.D. performed the experiments. T.H. contributed reagents. A.B., K.D., P.F., N.M., D.Sp. and D.Sch. analyzed the data. A.B., K.D. and D.Sch. wrote the manuscript and all authors approved it.

### **Acknowledgments**

We are grateful to Alasdair Cook and Bernhard Schink for helpful discussions, to Stefan Kreft for experimental support, to Andreas Marquardt for proteomic analyses and to students Emilia Amrou, Nail Özmen and Alexander Fiedler for their help in experimental work. A.B. and D.Sch. were supported by German Research Foundation (DFG) grants (SCHL1936/3 and 4) and by the Konstanz Research School Chemical Biology (KoRS-CB) and the Konstanz Young Scholar Fund (YSF).

## Supplementary material

**Table S2.1. Stoichiometry of fermentation of glucose and of SQ by *E. coli* K-12**

	Fermentative growth in 10 ml 6 mM glucose medium	Fermentative growth in 10 ml 12 mM SQ medium
<b>Total protein [mg]</b>	0.724	0.556
<b>Total cell dry mass [mg]</b>	1.45	1.11
<b>Assimilation equation</b>	$17 \text{ C}_6\text{H}_{12}\text{O}_6 \rightarrow 24 <\text{C}_4\text{H}_7\text{O}_3> + 6 \text{ CO}_2 + 18 \text{ H}_2\text{O}$	$17 \text{ C}_6\text{H}_{11}\text{O}_8\text{S}^- + \text{H}_2\text{O} \rightarrow 10 <\text{C}_4\text{H}_7\text{O}_3> + 17 \text{ C}_3\text{H}_7\text{O}_5\text{S}^- + 11 \text{ CO}_2$
<b>Substrate assimilation [mol/g dry mass]</b>	6.9	16.6
<b>Total substrate used [μmol]</b>	44	117
<b>Assimilated substrate [μmol]</b>	10.0	18.5
<b>Dissimilated substrate [μmol]</b>	34.0	98.5
<b>Succinate produced [μmol]</b>	6	12
<b>Formate produced [μmol]</b>	58	44
<b>Acetate produced [μmol]</b>	31	51
<b>Ethanol produced [μmol]</b>	11	0
<b>DHPS produced [μmol]</b>	0	96
<b>dissimilation equation</b>	34.0 glucose → 6 succinate + 58 formate + 31 acetate + 11 ethanol	98.5 SQ → 95.9 DHPS + 12 succinate + 44 formate + 51 acetate
<b>total carbon in dissimilated substrate[μmol]</b>	204.1	591.2
<b>total carbon in fermentation products[μmol]</b>	166.0	482.0
<b>Carbon recovery [%]</b>	81	82
<b>Molar growth yield for dissimilated substrate [g dry mass/mol diss. substrate]</b>	42.6	11.3
<b>Electrons gained by carbon oxidation</b>	$1 \text{ glucose} \rightarrow 6 \text{ CO}_2 + 24 \text{ e}^-$ $1 \text{ SQ} \rightarrow 6 \text{ CO}_2 + 24 \text{ e}^-$	$1 \text{ formate} \rightarrow 1 \text{ CO}_2 + 2 \text{ e}^-$ $1 \text{ ethanol} \rightarrow 2 \text{ CO}_2 + 12 \text{ e}^-$ $1 \text{ DHPS} \rightarrow 3 \text{ CO}_2 + 14 \text{ e}^-$
<b>Electrons in dissimilated substrate</b>	816	2365
<b>Electrons in fermentation products</b>	580	2008
<b>Electron recovery [%]</b>	71	85

**Table S2.2. PCR primers used for cloning**

Enzyme	Gene (IMG locus tag)	forward Primer (restriction: NdeI)	reverse primer (restriction: XbaI)
DHPS dehydrogenase	Ga0134130_130620	<i>CGTCATATG</i> CAGAT CGGATTATCGGC	<i>ATTCTCGAG</i> ATCCG GCTCTTCCACCTCA A
SLA dehydrogenase	Ga0134130_130623	<i>CGTCATATG</i> TTCAC AACATTGAACTCAT GCG	<i>ATTCTCGAG</i> GGTTG CCCTATCCTTATCCG TTTG
SuyA	Ga0134130_10402	<i>CGTCATATG</i> TCTATC CAATTATTGTCCAC GAA	<i>ATTCTCGAG</i> GTCCA TTCTCACGCCGATA CC
SuyB	Ga0134130_10403	<i>CGTCATATG</i> AAGAC CAAGTTCATGGGGT ATCG	<i>ATTCTCGAG</i> AACCG CCGGCCCCGACTAC

Letters in bold, restriction enzyme recognition site;  
letters in italic, base pairs added for restriction efficiency.

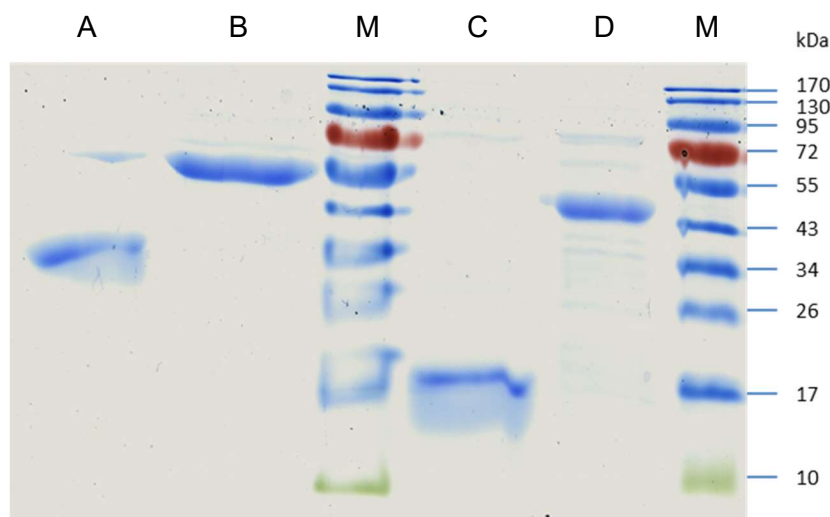


**Figure S2.1. Evaluation of the purity of recombinant His-tagged proteins by SDS-PAGE.** (A) DHPS dehydrogenase (locus tag Ga0134130\_130620, calculated mass 33.3 kDa); (B) SLA dehydrogenase (Ga0134130\_130623, 54.9 kDa); (C) SuyA (Ga0134130\_10402, 14.5 kDa); (D) SuyB (Ga0134130\_10403, 45.9 kDa); (M) molecular mass marker.

## Chapter 3: A glycyl radical enzyme enables hydrogen sulfide production by the human intestinal bacterium *Bilophila wadsworthia*

**Short title:** C-S bond cleaving glycyl radical enzymes in gut bacteria

Spencer C. Peck<sup>1</sup>, Karin Denger<sup>2,3</sup>, Anna Burrichter<sup>2,3</sup>, Stephanie M. Irwin<sup>1</sup>, Emily P. Balskus<sup>1</sup>, and David Schleheck<sup>2,4</sup>

### **Affiliations:**

<sup>1</sup> Department of Chemistry and Chemical Biology, Harvard University, Cambridge MA 02138, U.S.A.

<sup>2</sup> Department of Biology and Konstanz Research School Chemical Biology, University of Konstanz, D-78457 Konstanz, Germany

<sup>3</sup> These authors contributed equally

<sup>4</sup> Lead contact

### **Corresponding authors:**

**David Schleheck**

Department of Biology and Konstanz Research School Chemical Biology, University of Konstanz, D-78457 Konstanz, Germany

Email: david.schleheck@uni-konstanz.de

**Emily Balskus**

Department of Chemistry and Chemical Biology, Harvard University, Cambridge MA 02138, U.S.A.

Email: balskus@chemistry.harvard.edu

This chapter was published in Proceedings of the National Academy of Sciences of the United States of America (2019): <https://doi.org/10.1073/pnas.1815661116>

### **Keywords:**

Anaerobic bacterial metabolism, sulfite respiration, sulfidogenesis, H<sub>2</sub>S, organosulfonate degradation, desulfonation, taurine, isethionate, taurocholate, human gut microbiome, intestinal health and disease

## **Abstract**

Hydrogen sulfide ( $H_2S$ ) production in the intestinal microbiota has many contributions to human health and disease. An important source of  $H_2S$  in the human gut is anaerobic respiration of sulfite released from the abundant dietary and host-derived organic sulfonate substrate in the gut, taurine (2-aminoethanesulfonate). However, the enzymes that allow intestinal bacteria to access sulfite from taurine have not yet been identified. Here, we decipher the complete taurine desulfonation pathway in *Bilophila wadsworthia* 3.1.6 using differential proteomics, *in vitro* reconstruction with heterologously produced enzymes and identification of critical intermediates. An initial deamination of taurine to sulfoacetaldehyde by a known taurine:pyruvate aminotransferase (Tpa) is followed, unexpectedly, by reduction of sulfoacetaldehyde to isethionate (2-hydroxyethanesulfonate) by a NADH-dependent reductase (SarD). Isethionate is then cleaved to sulfite and acetaldehyde by a previously uncharacterized glycyl radical enzyme (GRE), isethionate sulfite-lyase (IsIA). The acetaldehyde produced is oxidized to acetyl-CoA by a dehydrogenase (AdhE) and the sulfite is reduced to  $H_2S$  by dissimilatory sulfite reductase (Dsr). This unique GRE is also found in *Desulfovibrio desulfuricans* DSM642 and *D. alaskensis* G20, which utilize isethionate but not taurine; corresponding knock-out mutants of *D. alaskensis* G20 did not grow with isethionate as the terminal electron acceptor. In conclusion, the novel radical-based C-S bond cleavage reaction catalyzed by IsIA diversifies the known repertoire of GRE superfamily enzymes and enables the energy metabolism of *B. wadsworthia*. This GRE is widely distributed in gut bacterial genomes and may represent a novel target for control of intestinal  $H_2S$  production.

## **Significance**

This paper describes a pathway for anaerobic bacterial metabolism of taurine (2-aminoethanesulfonate), an abundant substrate in the human intestinal microbiota, by the intestinal bacterium and opportunistic pathogen, *Bilophila wadsworthia*. This metabolism converts taurine to the toxic metabolite hydrogen sulfide ( $H_2S$ ), an activity associated with inflammatory bowel disease and colorectal cancer. A critical enzyme in this pathway is a new member of the glycyl radical enzyme family, isethionate sulfite-lyase. This enzyme catalyzes a novel, radical-based C-S bond cleavage reaction to convert isethionate (2-hydroxyethanesulfonate) to sulfite and acetaldehyde. This discovery improves our understanding of  $H_2S$  production in the human body and may also offer new approaches for controlling intestinal  $H_2S$  production and *B. wadsworthia* infections.

## Introduction

The metabolism of dietary and host-derived sulfur-containing compounds to H<sub>2</sub>S by members of the human gut microbiota has many prominent connections to host health and disease [e.g., (Carbonero, Benefiel *et al.* 2012; Singh and Lin 2015)]. H<sub>2</sub>S is a potent genotoxin and may contribute to the onset of colorectal cancer (Attene-Ramos, Nava *et al.* 2010). This metabolite can also reduce disulfide bonds in the mucus layer of the gut epithelium, disrupting its barrier function and potentially playing a role in inflammatory bowel disease (IBD) (Ijssennagger, van der Meer *et al.* 2016). As H<sub>2</sub>S can induce antibiotic resistance, production of this compound in the gut microbiota may trigger blooms of opportunistic bacteria during antibiotic treatment (Shatalin, Shatalina *et al.* 2011). However, H<sub>2</sub>S produced by gut microbes may also act as a signaling molecule in the host, potentially leading to beneficial effects such as cardioprotection (Singh and Lin 2015; Tomasova, Konopelski *et al.* 2016). Elucidating the influence of gut-microbial sulfur metabolism and H<sub>2</sub>S production on host health and disease represents an important but unresolved challenge in human microbiota research (Carbonero, Benefiel *et al.* 2012; Singh and Lin 2015; Wallace, Motta *et al.* 2018; Zhang, Deeke *et al.* 2018).

Significant gaps remain in our understanding of the gut-microbial metabolic pathways and enzymes that generate H<sub>2</sub>S (sulfidogenesis). For example, the human gut bacterium and opportunistic pathogen *Bilophila wadsworthia* (Baron, Summanen *et al.* 1989) produces H<sub>2</sub>S when respiring (bi)sulfite (HSO<sub>3</sub><sup>-</sup>) released from organosulfonate substrates (R<sub>3</sub>C-SO<sub>3</sub><sup>-</sup>), including the abundant dietary and host-derived molecule taurine (2-aminoethanesulfonate) as well as isethionate (2-hydroxyethanesulfonate) (Figure 3.1A) (Laue, Denger *et al.* 1997). Though *B. wadsworthia* is typically present in low abundances in the colonic microbiota of healthy humans (Nava, Carbonero *et al.* 2012), it has been associated with appendicitis and bone, brain, liver and ear abscesses (Baron, Curren *et al.* 1992) as well as colorectal cancer (Yazici, Wolf *et al.* 2017). In mice, *B. wadsworthia* can cause systemic inflammation (Feng, Long *et al.* 2017) and proliferates concomitantly with the onset of ulcerative colitis when taurine-conjugated bile acids are more abundant in the gastrointestinal tract (Devkota, Wang *et al.* 2012).

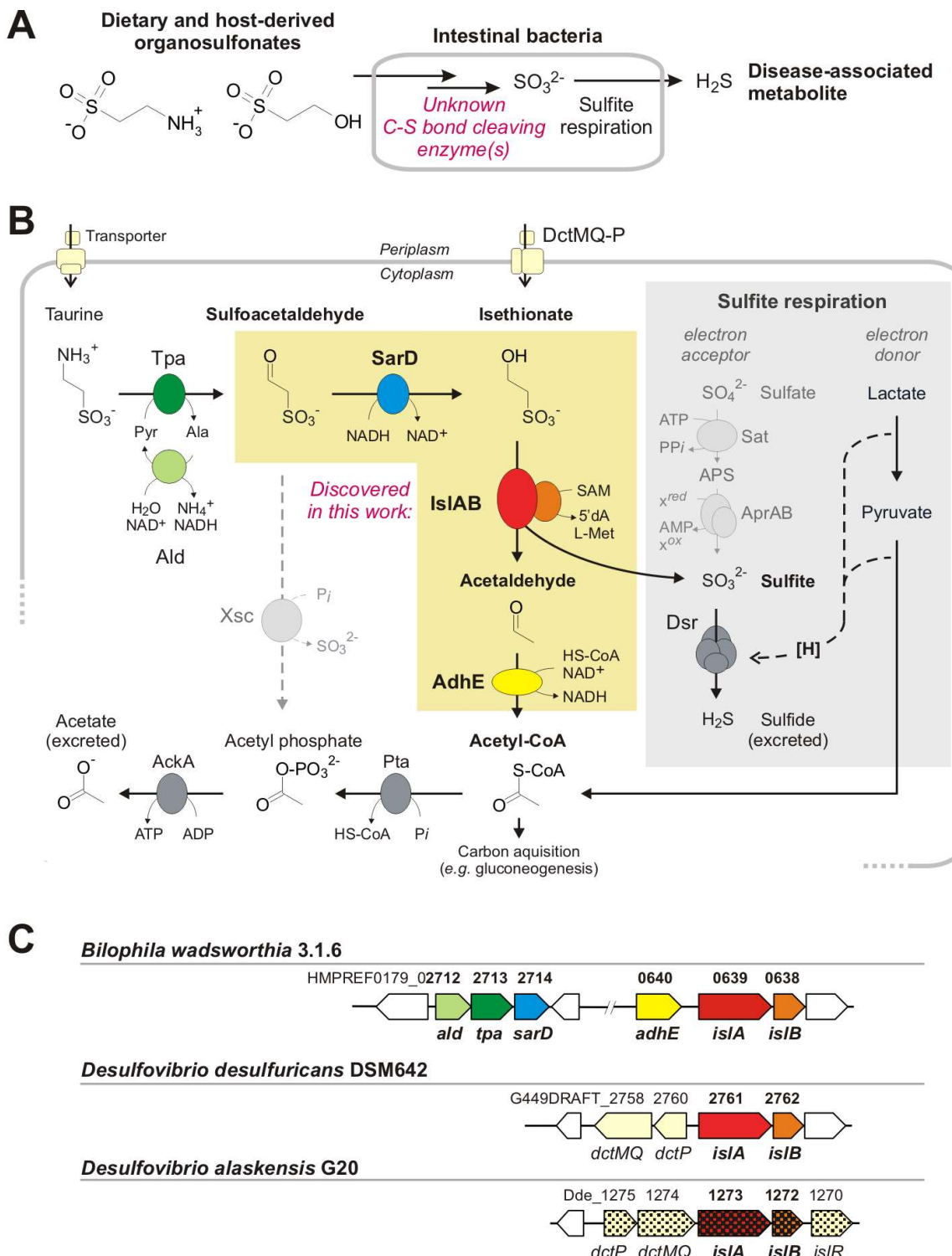


**Figure 3.1. Metabolism of taurine and isethionate by the human gut bacterium *Bilophila wadsworthia* and by *Desulfovibrio* spp.** (A) *B. wadsworthia* and other intestinal bacteria degrade dietary and host-derived organosulfonates in order to access sulfite as electron acceptor for their anaerobic respiration. The desulfonation reaction in *B. wadsworthia* has not yet been identified. (B) Summary of the pathways investigated in this study (no single organism represented). *B. wadsworthia* utilizes taurine and isethionate as electron acceptors and the two *Desulfovibrio* spp. strains can utilize isethionate, but not taurine. All three strains lack the sulfoacetaldehyde acetyltransferase (Xsc) enzyme known in many aerobic bacteria (dashed line on the left). Instead, the glycol radical enzyme (GRE) isethionate sulfite-lyase (IsIA) with its GRE-activase component (IsIB) are found in both *B. wadsworthia* and the *Desulfovibrio* spp., and a novel NADH-coupled, isethionate-

forming sulfoacetaldehyde reductase (SarD) is found only in *B. wadsworthia*. The sulfite released by the GRE is reduced to sulfide by dissimilatory sulfite reductase (Dsr) and coupled to proton translocation for ATP synthesis (symbolized as [H]), when using electrons from oxidation of an alternative electron donor such as lactate (gray box). Other enzyme abbreviations: Tpa, taurine:pyruvate aminotransferase; Ald, alanine dehydrogenase; AdhE, CoA acylating acetaldehyde dehydrogenase; Pta, phosphotransacetylase; AckA, acetate kinase. (C) The gene clusters identified in this study. In *B. wadsworthia*, two separate clusters encode for taurine transport and conversion to isethionate (*ald*, *tpa*, *sarD*), and for isethionate desulfonation and the conversion of acetaldehyde to acetyl-CoA (*adhE*, *islA*, *islB*). The *Desulfovibrio* strains harbor only a gene cluster for isethionate transport (*dctP*, fused *dctMQ*) and desulfonation (*islA*, *islB*), and acetaldehyde dehydrogenases are encoded elsewhere in their genomes (not depicted). Single-gene knockouts in *D. alaskensis* strain G20 that result in an inability to use isethionate (but not free sulfite) are indicated by squared gene symbols.

Metabolism of taurine and isethionate by *B. wadsworthia* involves a desulfonation reaction (Figure 3.1AB) to generate free sulfite, which is then reduced to H<sub>2</sub>S via the action of dissimilatory sulfite reductase (Dsr, desulfovirodin) for energy conservation by anaerobic sulfite respiration (Lie, Pitta *et al.* 1996; Laue, Denger *et al.* 1997). However, the enzymes involved in this critical C–S bond cleaving step have not yet been identified in *B. wadsworthia*. The known pathways for taurine and isethionate, deciphered almost exclusively in aerobic bacteria, are diverse but invariably involve sulfoacetaldehyde as the critical intermediate (Cook and Denger 2002) (see also METACYC pathways *Taurine degradation I-IV*). In these bacteria, sulfoacetaldehyde is desulfonated by the oxygen-insensitive, thiamine-diphosphate (TDP)-dependent sulfoacetaldehyde acetyltransferase (Xsc) (Denger, Ruff *et al.* 2001; Ruff, Denger *et al.* 2003) to produce acetyl phosphate, which is used to generate ATP or acetyl-CoA (Figure 3.1B), and sulfite, which is oxidized to sulfate by sulfite dehydrogenase in most aerobic bacteria (not depicted in Figure 3.1B). Notably, the sulfoacetaldehyde-desulfonating Xsc enzyme is employed also by strictly anaerobic *Desulfonospira thiosulfatigenes* GKNTAU that ferments taurine to acetate, ammonium and thiosulfate (Denger, Ruff *et al.* 2001).

Though an analogous C–S bond cleaving reaction has been proposed to operate in the strictly anaerobic, taurine- and isethionate-respiring, sulfidogenic bacterium *B. wadsworthia*, no valid Xsc homologs can be detected in the genomes of these organisms (*i.e.*, all homologs are annotated as catalytic, TDP-binding subunits of acetolactate synthase genes and are co-encoded with their small-subunit genes; <33% amino acid sequence identity). Further, no sulfoacetaldehyde-desulfonating Xsc enzyme activity can be observed in cell-free extracts of taurine-grown cells (Laue 2000).

In this study, we first investigated taurine and isethionate catabolism in the human microbiome project (HMP) reference strain *Bilophila wadsworthia* 3.1.6 (HMP-Consortium 2012), and later isethionate catabolism in *Desulfovibrio desulfuricans* subsp. *desulfuricans* DSM642 (Lie, Pitta *et al.* 1996) and *D. alaskensis* G20 (Kuehl, Price *et al.* 2014), after we

realized that these two pathways involve the same type of oxygen-sensitive desulfonation reaction. *Desulfovibrio* spp. are sulfate-reducing bacteria found in the human intestinal microbiota (Nava, Carbonero *et al.* 2012; Rey, Gonzalez *et al.* 2013) and they are also of clinical importance, e.g., associated with abdominal infections and bacteremia [e.g., (Goldstein, Citron *et al.* 2003)].

As taurine and isethionate catabolism are inducible in these bacteria, we adopted a differential-proteomics and reverse-genetics approach (Denger, Weiss *et al.* 2014; Felux, Spiteller *et al.* 2015) to identify the complete organosulfonate catabolic pathways.

## **Results**

### Proteomic experiments reveal putative desulfonating glycyl radical enzymes in *Bilophila* and *Desulfovibrio* strains.

We initially investigated the missing desulfonation step in taurine and isethionate catabolism using the HMP reference isolate *B. wadsworthia* 3.1.6 (HMP-Consortium 2012). Strain 3.1.6 was grown in media containing either taurine or isethionate as an electron acceptor.

Proteomics experiments implicated two gene clusters in taurine catabolism (Figure 3.2A), one of which was also linked to isethionate catabolism (Figure 3.1C). These gene clusters are conserved in all sequenced *Bilophila* genomes. The first gene cluster encodes the known enzymes Tpa and alanine dehydrogenase (Ald), as previously identified in a different *B. wadsworthia* isolate (Laue and Cook 2000b; Laue and Cook 2000a). Tpa converts taurine to sulfoacetaldehyde, and Ald regenerates the amino-group acceptor for Tpa (see Figure 3.1B). Both proteins were detected with a higher relative abundance (*i.e.*, with higher protein score and hit-rank) in taurine-grown cells, but not in isethionate-grown cells (Figure 3.2A). Another protein encoded in this gene cluster, a predicted iron-dependent alcohol dehydrogenase (SarD in Figure 3.1), was also detected in higher relative abundance specifically in taurine-grown cells, but had not been previously characterized. Surprisingly, the second gene cluster encodes a glycyl radical enzyme (GRE) and its cognate radical S-adenosylmethionine (SAM) activating enzyme (see Figure 3.1C). These proteins were consistently detected with much higher relative abundance (and with highest hit-rank) in both taurine- and isethionate-grown cells (Figure 3.2A). Another protein encoded directly upstream of the GRE was also detected in higher relative abundance in both taurine- and isethionate-grown cells (Figure 3.2A), a predicted CoA-acylating aldehyde dehydrogenase (AdhE) (Figure 3.1C).

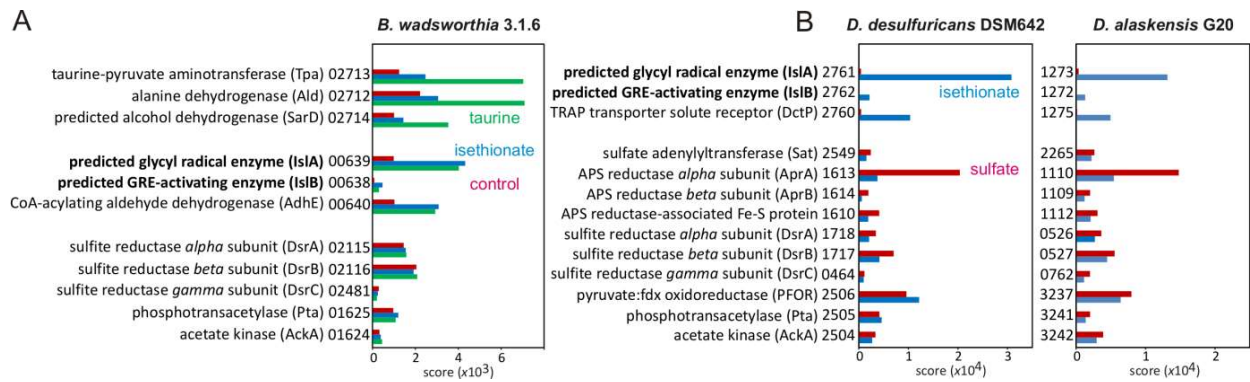


**Figure 3.2. Proteomics experiments with cell-free extracts reveal a putative desulfonating GRE.** Proteins encoded by the taurine- and isethionate-utilization gene clusters, including the predicted isethionate GRE (IslA) and GRE-activase (IslB) components, are specifically and strongly expressed during growth with taurine (*B. wadsworthia*, **A**) and isethionate (*B. wadsworthia*, *Desulfovibrio* strains, **B**). Constitutively expressed proteins, e.g. for sulfite reduction (Dsr) and metabolism of acetyl-CoA (Pta, AckA), are shown for comparison. IMG locus tag numbers are given; for their prefixes, see Figure 3.1C. Shown are results of representative total-proteomic analyses replicated at least twice with extracts prepared from independent growth experiments.

The discovery of these gene clusters allowed us to formulate a biochemical hypothesis for taurine catabolism in *B. wadsworthia*. Initial deamination of taurine would generate sulfoacetaldehyde (Figure 3.1B). Rather than undergoing C–S bond cleavage by an Xsc-type enzyme, we hypothesized that sulfoacetaldehyde could instead be reduced to isethionate by the co-induced alcohol dehydrogenase (sarD) encoded in the *tpa-ald* gene cluster. We then envisioned that the GRE from the second gene cluster might catalyze the conversion of isethionate to acetaldehyde and sulfite.

GREs are extremely oxygen-sensitive enzymes that use protein-centered radical intermediates in catalysis, with the key glycine-centered radical installed posttranslationally by a partner activating enzyme that is a member of the radical SAM enzyme family (see Figure S2.1). GREs catalyze challenging biochemical transformations that play important roles in primary metabolism under strictly anoxic conditions, including a range of C–C, C–O and C–N bond cleavage reactions (Backman, Funk *et al.* 2017). Though C–S bond cleavage had not been reported for any GRE, the amino-acid sequence of the identified *Bilophila* GRE resembles those of the C–O bond-cleaving GRE 1,2-propanediol dehydratase from *Roseburia inulinivorans* (32% identity), which converts 1,2-propanediol to water and propionaldehyde (propanal) (LaMattina, Keul *et al.* 2016), and the C–N bond cleaving GRE choline trimethylamine-lyase (CutC) from *D. alaskensis* G20 (31% identity), which metabolizes choline to trimethylamine and acetaldehyde (Craciun, Marks *et al.* 2014). This relationship suggested the potential for the *B. wadsworthia* GRE to function as a C–S bond cleaving, isethionate sulfite-lyase (IslA) of a desulfonation pathway for taurine (Figure 3.1A).

The acetaldehyde produced could then be further metabolized to acetyl-CoA by the CoA-acylating aldehyde dehydrogenases (*adhE*) encoded in the GRE gene cluster (Figure 3.1B).

To obtain further evidence for this biochemical hypothesis and the role of the putative isethionate metabolizing GRE, we examined the genomes and proteomes of two additional bacteria that use isethionate (but not taurine) as a terminal electron acceptor and, like *B. wadsworthia*, do not encode an Xsc homolog: *Desulfovibrio desulfuricans* subsp. *desulfuricans* DSM642 (Lie, Pitta *et al.* 1996) and *D. alaskensis* G20 (Kuehl, Price *et al.* 2014). Using an analogous differential-proteomics and reverse-genetics approach, we identified similar enzymatic machinery in these organisms specifically produced during growth with isethionate. A candidate GRE and GRE-activating enzyme were detected in high abundance in cells grown with isethionate, but not in control cells (Figure 3.2B). The sequences of these enzymes strongly resembled the corresponding GRE and activase from *B. wadsworthia* (pairwise identities of >73% and >52%, respectively). A protein encoded next to the putative isethionate-metabolizing GRE/activase was also detected in high abundance only in isethionate-grown cells (Figure 3.2B). This predicted substrate binding protein (DctP) of a tripartite ATP-independent periplasmic (TRAP) transporter (Figure 3.2B) may be involved in isethionate transport (Figure S3.2). We found highly similar gene clusters in the genomes of a wide range of sulfidogenic *Desulfovibrio* species, including *D. fairfieldensis*, *D. piger*, *D. termitidis*, *D. vulgaris* and *D. ruminis*, as well as in the genomes of many *Desulfitobacterium*, *Desulfomicrobium* and *Desulfotomaculum* strains (see below). The presence of the putative C–S bond cleaving GRE in these organisms strongly implicates this enzyme in isethionate metabolism.

#### Activities of cell-free extracts and genetic knockouts confirm the proposed organosulfonate catabolic pathways.

We next sought to further verify these proposed taurine and isethionate catabolic pathways by examining cell-free extracts of *B. wadsworthia* and *Desulfovibrio* for the newly postulated enzyme activities. First, high specific activity of an NADH-coupled sulfoacetaldehyde reductase was detected in extracts of taurine-grown *B. wadsworthia* cells (1.2 U/mg +/- 0.12, mean ± standard deviation of n=5), with much less activity observed in extracts of isethionate-grown cells (<0.5 U/mg). Second, formation of sulfite and acetaldehyde, the predicted products of the isethionate sulfite-lyase reaction, was detected in extracts of the two *Desulfovibrio* strains when grown with isethionate, only in the presence of isethionate as substrate. This activity (6.6 and 3.8 mU/mg for strains DSM642 and G20, respectively, calculated from the rate of sulfite formation and for representative reactions shown in Figure

S3.3) was observed only when great care was taken to perform the cell harvest, preparation of cell extracts and the enzyme assays under strictly anoxic conditions in presence of a strong reducing agent, titanium(III) nitrilotriacetate (Supplementary material, Materials and Methods). The oxygen sensitivity of this activity is consistent with involvement of a GRE. Extracts of taurine-grown *B. wadsworthia* cells, which were strictly kept free of oxygen, also exhibited sulfite formation when exposed to isethionate as substrate (5.3 mU/mg for a representative reaction shown in Figure S3.3), indicative of a desulfonation reaction taking place, but we were not able to detect acetaldehyde formation in these extracts (see below). When isethionate was replaced with taurine as potential substrate for the GRE, no sulfite formation was observed. We also observed no sulfite formation in reactions additionally containing the co-substrates needed to generate isethionate from taurine (pyruvate and NADH) in *B. wadsworthia* (see Figure 3.1B). In summary, we confirmed an oxygen sensitive isethionate sulfite-lyase activity in extracts of the two isethionate-grown *Desulfovibrio* strains and in taurine-grown *B. wadsworthia*, but we were not able to demonstrate a desulfonation of taurine by successfully coupling all three enzymes of *B. wadsworthia* (Tpa, SarD and putative GRE) in cell-free extract under the conditions tested.

In addition, we confirmed that the genes encoding the putative isethionate-metabolizing GRE, activase, and other proteins encoded in the gene cluster are required for isethionate utilization by examining single-deletion strains from a *D. alaskensis* G20 transposon library (Kuehl, Price *et al.* 2014). While wild type and mutant strains grew equally well in media containing sulfite as the sole electron acceptor, knock-out of any of the genes in the putative isethionate-utilization gene cluster (GRE, activase or transporter genes) or of a predicted regulator gene (*isR*) (see Figure 3.1B) abolished growth with isethionate (Figure S3.4), confirming that these genes are essential for utilizing isethionate-derived sulfite, but not free sulfite, as an electron acceptor.

#### *In vitro* reconstruction of taurine catabolism.

Having identified the complete pathways for taurine and isethionate metabolism in these strictly anaerobic bacteria, we sought to characterize the key enzymes from these processes *in vitro*. We first cloned and heterologously expressed the genes from the two *B. wadsworthia* gene clusters in *E. coli* and purified the enzymes (Figure S3.5). We verified that Tpa catalyzes the deamination of taurine with pyruvate to generate sulfoacetaldehyde and alanine (Laue and Cook 2000a). We then confirmed that the putative sulfoacetaldehyde reductase SarD reduces sulfoacetaldehyde to isethionate in an NADH-dependent manner (Figure S3.6 and Figure S3.7). SarD did not accept acetaldehyde as a substrate. Combining

Tpa and SarD resulted in the conversion of taurine to isethionate *via* sulfoacetaldehyde as confirmed by LC-MS (Figure S3.8). Together, these results confirm that the SarD enzyme provides the link between taurine and isethionate catabolism in *B. wadsworthia*.

We then investigated the proposed C–S cleaving GRE that generates sulfite, isethionate-sulfite lyase (IslA). The *B. wadsworthia* GRE-activating enzyme (IslB) was expressed, purified and characterized under anoxic conditions, whereas the *B. wadsworthia* IslA was expressed and isolated under oxic conditions and then rendered anoxic (see Material and Methods). The purified activase IslB was reconstituted by reduction with dithionite (Figure S3.9) and incubated with the purified GRE IslA in the presence of SAM and acriflavine as photosensitizer. This installed the glycyl radical on  $13 \pm 0.1\%$  (mean  $\pm$  standard deviation of three replicates) of all GRE polypeptides as determined by EPR spectroscopy (Figure 3.3A). Incubation of the activated IslA with isethionate resulted in substrate consumption (Figure S3.10) and formation of sulfite (Figure 3.3B) and acetaldehyde (Figure 3.3C). No reaction was observed when oxygen was present or when either the activase, GRE, or the substrate was omitted (Figure 3.3B,C). The steady-state kinetic parameters of the isethionate cleavage were determined spectrophotometrically using a coupled enzyme assay with yeast alcohol dehydrogenase (Figure 3.3D). The apparent  $k_{\text{cat}}/K_m$  ( $1.8 \times 10^3 \text{ M}^{-1} \text{ s}^{-1}$ ) under these conditions was lower than the catalytic efficiencies reported for other GRES (Craciun, Marks *et al.* 2014; Levin, Huang *et al.* 2017), but we did not detect turnover with any alternate organosulfonate (Figure S3.11) or with S-1,2-propanediol or choline as substrate (Figure S3.12), strongly suggesting that isethionate is the native substrate. Characterization of the recombinant and reconstituted activase IslB and the GRE IslA of *D. desulfuricans* DSM642 yielded similar results, including selectivity for the cleavage of isethionate to sulfite and acetaldehyde, but a modest apparent  $k_{\text{cat}}/K_m$  ( $1.2 \times 10^3 \text{ M}^{-1} \text{ s}^{-1}$ ) (Figure S3.13).

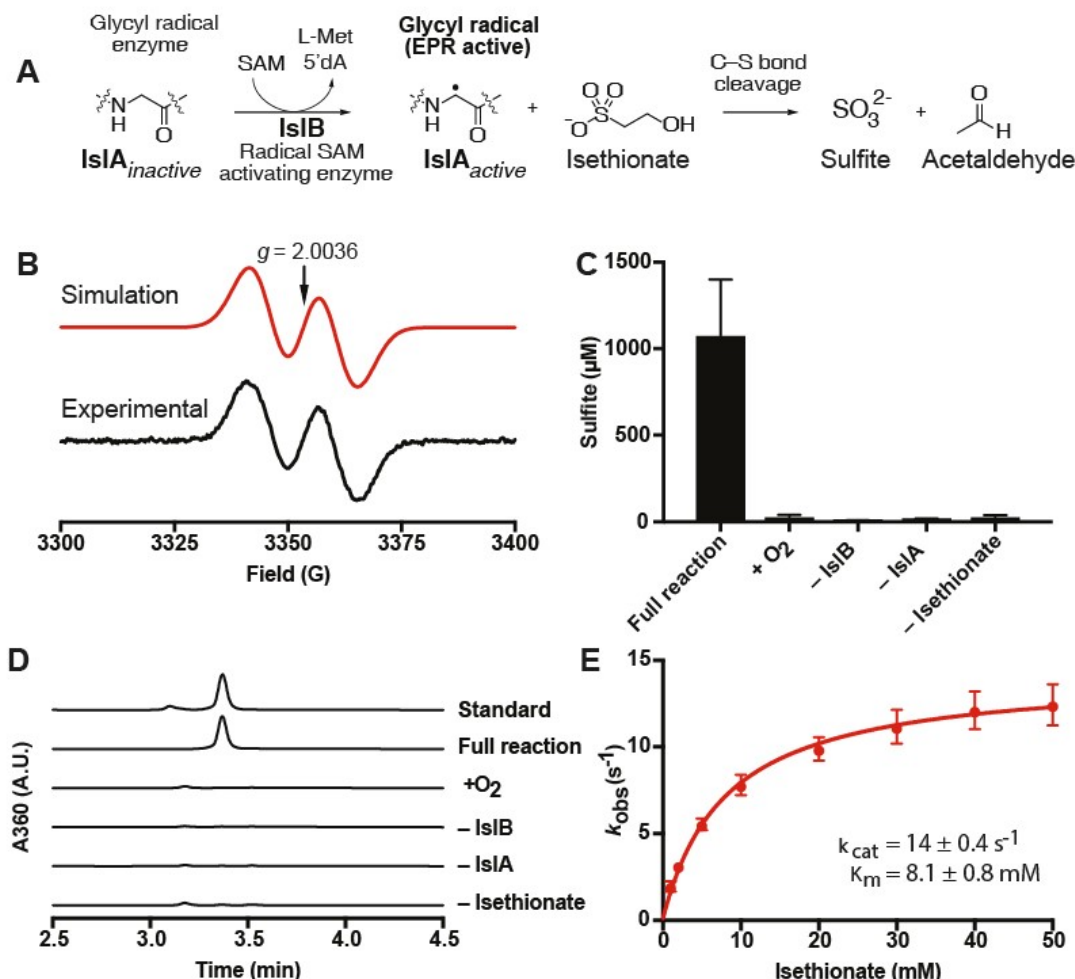


**Figure 3.3. The *B. wadsworthia* GRE is a C–S bond-cleaving isethionate sulfite-lyase.** (A) A radical generated by the GRE-activating, radical SAM enzyme IsIB is used to install a protein-centered, stable glycyl radical within the GRE IsIA. Activated IsIA then catalyzes a C–S bond cleavage reaction with isethionate as substrate. For an illustration of the mechanistic hypothesis, see Figure S3.1. (B) EPR spectroscopy demonstrating glycyl radical formation on recombinantly produced and purified IsIA after its activation by recombinant, purified and reconstituted GRE-activase IsIB. (C) Conversion of isethionate to sulfite by IsIA was observed only in the absence of molecular oxygen and in presence of all reaction components, as was acetaldehyde formation (D); the data in panel C is shown as the mean  $\pm$  standard deviation of three technical replicates and data in panel D as representative HPLC chromatograms of a minimum of two technical replicates. (E) The Michaelis-Menten kinetics of isethionate cleavage were determined by using a coupled spectrophotometric assay with yeast alcohol dehydrogenase and NADH. The  $k_{\text{cat}}$  was  $14 \pm 0.4 \text{ s}^{-1}$ , and the  $K_m$  was  $8.1 \pm 0.8 \text{ mM}$ . Data is shown as the mean  $\pm$  standard deviation of four technical replicates.

Finally, we examined the last putative enzyme from the *B. wadsworthia* taurine utilization pathway, AdhE. We found that the recombinant enzyme converted acetaldehyde to acetyl-CoA only in the presence of CoASH and NAD<sup>+</sup> (Figure S3.14); it preferred NAD<sup>+</sup> over NADP<sup>+</sup>. When we combined isethionate as substrate with activated GRE, NAD<sup>+</sup>, CoASH, and AdhE, we observed formation of acetyl-CoA, as confirmed by LC-MS (Figure S3.14C). Hence, the work with recombinant enzymes confirmed all four reactions of the taurine pathway of *B. wadsworthia* 3.1.6 (Figure 3.1B).

## **Discussion**

Our efforts to decipher the molecular basis for the conversion of taurine to sulfite in strictly anaerobic gut bacteria has uncovered a previously uncharacterized GRE, isethionate sulfite-lyase (IsIA) and its cognate activating enzyme (IsIB). This enzyme catalyzes a radical-based desulfonation, generating acetaldehyde, which can be further metabolized to acetyl-CoA, and sulfite, which can serve as a terminal electron acceptor. The reaction mechanism for isethionate desulfonation by the GRE IsIA (Figure 3.3A) may proceed in analogy to the mechanisms proposed for 1,2-propanediol dehydratase (PD) and choline trimethylamine-lyase (CutC), which have been supported experimentally (Bodea, Funk *et al.* 2016; Levin and Balskus 2018). This proposed mechanism would involve an initial hydrogen atom abstraction to form an  $\alpha$ -hydroxyalkyl radical at C<sub>2</sub> of isethionate, followed by a spin-center shift to eliminate the C<sub>1</sub> sulfonate group (see therefore Figure S3.1B). As this type of C–S bond cleavage reaction was not previously known to be catalyzed by GREs, the discovery of IsIA further diversifies the known repertoire of radical reactions catalyzed by this superfamily (Backman, Funk *et al.* 2017) and adds to the limited number of characterized microbial desulfonative enzymes (Cook and Denger 2002; Cook, Denger *et al.* 2006), including sulfoacetaldehyde acetyltransferase (Xsc) (EC 2.3.3.15) (Figure 3.1A), cysteate (3-sulfoalanine) sulfite-lyase (CuyA) (EC 4.4.1.25), sulfolactate sulfite-lyase (SuyAB) (EC 4.4.1.24), and the range of mono- and dioxygenases (EC 1.14.-) desulfonating aromatic and aliphatic sulfonates in aerobic bacteria [e.g., (Kertesz 2000)].

Remarkably, the logic of the two catabolic pathways that cleave taurine to, ultimately, acetyl-CoA and sulfite (Figure 3.1B), either in the absence of molecular oxygen in strictly anaerobic bacteria by the highly oxygen-sensitive GRE IsIA, or in aerobic bacteria *via* the oxygen-insensitive TDP-dependent Xsc, parallels the catabolism of pyruvate to acetyl-CoA in *Escherichia coli*. During anaerobic fermentation, *E. coli* can employ the GRE pyruvate formate-lyase (Knappe and Sawer 1990), while during aerobic respiration, this enzyme is replaced by a TDP-dependent, oxygen-insensitive pyruvate dehydrogenase. Further, the observation that anaerobic *Desulfonispora thiosulfatigenes* GKNTAU, which is highly specialized for taurine fermentation (Denger, Ruff *et al.* 2001), employs an Xsc enzyme (Ruff, Denger *et al.* 2003), while *B. wadsworthia* uses IsIA for the respiration of the sulfite from taurine with external electrons such as from lactate or H<sub>2</sub> (da Silva, Venceslau *et al.* 2008), may point to an interesting adaptation for maintaining redox balance under these different anoxic growth conditions.

Searches for additional putative IslA enzymes in sequenced microbial genomes revealed more than 250 sequences in the NCBI non-redundant protein database (>35% amino acid identity to the *B. wadsworthia* sequence). 115 of these sequences clustered together with the *B. wadsworthia* and the *Desulfovibrio* IslA sequences in a sequence similarity network (SSN) at a threshold of 62% (Figure S3.15A) (Levin, Huang *et al.* 2017) and are therefore likely to process isethionate or similar organosulfonate substrates. Bioinformatic analyses revealed distinctions between these sequences and GREs of known activity. For example, comparison of the sequences of characterized and putative IslAs with the sequences of other characterized GREs revealed a unique, conserved glutamine residue (Q193) positioned to interact with the sulfite leaving group in a homology model (Backman, Funk *et al.* 2017) (Figure S3.15B and C). Further, phylogenetic analysis (Figure 3.4A) reveals IslA to be part of a deeply branching group of sequences that were previously designated as ‘GREs of unknown function’ and that are typically not co-localized with genes encoding bacterial microcompartment (BMC) structural proteins [see (Zarzycki, Erbilgin *et al.* 2015)]. We note that, while IslA homologs are predominantly found in Deltaproteobacteria, these enzymes are also encoded in the genomes of many Firmicutes (Clostridia, Negativicutes) as well as several Gammaproteobacteria and Bacteroidetes (Figure 3.4B and Table S3.1). This observation suggests that anaerobic organosulfonate catabolism may be more widely distributed across microbial diversity than previously appreciated, and evaluating these organisms’ abilities to metabolize isethionate, taurine, or other organosulfonates, are important topics for future research.

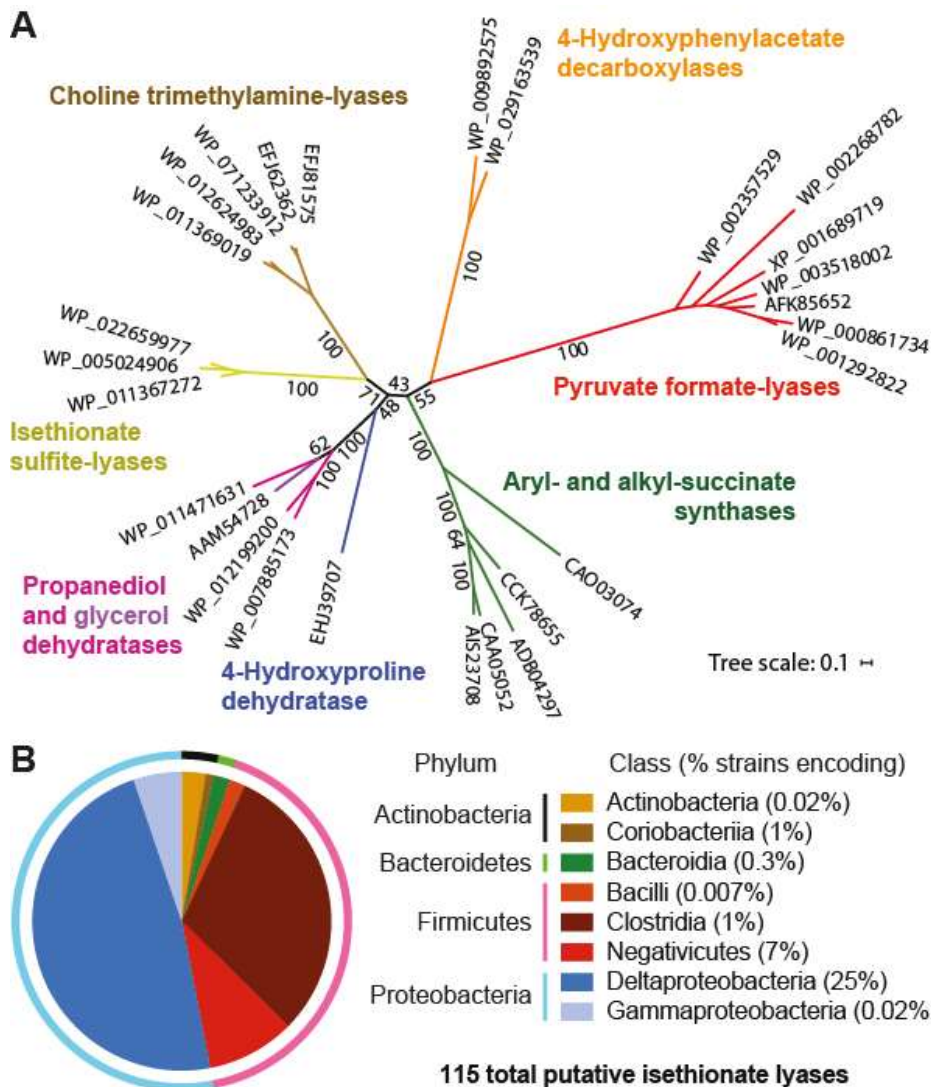


**Figure 3.4. Anaerobic organosulfonate metabolism has an unexpectedly broad distribution in sequenced bacteria. (A)** A maximum-likelihood phylogenetic tree illustrates that the IslAs are phylogenetically distinct from previously characterized GREs. The listed sequences identifiers are GenBank accession codes. **(B)** Illustration of the distribution of 115 putative IslA isethionate sulfite-lyases, as retrieved from the NCBI database at a threshold 62% identity, across sequenced bacterial genomes (see also Table S3.1). The pie chart showing their relative taxonomic distribution on the phylum level (outer ring) demonstrates that the majority are found in genomes of Proteobacteria and Firmicutes, and at the class level (inner circle) that they are predominantly distributed across Deltaproteobacteria, Clostridia and Negativicute genomes. The percent values shown in brackets indicate (at the class-level) the number of genomes with putative IslAs relative to all known genome sequences for this class, confirming the enrichment of IslAs in the Deltaproteobacteria (encoded in 25% of all known genomes).

Finally, the discovery of this gut microbial metabolic process reshapes our view of organosulfonate utilization in the human gut microbiota and unlocks new opportunities for investigating its contribution to human disease. Microbes derive several benefits from respiring organosulfonates, including the ability to occupy distinct metabolic niches. Compared to sulfate reduction, no ATP expenditure is required for generating sulfite as an electron acceptor (see Figure 3.1B). Notably, the two *Desulfovibrio* strains down-regulate

APS reductase during isethionate-utilization (Figure 3.2B) while *B. wadsworthia* is unable (or has lost the ability) to utilize sulfate (Laue, Denger *et al.* 1997). Furthermore, many sulfite-respiring bacteria exhibit a hydrogenotrophic lifestyle in the human gut (da Silva, Venceslau *et al.* 2008; Nava, Carbonero *et al.* 2012; Rey, Gonzalez *et al.* 2013), and in this respect, the taurine/isethionate pathway can serve both a dissimilatory and assimilatory function when the acetyl-CoA produced from isethionate is funneled directly into gluconeogenesis (Figure 3.1B).

The widespread distribution of these anaerobic taurine and isethionate pathways in microbiota-relevant sulfidogenic bacteria indicates an important role for organosulfonate respiration in this microbial habitat, potentially in the context of competition with sulfate-reducing bacteria and methanogenic archaea for the H<sub>2</sub> produced by gut bacterial fermentation (Rey, Gonzalez *et al.* 2013), or in the context of a high availability of these organosulfonate substrates during consumption of high-fat (high taurocholate) (Devkota, Wang *et al.* 2012) and/or high-meat (high taurine) diets (David, Maurice *et al.* 2014). Furthermore, given that taurine is present in high concentrations in mammalian tissues (2 - 20 mM; e.g. (Jacobsen and Smith 1968), this pathway may also be important for *B. wadsworthia* pathogenesis. The discovery of the molecular basis for taurine metabolism in this organism and other gut microbes will not only enable future efforts to understand the biological roles of this metabolic activity in the human body, but may also inform new approaches to controlling intestinal H<sub>2</sub>S production and *B. wadsworthia* infections.

## **Materials and methods**

A detailed material and methods section can be found in the supplementary material. The *Bilophila* and *Desulfovibrio* strains were grown in carbonate-buffered mineral salts medium reduced with Ti(III)-nitrilotriacetate. Cell-free extracts were prepared by French press-disruption followed by centrifugation to remove unbroken cells; these extract were used for proteomics and to measure Tpa, SarD and IslAB activity. Sulfite was detected by a colorimetric (fuchsin) assay as well as by HPLC after derivatization; acetaldehyde was detected by HPLC after derivatization; a HILIC column and HPLC-MS system was used to detect taurine, alanine, sulfoacetaldehyde and isethionate. His-tagged Tpa and SarD were produced using *E. coli* Rosetta 2 DE3 and the His-tagged GREs, AdhE and DctP using *E. coli* BL21. The His-tagged GRE activating enzymes were overexpressed in *E. coli* BL21(DE3) *ΔiscR::kan*. Before induction, these cultures were rendered anoxic by sparging with argon. Also cell lysis and enzyme purification were done under anoxic conditions. The recombinant GREs were rendered anoxic after purification and activated by incubation in

presence of the GRE-activating enzyme, SAM, and acriflavine as photosensitizer in HEPES-bicine buffer under ambient light. Kinetics and substrate range of the GREs were measured spectrophotometrically using a coupled assay with alcohol dehydrogenase, reducing the acetaldehyde to ethanol concomitant with NADH formation.

## **Acknowledgments**

The authors thank Emma Allen-Vercoe for kindly providing *B. wadsworthia* 3.1.6, Adam Deutschbauer and Jennifer Kuehl for kindly providing the *D. alaskensis* G20 mutant strains, Patric Cao for help with characterizing the *Bilophila* pathway, Benjamin Levin for construction of the  $\Delta iscR$  expression strain and synthesis of S-1,2-propanediol, Andreas Marquardt for proteomic analyses, Dieter Spitteler for LC-MS support and Thomas Huhn for chemical synthesis. We acknowledge the helpful discussions with Paul Boudreau, Alasdair Cook, Stefan Kreft and Bernhard Schink, and the helpful input offered by the anonymous reviewers of this manuscript. The work of AB and DS was funded by the German Research Foundation (DFG grants SCHL1936/3-4), the University of Konstanz (Young Scholar Fund) and Konstanz Research School Chemical Biology (KoRS-CB). The work of SCP and EPB was funded by the Bill & Melinda Gates Foundation (Howard Hughes Medical Institute-Gates Faculty Scholar Award) and the work of SMI by the NSERC Postgraduate Scholarship-Doctoral Program.

## **Author contributions**

DS and EPB conceived the study at International Symposium on Microbial Ecology 16. KD, AB and DS did the proteomic analyses and deduced the pathway and did the work with enzyme activities in *Bilophila* and *Desulfovibrio* cell extracts and the heterologous expression of Tpa and SarD at University of Konstanz. SCP characterized the recombinant GREs and AdhE as well as the *D. alaskensis* mutant strains at Harvard University. SMI characterized IsIA for its potential activity with S-1,2-propanediol and choline as substrates. SCP, EPB and DS wrote the manuscript and all authors improved it.

## **Supplementary material**

### **Material and methods**

#### **Chemicals**

Commercial chemicals were of the highest purity available and purchased from Sigma-Aldrich, Fluka, Roth, Merck or Biomol. Sulfonylpyruvate and sulfoacetaldehyde (as the bisulfite adduct) was synthesized as described previously (Denger, Ruff *et al.* 2001). Racemic 3-sulfolactate and 2,3-dihydroxypropanesulfonate (DHPS) were synthesized by Thomas Huhn (Department of Chemistry, University of Konstanz) as described elsewhere (Roy, Hewlins *et al.* 2003; Mayer, Huhn *et al.* 2010). S-1,2-propanediol was prepared as previously described (Schaus, Brandes *et al.* 2002). Luria-Bertani (LB) medium was prepared from its basic components (10 g/L tryptone, 5 g/L yeast extract, 5 g/L NaCl) or obtained from EMD Millipore or Alfa Aesar. Isopropyl  $\beta$ -D-1-thiogalactopyranoside (IPTG) was purchased from Teknova (Hollister, CA). Acetonitrile for LC-MS analyses was purchased as LC-MS grade solvent from Honeywell Burdick & Jackson or Sigma-Aldrich.

#### **Bacterial strains**

*Bilophila wadsworthia* 3.1.6 was kindly provided by Dr. Emma Allen-Vercoe, University of Guelph, Canada, and *Desulfovibrio desulfuricans* subsp. *desulfuricans* type-strain (DSM 642) and *Desulfovibrio alaskensis* G20 (DSM 17464) were purchased from the Leibniz Institute DSMZ-German Collection of Microorganisms and Cell Cultures, Braunschweig, Germany. The *D. alaskensis* G20 mutants (and parental strain) were kindly provided by Adam Deutschbauer at Lawrence Berkeley National Laboratory.

#### **Culture media for *Bilophila wadsworthia* and the *Desulfovibrio* strains**

Liquid cultures of *Bilophila wadsworthia* 3.1.6, *D. desulfuricans* DSM642 and *D. alaskensis* G20 were grown in a hydrogen-carbonate-buffered mineral salts medium, made with freshwater basal salts (Widdel and Pfennig 1981) plus trace elements (Widdel, Kohring *et al.* 1983), selenium-tungstate (Tschech and Pfennig 1984) and vitamins (Pfennig 1978) solutions, and 1 mM Ti(III)-nitrilotriacetate (NTA) as the reducing agent (Moench and Zeikus 1983), in serum bottles with butyl rubber stoppers under a gas phase of 20% CO<sub>2</sub> and 80% N<sub>2</sub>. For *B. wadsworthia*, the medium was supplemented with 1,4-naphthochinone (200 µg/l), and 20 mM sodium *L*-lactate was added as the electron and carbon source, and either 20 mM taurine or isethionate as the electron acceptor. For the *Desulfovibrio* strains, 20 mM

lactate was added and either 20 mM taurine, isethionate or sodium sulfate as the terminal electron acceptor. The cultures were incubated in the dark at 37°C (*Bilophila*) or at 30°C (*Desulfovibrio*), and harvested as appropriate (see below).

For the *D. alaskensis* G20 mutational analysis, the previously described lactate/sulfate medium (Craciun and Balskus 2012) was used with the exceptions that the 8 mM MgSO<sub>4</sub> was replaced by 8 mM MgCl<sub>2</sub> and that 52 mM Na<sub>2</sub>SO<sub>4</sub> was present as the sole electron acceptor; lactate/sulfite medium contained 52 mM Na<sub>2</sub>SO<sub>3</sub> as the sole electron acceptor, and lactate/isethionate medium 60 mM isethionate. For growing *D. alaskensis* on plates, the previously described MOYLS4 medium was used (Kuehl, Price et al. 2014) with 1 mM Na<sub>2</sub>S x 9 H<sub>2</sub>O as the reducing agent and 2 mM K<sub>2</sub>HPO<sub>4</sub> as the phosphorus source.

### Total proteomics

Anoxic extracts prepared for the enzyme assays (see below) were used, or extracts prepared under oxic conditions when the cells were disrupted in a bullet blender (Next Advance Inc.) in 50 mM Tris-HCl buffer (pH 8.0) containing Halt protease inhibitor cocktail (Thermo Fisher Scientific). Cell debris was removed by centrifugation (15,000 x g, 15 min, 4°C). The extracts were subjected to peptide fingerprinting-mass spectrometry at the Proteomics Facility of the University of Konstanz ([www.proteomics-facility.uni-konstanz.de](http://www.proteomics-facility.uni-konstanz.de)) as described previously (Schmidt, Müller et al. 2013; Denger, Weiss et al. 2014; Felux, Spiteller et al. 2015) with the exception that each sample was analyzed twice on a Orbitrap Fusion with EASY-nLC 1200 (Thermo Fisher Scientific), and that Tandem mass spectra were searched against an appropriate protein database (retrieved from IMG) using Mascot (Matrix Science) and Proteom Discoverer V1.3 (Thermo Fisher Scientific) with “Trypsin” enzyme cleavage, static cysteine alkylation by chloroacetamide, and variable methionine oxidation.

### Enzyme assays with cell-free extracts of *Bilophila* and *Desulfovibrio*

Cultures were harvested in the late exponential growth phase at an OD<sub>580</sub> of app. 0.3 – 0.4 by centrifugation of the serum bottles (2100 x g, 30 min, 4°C). Cells were resuspended in anoxic Tris-HCl buffer (50 mM pH 8.0) containing 5 mM MgCl<sub>2</sub> and disrupted by three passages through a cooled French pressure cell (140 MPa) (Aminco, MD, USA), which had been flushed with N<sub>2</sub> gas.

Taurine:pyruvate aminotransferase was assayed in 50 mM Tris-HCl buffer (pH 9.0) containing 5 mM taurine, 10 mM sodium pyruvate, and 0.1 mM pyridoxal-5-phosphate. Assays with cell free extract were performed with 200 or 400 µL of extract per mL reaction. Heat inactivation was done by heating the enzymes to 98°C for ten minutes in a heating

block. Samples for HPLC (see below) were mixed with acetonitrile (HPLC grade) in a ratio of 7:3 immediately after sampling in order to stop enzyme reaction, centrifuged to remove precipitate ( $16,100 \times g$ , 10 min, 4°C), and stored at -20°C until analysis.

Sulfoacetaldehyde reductase was assayed spectrophotometrically as the oxidation of NADH recorded at 365 nm for 1 min; the standard reaction mixture (1 mL) contained 50 mM Tris-HCl (pH 8.0), 5 mM MgCl<sub>2</sub>, 0.4 mM NADH and 2 mM sulfoacetaldehyde-bisulfite adduct at room temperature. The reactions were started either by addition of substrate or by addition of cell extract. Sulfoacetaldehyde disappearance and isethionate formation during the reactions was confirmed by HPLC (see below) in subsamples taken from the reactions, in which the reaction was stopped by addition of 30% (v/v) acetonitrile; these subsamples were stored at -20°C until analysis.

Isethionate sulfite-lyase was assayed discontinuously at room temperature by monitoring the formation of the two products sulfite and acetaldehyde. The reaction mixture (1 mL) contained 20 mM isethionate, 1 mM S-adenosylmethionine chloride (SAM), 1 mM Ti(III)-NTA, and about 0.2 – 0.9 mg total protein in 50 mM Tris-HCl (pH 8.0) containing 5 mM MgCl<sub>2</sub>. First, buffer including isethionate and SAM was degassed under vacuum in glass cuvettes with rubber stoppers, and flushed with nitrogen gas, three times each. Then, Ti(III)-NTA was added, and the reaction was initiated by the addition of anoxic crude extract, each with a syringe and needle through the rubber stoppers. At appropriate time intervals, samples (100 µL) were taken by syringes for routine quantification of sulfite by two independent methods, through a colorimetric assay and by derivatization and HPLC-UV analysis (see below), and for routine quantification of acetaldehyde by derivatization and HPLC-UV analysis (see below).

#### Analytical chemistry for enzyme assays with *Bilophila* and *Desulfovibrio* cell extracts

For routine HPLC with ELSD detection, a Shimadzu Prominence HPLC-DAD system coupled with a ZAM3000 ELSD detector (Schambeck SFD GmbH, Germany) was used with a SeQuant ZIC-HILIC hydrophilic interaction liquid chromatography column (5µm, 200 Å, 150 mm x 2.1 mm; Merck). The HPLC conditions were: acetonitrile as eluent A, and 0.1 M ammonium acetate buffer (pH 7.0) containing 10% acetonitrile as eluent B; total flow rate 0.3 mL/min. The elution gradient was: from 90% eluent A to 75% in 20 minutes; from 75% to 65% in 10 minutes; plateau at 65% A for 10 minutes. Under these conditions isethionate eluted at 11.5 min, taurine at 19.5 min, alanine at 20.6 min, NADH at 26.6 min, and NAD<sup>+</sup> at 28.7 min, while sulfoacetaldehyde eluted only poorly separated in between 5–16 min retention time. Sulfoacetaldehyde (and acetaldehyde) was determined also by HPLC-UV

against authentic standards after derivatization with DNPH. Samples were mixed in a 1:1 ratio with the derivatization agent (0.5 mg/mL 2,4-dinitrophenylhydrazine [DNPH] in acetonitrile with 0.1% H<sub>3</sub>PO<sub>4</sub>), after which subsamples (5 µL) were analyzed by HPLC-UV. A mixed mode C<sub>18</sub> column (Luna Omega, 5 µm, PS, C18, 100 Å, 140 mm x 3 mm; Phenomenex) was used. The flow rate was 1 mL/min with acetonitrile as eluent A and 0.1% formic acid in MilliQ water as eluent B. HPLC conditions were as follows: three minutes at 25% A, gradient from 25 to 80% A for ten minutes, reequilibration to 25% A for seven minutes. Under these conditions, DNPH-derivatized sulfoacetaldehyde eluted at 5.7 min, derivatized acetaldehyde at 6.8 min, and free DNPH at 8.8 min.

Sulfite concentration in enzyme reactions was routinely determined by a colorimetric assay described previously (Denger, Ruff *et al.* 2001). Samples taken from the reactions were immediately added in a ratio of 1:20 to a mixture of 0.56 M H<sub>2</sub>SO<sub>4</sub>, 0.16% (w/v) fuchsine and 0.16% formaldehyde. The absorption at 580 nm was measured after 10 minutes against sulfite standards prepared from a fresh sodium sulfite stock solution. Sulfite in enzyme reactions was also determined by HPLC-UV after derivatization with *N*-(9-acridinyl)maleimide (NAM) (see below) against authentic standards; the column and gradient system for analysis of DNPH-derivatized aldehydes (see above) was used for separation of the sulfite reaction product, which eluted at 3.8 – 4.2 min under these conditions.

#### PCR primers and DNA sequencing

Primers for cloning were synthesized by Microsynth AG (Balgach, Switzerland), Integrated DNA Technologies (Coralville, IA) or Sigma Aldrich. PCR was conducted on Biometra T-Gradient or BioRad C1000 thermocyclers. Constructed plasmids were sequenced by GATC Biotech (Konstanz, Germany) or Eton Biosciences (Charlestown, MA). DNA sequencing results were visualized in Geneious 8.1.7, Jalview 2.9.0. or DNASTAR Lasergene 7. Primer sequences are given in Table S3.2.

#### Experiments with mutants of *Desulfovibrio alaskensis* G20

Transposon insertion mutagenesis was previously used to inactivate *Dde\_1270*, *Dde\_1272*, *Dde\_1273*, *Dde\_1274*, and *Dde\_1275* (Kuehl, Price *et al.* 2014). The frozen strains were revived on MOYLS4 plates amended with G418 (geneticin, 400 µg/mL) at 37 °C, and colonies were inoculated into Hungate tubes containing 5 mL lactate/sulfate medium amended with 800 µg/mL G418. For confirmation of specific transposon insertion by PCR, 20 µL of outgrown lactate/sulfate culture was heated at 95 °C for 10 min, and the lysed cells were diluted 1:10 in nuclease-free H<sub>2</sub>O and used as PCR template. The reactions (10 µL)

contained 1 µL template, 0.5 µM pRL27\_IE\_rev1 and 0.5 µM gene-specific primer (see Table S3.2), and 5 µL 2x Q5 polymerase master-mix. The PCR program was: denaturation for 12 min at 95°C, followed by 25 cycles of 30 s denaturation at 95°C, 30 s annealing at 55°C, and 90 s elongation at 72°C. Specific transposon insertion for each mutant was confirmed by the presence of an amplicon at 800–1000 bp on agarose gels. The growth of the mutants in lactate/sulfite and lactate/isethionate medium was monitored also in 96-well plates with a plate reader in an anoxic chamber. Therefore, precultures in Hungate tubes containing 5 mL lactate/sulfate medium (wildtype) or 5 mL lactate/sulfate medium amended with 800 µg/mL G418 (mutants) were grown at 37°C for 48 h, and 100 µL of each culture was inoculated into fresh 5 mL medium and incubated further for 24 h. Then, 200 µL of each culture was inoculated into a well plate (in quadruplicate) containing 200 µL lactate/sulfite or lactate/isethionate medium, such that the initial OD<sub>600</sub> was 0.02 (pathlength-corrected). For 30 h, the OD<sub>600</sub> was recorded every 1 h with shaking every 20 min.

Heterologous over-production and purification of taurine-pyruvate aminotransferase (Tpa) and sulfoacetaldehyde reductase (SarD)

Chromosomal DNA was isolated from *B. wadsworthia* 3.1.6 using the protocol published by the DOE Joint Genome Institute (JGI), “JGI Bacterial DNA Isolation CTAB-2012” (<https://jgi.doe.gov/user-program-info/pmo-overview/protocols-sample-preparation-information/>). The constructs for the production of recombinant and His-tagged Tpa and SarD of *B. wadsworthia* were generated when the genes were amplified by PCR using Phusion polymerase (New England BioLabs) and the primers given in Table S3.2; the primers introduced a NdeI and Xhol site in front of the start and after the stop codons, respectively. The following PCR conditions were used: denaturation for 90 s at 98°C, followed by 30 cycles of 30 s denaturation at 98°C, 30 s annealing at 68°C, and 60 s elongation at 72°C; final elongation was for 5 min at 72°C. The PCR products were purified (QIAquick MiniElute Purification Kit) and blunt-end cloned into a pJet suicide vector (CloneJet PCR cloning kit, ThermoFisher Scientific). 2 µL of the reaction were transformed into chemically competent *E. coli* NovaBlue cells, by incubating 50 µL competent cells with 10 ng plasmid for 15 minutes on ice, followed by a heat shock at 42°C for 30 s, and recovery on ice for 1 min. Then, 200 µL of SOC medium (2% w/v tryptone, 0.5% w/v yeast extract, 10 mM NaCl, 2.5 mM KCl, 10 mM MgCl<sub>2</sub>, 20 mM glucose) was added and the cells were incubated at 37°C for 45 minutes before streaking them onto selective LB agar plates (100 µg/mL ampicillin). Positive clones from the agar plates were selected by colony PCR using the insert primers, cultivated overnight in LB medium, and the plasmid was extracted (Zyppy Plasmid Miniprep kit, Zymo Research). Each 0.5 µg of pJet plasmid from a positive clone was digested with

20 U NdeI and 80 U XbaI (New England BioLabs) in CutSmart buffer for 2h at 37°C. The inserts were then purified (Gel extraction Mini Spin Column kit, Genaxxon biosciences), and ligated (overnight, 16°C; T4 ligase, NEB) into the expression vector pET 28a(+) (Novagen), which had been linearized by digestion with NdeI and XbaI as described above. 2 µL of the ligation reaction were transformed into chemically competent *E. coli* NovaBlue and the cells streaked onto selective LB plates (30 µg/mL kanamycin). Positive clones were selected by colony PCR, and the constructs confirmed by DNA sequencing (GATC Biotech).

For heterologous overproduction of Tpa and SarD, the pET28 constructs were transformed into chemically competent *E. coli* Rosetta 2 DE3 cells as described above, and the cells grown in 5 mL selective LB medium (30 µg/mL kanamycin, 35 µg/mL chloramphenicol) at 37°C overnight. 100 mL LB medium with kanamycin and chloramphenicol were inoculated with 2 mL of this overnight culture and grown at 37°C with shaking. When the cultures reached an OD<sub>580</sub> of 0.5, expression was induced by addition of IPTG to a concentration of 1 mM. The cells were incubated further for 6 hours at 37°C, and harvested by centrifugation (26,000 x g, 15 min, 4°C). Cells were resuspended in 2 mL 20 mM potassium phosphate buffer (pH 7.2) containing 500 mM NaCl, 2.5 mM MgCl<sub>2</sub>, 10 U DNaseI, protease inhibitor (Halt, ThermoFisher Scientific) and 20 mM imidazole (buffer A). Cells were disrupted by four passages through a cooled French pressure cell (140 MPa). Whole cells and debris were removed from the extracts by centrifugation (17,000 x g, 15 min, 4°C). The His-tagged proteins were purified using affinity columns (His SpinTrap kit, GE Healthcare) with washing steps at 20, 40 and 60 mM imidazole in buffer A, followed by elution with 500 mM imidazole in buffer A. The imidazole buffer was exchanged by gel filtration (Illustra™ Nap™-5 columns, GE Healthcare) against phosphate buffer (20 mM, pH 7.2) containing 5 mM NaCl, and SDS-PAGE was used to identify the fractions containing protein and its purity (see below). The recombinant and purified proteins were stored at -20°C in glycerol (30% v/v final concentration). For purification and storage of Tpa, pyridoxal-5-phosphate (0.1 mM) was added to all buffers.

Heterologous over-production and purification of glycyl radical enzymes (GREs), GRE activating enzymes, acetaldehyde dehydrogenase (AdhE) and substrate binding protein (DctP)

The GRE genes were assembled into pET28a plasmids, and the GRE activating enzyme, AdhE, and DctP genes were assembled into pET29b plasmids, each via Gibson assembly. Inserts were prepared when 20 ng of genomic DNA of *B. wadsworthia* or *D. desulfuricans* (prepared as described above) was mixed with primers (0.5 µM of each, see Table S3.2) and

1x Phusion master-mix (New England BioLabs) on a 50 µl scale. The inserts were amplified using the following protocol: denaturation for 30 s at 95°C, followed by 25 cycles of 30 s denaturation at 95°C, 30 s annealing at 66°C, and 90 s elongation at 72°C. The amplifications were assessed on agarose gel, and the amplicons purified using an Illustra GFX PCR DNA and Gel Band Purification Kit (GE Healthcare). Linearized vector was prepared by incubating 5 µg of circular empty vector with 60 U each of NdeI and XbaI in 1x CutSmart buffer on a 50 µl scale at 37 °C for 1 h. The vector was then purified using an Illustra GFX PCR DNA and Gel Band Purification Kit. Each insert was assembled into the vector using Gibson assembly by incubating vector (50 ng, pET28a or pET29b) with the insert (3 equivalents) in 1x Gibson Assembly Master-mix (New England Biolabs) on a 10 µl scale at 50 °C for 1 h. Then, 2 µl from each reaction was transformed into 50 µl chemically competent *E. coli* Top10 cells by incubating them on ice for 2 min, incubating the cells and DNA at 42 °C for 30 s, and recovering on ice for 1 min; SOC medium (see above) (200 µl) was added and the cells were incubated at 37 °C for 1.5 h. The cells were plated on LB supplemented with kanamycin (50 µg/ml, hereafter referred to as LB-Kan50) and then grown at 37 °C overnight. Individual colonies were inoculated into 5 mL LB-Kan50 and grown overnight at 37 °C. The plasmids were isolated using an E.Z.N.A. Plasmid Mini Kit I (Omega Bio-tek, D6942-02), and the plasmid inserts were confirmed to have the desired sequence by sequencing (Eton Bioscience).

The expression host *E. coli* BL21(DE3) *ΔiscR* (Akhtar and Jones 2008) for expression of the GRE activating enzyme (see below) was constructed as follows. The strain *E. coli* BL21(DE3) *ΔiscR::kan* was generated using P1 transduction with *E. coli* strain JW2515-3 (Coli Genetic Stock Center), which contains the *ΔiscR777::kan* mutation, as the donor strain and *E. coli* BL21(DE3) as the recipient strain as previously described (Thomason, Costantino *et al.* 2007). The antibiotic resistance cassette was removed from *E. coli* BL21(DE3) *ΔiscR::kan* to produce *E. coli* BL21(DE3) *ΔiscR* using the plasmid pCP20 (Coli Genetic Stock Center) (Cherepanov and Wackernagel 1995; Datsenko and Wanner 2000).

Recombinant enzymes that required anoxic conditions (see below) were handled in an anoxic cabinet (MBraun) (100% N<sub>2</sub> atmosphere) or an anoxic soft vinyl chamber (Coy Laboratories) (97% N<sub>2</sub>/3% H<sub>2</sub> atmosphere). Samples were routinely rendered anoxic by one of the following methods. Consumable goods were brought into the glovebox the day before being used. Solid chemicals were brought into the anoxic chamber in Eppendorf tubes that had been perforated. Protein solutions were rendered anoxic as described in the specific section related to their purification. Media components were routinely rendered anoxic by sparging them with argon or N<sub>2</sub> prior to sterilization.

For heterologous overexpression, 50 ng of plasmid was transformed into 50 µL chemically competent *E. coli* BL21, or chemically competent *E. coli* BL21 *ΔiscR* (GRE activating enzymes). The cells were incubated on ice with DNA (5 min), incubated at 42 °C (30 s), and recovered on ice (2 min); SOC (200 µL) was added, and the cells were shaken at 37 °C for 1 h. Cells were then plated on LB-Kan50 and grown overnight. Single colonies were inoculated into 5 mL LB-Kan50, and these cultures transferred further into 100 ml LB-Kan50, if appropriate. For expression of GREs and the GRE activating enzymes, an entire 100 ml starter culture was inoculated into 4 L LB-Kan50, which was split equally between two 4 l shake-flasks, and for AdhE and DctP, a 5 mL starter culture was inoculated into 1 l LB-Kan50. For overexpression of the activase, the LB medium was supplemented with glucose (1% w/v) and Fe(III)-ammonium-citrate (2 mM). The cultures were grown at 37 °C until they reached an OD<sub>600</sub> of 0.6, at which point IPTG (0.3 mM) was added. Then, the temperature was lowered to 15 °C and the cultures incubated overnight. At the point of induction, the cultures expressing the GRE activating enzymes were additionally sparged with argon for 20 min, and cysteine (2 mM) and sodium fumarate (20 mM) were added, before the cultures were sealed with screw-cap tops. These cultures were then transferred into the anoxic chamber that had been chilled to 15 °C and incubated overnight without shaking.

For the preparation of the GRE activating enzymes, all subsequent steps took place at 4 °C in an anoxic chamber unless otherwise specified. For the steps taking place outside of the anoxic chamber (centrifugation and incubation on a nutator), the containers were sealed with electrical tape before removing them from the chamber.

After overnight growth, the cells were harvested by centrifugation (6,770 × g, 10 min). The supernatant was decanted, and the cells were resuspended in 35 ml lysis buffer. For the GREs, the lysis buffer was 50 mM HEPES pH 7.5, 200 mM NaCl, 20 mM imidazole, for the GRE activating enzymes the same buffer supplemented with lysozyme (8 mg), half of an EDTA-free protease inhibitor tablet (Sigma S8830) and DTT (5 mM); for AdhE and DctP, 50 mM HEPES pH 8.0, 200 mM NaCl and 20 mM imidazole was used.

For the GREs, AdhE and DctP, the cells were lysed by two passages through an Avestin EmulsiFlex-C3 cell disruptor (35–70 MPa). The lysates were clarified by centrifugation (30 min, 20,000 × g). For the GRE activating enzymes, the cells were incubated with the lysozyme at 4 °C for 1 h. The cells were then lysed by sonication with a ½" horn (7 min total sonication, 10 s on, 30 s off, 25% amplitude) in a cold water bath. The dark gray solution was transferred into a fresh 50 ml plug-seal conical vial that was sealed with electrical tape, and the lysates were clarified by centrifugation (20,000 'x g, 30 min).

For protein purification, the supernatant was incubated with Ni-NTA resin (Qiagen) (6 ml for the GREs, 3 ml for the activating enzymes, 1 ml for AdhE and DctP) that had been equilibrated with 10 column volumes of the respective lysis buffer for 1 h. The resin was pelleted ( $500 \times g$ , 5 min), and the supernatant was decanted. The resin was resuspended in a minimal volume of lysis buffer and then transferred into a column, except for purification of the GREs, where the mixture was directly decanted into a column. After the flowthrough was collected, the resin was washed with 50 ml lysis buffer (10 mL for AdhE and DctP). The proteins were eluted by sequential washes with elution buffer (50 mM HEPES pH 7.5, 200 mM NaCl, 250 mM imidazole, pH 8.0 for the acetaldehyde dehydrogenase); for the GREs, this was four steps with 6 ml each, for the activating enzymes three steps of 4 ml, and for AdhE four steps of 1 ml. SDS-PAGE was used to identify the fractions containing the proteins and their purity.

Purified proteins were loaded into a dialysis cassette of an appropriate size; for GREs, the dialysis cutoff was 20 kDa MWCO, and 10 kDa for activating enzymes, AdhE and DctP. The proteins were dialyzed three times against 1.3 L dialysis buffer (50 mM HEPES pH 7.5, 50 mM NaCl, 10% (v/v) glycerol) for two 2 h steps and one overnight step; for AdhE and DctP, one of the 2 h steps was omitted.

In order to render the GREs anoxic, the dialyzed protein solution was concentrated *via* repeated spins in a 20 mL 30 kDa centrifuge filter ( $3,220 \times g$ , 10–20 min spins) until a volume of 5 ml was reached. Thereafter, degassing was accomplished by 12 cycles of a short vacuum pull followed by refilling with argon, then a 5 min pull of vacuum and a 5 min refill with argon; the entire process was repeated two times. Then the flasks were sealed and transferred into the anoxic chamber (97% N<sub>2</sub>/3% H<sub>2</sub>). Finally, all proteins were aliquoted into 200  $\mu$ L portions in cryovials fitted with an O-ring, flash frozen in liquid N<sub>2</sub>, and stored at -80°C. The cryovials with GREs and activating enzymes were sealed in anoxic Hungate tubes before freezing.

#### In vitro assays for recombinant Tpa and SarD

Enzyme assays were conducted in 50 mM Tris-HCl buffer at a pH of 9.0 containing 5 mM taurine, 5 mM sodium pyruvate, and 0.1 mM pyridoxal-5-phosphate. Typically, 50  $\mu$ g/mL Tpa and 25  $\mu$ g/mL SarD were used in an assay, and SarD and 2 mM NADH were added to the reactions after 90 minutes. Samples taken for HPLC were mixed with acetonitrile (HPLC grade) in a ratio of 7:3 immediately after sampling and stored at -20°C until analysis.

For separation of taurine, isethionate, sulfoacetaldehyde, alanine, pyruvate, NAD<sup>+</sup>, NADH, sulfate and sulfite, the HPLC-DAD-ELSD system (see above) fitted with the hydrophilic interaction liquid chromatography column (ZIC-HILIC, see above) was used as follows: acetonitrile as the eluent A, and 0.1 M ammonium acetate buffer (pH 7.0) containing 10% acetonitrile as the eluent B; total flow rate 0.3 mL/min. The elution gradient was: from 90% eluent A to 75% in 20 minutes; from 75% to 65% in 10 minutes; plateau at 65% A for 10 minutes. Under these conditions, pyruvate eluted at 6.6 min, isethionate at 11.5 min, alanine at 20.6 min, NADH at 26.6 min, and NAD<sup>+</sup> at 28.7 min. Sulfoacetaldehyde eluted only poorly separated in between 5–16 min retention time, and taurine eluted at 19.5 min but co-eluted with the peaks for Tris and sodium.

For HPLC with ESI-MS-MS detection, an Agilent 1100 HPLC system fitted with the same chromatography system was connected to a ThermoFisher LCQ ion trap mass spectrometer. The fragmentation spectra for each analyte were recorded from the total ion counts (TIC) with the following ranges (exact mass of the [M-H]<sup>-</sup> ion as well as the mass determined in the MS tuning step in brackets): taurine (*m/z* = 124.01/124.20): 124–125; sulfoacetaldehyde (*m/z* = 122.98/123.20): 123–124; isethionate (*m/z* = 124.99/125.20): 125–126; alanine (*m/z* = 89.05 for the zwitter ion): 88–90.

For the kinetic measurement of SarD, the oxidation of NADH was measured spectrophotometrically as the decrease of absorbance recorded at 365 nm for 1 min. The reaction mixture (1 ml) contained 50 mM Tris-HCl (pH 9.5), 0.128 mg recombinant protein, 1 mM NADH and 0.02–0.6 mM sulfoacetaldehyde-bisulfite adduct at room temperature. The reactions were started by addition of sulfoacetaldehyde. Each concentration point was measured in triplicate. The mean of the calculated specific activity was plotted against the sulfoacetaldehyde concentration and the data points were fitted to the Michaelis-Menten steady-state equation ( $k_{\text{obs}} = k_{\text{cat}}^* [\text{S}] / (K_m + [\text{S}])$ ) in Origin 8.0.

#### In vitro activation of GREs and glycyl radical detection and quantification by electron paramagnetic resonance (EPR) spectroscopy

The GRE was activated in an anoxic chamber by incubating activating enzyme (80 µM), GRE (40 µM), acriflavine (100 µM), SAM (1 mM), and bicine (50 mM pH 7.5) in reaction buffer (50 mM HEPES pH 7.5, 50 mM NaCl) at 25 °C for 2 h under ambient light, in a 250 µl scale for EPR spectroscopy.

The entire activation mixture was then loaded into a J. Young EPR tube (4 mm outer diameter and 8" length, from Wilmad Lab-Glass), sealed, removed from the anoxic chamber,

and slowly frozen in liquid N<sub>2</sub>. Perpendicular mode X-band EPR spectra were recorded on a Bruker ElexSysE500 EPR instrument equipped with a quartz finger dewar (Wilmad Lab-Glass) for acquiring spectra at 77 K with liquid N<sub>2</sub>. The samples were acquired with the following parameters: microwave frequency: 9.45 GHz; power: 20 µW (40 dB attenuation); center field: 3350 Gauss; sweep width: 200 Gauss; conversion time: 20.48 ms; modulation gain: 60 dB modulation gain for samples; 30 dB for external standards; time constant: 20.48 ms; modulation amplitude: 4 G; modulation frequency: 100 kHz. Normalization due to differences in modulation gain were automatically performed by the spectrometer. Typically, only a single scan was recorded to minimize any disruption due to bubbling from the liquid N<sub>2</sub>. The field was calibrated by using an external standard of bisdiphenylene-β-phenylallyl (BDPA) with g = 2.0026. An external standard of Frémy salt was prepared by dissolving K<sub>2</sub>(SO<sub>3</sub>)<sub>2</sub>NO in anoxic 0.5 M KHCO<sub>3</sub> and diluting the standard to ~0.5 mM. The concentration of the standard was more precisely ascertained by measuring its absorbance at 248 nm ( $\varepsilon = 1,690 \text{ M}^{-1} \text{ cm}^{-1}$ ) using a NanoDrop 2000 UV-Vis Spectrophotometer. The double integral of the Frémy salt standard was calculated on the EPR spectrometer and then used to determine the concentrations of each of the protein samples. The EPR spectra from the activation mixtures were simulated using EasySpin in MatLab using the genetic algorithm followed by the Levenberg/Marquardt algorithm after sufficient optimization. These simulations yielded the g-value, the hyperfine coupling constant, and the linewidth associated with the GRE signal.

### Enzyme assays with activated GREs

The GRE was first activated as described above for EPR spectroscopy. Activated GRE (1 µM) was then added to reaction buffer (50 mM HEPES pH 7.5, 50 mM NaCl) in a 50 µl, 250 µl or 500 µl scale, as specified in the following sections, and the reaction initiated by addition of isethionate. If appropriate, reaction buffer containing yeast alcohol dehydrogenase (8 µM) and NADH (3 mM) was used, and then activated GRE and isethionate was added. In the coupled assay with yeast alcohol dehydrogenase, acetaldehyde is reduced to ethanol, which allows for monitoring the GRE reactions spectrophotometrically *via* the NADH conversion (see below). Further, without including these components, sulfite and acetaldehyde condense to form 1-hydroxyethanesulfonate, which can be indistinguishable from isethionate by LC-MS. Aerobic control reactions were first removed from the anoxic chamber and gently aerated by pipetting, prior to mixing with the isethionate.

For monitoring isethionate consumption by HPLC-MS in reactions mixtures in a 500 µl scale with 2 mM isethionate, and in the presence of yeast alcohol dehydrogenase and NADH (see above), 50 µl aliquots were withdrawn at intervals and quenched with 50 µl acetonitrile in the anoxic chamber. The samples were centrifuged (16,100 x g, 10 min, 4 °C) and the supernatant was diluted into 90% acetonitrile and then analyzed under chromatographic conditions as described in the following: a ZIC-HILIC column (100 x 2.1 mm, 3.5 µm, 200 Å) was used; eluent A was 10 mM ammonium acetate in H<sub>2</sub>O and eluent B was acetonitrile; flow rate was 0.4 mL/min; the gradient was started at 90% B, decreased to 65% B over 5 min, ramped down to 35% B over 1 min, held at 35% B for 2 min, increased to 90% B over 2 min, and reequilibrated at 90% B for 4 min. Single ion monitoring was used to record the abundance of the [M-H]<sup>-</sup> charge state of isethionate (125.1 m/z, 0.5 m/z span, 50 ms dwell); the capillary temperature was 275 °C, the capillary voltage was 140 V, the source voltage offset was 20 V, the source voltage span was 20 V, the source gas temperature was 200 °C, and the ESI voltage was 2500 V.

For sulfite quantification and testing of the substrate range, reactions mixtures in a 50 µl scale in the presence of yeast alcohol dehydrogenase and NADH (see above) were incubated with 10 mM isethionate, ethanesulfonate, sulfoacetate, 3-sulfolactate, sulfopyruvate, taurine, hypotaurine or L-cysteine sulfinic acid, and transferred after 1 h out of the anoxic chamber and derivatized according to a modified procedure that was previously reported (Akasaka, Matsuda *et al.* 1990). A 100 ml solution of 0.3 M boric acid, 0.3 M KCl, and 0.02 M Na<sub>2</sub>-EDTA was mixed with a 50 ml solution of 0.3 M Na<sub>2</sub>CO<sub>3</sub> and 0.02 M Na<sub>2</sub>-EDTA to adjust the solution of the mixture to pH 8.8. 150 µl of this solution was added to each reaction, followed by 50 µl of an acetone solution containing NAM (0.1% w/v). Freshly prepared sodium sulfite standards were derivatized at the same time. The reactions were incubated at 37 °C for 2 h, and then transferred to a UV-transparent 96-well plate. The fluorescence intensity was recorded using a Spectramax i3 Plate Reader. The excitation wavelength was 362 nm (9 nm bandwidth); the emission wavelength was 436 nm (15 nm bandwidth). The photomultiplier setting set to “low” and 2 flashes per read were used.

For acetaldehyde quantification, reactions in a 50µl scale with 10 mM isethionate were transferred after 1 h out of the anoxic chamber and quenched by addition of 50 µl of derivatization solution (3.8 mg DNPH dissolved in 3 ml acetonitrile and acidified with 7.5 µl 85% H<sub>3</sub>PO<sub>4</sub>). Acetaldehyde standards in reaction buffer were derivatized at the same time. The samples were incubated in the dark for 1 h at room temperature, centrifuged (16,100 x g, 10 min), and then held at 10 °C until analysis was carried out (<24 h). HPLC analysis was used to detect the DNPH-derivatized acetaldehyde, when separated using a Dikma C<sub>18</sub>

Inspire (50 x 4.6 mm, 5 µm) column. Eluent A was 0.1% formic acid in H<sub>2</sub>O and eluent B 100% acetonitrile, and the flow rate was 1.0 mL/min. The gradient was started at 20% B, was held at 20% B for 1 min, ramped to 80% B over 1.5 min, held at 80% B for 0.5 min, decreased to 20% B over 1 min, and reequilibrated at 20% B for 2 min. The absorption at 360 nm was monitored. 5 µL of sample was injected.

For the spectrophotometrically coupled GRE assay for kinetics determination, activated GRE (0.1 µM) was mixed with yeast alcohol dehydrogenase (2 µM) and NADH (200 µM) on a 200 µL scale in a 96 well plate. The reactions were initiated by addition of isethionate (1, 2, 5, 10, 20, 30, 40 or 50 mM), and the plate was loaded into a plate reader set to 27 °C. These reactions were repeated in quadruplicate. The pathlength-corrected absorbance at 340 nm was recorded every 10 s for up to 5 min. The rate of NADH disappearance was assumed to correlate 1:1 with acetaldehyde production. The initial rate of product formation was then normalized for the amount of active enzyme in solution. The observed rate constant was fit to the standard Michaelis-Menten steady-state equation ( $k_{obs} = k_{cat}^* [S]/(K_m + [S])$ ) in Graphpad Prism.

For the coupled GRE assay with the potential substrates 2-mercaptopethanesulfonate (coenzyme M), 2-hydroxyethylphosphonate (2-HEP), 2,3-dihydroxypropanesulfonate (DHPS), 3-sulfolactate, choline, and S-1,2-propanediol the GRE was first activated as described above. Then, on a 200 µL scale, activated GRE (0.1 µM for choline or S-1,2-propanediol and 0.5 µM for all other potential substrates) was mixed with NADH (200 µM) and an alcohol dehydrogenase (2 µM) that would reduce the predicted organic product: this was yeast alcohol dehydrogenase for coenzyme M, 2-HEP, choline, and S-1,2-propanediol (the predicted organic product would be acetaldehyde for all except S-1,2-propanediol which would yield propionaldehyde), glycerol dehydrogenase from *Cellulomonas* sp. for DHPS (the predicted organic product would be hydroxyacetone, which glycerol dehydrogenase has activity towards) and L-lactate dehydrogenase from rabbit muscle for 3-sulfolactate (the predicted organic product would be pyruvate). The reactions were initiated by addition of the substrates, and the plate was loaded into a plate reader set to 30 °C (for choline and S-1,2-propanediol) or 22 °C (all other substrate analogs). The pathlength-corrected absorbance at 340 nm was recorded every 10 s for up to 5 min.

#### Characterization of the recombinant acetaldehyde dehydrogenase AdhE

Recombinant and purified AdhE (10 µM) was incubated with CoASH (500 µM), NAD<sup>+</sup> or NADP<sup>+</sup> (1 mM), and acetaldehyde (10 mM) in reaction buffer (50 mM HEPES pH 8.0, 50 mM NaCl) on a 200 µL scale at 22 °C, with addition of the acetaldehyde last to initiate the

reaction. The pathlength-corrected absorption at 340 nm was recorded every 30 s for 15 min. No reaction was observed when the reaction was run at pH 7.5; presumably the catalytic active site cysteine is protonated at this lower pH and, hence, AdhE is unable to initiate attack on the aldehyde. Addition of unactivated GRE did not stimulate formation of NADH. The reactions were quenched by addition of acetonitrile (100  $\mu$ L) to each reaction. 200  $\mu$ L of each sample was transferred to an Eppendorf tube, and the precipitated proteins were pelleted by centrifugation (16,100 g, 10 min, 4 °C). 100  $\mu$ L of each tube was then transferred into an LC-MS vial.

For detection of CoASH and acetyl-CoA, 5  $\mu$ L of each sample was injected onto the Sequent ZIC-HILIC column (see above). Eluent A was 20 mM ammonium acetate pH 8.0, and eluent B was acetonitrile. The flow rate for the column was 0.4 mL/min, and the column was started at 100% B which was decreased linearly to 0% B over 10 min, held at 0% B for 2 min, increased to 100% B over 2 min, and held at 100% B for 6 min. The absorbance at 260 nm was recorded with a 4 nm bandwidth. For MS analysis, single ion monitoring of the [M-2H]<sup>2-</sup> charge state for acetyl CoA (403.6 *m/z*) and CoASH (382.5 *m/z*) were recorded with a 50 ms dwell time and a 0.5 *m/z* span. The MS settings were: capillary temperature, 275 °C; capillary voltage, 180 V; voltage offset, 20 V; voltage span, 0 V; source gas temperature, 150 °C; ESI voltage, 2500 V.

#### Determination of DctP ligand specificity and binding constant

For determining the ligand specificity of *D. desulfuricans* DSM642 DctP, the protein (10  $\mu$ M) was incubated with or without ligand (10 mM) and 5x SYPRO Orange in 50 mM HEPES pH 7.5, 50 mM NaCl on a 20  $\mu$ L scale (in quadruplicates) in a bright white 96 well real-time PCR plate. The plate was loaded into a BioRad CFX 96 RT-PCR instrument. The plate was heated at 25 °C for 1 min, and the fluorescence was recorded. The temperature was increased by 1 °C per minute with a fluorescence reading recorded at the end of each minute until 95 °C had been reached. The fluorescence setting used was the “FRET” setting with an opaque plate setting. Ligands tested included isethionate, hypotaurine, taurine, sulfite, sulfoacetaldehyde (protected as the bisulfite adduct), sulfopyruvate, 3-sulfolactate, sulfoacetate, ethylsulfonate, vinylsulfonate, 1-hydroxyethanesulfonate, 2,3-dihydroxypropanesulfonate, 2-hydroxyethylphosphonate, and *L*-cysteine sulfinic acid. The melting temperature for each well was calculated by the instrument based on where the change in fluorescence as a function of temperature was maximal (*i.e.* d(Fluorescence)/dT was at its highest). The average melting temperature across four separate wells was subtracted from the average melting temperature across the apo wells to determine the  $\Delta T_m$ .

To determine the  $K_d$  of the *D. desulfuricans* DctP to isethionate, protein (10  $\mu$ M) was incubated in quadruplicate with isethionate (0, 0.01, 0.025, 0.05, 0.1, 0.25, 0.5, 0.75, 1, 2, 5, 10, 20, 30 or 50 mM) and 5x SYPRO Orange in 50 mM HEPES pH 7.5, 50 mM NaCl on a 20  $\mu$ L scale in a bright white 96 well rt PCR plate. The average melting temperature at each concentration was determined as above. The average  $\Delta T_m$  as a function of isethionate concentration was fit in GraphPad Prism 7 to the “One site — Specific binding” equation,  $\Delta T_m = \Delta T_{max} * [S] / (K_d + [S])$  (all abbreviations have the standard meaning).

#### Construction of multiple sequence alignments

Multiple sequence alignments were routinely constructed using the default parameters of Clustal Omega (<https://www.ebi.ac.uk/Tools/msa/clustalo/>) with a Pearson/FASTA output format, and the results were visualized in Geneious 8.1 (Biomatters Ltd).

#### Bioinformatic identification of putative sulfoacetaldehyde reductases

The distribution of the sulfoacetaldehyde reductase was examined by using the *B. wadsworthia* sequence as the query for a BLAST search in the NCBI non-redundant protein database (September 7, 2017). Authentic acetaldehyde dehydrogenases, such as CutO from the choline utilization cluster, exhibit only modest sequence identity to SarD (33% ID/E-55). To identify putative SarD homologs, we gathered only the sequences that exhibited substantially more homology than that relationship (27 sequences in total; the least similar sequence was 39% ID/5E-90 to the query sequence). The primary sequences of these proteins and several experimentally verified alcohol dehydrogenases were aligned as outlined above.

The putative metal-binding residues within all proteins (36 proteins in total, 9 of verified function including *B. wadsworthia* SarD, and 27 of completely uncharacterized function) are completely conserved (Asp193, His197, His262, and His276, numbering according to *B. wadsworthia* SarD), supporting the annotation of these sequences as group(III) alcohol dehydrogenases. Thr266 in *B. wadsworthia* SarD is aligned with His267 in FucO from *E. coli*; in the latter protein, this residue is hypothesized to be critical for interacting with, and determining the, substrate specificity of the protein (Obradors, Cabiscol *et al.* 1998; Montella, Bellsolell *et al.* 2005). The other 10 proteins that have a threonine at this position in the multiple sequence alignment are the most closely-related 10 proteins by sequence identity/E-score, ranging from 61%-100% ID (E-167 to under E-200). The next most similar proteins are <50% ID to the query sequence (>E-127) and contain a methionine or tyrosine at this position. By contrast, proteins other than FucO that reduce acetaldehyde or propionaldehyde

also have an essential histidine at this position. Based on the residue identity of position 267 and the large discontinuity in sequence identity percentage, we believe there were only 10 other sulfoacetaldehyde reductases in the NCBI non-redundant protein database.

A homology model of the *B. wadsworthia* SarD was generated using the MPI Bioinformatics Toolkit (<https://toolkit.tuebingen.mpg.de/>). This protein was used as the query sequence for an HHpred search of the most recent PDB release (as of August 8, 2017), yielding a series of proteins with similarity scores of E-55 to E-61. The ten most similar, structurally-solved proteins were used as the templates for homology model construction with Modeller. The homology model, the crystal structure of 1,3-propanediol dehydrogenase from *K. pneumoniae* (PDB ID: 3BFJ) and the crystal structure of lactaldehyde reductase from *E. coli* (PDB ID: 1RRM) were visualized in Pymol. A structural alignment in Pymol indicated that T266 in SarD occupies the same site as the catalytically essential histidine in the other two proteins, again underscoring that likely only proteins that have a Thr in this position are authentic SarD homologs.

#### Bioinformatic compilation of strains containing a putative isethionate sulfite-lyase

The *B. wadsworthia* IsIA-GRE (GenBank accession, EFV43471) was used as the query sequence for a BLAST search of the NCBI non-redundant protein database (September 7, 2017). The 250 highest-scoring sequences were exported (down to ~35% ID/E-145 score). As many of these sequences are unlikely to be authentic isethionate sulfite-lyases, these sequences were then clustered into a sequence similarity network using Option C of the Enzyme Function Initiative's Enzyme Similarity Tool [EFI-EST; (Gerlt, Bouvier *et al.* 2015)]. The network was generated with a sequence length requirement of >750 amino acids and with an initial alignment score of E-200. The full network was downloaded, and the edge value was subsequently refined in Cytoscape 3.2 to 62% ID, as this edge value had previously been determined to be likely sufficient to separate proteins that catalyze distinct reactions into distinct sequence similarity clusters (Levin, Huang *et al.* 2017). The three confirmed isethionate sulfite-lyases (from *B. wadsworthia*, *D. desulfuricans*, and *D. alaskensis*) co-occurred in the same cluster with 115 GRE sequences, suggesting that this cluster encodes isethionate sulfite-lyases or other C–S bond cleaving GREs.

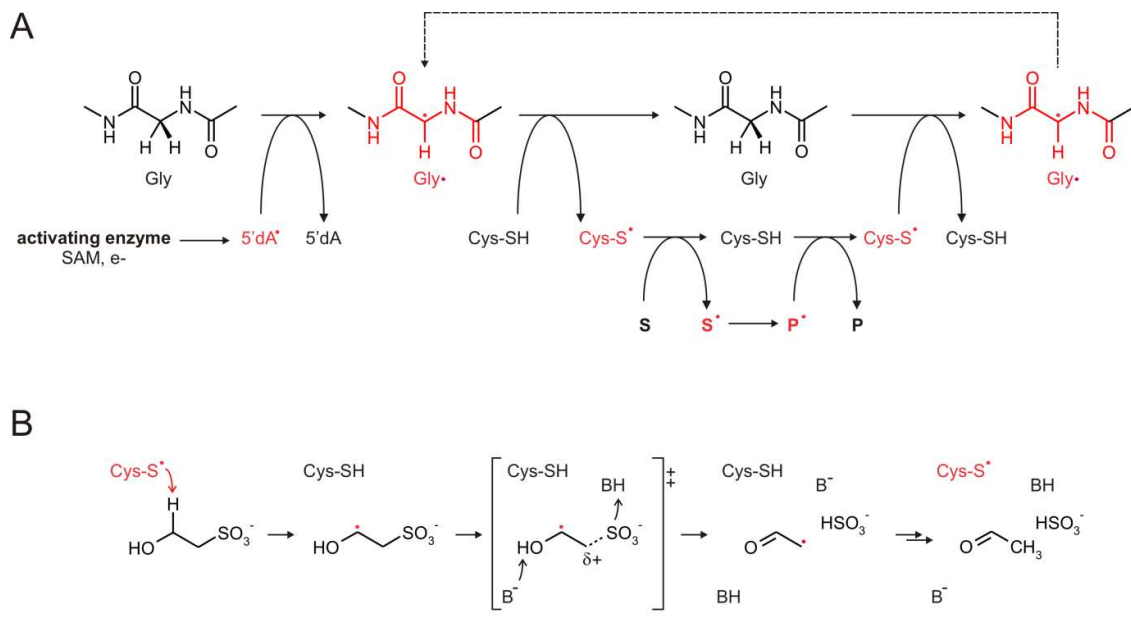
Multiple tactics were taken to validate this hypothesis. First, a multiple sequence alignment of these sequences was constructed as described above. A homology model was also constructed of the *B. wadsworthia* IsIA by using the MPI Bioinformatics Toolkit. The protein was used as the query sequence for an HHpred search of the most recent PDB release (as of January 3, 2017), yielding structurally characterized proteins with significant sequence

similarity. The top 8 returned hits had similarity scores more stringent than E-138 and represented all structurally-characterized GREs other than ribonucleotide reductase. These proteins were used as the templates for homology model construction with Modeller. The homology model, 1,2-propanediol dehydratase from *Roseburia inulinivorans* (PDB ID 1R9D), and choline trimethylamine-lyase from *D. alaskensis* (PDB ID 1FAU) were visualized in Pymol. The multiple sequence alignment and a structural alignment in Pymol indicated that residues Q193, C468, E470, and G805 in the *B. wadsworthia* IslA align with the residues critical for dehydration in 1,2-propanediol dehydratase or trimethylamine elimination in choline trimethylamine-lyase. These residues may thus dictate specificity for bisulfite elimination; notably, these four residues are universally conserved in the 115 putative isethionate sulfite-lyases. Other residues in the active site may be less than 100% conserved, and hence it will take more (structural) work to discern whether the proteins are likely isethionate sulfite-lyases or operate on other organosulfonates.

The organisms encoding these putative IslAs were tabulated. The number of sequenced strains within the NCBI non-redundant protein database in a given taxonomic class was estimated by searching the NCBI RefSeq assemblies using “Desulfovibrio[orgn] AND latest refseq[filter]”, where the “Desulfovibrio” portion was replaced with the taxon of interest. Thus, we could roughly calculate the proportion of strains within a given taxonomic order that encode an isethionate sulfite-lyase.

#### Construction of a phylogenetic tree for the glycyl radical enzymes

A literature search was performed to identify functionally-characterized GREs. The class II choline trimethylamine-lyase proteins contain an N-terminal extension of ~300 amino acids that hinders phylogenetic tree construction. The first ~300 amino acids from these sequences were trimmed, and then the proteins (27 sequences in total) were aligned using the Clustal Omega webserver tool with the output as “Clustal w/o numbers.” The file was visualized in Mega 7 and then this file was used to construct a maximum likelihood phylogenetic tree in Mega 7. A maximum likelihood Jones-Taylor-Thornton model with uniform rates for the substitution pattern with complete deletion of any gaps and 200 bootstraps was used to construct the phylogenetic tree. A total of 670 positions were used in the final analysis. The Newick tree files were uploaded to the Interactive Tree of Life webserver (<https://itol.embl.de/>) to annotate the trees (Letunic and Bork 2016).

Additional Figures and Tables

**Figure S3.1. Overview of glycyl radical enzyme (GRE) mechanism and of the desulfonation reaction for isethionate as catalyzed by IsIA.** (A) General mechanistic hypothesis for GRE function. The 5'deoxyadenosyl radical ( $5'dA^\bullet$ ) generated by a GRE-activating, radical SAM enzyme is used to install a protein-centered, stable glycyl radical ( $Gly^\bullet$ ) within the GRE. A thiyl radical ( $Cys-S^\bullet$ ) is proposed to serve as the active oxidant in all GREs and would be generated transiently within the active site. S, substrate; P, product. (B) The proposed reaction mechanism for isethionate desulfonation in analogy to the mechanisms proposed for 1,2-propanediol dehydratase (PD) and choline trimethylamine-lyase (CutC), which have been supported experimentally (Bodea, Funk *et al.* 2016; Levin and Balskus 2018). Following initial hydrogen abstraction by the thiyl radical to form an  $\alpha$ -hydroxyalkyl radical at C<sub>2</sub> of isethionate, IsIA may perform a spin-centered shift to eliminate the sulfonate group at C<sub>1</sub>.

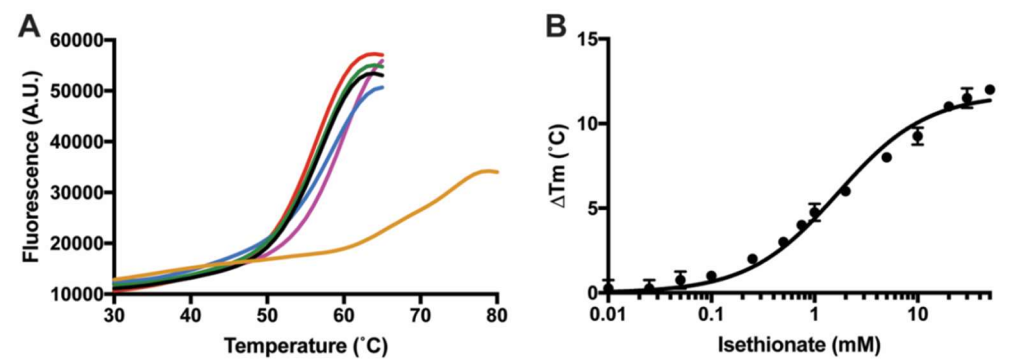


**Figure S3.2. Characterization of the DctP homolog of *D. desulfuricans* DSM642.** (A) Recombinantly produced and purified DctP solute-binding protein was incubated without ligand (red) or with isethionate (orange), taurine (black), hypotaurine (green), sulfoacetaldehyde (blue), or ethylsulfonate (purple) in the presence of SYPRO Orange, and the increase in fluorescence was monitored while the protein was heated. Only isethionate significantly stabilized the protein to thermal denaturation. Data is shown as the mean of four technical replicates; error bars are omitted for clarity. (B) The melting temperature as a function of isethionate concentration was determined, and the curve was fit to a single-site binding equation. The  $K_d$  was  $1.7 \pm 0.1$  mM. The melting temperature at each concentration represents the mean of four technical replicates; error bars indicate the standard deviation.

**Isethionate sulfite-lyase activity  
in cell-free extracts:**

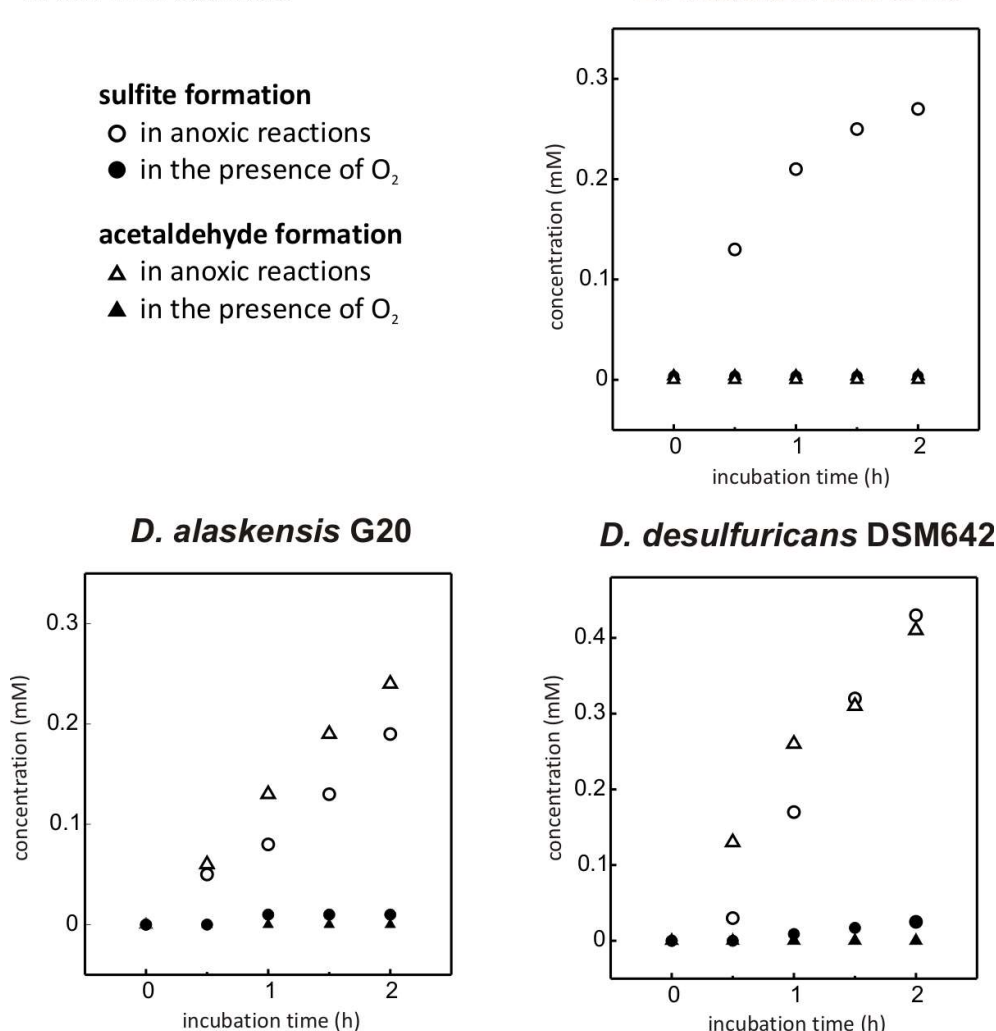


**Figure S3.3.** Experiments with cell-free extracts reveal a putative desulfonating GRE. Formation of sulfite and acetaldehyde from isethionate in strictly anoxic cell-free extracts prepared of taurine-grown *B. wadsworthia* and isethionate-grown *Desulfovibrio* spp. The specific activity of isethionate sulfite-lyase calculated from the rate of sulfite formation was 5.3 mU/mg for *B. wadsworthia* and 6.6 and 3.8 mU/mg for the *Desulfovibrio* sp. strains DSM642 and G20, respectively. The reaction mixtures contained cell-free extract, isethionate, SAM and Ti(III)-NTA in Tris-HCl buffer, pH 8.0. Shown are results of representative enzyme reactions replicated at least three times with material from independent growth experiments.

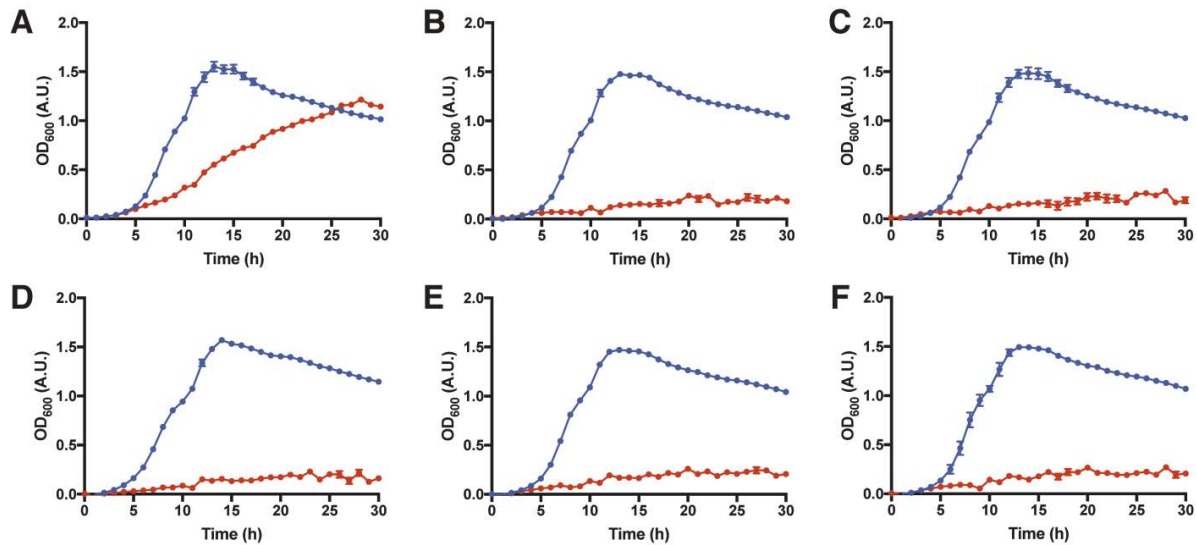


**Figure S3.4. Growth experiments with transposon mutants of *D. alaskensis* G20.** *D. alaskensis* without any mutation (wild-type) (**A**), or strains with a single disruption in the genes (Figure 3.1B) for a (**B**) putative regulator (IMG locus tag Dde\_1270), (**C**) GRE-activating enzyme (*islB*, Dde\_1272), (**D**) GRE (*islA*, Dde\_1273), and (**E**) fused DctMQ transporter (Dde\_1274) and (**F**) DctP solute-binding protein (Dde\_1275) of a TRAP-transport system. Cultures were grown in either lactate/sulfite medium (blue) or lactate/isethionate medium (red). The data shown is the mean of four replicate growth experiments  $\pm$  standard error of the mean after baseline correction.

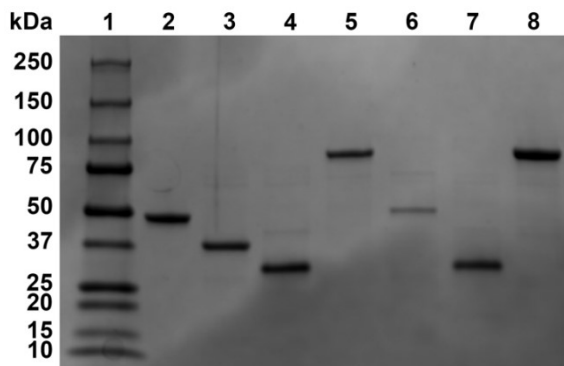


**Figure S3.5. SDS-PAGE of purified recombinant enzymes.** Precision Plus Protein™ All Blue Standards (lane 1), *B. wadsworthia* Tpa (51 kDa, lane 2), SarD (42 kDa, lane 3), IslB (36 kDa, lane 4), IslA (96 kDa, lane 5), AdhE (52 kDa, lane 6), and *D. desulfuricans* IslB (36 kDa, lane 7) and IslA (96 kDa, lane 8).

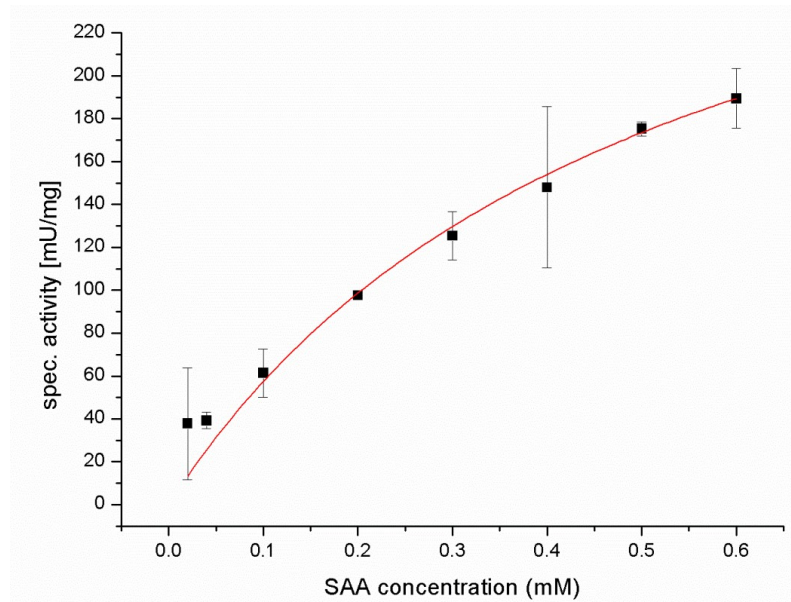


**Figure S3.6. Sulfoacetaldehyde reduction by SarD of *B. wadsworthia* 3.1.6.** The reactions contained 130 µg/mL recombinant SarD in 50 mM Tris-HCl buffer at pH 9.5. The sulfoacetaldehyde (SAA) concentration was varied between 0–0.6 mM in the presence of 1 mM NADH, and the initial rates of NADH consumption were determined spectrophotometrically as decrease of absorbance at 340 nm. The data shown represents the mean ± standard deviation of at least three technical replicates. The  $K_m^{\text{app}}$  was estimated at 0.51 mM ± 0.08 mM SAA and  $V_{\text{max}}$  at 351 ± 38 mU/mg protein (mean ± standard error of the mean).

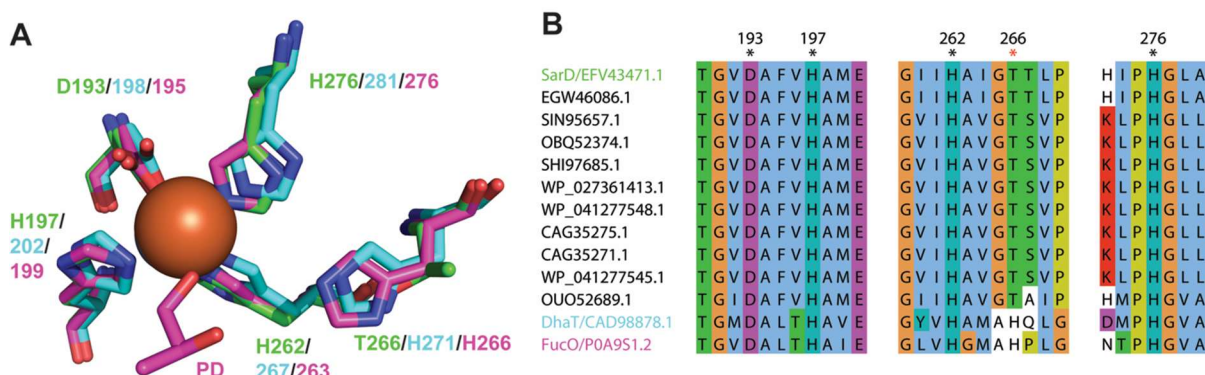


**Figure S3.7. Bioinformatic analysis of sulfoacetaldehyde reductase SarD.** **(A)** Structural alignment of the crystal structures of DhaT (blue), FucO (magenta), and the homology model of the characterized SarD of *B. wadsworthia* (green) generated with Modeller. SarD reduces sulfoacetaldehyde, DhaT reduces 3-hydroxypropionaldehyde, and FucO reduces lactaldehyde. FucO was crystallized in the presence of the product propanediol, which is abbreviated as “PD” in the figure. Labels are the same color as the structures. PDB IDs are 3BFJ for DhaT and 1RRM for FucO. **(B)** Multiple sequence alignment of putative sulfoacetaldehyde reductases compared to DhaT (blue), FucO (magenta), and SarD of *B. wadsworthia* (green label for the protein and black labels for the putative SarD homologs). The black asterisks indicate the metal-binding residues in DhaT and FucO; these residues are completely conserved in SarD of *Bilophila* and the putative SarDs. The catalytically essential His from DhaT and FucO is hypothesized to mediate a critical interaction with the substrate. In SarD and candidate SarD homologs, this residue is instead a Thr. Only the 10 most similar proteins contain a Thr at this position; other less similar proteins contain a variety of other residues at this position. The putative SarD sequences occur exclusively in the order Desulfobacterales and Desulfovibrionales of Deltaproteobacteria. The listed numbering is according to the *B. wadsworthia* SarD.

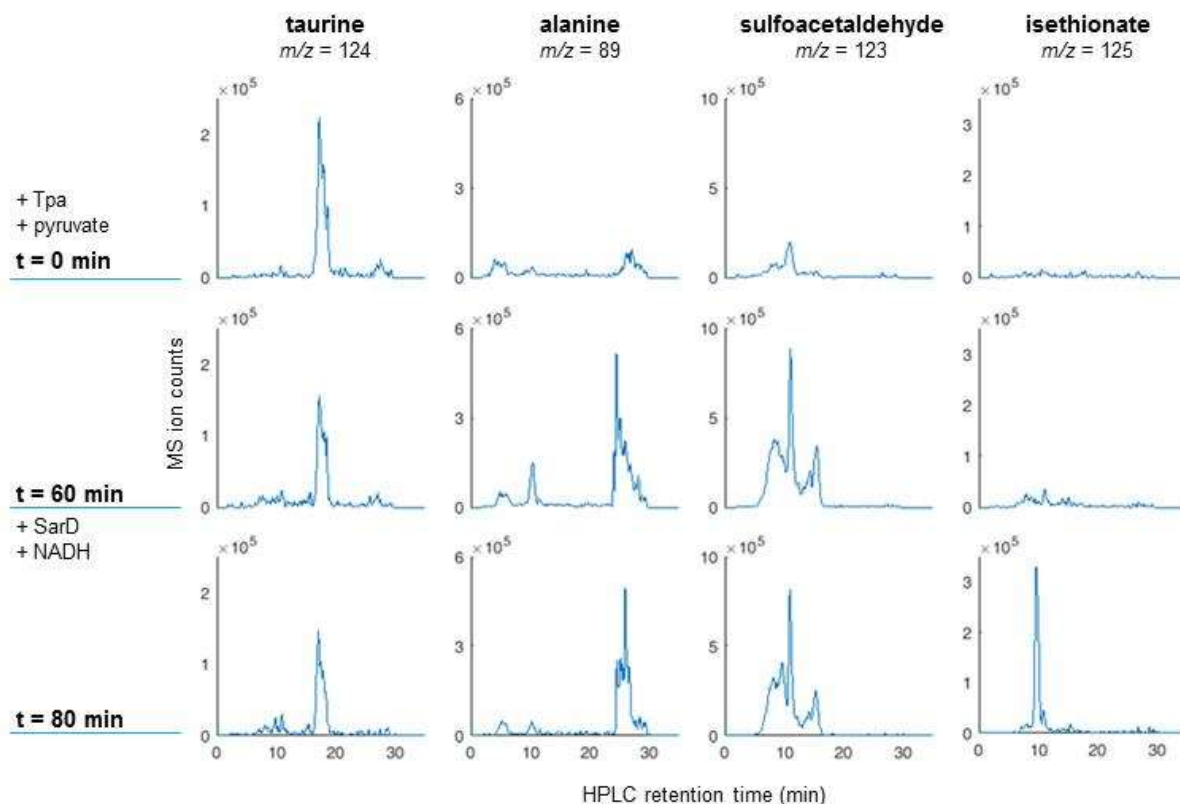


**Figure S3.8.** Transformation of taurine via sulfoacetaldehyde to isethionate by recombinantly produced and purified Tpa and SarD of *B. wadsworthia* 3.1.6. LC-MS ion-extract chromatograms are shown when scanning for [M-H]<sup>-</sup> ions of taurine, alanine, sulfoacetaldehyde and isethionate. Top row: sample taken from a reaction mixture containing taurine (5 mM), pyruvate (5 mM) and pyridoxal-5-phosphate (0.1 mM) directly after addition of recombinant Tpa (50 µg/ml). Middle row: sample taken after 60 min incubation time, directly before the addition of recombinant SarD (25 µg/ml) and NADH (1 mM). Bottom row: sample taken after 20 min additional incubation time. No formation of alanine, sulfoacetaldehyde and isethionate was detectable in absence of the cosubstrates pyruvate and NADH, respectively. Note that also the sulfoacetaldehyde standard was only poorly separated by hydrophilic interaction liquid chromatography (Material and Methods).

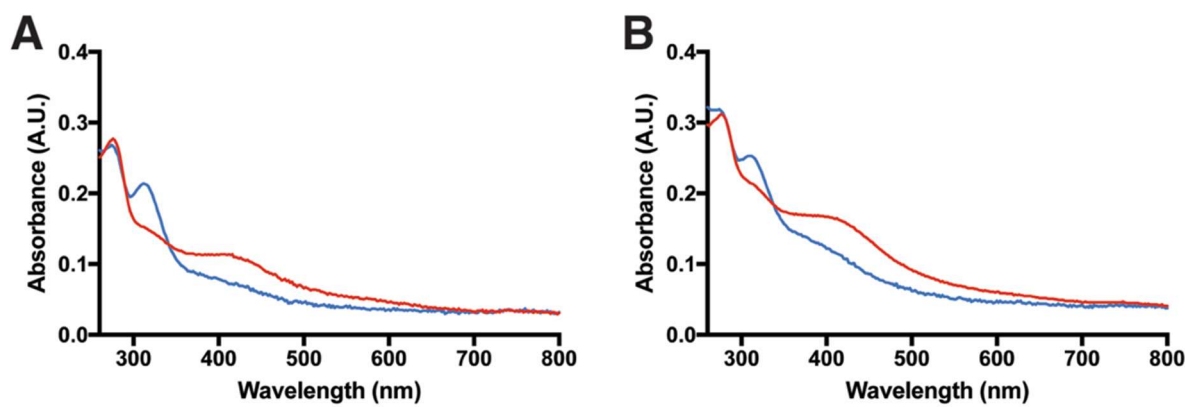


**Figure S3.9.** Reduction of IsIB of *B. wadsworthia* and *D. desulfuricans* as characterized by UV-visible spectroscopy. Recombinant and purified (A) *B. wadsworthia* or (B) *D. desulfuricans* GRE-activating enzyme (10 µM) was incubated without sodium dithionite (red line) or with sodium dithionite (50 µM, blue line). For both enzymes, sodium dithionite abated the broad absorption feature of the oxidized iron-sulfur chromophore at 410 nm.

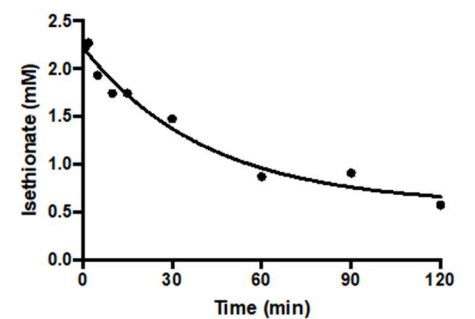


**Figure S3.10. Isethionate consumption by the *B. wadsworthia* IsIA.** Activated IsIA (1  $\mu$ M) was incubated with isethionate (2 mM) and at selected timepoints, a portion of the reaction was withdrawn and quenched for determination of the residual isethionate by LC-MS. The reaction shown was conducted in the presence of yeast alcohol dehydrogenase (8  $\mu$ M) and NADH (3 mM) in order to also monitor acetaldehyde formation as NADH consumption (see Material and Methods and Figure 3.3).

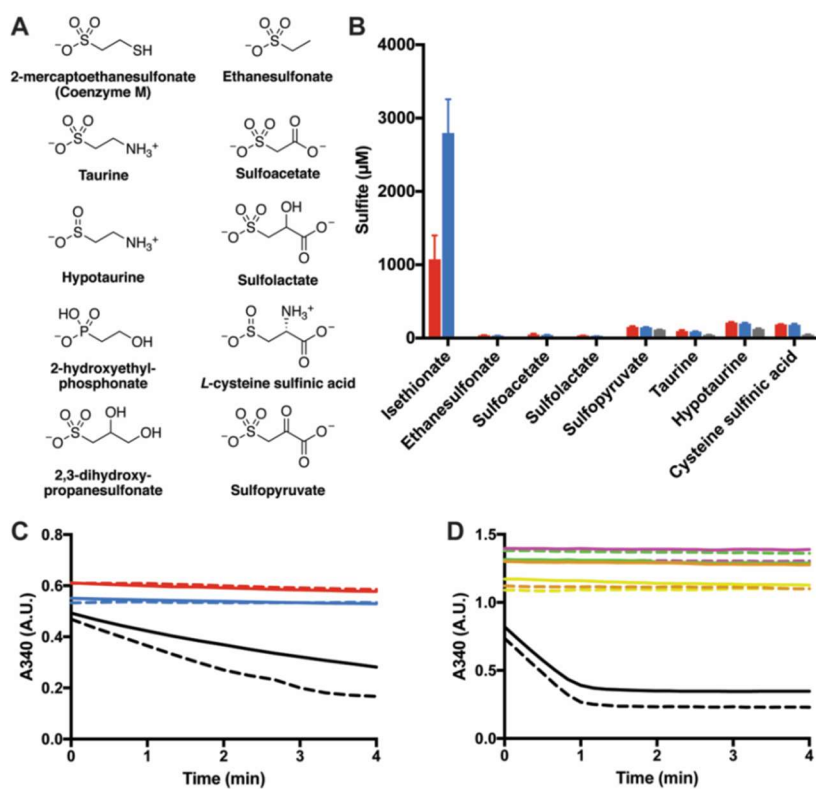


**Figure S3.11. Alternative substrates evaluated for turnover by IsIA.** (A) A range of substrates was evaluated for turnover either by quantifying sulfite formed or by monitoring the formation of the predicted carbon-containing product using a coupled enzyme assay. (B) For certain substrates, sulfite was quantified after incubations with the *B. wadsworthia* (red) or *D. desulfuricans* (blue) IsIA, or without enzyme (gray). Data is shown as the average  $\pm$  the standard deviation of three technical replicates. Activity was only observed with isethionate as substrate. (C) The *B. wadsworthia* (solid traces) or *D. desulfuricans* (dashed traces) IsIA were incubated with isethionate (black), taurine (blue), or hypotaurine (red) in the presence of yeast alcohol dehydrogenase and NADH; formation of aldehydes was monitored by the consumption of NADH. Activity was only observed with isethionate as the substrate. (D) The *B. wadsworthia* (solid traces) or *D. desulfuricans* IsIA (dashed traces) were incubated with isethionate (black), 2-mercaptopropanesulfonate (orange), 2-hydroxyethylphosphonate (yellow), 2,3-dihydroxypropanesulfonate (green), or 3-sulfolactate (magenta) in the presence of an appropriate alcohol dehydrogenase (see Material and Methods) and NADH. Activity was only observed with isethionate as substrate.

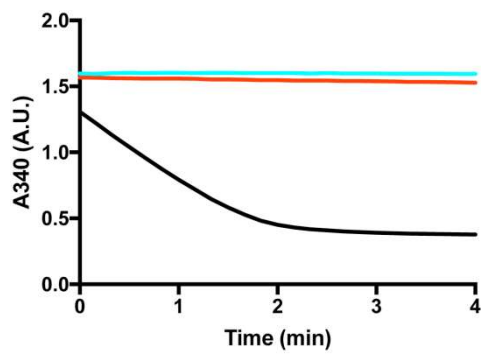


**Figure S3.12. Substrates of other GREs evaluated for turnover by IslA.** Choline is processed by the GRE choline trimethylamine-lyase (CutC) to generate acetaldehyde and trimethylamine; S-1,2-propanediol is turned over by the GRE S-1,2-propanediol dehydratase to yield propionaldehyde and H<sub>2</sub>O. Recombinant IslA from *B. wadsworthia* was incubated with 50 mM choline (cyan), 50 mM S-1,2-propanediol (red), or 50 mM isethionate as a positive control (black) in the presence of yeast alcohol dehydrogenase and NADH. Formation of aldehydes was monitored by consumption of NADH. Activity was only observed with isethionate as the substrate.

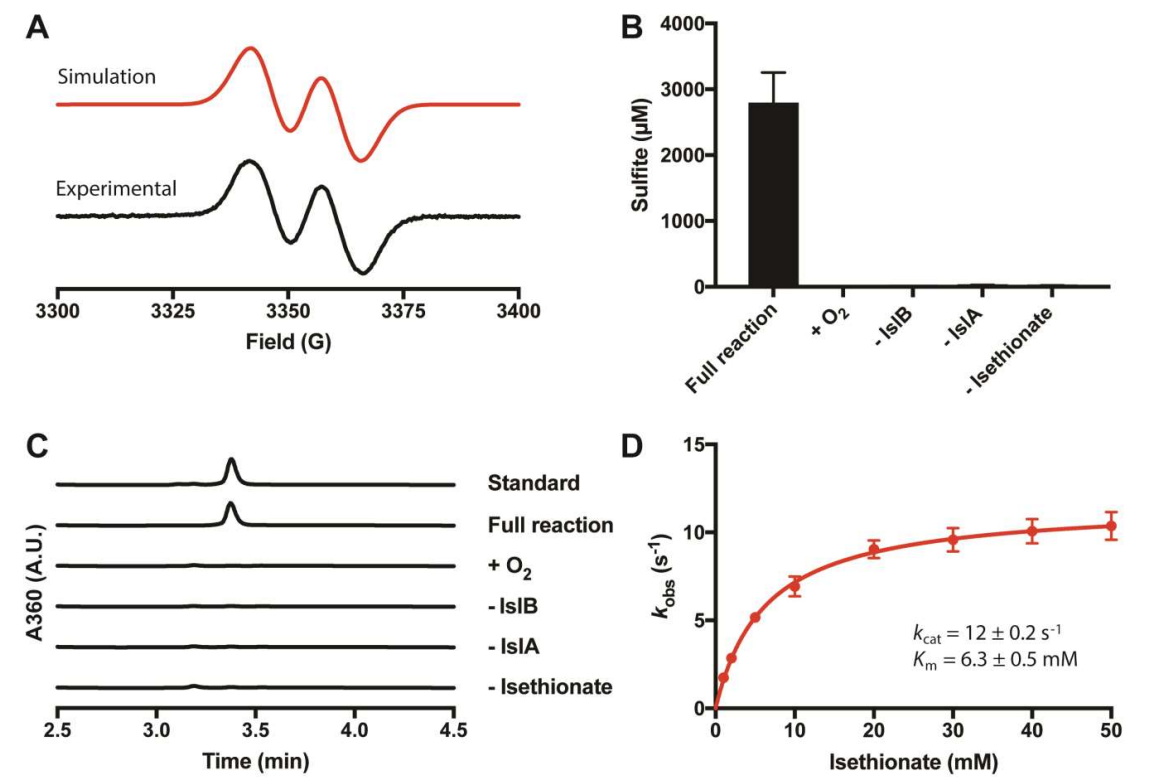


**Figure S3.13. Characterization of the *D. desulfuricans* IslA.** (A) A representative EPR spectrum of the recombinant and purified *D. desulfuricans* IslA is shown. Simulation of the data revealed that the radical has parameters similar to those previously reported for other GREs ( $g = 2.0034$ ,  $A = 1.4$  mT). Comparison to an external standard indicated that  $38 \pm 3\%$  of all GRE polypeptides are activated (mean  $\pm$  standard deviation of three replicates). (B) Sulfite and (C) acetaldehyde formation was observed only with activated IslA and isethionate as substrate under strictly anoxic reaction conditions, and no reaction was observed when oxygen was present or either the activase, GRE, or the substrate was omitted. (D) The Michaelis-Menten steady-state kinetics of isethionate cleavage were determined using the spectrophotometric coupled enzyme assay with yeast alcohol dehydrogenase and NADH. The  $k_{\text{cat}}$  was  $12 \pm 0.2 \text{ s}^{-1}$ , and the  $K_m$  was  $6.3 \pm 0.5 \text{ mM}$ . Data in this figure is shown as the mean  $\pm$  standard deviation of at least three technical replicates.

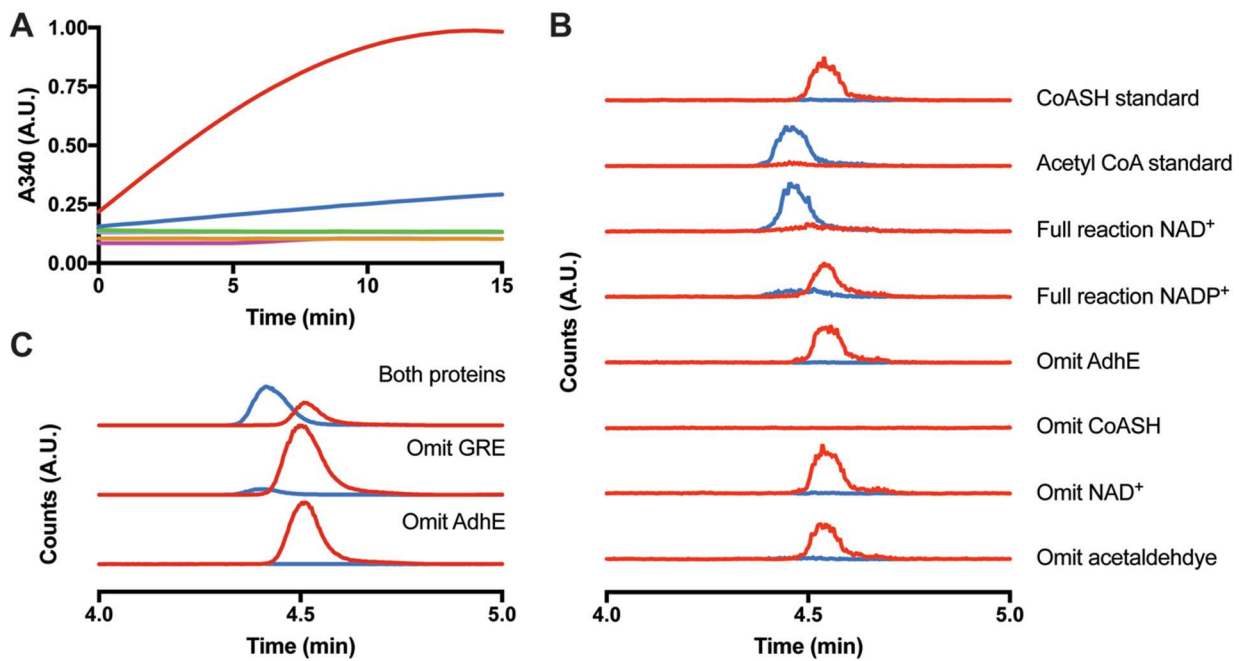


**Figure S3.14. Characterization of the *B. wadsworthia* CoA-acylating acetaldehyde dehydrogenase (AdhE).** (A) A spectrophotometric assay with recombinant and purified AdhE demonstrated conversion of NAD<sup>+</sup> to NADH in the presence of all reaction components (red) but strongly reduced conversion with NADP<sup>+</sup> instead of NAD<sup>+</sup> (blue). No conversion was observed when protein (orange), CoASH (green), NAD<sup>+</sup> (purple), or acetaldehyde (gray) was omitted. (B) The reactions from panel A were analyzed by LC-MS for the conversion of CoASH (red traces) to acetyl-CoA (blue traces). Robust conversion was only observed in the full reaction with NAD<sup>+</sup>. (C) Acetaldehyde was generated *in situ* by the action of the recombinant *Bilophila* sulfite-lyase when cleaving isethionate, and the AdhE converted CoASH (red traces) to acetyl CoA (blue traces), as determined by LC-MS analysis.

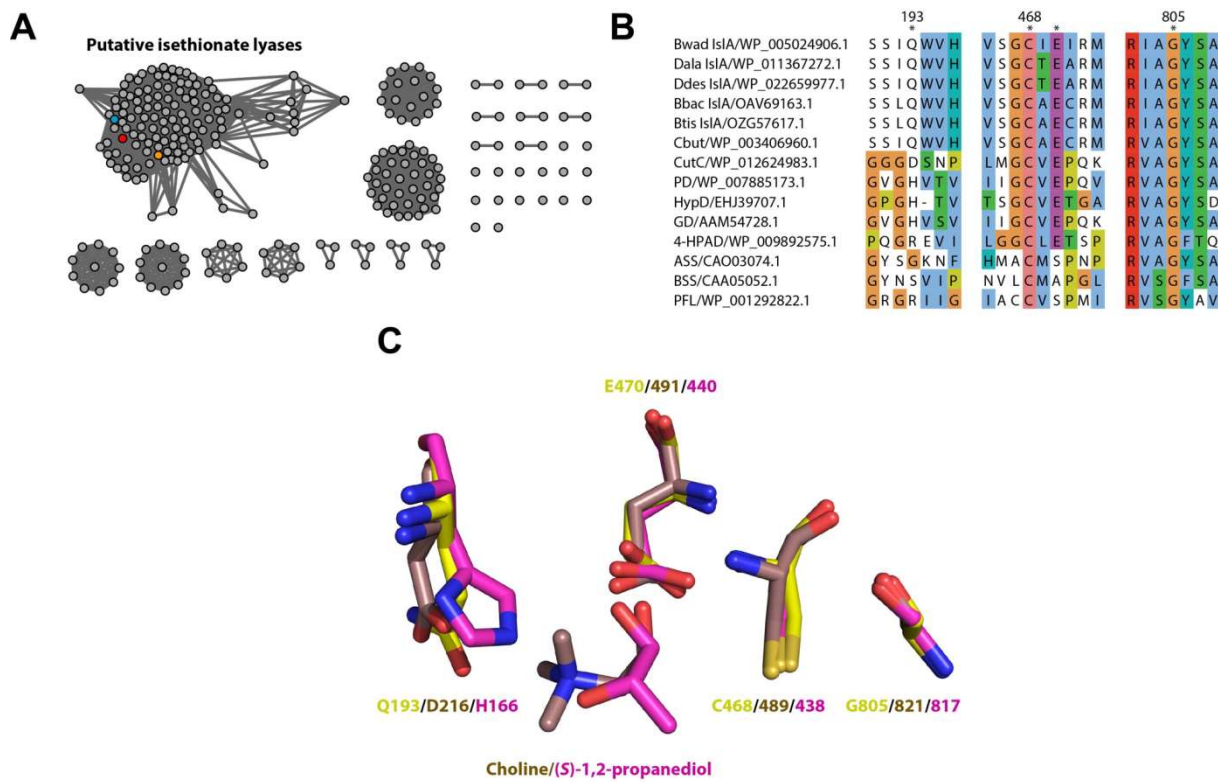


**Figure S3.15. Bioinformatic characterization of the isethionate sulfite-lyases.** (A) Sequence similarity network of the 250 sequences most similar to the *B. wadsworthia* isethionate sulfite-lyase (IsIA) amino acid sequence. The edge threshold was set to a minimum of 62% identity. At this edge value, the three IsIA characterized in this study occur in the same cluster. The node in red represents IsIA of *B. wadsworthia*, and blue IsIA of *D. desulfuricans*, orange IsIA of *D. alaskensis*, and gray uncharacterized proteins. (B) Multiple sequence alignment of selected GREs. The starred residues denote positions in CutC and PD that are critical for catalysis; numbering is according to *B. wadsworthia* IsIA. All sequences of characterized IsIAs conserve Q193, C468, E470, and G805, as well as all candidate IsIAs, for which three representative sequences from *Bacteriodales* bacterium (Bbac), *Bifidobacterium tissieri* (Btis) and *Clostridium butyricum* (Cbut) are shown. For a complete list of all 115 candidate IsIA or of other C-S bond cleaving GREs, see Table S3.1. (C) Alignment of the crystal structures of CutC (brown), PD (magenta), and the homology model of *B. wadsworthia* IsIA (yellow) generated with Modeller. In addition to the substrates of CutC and PD, choline and S-1,2-propanediol, respectively, the residues identified from panel B are also shown; labels are the same color as for the structures. The homology model suggests that Q193 of IsIA might facilitate elimination of sulfite in the same way as Asp216 does for trimethylamine in CutC and His166 does for water in PD. The importance of the residues in this position have been noted by others as predictive of the reactivity of the GRE (Backman, Funk et al. 2017). PDB IDs are 5FAU for CutC and 5I2G for PD.

**Table S3.1. List of predicted isethionate sulfite-lyases or other C-S bond cleaving GREs as retrieved from the non-redundant NCBI database at a threshold of 62% identity.**

Due to its size, Table S3.1 has been moved to the back of this thesis (pages 130ff.).

**Table S3.2. PCR Primers used**

<b>IMG locus tag (gene)</b>	<b>forward primer</b>	<b>reverse complements primer</b>
<b>HMPREF0179_02714 (<i>B. wadsworthia</i> SarD)</b>	<b>CGTCATATGACTTACGATAAA GCTGAATTGGTCG</b>	<b>ATTCTCGAGAGTCCCGATGC CTCCGGATGAAGG</b>
<b>HMPREF0179_02713 (<i>B. wadsworthia</i> Tpa)</b>	<b>CGTCATATGGCTTTGTGCAT TACACCGTC</b>	<b>ATTCTCGAGTTGTTCAGGGCT TTTCTTCGTTTT</b>
<b>pET28a / HMPREF0179_00639 (<i>B. wadsworthia</i> lsIA)</b>	<b>GCAGCGGCCTGGTGCCGCG CGGCAGCCATATGACTCAGG TAGCTGAAATCAAATC</b>	<b>GGATCTCAGTGGTGGTGGTG GTGGTGCTCGAGTTACATCT GGTCTGTGCCGGTACG</b>
<b>pET29b / HMPREF0179_00638 (<i>B. wadsworthia</i> lsIB)</b>	<b>GTTTAACTTAAGAAGGAGAT ATACATATGGGTCCTTGAA GATAGAAAAGG</b>	<b>GATCTCAGTGGTGGTGGTGG TGGTGCTCGAGTGAACATCTT TCTTCGTCACGGC</b>
<b>pET29b / HMPREF0179_00640 (<i>B. wadsworthia</i> AdhE)</b>	<b>GTTTAACTTAAGAAGGAGAT ATACATATGGACGTGCGCCA ACAAGACG</b>	<b>GATCTCAGTGGTGGTGGTGG TGGTGCTCGAGTGAACGAT GCGGAAGTTGTCC</b>
<b>pET28a / G449DRAFT_2761 (<i>D. desulfuricans</i> lsIA)</b>	<b>GCAGCGGCCTGGTGCCGCG CGGCAGCCATATGAGCACCA CCACTTGCAGATGCC</b>	<b>GGATCTCAGTGGTGGTGGTGG GTGGTGCTCGAGTTACATCA CGTCGTGTTCACTAC</b>
<b>pET29b / G449DRAFT_2762 (<i>D. desulfuricans</i> lsIB)</b>	<b>GTTTAACTTAAGAAGGAGAT ATACATATGTGCCTGGAAGAC AGCCAACAGC</b>	<b>GATCTCAGTGGTGGTGGTGG TGGTGCTCGAGTGAACGCG TACGCGGAGCCGATC</b>
<b><i>D. desulfuricans</i> DctP pET29b Fw</b>	<b>GTTTAACTTAAGAAGGAGAT ATACATATGAGGCCGTCCAG GTTTATG</b>	<b>GATCTCAGTGGTGGTGGTGG TGGTGCTCGAGCAGACTCTG CGTTGCAGCGATCAG</b>
<b>pRL27_IE_rev1</b>	<b>ACTGAGAAGCCCTAGAGCC</b>	
<b><i>D. alaskensis</i> Δ1270</b>	<b>CCACCATGCTTATTCTGGGT</b>	<b><i>D. alaskensis</i> Δ1270</b>
<b><i>D. alaskensis</i> Δ1272</b>	<b>GGCATTACCGAACCTGCTA</b>	<b><i>D. alaskensis</i> Δ1272</b>
<b><i>D. alaskensis</i> Δ1273</b>	<b>AGACATAGAAGAAGGCCGCA</b>	<b><i>D. alaskensis</i> Δ1273</b>
<b><i>D. alaskensis</i> Δ1274</b>	<b>CCTTCTACGGCCTCATCATC</b>	<b><i>D. alaskensis</i> Δ1274</b>
<b><i>D. alaskensis</i> Δ1275</b>	<b>CAGCAGGTGCATGCTGTAGT</b>	<b><i>D. alaskensis</i> Δ1275</b>

## **Chapter 4: Bacterial microcompartments as part of taurine metabolism in *Bilophila wadsworthia***

**Anna G. Burrichter<sup>1,2</sup>, Stefanie Dörr<sup>1</sup>, Paavo Bergmann<sup>3</sup>, Sebastian Haiß<sup>1</sup>, Anja Keller<sup>1,2</sup>  
David Schleheck<sup>1</sup>**

<sup>1</sup>Department of Biology, University of Konstanz, 78457 Konstanz, Germany

<sup>2</sup>Konstanz Research School Chemical Biology, University of Konstanz, 78457 Konstanz, Germany

<sup>3</sup>Electron Microscopy Centre, Department of Biology, University of Konstanz, 78457 Konstanz, Germany

### **Abstract**

*Bilophila wadsworthia*, a strictly anaerobic, sulfite-reducing bacterium of the family Desulfovibrionaceae, is a member of the human-gut microbial community and has been associated with the development of diseases such as appendicitis and colitis. *B. wadsworthia* is specialized on the utilization of organosulfonates, such as the dietary and host-derived taurine (2-aminoethanesulfonate), as sulfite donors for sulfite respiration. This process has been termed 'organosulfonate respiration' and produces harmful hydrogen sulfide ( $H_2S$ ). The taurine desulfonation pathway of *B. wadsworthia* was recently shown to involve a glycyl radical enzyme (GRE), isethionate sulfite-lyase (IslAB), which cleaves isethionate (2-hydroxyethanesulfonate) derived of taurine into acetaldehyde and sulfite. Here, we show that this reaction takes place isolated within bacterial microcompartments (BMCs). First, we confirmed an inducible production of BMCs during growth with taurine by proteomic, transcriptomic and electron microscopical analyses. Then, we isolated the BMCs from taurine-grown cells by density-gradient ultracentrifugation and analyzed their composition by proteomic analysis as well as by enzyme assays, which suggested that the GRE reaction and the further conversion of the acetaldehyde take place within the BMCs. Hence, we characterized a novel subclass of BMCs involved in the desulfonation of organosulfonates for microbial energy generation by sulfite respiration and, thus, provide more details also on the biomedically relevant microbial  $H_2S$  formation in the human gut.

## Introduction

*Bilophila wadsworthia* is an obligately anaerobic, sulfite-reducing bacterium and part of the normal human gut flora. It has also been associated with diseases such as abscesses, appendicitis or colitis (Baron, Summanen *et al.* 1989; Gibson, Cummings *et al.* 1991; Arzese, Mercuri *et al.* 1997; Baron 1997; Devkota, Wang *et al.* 2012) and therefore is classified as an opportunistic pathogen. *B. wadsworthia* uses taurine (2-aminoethanesulfonate) as well as isethionate (2-hydroxyethanesulfonate) as sources of sulfite as terminal electron acceptor in a process termed organosulfonate respiration (Peck, Denger *et al.* 2019) producing hydrogen sulfide ( $H_2S$ ) as end product (Laue, Denger *et al.* 1997). This bacterial degradation of organosulfonates is, next to the reduction of inorganic sulfate, an important source of  $H_2S$  in anoxic habitats such as the human gut.  $H_2S$  has previously been implicated as an important factor in the development of inflammatory bowel diseases such as colitis (Roediger, Moore *et al.* 1997; Levine, Ellis *et al.* 1998; Wallace 2010) and colon cancer (Carbonero, Benefiel *et al.* 2012). Its negative effect may be based on its destructive influence on the mucus barrier of the colon (Ijssennagger, Belzer *et al.* 2015; Ijssennagger, van der Meer *et al.* 2016) and its genotoxicity (Attene-Ramos, Wagner *et al.* 2006; Attene-Ramos, Wagner *et al.* 2007).

Taurine as substrate for *B. wadsworthia* can be part of the human diet, e.g. as a constituent of meat (Huxtable 1992; Rипps and Shen 2012) and energy drinks (Farag, Klikarova *et al.* 2019), while isethionate can be found in different kinds of seafood (Koechlin 1954; Holst, Nielsen *et al.* 1994). More importantly, taurine is produced by the human body for example as a conjugate for bile salts such as taurocholate (Spaeth and Schneider 1974; Brand, Jorning *et al.* 1998; Ridlon, Wolf *et al.* 2016); for an overview of its many other functions in the human body, see (Huxtable 1992; Rипps and Shen 2012). Both a diet rich in saturated fats stimulating bile salt production, including taurocholate, and a diet supplemented directly with taurocholate, can in mice lead to *B. wadsworthia* blooms and subsequent development of colitis (Devkota, Wang *et al.* 2012). The taurine catabolism of *B. wadsworthia* thus provides an intriguing link between dietary conditions, microbial  $H_2S$  production and disease development in animals and humans.

While *B. wadsworthia* produces  $H_2S$  from organosulfonates, it is unable to carry out reduction of inorganic sulfate (Laue, Denger *et al.* 1997). Its genome lacks the genes for sulfate adenylyltransferase (Sat) and adenosine 5'-phosphosulfate reductase (AprAB).

*B. wadsworthia* is thus unable to activate sulfate and reductively cleave adenosine 5'-phosphosulfate to sulfite and adenosine monophosphate. It does contain the genes for the subunits of the dissimilatory sulfite reductase complex (Dsr), enabling it to reduce sulfite released from organosulfonates (or free sulfite provided in the culture fluid) further to  $H_2S$ .

Previously, the complete degradation pathway of taurine (see Figure 4.1A) in *B. wadsworthia* was elucidated and shown to include a new class of glycyl radical enzymes (GREs) that is able to cleave the carbon-sulfur bond in isethionate (Peck, Denger *et al.* 2019; Xing, Wei *et al.* 2019). Until then, GREs were known to cleave C-C, C-O, and C-N bonds, so this novel GRE class significantly broadens the substrate spectrum and the range of metabolic pathways in which they can be employed.

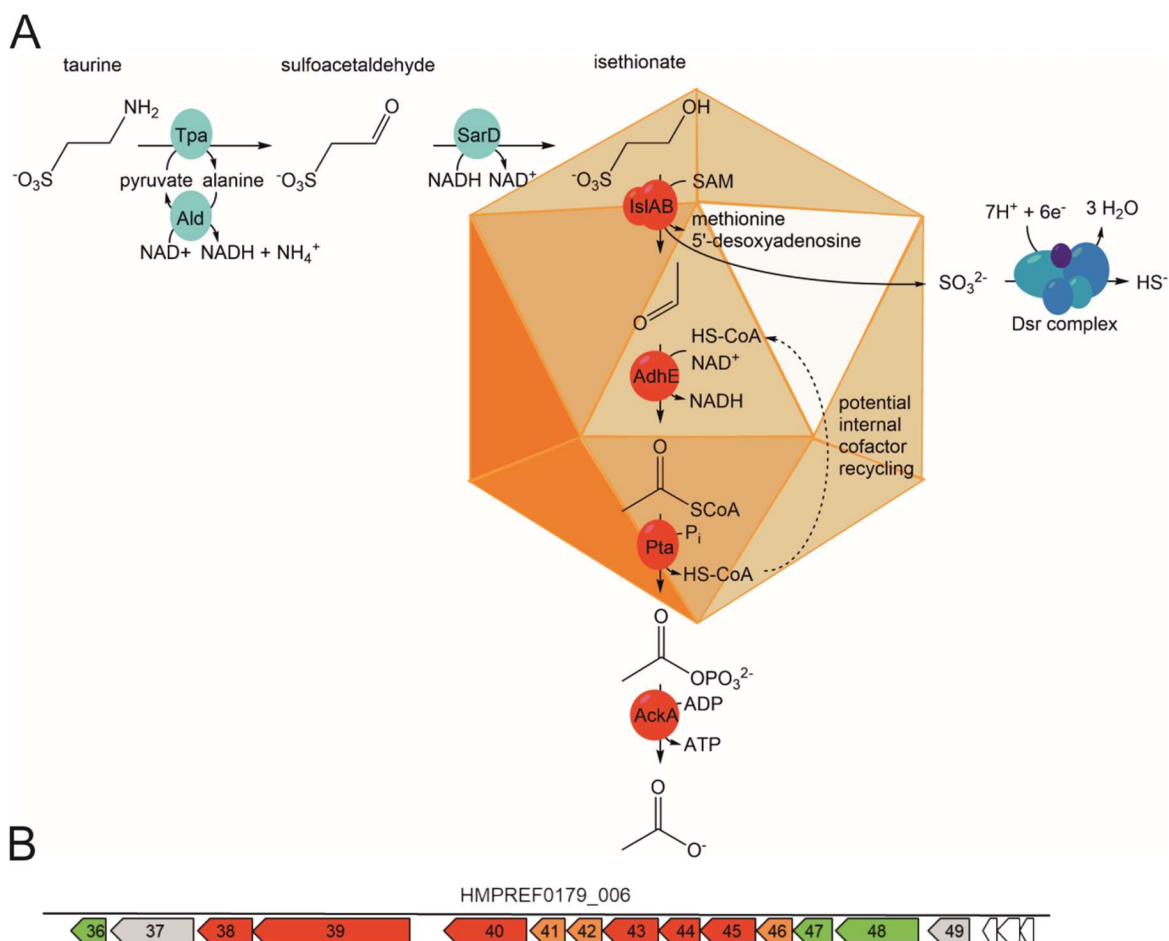


**Figure 4.1. Overview of the taurine degradation pathway in *B. wadsworthia* 3.1.6, as revealed previously (Peck, Denger *et al.* 2019), and of the containment of key enzymes of the pathway in bacterial microcompartments (BMCs), as inferred from the results of this study. (A)** Enzymatic reactions of the taurine degradation pathway via isethionate desulfonation by a glycyl radical enzyme (IslAB) and the subsequent conversion of the produced acetaldehyde to acetyl phosphate and of the produced sulfite to  $\text{H}_2\text{S}$ . Please note that  $\text{H}_2\text{S}$ ,  $\text{HS}^-$  and to a small extent  $\text{S}^{2-}$  are in equilibrium at physiological pH, but that  $\text{H}_2\text{S}$  will be used throughout this study to refer to all three species. Enzyme abbreviations used: Tpa, taurine:pyruvate aminotransferase; Ald, alanine dehydrogenase; SarD, sulfoacetaldehyde reductase; IslAB, isethionate-sulfite lyase; AdhE, acetylating acetaldehyde dehydrogenase; Pta, phosphotransacetylase; AckA, acetate kinase; Dsr, dissimilatory sulfite reductase. **(B)** The gene cluster in *B. wadsworthia* 3.1.6 encoding isethionate sulfite-lyase IslAB (IMG locus tags HMPREF0179\_00638 and \_00639) and BMC-associated proteins. The IMG locus tag prefix HMPREF0179\_ is omitted in the following and only gene numbers are used. Genes marked in red are genes for catabolic enzymes: 00640, acetylating acetaldehyde dehydrogenase gene; 00643, phosphotransacetylase gene; 00644, annotated to encode EutT, a cobalamin adenosyltransferase whose function is unclear (see main text); 00645, annotated to encode EutQ, a putative acetate kinase (Moore and Escalante-Semerena 2016). Genes marked in orange encode BMC shell proteins: 00641

and 00642 are annotated to encode EutN, a known BMC shell protein (Kofoid, Rappleye *et al.* 1999; Tanaka, Kerfeld *et al.* 2008); 00646, annotated to encode a BMC domain-containing CcmK-like shell protein (CcmK is a cyanobacterial carboxysome shell protein (Price, Howitt *et al.* 1993; Cai, Sutter *et al.* 2015). Genes marked in green may encode proteins that we suspect to be involved in maintaining the redox balance within the BMC (see Discussion); 00636, this gene is annotated to be a member of the uncharacterized TIGR04076 family; 00647, annotated to encode a CcmL/EutN protein, though BLAST search revealed it to be also similar to PduT, a shell protein from propanediol utilization microcompartments that contain 4Fe-4S cluster (Parsons, Dinesh *et al.* 2008; Crowley, Cascio *et al.* 2010; Pang, Warren *et al.* 2011) (see also Discussion); it will be shown as CcmL/PduT from here on for clarity; 00648, annotated to encode a  $\text{Na}^+$ -translocating ferredoxin:NAD $^+$  oxidoreductase (RnfC subunit), though based on its four protein family (pfam) domains, we conclude it to be a PduS homolog (see Discussion). The genes marked in gray are annotated as a transcriptional regulator gene (00637) and as a hypothetical protein gene (00649) with an amidohydrolase domain. All initial annotations were taken from the original IMG annotation for *Bilophila wadsworthia* 3.1.6.

In the *B. wadsworthia* catabolic pathway for taurine as electron acceptor (Figure 4.1A), taurine is first deaminated to sulfoacetaldehyde by a taurine:pyruvate aminotransferase (Tpa), which is then reduced to isethionate by a NADH-dependent sulfoacetaldehyde reductase (SarD). Isethionate is the substrate for the GRE isethionate-sulfite lyase (IsIA), which is activated by its activating enzyme IsIB using S-adenosylmethionine (SAM) as the initial radical donor. This radical-mediated cleavage reaction, which is extremely oxygen sensitive (Peck, Denger *et al.* 2019), results in the sulfonate group of isethionate being released as sulfite and of the carbon moiety as acetaldehyde. The sulfite is utilized as a terminal electron acceptor by the Dsr complex, producing  $\text{H}_2\text{S}$ . Notably, this choice of electron acceptor is beneficent in energetic terms compared to sulfate reduction, as it eliminates the investment of two ATP equivalents for the activation of sulfate (Peck, Denger *et al.* 2019). The acetaldehyde formed (Figure 4.1A) is oxidized by an acetylating aldehyde dehydrogenase (AdhE) to acetyl-CoA, converted to acetyl phosphate by a phosphotransacetylase (Pta) and finally to acetate after transfer of the phosphate to ADP to form one ATP by an acetate kinase (AckA); the acetate is excreted. As this pathway is not balanced in respect to electrons, an additional electron donor such as lactate, formate or hydrogen (da Silva, Venceslau *et al.* 2008) is necessary to provide electrons to the Dsr complex for respiration and energy conservation. Indeed, *B. wadsworthia* is able to use organosulfonates as terminal electron acceptors but not as sole substrates for fermentation (Laue, Denger *et al.* 1997; da Silva, Venceslau *et al.* 2008).

The genes for the taurine desulfonation pathway are encoded in two clusters that are regulated independently (Peck, Denger *et al.* 2019): one taurine-inducible cluster encoding for the enzymes for conversion of taurine to isethionate (*i.e.*, genes for Tpa, for a pyruvate-regenerating alanine dehydrogenase Ald and for SarD; not shown in Figure 4.1B) and a second, taurine- and isethionate-inducible gene cluster (shown in Figure 4.1B) comprising the genes for IsIA, IsIB and AdhE. Intriguingly, this second gene cluster contains also several genes that are predicted to encode for shell proteins of bacterial microcompartments (see

Figure 4.1B). Bacterial microcompartments (BMCs) are small (40–600 nm in diameter (Liberton, Austin *et al.* 2011; Erbilgin, McDonald *et al.* 2014; Kerfeld, Aussignargues *et al.* 2018) organelle-like compartments constructed entirely from protein that exist within the bacterial cytosol. Their function is to isolate reactions either to protect the cell from reactive or volatile intermediates, usually aldehydes, or to improve the efficiency of multistep pathways (Kerfeld, Aussignargues *et al.* 2018). BMCs have first been described in cyanobacteria, in which the CO<sub>2</sub>-fixing ribulose-1,5-bisphosphate carboxylase/oxygenase is contained within the so-called carboxysome (Shively, Ball *et al.* 1973; Codd and Marsden 1984; Tabita 1999; Cannon, Bradburne *et al.* 2001). Later, BMCs were described also in cells catabolizing ethanolamine (Stojiljkovic, Bäumler *et al.* 1995; Kofoid, Rappleye *et al.* 1999; Brinsmade, Paldon *et al.* 2005) or propanediol (Bobik, Havemann *et al.* 1999) by B<sub>12</sub>-dependent enzymes (Kerfeld, Heinhorst *et al.* 2010; Chowdhury, Sinha *et al.* 2014). These catabolic BMCs, also called metabolosomes, are typically defined by their signature enzymes, e.g choline-trimethylamine lyase or B<sub>12</sub>-dependent diol dehydratases. In addition to these aldehyde-forming signature enzymes, metabolosomes generally contain also an aldehyde dehydrogenase that further processes the aldehyde, an alcohol dehydrogenase and a phosphotransacetylase (Kerfeld, Aussignargues *et al.* 2018).

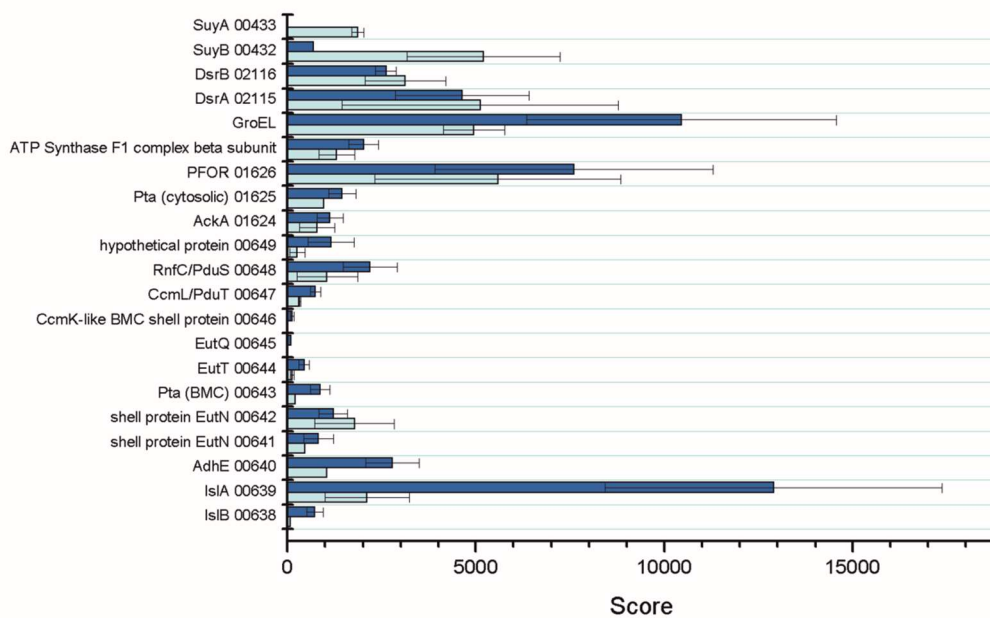
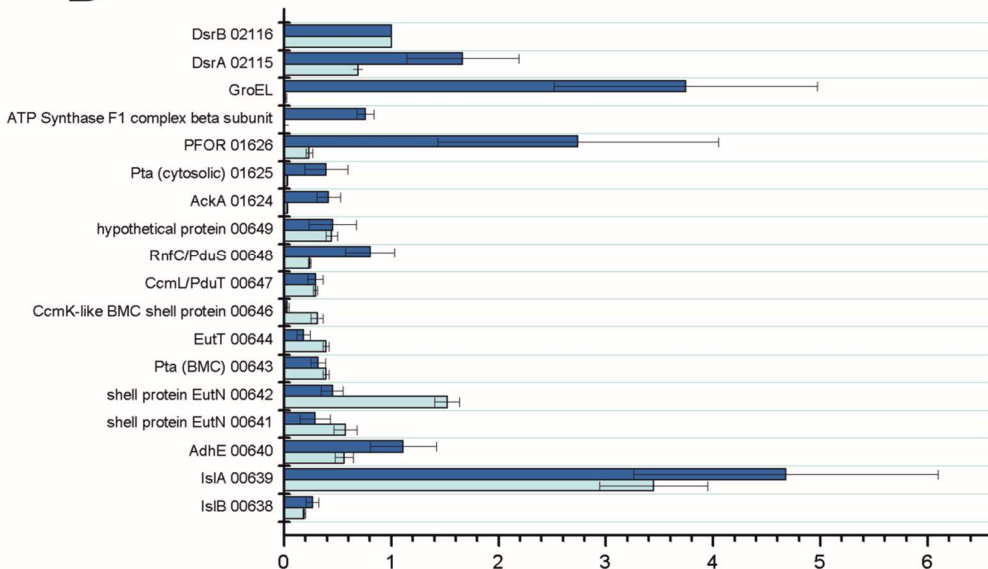
Glycyl radical enzymes (GREs) are the signature enzymes of a specific range of BMCs. The two well-defined examples are choline trimethylamine-lyase (CutC) in, for example, *Desulfovibrio desulfuricans* and *Escherichia coli* (Craciun and Balskus 2012; Herring, Harris *et al.* 2018) and B<sub>12</sub>-independent glycerol dehydratase in *Clostridium butyricum* (Raynaud, Sarçabal *et al.* 2003; O'Brien, Raynaud *et al.* 2004; Petit, LaTouf *et al.* 2013; Schindel, Karty *et al.* 2018). Other classes of potentially GRE-containing BMCs were defined by genomic analyses (Axen, Erbilgin *et al.* 2014; Zarzycki, Erbilgin *et al.* 2015), but as of yet their function has not been revealed. For *B. wadsworthia*, it can be assumed that the radical cleavage of isethionate by the extremely oxygen-sensitive IslAB, which leads in addition to the formation of two toxic products, sulfite and acetaldehyde, may as well be isolated within a BMC, given the putative genes for BMC shell proteins co-located in the same gene cluster as the genes for IslAB and AdhE (see Figure 4.1B).

In this study, we confirmed the formation of BMCs during the degradation of taurine and investigated their association with the enzymes of the taurine desulfonation pathway. The BMCs were isolated using a gradient centrifugation method and their protein constituents were examined using peptide mass fingerprinting as well as specific enzyme assays.

## **Results**

### **Total transcriptomic and proteomic analysis confirms expression of microcompartment shell proteins during metabolism of taurine**

The *B. wadsworthia* gene cluster encoding for IslAB and AdhE also contains four predicted genes annotated as BMC shell protein genes (Figure 4.1B). We therefore assumed that *B. wadsworthia* may form BMCs during degradation of taurine and isethionate. This assumption was supported by proteomic and transcriptomic analyses, which both showed strong, inducible expression of IslAB and AdhE together with the shell proteins 00641 and 00642 (both annotated as EutN), 00646 (CcmK-like shell protein) and 00647 (CcmL/PduT) on both the transcriptional (Figure 4.2A) and the protein (Figure 4.2B) level during growth with taurine as electron acceptor (IMG locus tag prefix HMPREF0179\_ is omitted and only gene numbers are used).

**A****B**

**Figure 4.2. Total transcriptomic and proteomic analysis of *B. wadsworthia* in respect to the expression of BMC proteins.** **(A)** Comparison of proteomic (dark blue) and transcriptomic (light blue) data for *B. wadsworthia* grown each with taurine as electron acceptor. The transcription rate for shell proteins such as 00641, 00642 (both annotated as EutN) and 00646 (CcmK-like shell protein) appeared to be higher compared to the proteomic scores detected, however this observation may be attributed to technical constraints since small proteins are detected with lower score by total proteomic analysis than larger proteins. **(B)** Total proteomic data for *B. wadsworthia* grown with taurine (dark blue) or sulfolactate (light blue) as electron acceptors. Taurine respiration led to a much higher expression of IslAB, as well as of other BMC-associated proteins from the gene cluster represented in Figure 4.1B, such as the shell proteins EutN (00641), a CcmK-like shell protein (00646) and CcmL/PduT (00647). Sulfolactate respiration on the other hand led to much higher expression of SuyAB in comparison to taurine respiration.

Confirmation of BMC production by transmission electron microscopy.

Ultramicrosections of *B. wadsworthia* cells grown with taurine as electron acceptor were examined for the formation of BMCs by transmission electron microscopy (TEM) in comparison to sulfolactate-grown cells (Figure 4.3AB). Multiple polyhedral structures of 50–100 nm in diameter were visible in each taurine-grown cell (see Figure 4.3A), which were identified as BMCs by comparing them to structures in *Desulfovibrio alaskensis* cells grown with choline, hence, conditions that are known to lead to BMC formation in this organism (Craciun, Marks *et al.* 2014). These structures were not found in *B. wadsworthia* cells grown with sulfolactate (Figure 4.3B) as negative control: sulfolactate is desulfonated by sulfolactate sulfite-lyase (SuyAB) (Rein, Gueta *et al.* 2005; Burrichter, Denger *et al.* 2018) in *B. wadsworthia* (see also Figure 4.2B for proteomic data showing the expression of SuyAB during growth with sulfolactate as electron acceptor), and SuyAB is not oxygen sensitive and produces sulfite and non-toxic pyruvate. Further, the gene cluster for SuyAB does not contain BMC shell protein genes (Figure S4.1), and the shell proteins encoded in the IsIAB gene cluster are expressed only at low level during growth with sulfolactate as electron acceptor (Figure 4.2B).

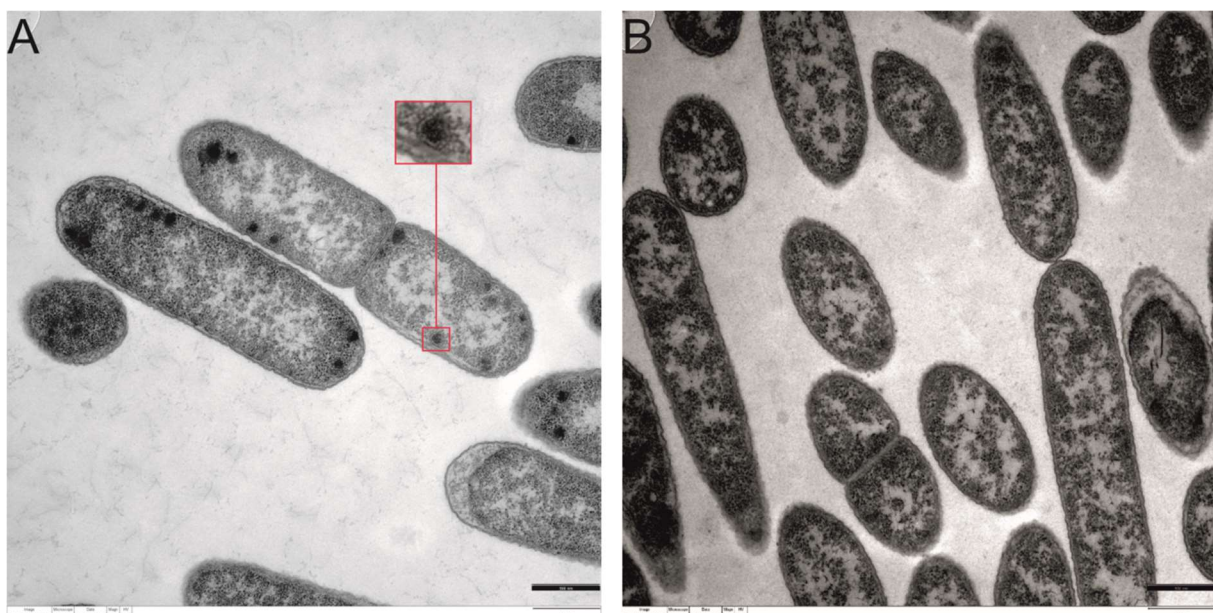


**Figure 4.3.** Transmission electron microscopy (TEM) images of negatively-stained ultramicrosections of *B. wadsworthia* cells grown with taurine (A) or sulfolactate as electron acceptor (B). Polyhedral structures characteristic of BMCs were observed specifically for taurine-grown cells. Scale bars: 500 nm.

### Purification of microcompartments by sucrose gradient centrifugation

The BMCs were purified using a sucrose gradient centrifugation which separated the cell components according to their sedimentation speed in sucrose solutions of increasing viscosity. In total, ten clearly distinguishable bands were observed after the centrifugation and collected separately into ten fractions, as shown in Figure 4.4A. From SDS-PAGE analysis of these fractions, a preliminary distribution was attributed (Figure 4.4C): the distinctive band of the glycyl radical enzyme IsIA (93.9 kDa molecular weight) was found in fractions 3–5 and was strongest in fraction 4, suggesting that this was the main fraction in which also intact BMCs may be contained; this band (marked by the upper red box in Figure 4.4C) was confirmed to represent IsIA by peptide mass-fingerprinting. Fraction 2 contained a high concentration of protein, no distinct 94 kDa band but many other bands, and we attributed this to be the fraction containing predominantly soluble cytosolic proteins. Fraction 4 was analyzed by TEM and found to contain microcompartment-like structures (Figure 4.4B), thus confirming that fraction 4 indeed contained intact BMCs.

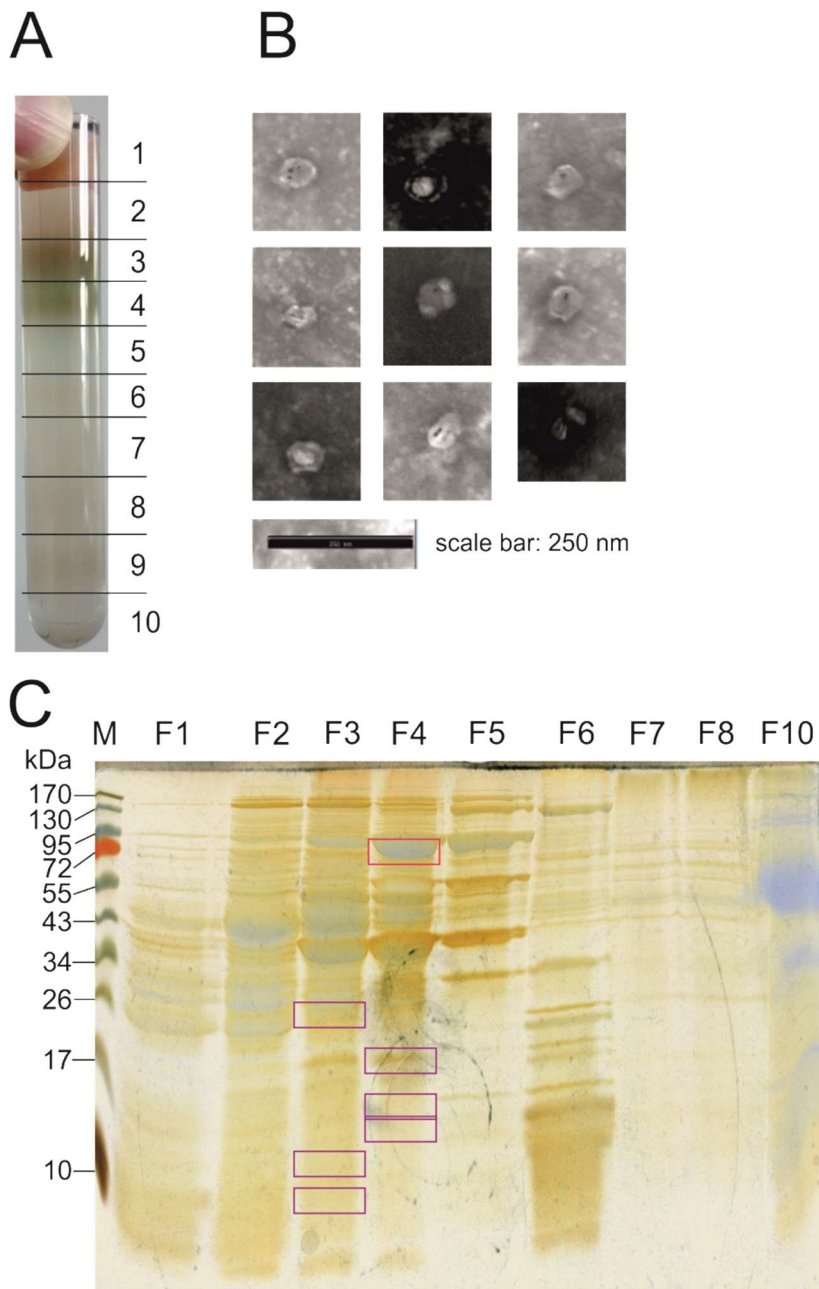


**Figure 4.4. Sucrose gradient purification of BMCs from cell-free extracts of *B. wadsworthia*.** (A) Sucrose gradient after centrifugation. The numbers mark the fractions that were collected from each gradient. Fraction 2 contained most of the cytosolic proteins as well as broken BMCs while fraction 4 contained intact BMCs (see Figure 4.4C). Fraction 10 refers to the centrifugation pellet that was resuspended in 500 µl of the sucrose solution directly above it. (B) Negative-stained TEM image of purified BMCs as obtained from fraction 4. (C) Coomassie- and silver-stained SDS-PAGE of gradient fractions (F) (excluding fraction 9 which contained very low amounts of protein). The upper red box marks the size of the signature enzyme of the BMC, the glycyl radical enzyme IslA at approx. 94 kDa molecular weight. The strong band above it at 130 kDa corresponds to the size of pyruvate:ferredoxin oxidoreductase (PFOR) (130.0 kDa). The strong band at 40 kDa molecular weight corresponds to SarD (40.8 kDa) and Ald (39.8 kDa). The lower purple boxes mark bands that have been identified by proteomic analysis as BMC shell proteins (see main text and Table S4.2). M, protein molecular weight markers.

### Proteomic analysis of the microcompartment-containing fractions

To specifically identify shell proteins of the BMCs, SDS-PAGE bands from fractions 3 and 4 in the size range of predicted shell proteins were submitted to peptide mass-fingerprinting (Table S4.2). Bands in both fractions contained proteins annotated as, among others, EutN (00642 and 00647), a known shell protein from ethanolamine utilization BMCs. Especially fraction 4 also contained fragments of ribosomal proteins. We concluded that ribosome complexes, in size and composition comparable to small BMCs, may have been co-purified with the BMCs with our method.

To gain further insight into the content of these structures, fractions 2–5 were also submitted to total proteomic analysis. Figure 4.5 shows the distribution of taurine degradation enzymes throughout the central gradient fractions 2–5 (light blue: fraction 2, medium light blue: fraction 3, medium dark blue: fraction 4, dark blue: fraction 5).

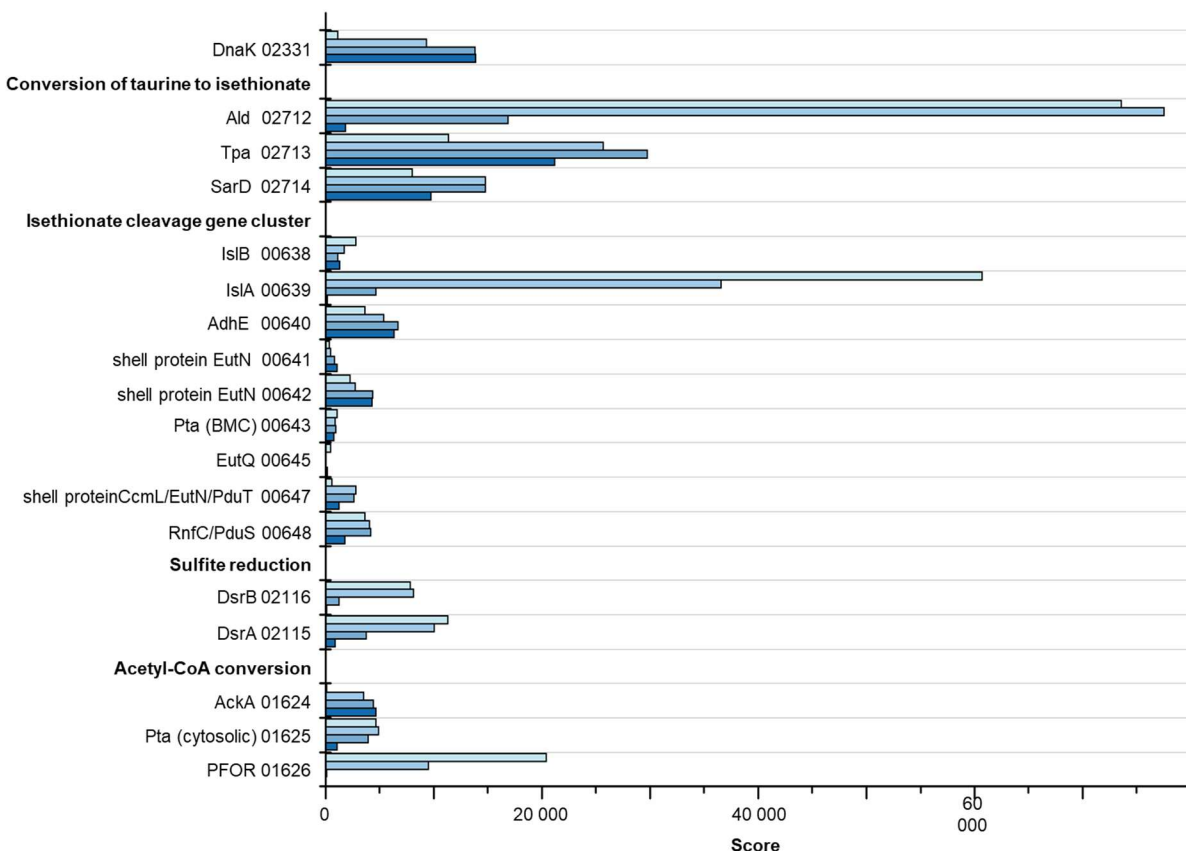


**Figure 4.5. Total proteomic analysis of purified sucrose gradient fractions.** Light blue, fraction 2; medium light blue, fraction 3; medium dark blue, fraction 4; dark blue, fraction 5. The protein description includes a shortened IMG locus tag which can be completed by adding the shown number to the following prefix: HMPREF0179\_.

The cytosolic chaperone DnaK was used as a control; it was evenly distributed in fractions 2 and 3 and its content declined in fractions 4 and 5, as expected for a cytosolic protein.

The BMC signature enzyme IsIAB showed a contrasting distribution: it was mostly found in fractions 4 and 5, where intact BMCs were expected given the results described above. This further confirmed that these were the BMC-containing fractions. Interestingly, a similar distribution pattern was observed for the components of sulfite reductase DsrAB, for pyruvate:ferredoxin oxidoreductase and to a certain extent also for aldehyde dehydrogenase, phosphotransacetylase, the RnfC subunit oxidoreductase and alanine dehydrogenase. Shell proteins, acetate kinase, and the enzymes converting taurine to isethionate (Tpa, SarD) are more evenly distributed between the cytosolic fraction and the intermediate fraction 3 and in a lower amount in fraction 4. The shell proteins detected in the soluble protein fractions are likely part of fractured BMCs, and since the monomeric shell proteins are very small (10–20 kDa), they may have ended up in the higher gradient fractions.

### Enzyme activities

We also measured specific activities of the taurine pathway enzymes associated to the different gradient fractions, relating the activities observed to the proteins identified in these fractions by proteomic analysis (Figure 4.6).

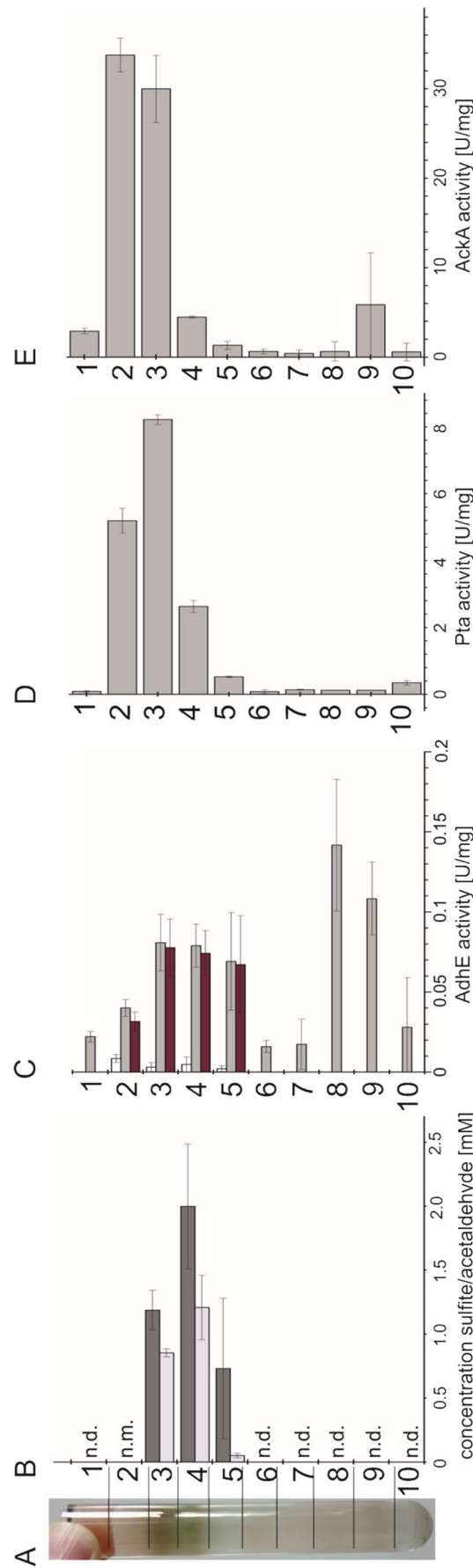


**Figure 4.6. Specific enzyme activities detected in the different sucrose gradient fractions (B-E) in comparison to an image of a representative gradient.** (A) Protein concentrations in the fractions 7–9 were typically very low and, thus, apparently high specific enzyme activities detected were considered unreliable. Specific protein activities are given as Units per mg of total protein. (B) IsAB activity represented as sulfite (light gray bars) and acetaldehyde (dark gray bars) production in anoxic incubations with isethionate and S-adenosylmethionine. n.d.: not determined; n.m.: not measurable. (C) Specific acetaldehyde dehydrogenase activity determined photometrically as rate of NADH formation from NAD<sup>+</sup>. Gray bars, total acetaldehyde dehydrogenase activity (measured in presence of free coenzyme A); red bars, acetylating acetaldehyde dehydrogenase activity, calculated by subtracting non-acetylating acetaldehyde dehydrogenase activity (measured in absence of free coenzyme A). (D) Specific phosphotransacetylase activity measured as acetyl-CoA formation from acetyl phosphate in the presence of free coenzyme A. (E) Specific acetate kinase activity measured as acetyl phosphate consumption in the presence of ADP.

Isethionate cleaving-activity of IslAB was measurable in the BMC fraction 4 and to a lower extent in the neighboring fractions 3 and 5, confirming the distribution displayed by the proteomic data (Figure 4.6B). Both the formation of acetaldehyde and sulfite was detectable in the BMC fractions after incubation with isethionate and S-adenosylmethionine in assays under strictly oxygen-free, reducing conditions (see Material and Methods). For comparison, there was no acetaldehyde or sulfite formation measurable in the soluble fraction 2. The detected acetylating aldehyde dehydrogenase activity was similar in the BMC-associated fraction 4 and the neighboring fractions 3 and 5, again confirming the distribution pattern found in the proteomic data (Figure 4.6C). Almost all of the aldehyde-oxidizing activity was found to be coenzyme A-dependent, while non-acetylating acetaldehyde oxidation was negligible.

Phosphotransacetylase activity was detected highest in the intermediate fraction 3 and slightly lower in fractions 2 and 4 (Figure 4.6D). As discussed below, *B. wadsworthia* encodes two phosphotransacetylases in its genome (Figure 4.5: locus tags 00643 and 01625), which cannot be distinguished by the activity measurement; they might both be present in a different distribution along the gradients.

Acetate kinase activity was detected highest in the soluble fractions 2 and 3, confirming its distribution as suggested by the proteomic data (Figure 4.6E). The activity was markedly lower in the BMC-containing fractions 4 and 5. This shifted activity pattern of acetate kinase compared to phosphotransacetylase, which seemed to be more closely associated to the BMCs, is consistent with the different distribution pattern displayed by the proteomics data. The activity of Tpa was not measurable as the enzyme did not remain active throughout the centrifugation. Further, it was impossible to determine sulfoacetaldehyde reductase (SarD) activity in a photometrical assay against a high background NADH-oxidizing activity.

## Discussion

The existence of BMCs in *B. wadsworthia* growing with taurine as electron acceptor was indicated first by genomic analysis, and then confirmed by total-proteomic and transcriptomic analyses as well as by electron microscopy, each specifically in *B. wadsworthia* cells grown with taurine. Further, we have also succeeded in enriching the BMCs by gradient centrifugation, as confirmed both by electron microscopy and proteomic analysis, and were able to confirm the IslAB enzyme activity associated to them. Based on the clear distribution patterns of IslAB found in both the proteomic data and the activity measurements, we conclude that this is indeed the signature enzyme of the BMCs. *B. wadsworthia* likely employs these BMCs in order to isolate the desulfonating GRE IslAB, which cleaves

isethionate to harmful acetaldehyde and sulfite, from the cytosol. Furthermore, enzymes that process the toxic reaction products of IsIAB, such as the aldehyde dehydrogenase as discussed in the following, may be associated with the BMC as well, though it remained unclear whether they are contained within, or are merely associated to the outside of the BMC.

These BMC-enriched gradient fractions also contained the soluble complex DsrAB, which reduces sulfite to H<sub>2</sub>S, suggesting that also this enzyme system may be associated to the BMCs in order to ensure that the cells are exposed only to very low concentrations of toxic sulfite. Since DsrAB requires electrons from the membrane quinone pool shuttled by DsrC, it is probably not located inside the BMC but rather associated to the outside.

Similarly, the activity of acetylating acetaldehyde dehydrogenase closely associated to or contained within the BMC, as known from other types of BMC (Kerfeld, Aussignargues *et al.* 2018), would be keeping concentrations of free acetaldehyde low. The acetyl-CoA resulting from the oxidation of acetaldehyde can be further metabolized in two directions: it could be transesterified to acetylphosphate by Pta, a protein that based on our proteomic data and activity measurements seemed to be associated with the BMC, and then converted to acetate and ATP by cytosolic acetate kinase; or it could be reductively transformed to pyruvate by pyruvate:ferredoxin oxidoreductase (PFOR) (incorporating one molecule of CO<sub>2</sub>), an enzyme which appeared to be also enriched in the BMC fraction based on the proteomic measurements and SDS-PAGE. As our enzyme assay data shows high Pta activity also in the BMC fraction, transformation to acetylphosphate is the more likely route. The acetylphosphate would likely be shuttled out of the BMC and dephosphorylated (with ATP formation) to acetate by AckA, which enzyme assays strongly indicate to be a cytosolic enzyme.

In both cases, the free coenzyme A that is required by acetylating acetaldehyde dehydrogenase could be regenerated within the BMC if the respective enzyme was located inside of the BMC. As coenzyme A is a large cofactor compared to, for example, phosphate, regeneration within the BMC would save substantial transport across the shell. Such an internal cofactor recycling has been shown for ethanolamine- (Huseby and Roth 2013) and 1,2-propanediol-utilization (Cheng, Fan *et al.* 2012) microcompartments. For ethanolamine utilization of *Salmonella enterica*, the gene for phosphotransacetylase EutD in the BMC gene cluster has been shown to be essential even though it is functionally redundant since a second, housekeeping phosphotransacetylase gene exists elsewhere in the genome (Huseby and Roth 2013). The authors assumed that the BMC-contained Pta is essential due to its ability to recycle free coenzyme A within the BMC. A similar situation may be the case

in *B. wadsworthia*, which was found to express two phosphotransacetylases as well: one whose respective gene is located within the BMC gene cluster (00643) and one that is encoded next to cytosolic acetate kinase (01625). Both of these phosphotransacetylases were found associated with the BMC by proteomic analysis; however the assay we used cannot distinguish between the activities of these two enzymes. It is possible that one is indeed located within the BMC and one in the cytosol. The BMC gene cluster even contains a gene annotated as EutQ which has been described as having an acetate kinase activity (Moore and Escalante-Semerena 2016) and could catalyze the last reaction step from acetyl phosphate to acetate, but it was only detectable in low amounts in the proteomic analysis; in addition, the acetate kinase activity was mainly detected in the soluble protein fraction.

The potential internal recycling of NAD<sup>+</sup> from NADH formed by acetaldehyde oxidation to acetyl-CoA is less clear, though an intriguing candidate can be found in the protein annotated as Na<sup>+</sup>-translocating ferredoxin:NAD<sup>+</sup> oxidoreductase (RnfC, 00648). In the proteomic analysis, this protein is found associated with the BMCs where it could serve as part of a redox shuttle to remove excess electrons from the BMC across the shell, internally regenerating NAD<sup>+</sup> from NADH. Based on the pfam domains, of which the motif of the RnfC subunit (pfam13375) is only one of four (Ferlez, Sutter *et al.* 2019), it is more similar to the cobalamin reductase PduS from *Salmonella enterica* or *Citrobacter freundii* than to the actual Rnf complex subunit. PduS in propanediol utilization microcompartments reduces the cobalamin cofactor of B<sub>12</sub> from Co<sup>3+</sup> to Co<sup>2+</sup> (Cheng and Bobik 2010; Parsons, Lawrence *et al.* 2010) and also associates with PduT, a shell protein bearing a 4Fe-4S cluster (Parsons, Lawrence *et al.* 2010). A PduT homolog could possibly be encoded in the *B. wadsworthia* gene cluster annotated as CcmL/EutN (00647): BLAST search revealed the most closely related protein (69.7% identity) to be a protein of the PduT family in *Telmatospirillum siberiense*. Its identity to the experimentally verified PduT sequences of *C. freundii* and *Salmonella typhimurium* strain LT2 is 43.9 and 41.2% respectively. In the GRE-containing BMCs of *B. wadsworthia*, which do not involve B<sub>12</sub> as a cofactor, the function of PduS and PduT is yet unclear, however, it is tempting to speculate that they may also serve to shuttle electrons between the outside and the inside of the BMC using the FeS cluster of PduT, as it was suggested for propanediol utilization microcompartments (Parsons, Lawrence *et al.* 2010; Ferlez, Sutter *et al.* 2019). Since the *B. wadsworthia* gene cluster contains no gene for alcohol dehydrogenase in order to recycle NAD<sup>+</sup> within the BMCs (Cheng, Fan *et al.* 2012; Huseby and Roth 2013), it remains unclear how the electrons released by the acetaldehyde dehydrogenase are being shuttled further. Hence, a potential transfer of these electrons to the cytosol *via* the iron-sulfur clusters of PduS in the BMC lumen and PduT in the BMC shell is a viable hypothesis.

It could even provide a link to the annotated PFOR (01626), which is highly expressed, but whose function in relation to the BMCs is unclear: PFOR cannot regenerate NAD<sup>+</sup> from NADH directly, since it requires reduced ferredoxin as an electron donor. However, a transfer of electrons from NADH to ferredoxin is generally possible *via* electron bifurcation (Buckel and Thauer 2018). Both PduS and PduT are known to use flavins as electron carriers, which are also used in electron bifurcating enzymes (Buckel and Thauer 2018). The electrons on oxidically purified recombinant PduS, binding only the flavin cofactor, are at a potential of -262 mV, in anoxically produced PduS, binding both the flavin cofactor and an [4Fe-4S] center, the electron potential is -150 mV (Parsons, Lawrence *et al.* 2010). This means that the electrons could theoretically be used by DsrAB for sulfite reduction (-116 mV). However, the potential of electrons on the [4Fe-4S] cluster of PduT, the proposed redox link in the BMC shell, is +99 mV (Parsons, Dinesh *et al.* 2008) and not sufficient for sulfite reduction.

Inside the BMC, these flavins could additionally be used to shuttle electrons to IslB, which like other GRE activating enzymes might require electrons transferred by flavins to install the glycyl radical on IslA (Bianchi, Eliasson *et al.* 1993; Shisler and Broderick 2014; Backman, Funk *et al.* 2017). However, as the radical, once installed, is regenerated after each reaction of IslA without further electron input (Bodea, Funk *et al.* 2016; Levin and Balskus 2018; Peck, Denger *et al.* 2019), IslB cannot take up the stoichiometric amounts of electrons produced by AdhE, making a second electron sink necessary, such as a transport out of the BMC, for example, to PFOR or DsrAB. The detailed function of B<sub>12</sub>-regenerating enzymes in BMCs with B<sub>12</sub>-independent signature enzymes in combination with the unclear redox balance of the BMC is an exciting field for further study and could provide valuable insight into the very specialized metabolism of the human gut bacterium *B. wadsworthia*.

## **Materials and methods**

### Growth and harvest of *B. wadsworthia*

*B. wadsworthia* 3.1.6 was grown in anoxic, carbonate-buffered, Ti(III)-reduced minimal medium as described before (Peck, Denger *et al.* 2019). The medium additionally contained 2 µg/l naphthochinone; 20 mM lactate and 20 mM taurine were supplied as electron donor and electron acceptor, respectively. The cells were harvested by centrifugation after 20 hours of growth and the cell pellets stored at -20°C. For BMC purification, the cells were opened by three passages through a cooled French pressure cell and then centrifuged for 10 minutes at 16 000 x g to remove cell debris. *Desulfovibrio alaskensis* G20 was grown as a positive

control for BMC formation in the same medium without naptochinone and supplied with 40 mM choline as sole substrate (Craciun and Balskus 2012).

### Transcriptomics

For RNA isolation, 50 ml of overnight culture were centrifuged and the pellet was washed with 1 ml RNA/*ater*<sup>TM</sup> (Invitrogen/Thermo Fisher Scientific, Waltham, MA, USA), then resuspended in 100 µl RNA/*ater*<sup>TM</sup> and stored at -80°C. RNA was isolated using a *Quick*-RNA Miniprep kit (Zymo Research, Irvine, CA, USA) and DNA removed using a TURBO DNA-free<sup>TM</sup> kit (Invitrogen/Thermo Fisher Scientific, Waltham, MA, USA). PCR using 16S forward and reverse primers was performed to confirm the absence of DNA contamination. Libraries were constructed at Eurofins Genomics (Ebersberg/Konstanz, Germany) after ribosomal RNA depletion and cDNA synthesis using random hexamer primers and sequenced single-end 50bp on an Illumina HiSeq4000 platform.

For data analysis, the reference genome and annotation file for *Bilophila wadsworthia* 3\_1\_6 were obtained from NCBI (reference sequence: NZ\_ADCP00000000.2). The sequence results were quality trimmed with Trimmomatic 0.39 (Bolger, Lohse *et al.* 2014) using the following parameters: minimum read length 30 bp, minimum average phred quality must be at least 15 in a sliding window of 4, bases at the start and end of sequences are removed if the phred quality is lower than 3. Only a small amount of reads (< 0.5%) were dropped this way (Table S4.1). The trimmed reads were aligned to the reference genome using Bowtie2 [version 2.3.5.1; (Langmead and Salzberg 2012)] with default settings and thresholds. The program Samtools [version 1.9 (Li, Handsaker *et al.* 2009)] was used to convert mapping files from “sam” to “bam” format and sort them by genomic coordinates. Stringtie [version 1.3.5 (Pertea, Pertea *et al.* 2015)] was used to assign read counts to each gene present in the provided annotation described above in combination with the PERL script prepDE.pl (<http://ccb.jhu.edu/software/stringtie/>). The obtained raw count table was analyzed using the R package DESeq2 [version 1.8.2 (Love, Huber *et al.* 2014)].

### Sucrose gradient centrifugation

The sucrose gradient was prepared from solutions containing 10, 20, 30, 40, and 50% (w/v) sucrose in 50 mM Tris(hydroxymethyl)-aminomethan(Tris)-HCl at pH 7.4. 2.5 ml each of each gradient step were used to form the gradient in a 14 ml Ultra-Clear<sup>TM</sup> centrifuge tube (Beckman Coulter, Brea, CA, USA), with the highest sucrose concentration at the bottom of the tube. The cell-free extract was layered on top and the gradients were centrifuged at 85365 x g (average relative centrifugal force in a Beckman Coulter SW 40 Ti swing bucket

rotor) for 16 hours at 4°C (Huber 2017). The resulting gradient fractions were removed in the same pattern for every individual gradient.

For proteomic analysis, the buffer was exchanged to 50 mM Tris-HCl pH 7.9 without sucrose using 10 kDa mass cutoff centrifugal filters (Sartorius Vivaspin 500, Sartorius AG, Göttingen, Germany), the samples were then brought to comparable protein concentrations and submitted to the Proteomics Facility of the University of Konstanz for protein mass fingerprinting. For electron microscopy the buffer was exchanged in the same way to 5 mM Tris-HCl pH 7.9 without sucrose.

#### SDS-PAGE and enzyme identification

The protein content of the individual fractions was determined by Bradford assay on a 1 ml scale (Bradford 1976). For SDS-PAGE, routinely an amount of gradient fraction corresponding to 50 µg of protein was boiled with loading dye (Roti®-Load 1, Carl Roth, Karlsruhe, Germany) and loaded onto a gel (12% acrylamide in the resolving gel, 4% in the stacking gel). The gels were run at 100 V for 1 hour and the proteins visualized by Coomassie and/or silver staining (Table S4.3).

Individual bands were cut out of the gel and submitted for protein mass fingerprinting at the Proteomics Facility of the University of Konstanz.

#### Transmission electron microscopy

##### Negative staining of isolated BMCs

Glow discharge carbon-coated nickel grids were cleaned by oxygen plasma for 45 seconds in a Harrick PDC-32G2 PlasmaCleaner (Harrick Plasma, Ithaca NY, USA). 15 µl sample were applied to the grid by floating the grid on top of the sample for 2 minutes. The grid was then rinsed four times with double-distilled water and contrasted with 1% neutralized phosphotungstic acid (5 second rinse followed by 45 second incubation in the contrasting solution). The grids were carefully blotted from the edge and dried thoroughly before imaging.

##### Embedding and ultrathin sectioning of cells

Culture samples of *B. wadsworthia* grown with taurine and lactate, of *B. wadsworthia* grown with sulfolactate and lactate and of *D. alaskensis* grown on choline were submitted to the Electron Microscopy Centre at the University of Konstanz.

The cells were enclosed in agarose and fixed with 2.5% glutardialdehyde in 0.05M HEPES

(2-[4-(2-hydroxyethyl)piperazin-1-yl]ethanesulfonic acid and its sodium salt) buffer at pH 7. Postfixation was performed with 2% OsO<sub>4</sub> and en-bloc staining with uranyl acetate saturated in 70% ethanol, after initial dehydration in a graded ethanol series. Following further dehydration in a graded acetone series the agarose blocs were embedded in Spurr's resin (Spurr's Low Viscosity embedding kit, Sigma Aldrich, St Louis, USA) using acetone as intermedium, and polymerized at 65°C for 48 hours. A detailed description of the process can be found in Table S4.4.

Ultramicrotomy was performed on a Leica UC7 ultramicrotome (Leica Microsystems, Wetzlar, Germany) using diamond knives (Diatome 45°Ultra, Diatome, Nidau, Switzerland). Ultrathin sections (50nm) were mounted on formvar-coated copper mesh grids, incubated on a drop of saturated aqueous uranylacetate solution (~7.8%) for 20 minutes in the dark, then rinsed with double distilled water for 10 seconds and dried. They were then incubated for 90 seconds on a drop of 0.4% lead citrate and 0.4% sodium hydroxide solution under carbon dioxide-free conditions, rinsed for 10 seconds with double distilled water and dried overnight under air according to (Venable and Coggeshall 1965).

#### Transmission electron microscopy imaging

Imaging was performed on a Zeiss EM 912 Omega (Zeiss, Oberkochen, Germany) transmission electron microscope equipped with a tungsten electrode, and a TRS slow scan CCD-camera for TEM (Tröndle Restlichtverstärker Systeme, Moorenweis, Germany). The images were taken at an acceleration voltage of 80 kV and processed using ImageSP ver.1.2.3.36 (SYS-PROG, Minsk, Belarus & Tröndle Restlichtverstärker Systeme, Moorenweis, Germany).

#### Enzyme assays

##### Taurine:pyruvate aminotransferase (*Tpa*)

Taurine:pyruvate aminotransferase activity was measured aerobically as taurine consumption and alanine formation in a solution of 5 mM taurine and 5 mM pyruvate in 50 mM Tris-HCl at pH 7.9. The cofactor pyridoxal-5-phosphate was additionally supplied in a concentration of 0.1 mM in all buffers used in the assay or during purification. Typically, 0.2 ml of cell-free extract or gradient fraction were used for an assay on a 1 ml scale. Taurine and alanine concentrations were measured by HPLC as described in (Peck, Denger *et al.* 2019). Each fraction was assayed in triplicates.

### Sulfoacetaldehyde reductase (SarD)

SarD activity was measured under oxic conditions in 50 mM Tris-HCl buffer at pH 7.9 with 0.4 mM sulfoacetaldehyde and 0.2 mM NADH provided as substrates. The decrease of NADH concentration was measured at 340 nm in a spectrophotometer (JASCO, Tokyo, Japan). 100 µl of gradient fraction were used in one assay and the background activity of the protein solution with NADH only was measured separately before adding sulfoacetaldehyde. Each fraction was assayed in triplicates.

### Isethionate sulfite-lyase (IslAB)

For measuring isethionate sulfite-lyase activity, the gradient was prepared from anoxic sucrose solutions under a 95% N<sub>2</sub>/5%H<sub>2</sub> atmosphere and centrifuged in sealed tubes as described above. The fractions were separated in a 95% N<sub>2</sub>/5%H<sub>2</sub> atmosphere. The enzyme assays were carried out in anoxic 50 mM Tris-HCl buffer at pH 7.9. The reaction mixture contained 20 mM isethionate, 1 mM SAM hydrochloride, 2 mg/l resazurin as a redox indicator and 1 mM Ti(III)-NTA as a reducing agent. The reactions were carried out in anoxic stoppered 1 ml glass cuvettes with a 95% N<sub>2</sub>/5%H<sub>2</sub> gas phase. The reaction was started by addition of 200 µl/ml gradient fraction solution. Samples were taken at one hour intervals using analytical syringes. Each fraction was assayed in triplicates.

For acetaldehyde quantification, 50 µl sample were added to a 2.5 mM solution of 2,4-dinitrophenylhydrazine (DNPH) in acetonitrile with 0.1% phosphoric acid. The derivatization reaction was incubated for at least 30 minutes at room temperature [modified from (Frey, Schneider *et al.* 2018)].

For sulfite quantification, 50 µl sample were added to 0.25 M borate buffer with 0.25 M KCl and 20 mM EDTA, adjusted to pH 10 with sodium carbonate. 50 µl of a 10 mM solution of *N*-(9-acridinyl)-maleimide (NAM) in acetone were added and the reaction was incubated for 30 minutes at 50°C (Akasaka, Matsuda *et al.* 1990).

All derivatized samples were frozen once to precipitate proteins and then centrifuged for 30 seconds. Derivatized sulfite respectively acetaldehyde were analyzed by HPLC on a phenomenex Luna Omega C18 column (5 µm PS, 100 Å, 150 x 3 mm, phenomenex/Danaher; Washington D.C., USA) with acetonitrile and 0.1% formic acid in water as mobile phases. The Shimadzu Prominence HPLC (Shimadzu, Kyoto, Japan) was equipped with a SPD-M20A photodiode array detector and the detection wavelengths were 254 nm for NAM-sulfite adducts and 360 nm for DNPH derivatives. The HPLC gradient programmes were as follows: for DNPH derivates: 25% acetonitrile for 4.5 minutes, followed by a rise to 70% acetonitrile over 15 minutes and 10 minutes reequilibration to 25%

acetonitrile. For NAM-sulfite: 3 minutes at 10% acetonitrile, gradient to 80% acetonitrile during 10 minutes, reequilibration to 10% acetonitrile for 7 minutes.

#### Acetylating acetaldehyde dehydrogenase (*AdhE*)

To determine acetaldehyde dehydrogenase activity the reduction of NAD<sup>+</sup> to NADH was measured photometrically [modified after (Hensgens, Hagen *et al.* 1995)] under oxic conditions. One assay typically contained 0.25 mM NAD<sup>+</sup>, 5–25 µl gradient fraction, 2 mM acetaldehyde and 0.33 mM coenzyme A in a total volume of 1 ml anoxic 50 mM potassium phosphate buffer with 3 mM dithiothreitol (DTT) at a pH of 7.5. The formation of NADH was monitored for one minute at 340 nm. To be able to calculate the activity of acetylating acetaldehyde dehydrogenase specifically, each fraction was measured in one assay with coenzyme A, yielding total acetaldehyde dehydrogenase activity, and one without coenzyme A to measure non-acetylating acetaldehyde dehydrogenase activity. The activity of acetylating acetaldehyde dehydrogenase was calculated as the difference between these two measurements. Each fraction was assayed in triplicates.

#### Phosphotransacetylase (*Pta*)

Phosphotransacetylase activity was measured as the backwards reaction from acetyl phosphate to acetyl-CoA, with the acetyl-CoA formation being measured photometrically [(Müller, Griffin *et al.* 2008) modified after (Bergmeyer 1970)]. 3.33 mM acetyl phosphate and 0.33 mM coenzyme A were incubated in 50 mM Tris-HCl buffer at a pH of 7.5. 10–100 µl of gradient fraction per ml were added and the formation of acetyl-CoA was monitored for one minute at 233 nm. Each fraction was measured in triplicates.

#### Acetate kinase (*AckA*)

The activity of acetate kinase was measured as the consumption of acetyl phosphate, which was quantified using a colorimetric assay based on the formation of acyl-hydroxamate chelation with Fe<sup>3+</sup> [(Müller, Griffin *et al.* 2008) modified after (Nishimura and Griffith 1981)]. The enzymatic reaction was set up in a volume of 1 ml containing 5 mM ADP, 5 mM MgCl<sub>2</sub>, 3.33 mM acetyl phosphate and 5–25 µl gradient fraction in 50 mM Tris-HCl buffer at a pH of 7.4. The reactions were incubated shaking at room temperature (23°C) and samples of 300 µl for the determination of acetyl phosphate concentration were taken at time intervals of 2 or 5 minutes depending on the reaction speed.

The samples were added to 200 µl of a 2.5 M solution of hydroxylamine hydrochloride in water, freshly neutralized with NaOH. This mixture was stored on ice until the complete batch

could be incubated at room temperature for ten minutes. 0.5 ml of the Fe(III) reagent were then added: 3% (w/v)  $\text{FeCl}_3$  dissolved in 0.1 M HCl, 12% (w/v) trichloroacetic acid in water, and 3 M HCl were mixed in equal amounts to obtain this reagent. The reaction was mixed thoroughly and the absorption of the Fe(III) chelates was measured at 540 nm. The absorption values were quantified using a freshly prepared acetyl phosphate standard. Each fraction was measured in triplicates.

### Protein Alignment

Genome search was performed and annotations were taken from JGI IMG/M on 28.6.2019. HMPREF0179\_00647 was identified as PduT by Basic Local Alignment Search Tool on UniProt. The search was conducted using the amino acid sequence of HMPREF0179\_00647 against UniProt reference proteomes plus Swiss-Prot, with an E-threshold of 10 and no filtering and gapping allowed. For alignments with PduT of *Citrobacter freundii* and *Salmonella typhimurium*, the respective proteins sequences were taken from the UniProt database and aligned with the amino acid sequence of HMPREF0179\_00647 using default settings.

### Acknowledgments

We thank Karin Denger for help with cultivation, Alexander Fiedler, Alina Kindinger, Anne Van Humbeeck, and Prof. Dr. Erika Isono for experimental support. We are grateful to Dr. Paolo Franchini and Corentin Fournier for help with transcriptomic data analysis and Dr. Andreas Marquardt and the Proteomics Facility for proteomic measurements. This work was funded by the Deutsche Forschungsgemeinschaft and the Konstanz Research School Chemical Biology.

### Author contributions

AGB and DS designed the experiments. AGB, SD, PB and SH performed and analysed them. AK contributed further analysis. AGB and DS wrote the manuscript.

## Supplementary Material

HMPREF0179\_004

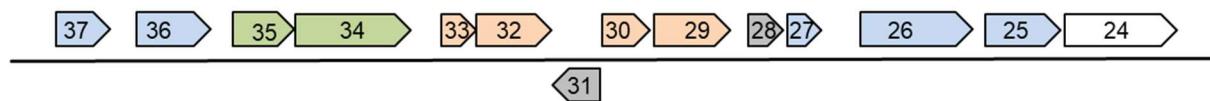


**Figure S4.1. Illustration of the gene cluster in *B. wadsworthia* encoding sulfolactate degradation enzymes including sulfolactate sulfite-lyase (SuyAB).** Genes marked in orange are directly involved in sulfolactate degradation: 00433, SuyA; 00432, SuyB; 00430, S-sulfolactate dehydrogenase; 00429, R-sulfolactate dehydrogenase. The two dehydrogenases most likely interconvert sulfolactate enantiomers, analogous to the pathway described by (Mayer, Huhn et al. 2010). Genes marked in green encode transport components: 00435, tripartite-type tricarboxylate transporter, receptor component TctC; 00434, putative tricarboxylic transport membrane protein. Genes marked in blue are annotated to encode metabolic enzymes but their function related to sulfolactate metabolism is not clear: 00437, hydroxyethylthiazole kinase (from thiamine metabolism); 00436, Formate dehydrogenase maturation protein FdhE; 00427, methylglyoxal synthase; 00426, D-lactate dehydrogenase; 00425, glycolate oxidase iron-sulfur subunit. Genes marked in gray may serve a regulatory function: 00431, GntR family transcriptional regulator; 00425, regulator of RNase E activity RraA. 00424 annotated to encode a hypothetical protein. Notably, there are no genes found in the gene cluster that are annotated to encode BMC shell proteins. All annotations were taken from IMG for *Bilophila wadsworthia* 3.1.6. and the shortened IMG locus tag can be completed by adding the given number to the following prefix: HMPREF0179\_.

**Table S4.1. Number of reads and alignment rate of RNA samples.**

		Taurine_1	Taurine_2	Taurine_3	DHPS
<b>Raw reads</b>		25,780,974	21,425,313	12,520,332	14,901,949
<b>Dropped reads by trimming/filtering</b>		88,953 (0.35%)	77,948 (0.36%)	47,309 (0.38%)	47,413 (0.32%)
<b>Alignment to reference genome</b>	Overall alignment rate	99.66%	99.11%	99.66%	99.69%
	Aligned exactly 1 time	1,517,999 (5.91%)	1,413,868 (6.62%)	681,150 (5.46%)	2,296,417 (15.46%)
	Aligned >1 time	24,086,278 (93.75%)	19,743,584 (92.49%)	11,749,218 (94.20%)	12,511,736 (84.23%)
<b>Final reads</b>		17,033,545	14,057,112	8,296,581	7,228,077

**Table S4.2. Proteomic results for the SDS-PAGE bands (see Figure 4.4C).** The protein description includes a shortened locus tag, which can be completed by adding the shown number to the following prefix: HMPREF0179\_. BMC shell proteins are marked bold.

Fraction	approximate protein size	identified as	Score
3	10 kDa (1)	<b>ethanolamine utilization protein EutN (00642)</b>	115 (top score)
	10 kDa (2)	integration host factor subunit alpha (01532) taurine:pyruvate aminotransferase (02713) chaperonin GroES (03535) DNA-binding protein HU-β(00718) hypothetical protein (00544)	242.03 225.79 196.43 191.42 188.06
		<b>ethanolamine utilization protein EutN (00642)</b>	157.39
	25 kDa	dissimilatory sulfite reductase β subunit (02116)	655.11
	14 kDa	large subunit ribosomal protein L10P (02084)	227.30
	15 kDa	large subunit ribosomal protein L10P (02084) periplasmic chaperone for outer membrane proteins Skp (02805) small subunit ribosomal protein S5P (02023) large subunit ribosomal protein L9P (02745) Class III cytochrome C family protein (01235) small subunit ribosomal protein S9 (00867) small subunit ribosomal protein S7P (02067) hypothetical protein (02302) Flavorubredoxin (03149)	287.38 234.45 234.24 193.54 189.18 187.27 161.72 151.57 140.29
4		<b>Carboxysome shell and ethanolamine utilization microcompartment protein CcmL/EutN (00647)</b>	117.07
	18 kDa	ATP-dependent Clp protease, protease subunit (02214) transcriptional regulator, TetR family (00863) hypothetical protein (00984) large subunit ribosomal protein L9P (02745) pyrimidine operon attenuation protein / uracil phosphoribosyltransferase (03139) Rubrerythrin (02466) Putative exonuclease, RdgC (01649) bacterioferritin (00484)	138.21 135.34 134.65 130.60 119.28 95.03 87.47 82.44
		<b>Carboxysome shell and ethanolamine utilization microcompartment protein CcmL/EutN (00647)</b>	81.44

**Table S4.3. Coomassie and silver staining of SDS polyacrylamide gels, modified after (Laemmli 1970; Heukeshoven and Dernick 1985).**

	Substance	time
Coomassie staining	0.25% (w/v) Coomassie brilliant blue R-250, 45% (v/v) ethanol, 10% (v/v) acetic acid in water	1 h
Washing/initial destaining	45% (v/v) ethanol, 10% (v/v) acetic acid in water	1 h
Destaining/Fixation	45% (v/v) ethanol, 10% (v/v) acetic acid in water	overnight
Reduction	30% (v/v) ethanol, 0.8 M acetate, 2 g/l thiosulfate	30 min
Washing	distilled water	3x 5 min
Silver solution	2 g/l (11.8 mM) silver nitrate, 200 µl/l 37% formaldehyde	20 min
Developing	25 g/l (0.236 M) sodium carbonate, 100 µl/l 37% formaldehyde	2–8 min
Stopping	10 g/l glycine	10 min

**Table S4.4. Cell fixation and embedding protocol for transmission electron microscopy**

	<b>Substance</b>	<b>pH</b>	<b>°C</b>	<b>time</b>
<b>Pre fixation</b>	50/50 culture medium with 5% glutardialdehyde in 0.05M HEPES	7	0	45 min
<b>Enclosing</b>	Agarose-enclosure			
<b>Fixation</b>	2.5% glutardialdehyde in 0,1M HEPES	7	0–4	2.5 h
<b>Washing</b>	0.05M HEPES	7	0	3x 10 min
<b>Postfixation / osmification</b>	2% OsO <sub>4</sub> in 0.05M HEPES	7	4	1h
<b>Washing</b>	0.05M HEPES	7	0	3x 10 min
<b>Drainage</b>	30% ethanol, precooled		4	10 min
	50% ethanol, precooled		4	15 min
<b>En-bloc staining</b>	Uranylacetat saturated in 70% ethanol		4	overnight
<b>Dehydration</b>	70% ethanol, precooled		RT	3x 10 min
	80% acetone, precooled		RT	3x 10 min
	90% acetone, precooled		RT	3x 10 min
	96% acetone, precooled		RT	3x 10 min
	100% acetone, dried on molecular sieve		RT	3x 10 min
<b>Intermedium</b>	100% acetone, dried on molecular sieve		RT	1 h
<b>Embedding</b>	15% Spurr resin in acetone		RT	1 h
	33% Spurr resin in acetone		RT	2 h
	50% Spurr resin in acetone		RT	2 h
	75% Spurr resin in acetone		RT	o.n.
	pure Spurr resin in closed Eppies		RT	2x 2 h
<b>Polymerisation</b>			65	48 h
<b>Cooling</b>	In extractor hood		RT	overnight

## Chapter 5: General Discussion and Outlook

Natural organosulfonates are a significant pool of organically bound, partially oxidized sulfur in nature (Autry and Fitzgerald 1990; Vairavamurthy, Zhou *et al.* 1994; Anderson and Pratt 1995; Werne and Hollander 2004; Zhu, Chen *et al.* 2016; Fakhraee, Li *et al.* 2017).

Previously, their degradation pathways have mainly been studied in aerobic bacteria, where they can be mineralized to CO<sub>2</sub> and sulfate by single organisms or, in case of molecules such as the C<sub>6</sub>-sugar SQ, by two-member consortia (for more details, please refer to the Introduction) (Rein, Gueta *et al.* 2005; Denger, Mayer *et al.* 2009; Mayer, Huhn *et al.* 2010; Denger, Weiss *et al.* 2014; Felux, Spiteller *et al.* 2015). Significant amounts of organic matter, however, are degraded also in anoxic or microoxic environments, such as in the subsurface layers of soils and sediments and in the digestive tracts of animals. Under these conditions, organosulfonates can be a substrate for the production of H<sub>2</sub>S instead of sulfate as with aerobic bacteria (Lie, Pitta *et al.* 1996; Laue, Denger *et al.* 1997). Such H<sub>2</sub>S production can have major impacts on human health and wealth. For example, H<sub>2</sub>S-mediated corrosion of metals (Little, Lee *et al.* 2008) is a source of danger in, e.g., the oil industry (Muyzer and Stams 2008; Hubert 2010), sulfidogenic processes can compete with methane formation during biogas production (Stefanie, Visser *et al.* 1994; Weijma, Gubbels *et al.* 2002), H<sub>2</sub>S can be used in the recovery of heavy metals (Muyzer and Stams 2008) and, importantly, H<sub>2</sub>S production in the human gut is linked to the development of multiple diseases such as inflammatory bowel diseases (see Introduction). It is therefore important to uncover and describe in detail the bacterial organosulfonate degradation pathways that lead to H<sub>2</sub>S production, in addition to the much better studied H<sub>2</sub>S production through sulfate reduction.

Indeed, the fact that small (C<sub>2</sub>- and C<sub>3</sub>-) organosulfonates can be utilized by bacteria as substrates for fermentations or as electron acceptors for respirations, has been known for more than 20 years (Lie, Pitta *et al.* 1996; Laue, Denger *et al.* 1997; Lie, Godchaux *et al.* 1999), but most of the pathways, enzymes and genes involved were not characterized in detail until today. Importantly, as much of microbiological research today is done *via* metagenomic and metatranscriptomic sequencing, it is vital to identify and correctly annotate the genes responsible for organosulfonate degradation in the reference databases in order to be able to correctly detect these processes in DNA- or RNA-based approaches. In this work, I described the genes responsible for fermentative degradation of SQ to DHPS in the model organism *E. coli* and identified a first pathway for the subsequent degradation of the DHPS to sulfide by *Desulfovibrio* sp. strain DF1 (Chapter 2). Further, we identified the pathway, enzymes and genes responsible for taurine (Chapter 3) and sulfolactate degradation

(Chapter 4) in the disease-relevant human-gut bacterium *B. wadsworthia*. Finally, I characterized bacterial microcompartments in *B. wadsworthia* that are involved in the desulfonation pathway for utilization of taurine and isethionate as electron acceptors (Chapter 4).

It was previously demonstrated that *E. coli* degrades SQ under oxic conditions through the SQ-Embden-Meyerhof-Parnas pathway, analogous to, but genetically independent of, the Embden-Meyerhof-Parnas pathway for glucose (Denger, Weiss *et al.* 2014), thereby releasing the sulfonate moiety in form of DHPS. It was already speculated (Felux 2015; Felux, Spitteler *et al.* 2015) that also under anoxic conditions, *E. coli* might employ sulfoglycolysis as it yields one ATP per SQ molecule by substrate-level phosphorylation and because the reduction of the intermediate sulfolactaldehyde to DHPS serves as an additional fermentation step in order recover NAD<sup>+</sup> (as discussed extensively in Chapter 2). In this work, I confirmed that under fermentative conditions, *E. coli* degrades SQ in a modified mixed-acid fermentation to DHPS, succinate, acetate and formate. DHPS in turn can be used by *Desulfovibrio* sp. strain DF1, which was isolated specifically for the ability to ferment DHPS. In the previously studied aerobic DHPS-degrader *Cupriavidus pinatubonensis* JMP134, DHPS is oxidized in one step to sulfolactate by the DHPS 3-dehydrogenase HpsN. Sulfolactate is then the substrate for sulfolactate sulfite-lyase SuyAB, which cleaves it into pyruvate and sulfite (Mayer, Huhn *et al.* 2010). In comparison, the anaerobic *Desulfovibrio* strain does not have a HpsN homolog, while instead two other enzymes were highly expressed, annotated as 3-hydroxyisobutyrate dehydrogenase and succinate semialdehyde dehydrogenase, respectively. Using recombinant enzymes, I demonstrated that these two NAD<sup>+</sup>-dependent enzymes indeed oxidize DHPS to sulfolactate in two steps with sulfolactaldehyde as intermediate. They were therefore re-annotated as DHPS dehydrogenase (DhpA), which oxidizes DHPS at the terminal alcohol function to the corresponding aldehyde, sulfolactaldehyde, and sulfolactaldehyde dehydrogenase (SlaB), which oxidizes the sulfolactaldehyde to sulfolactate. For the following desulfonation step, a SuyAB homolog was identified for the first time as a desulfonation enzyme in a strictly anaerobic bacterium, cleaving sulfolactate into pyruvate and sulfite, as in aerobic bacteria (see above). While most of the aerobic organisms oxidize and detoxify sulfite to sulfate and excrete it, anaerobes like *Desulfovibrio* sp. strain DF1 can use sulfite as a terminal electron acceptor using the dissimilatory sulfite reductase (Dsr) complex. In comparison to sulfate reduction, this saves the investment of two ATP equivalents that are needed to activate the sulfate (as is extensively discussed in Chapter 3).

With these two species as model organisms, I demonstrated for the first time that anaerobic degradation of SQ by two member bacterial consortia *via* DHPS to H<sub>2</sub>S exists and identified

a first set of genes especially for the anaerobic degradation of DHPS. It remains unclear whether these model organisms and pathways are indeed representative for the SQ degradation and H<sub>2</sub>S formation taking place in the human gut. *E. coli* is generally present in the human gut flora, as are *Desulfovibrio* species (Loubinoux, Bronowicki *et al.* 2002; Rowan, Docherty *et al.* 2010; Fuchs, Eitinger *et al.* 2014; Chen, Zhou *et al.* 2019), but only to a small percentage (Hayashi, Sakamoto *et al.* 2002; Wang, Heazlewood *et al.* 2003; Eckburg, Bik *et al.* 2005). However, my first demonstration of SQ conversion to H<sub>2</sub>S using the two model bacteria prompted ongoing collaborative research led by Buck Hanson at the University of Vienna (co-authored manuscript in generation): surprisingly, the most prominent SQ- and DHPS-degrading species in incubations of SQ-amended human fecal samples were identified as *Clostridium symbiosum* and *Agathobacter rectalis* (previously *Eubacterium rectale*), degrading SQ to DHPS instead of *E. coli*, and *Bilophila wadsworthia*, degrading DHPS to H<sub>2</sub>S instead of *Desulfovibrio* sp. Further, in a Master's thesis, Alexander Fiedler in our group performed growth experiments and proteomic analyses on representative strains of *C. symbiosum*, *A. rectalis* and *B. wadsworthia* (Fiedler 2018). For the *C. symbiosum* and *A. rectalis* strains, it was found that they employ a third SQ degradation pathway, which had in the meantime been discovered in an aerobic *Bacillus* strain by Benjamin Frommeyer in our group (manuscript in generation): in this so-called transaldolase pathway, SQ is first isomerized to 6-deoxy-6-sulfofructose (SF) and then cleaved without previous phosphorylation by a novel transaldolase enzyme. The latter reaction releases sulfolactaldehyde, as with the first two known SQ pathways, but couples the non-sulfonated C<sub>3</sub>-half of SF with glyeraldehyde-3-phosphate to form fructose-6-phosphate, which can be further metabolized as carbon and energy source. Sulfolactaldehyde is reduced to DHPS as an additional fermentation step, as with *E. coli*, and excreted. This is not only the shortest but also the most efficient, in terms of energy conservation, degradation pathway known for SQ. Interestingly, an anaerobic, fermentative *Enterococcus gilvus* strain that also employs this transaldolase pathway for SQ degradation excretes sulfolactate, instead of DHPS like *A. rectalis* and *C. symbiosum*. Hence, while these three anaerobic Firmicutes strains all express the transaldolase pathway, they vary in that they excrete either a more reduced (DHPS) or more oxidized form (sulfolactate) of the sulfolactaldehyde intermediate. It is yet unknown what the physiological role of this branching of the pathway in either a reductive or oxidative route for these anaerobic bacteria may be or how it is regulated. Hence, this is an intriguing topic for future examinations. In conclusion, this means there are now three pathways known for anaerobic SQ degradation (see Figure 5.1): the anaerobic SQ-Embden-Meyerhof-Parnas pathway with modified mixed acid fermentation and reduction of sulfolactaldehyde to DHPS (*E. coli*; this work, Chapter 2), the transaldolase pathway with

reduction of sulfolactaldehyde to DHPS [*A. rectalis*, *C. symbiosum*; Frommeyer et al., manuscript in preparation, and (Fiedler 2018)], and the transaldolase pathway with oxidation of sulfolactaldehyde to sulfolactate [*E. gilvus*; Frommeyer et al., manuscript in preparation, and (Fiedler 2018)]. Notably, a fourth pathway for SQ degradation yielding the C<sub>2</sub>-organosulfonate isethionate as the degradation product instead of the C<sub>3</sub>-sulfonates DHPS or sulfolactate may exist based on preliminary work on enrichment cultures done by Karin Denger (note that this potential route, from SQ via isethionate to H<sub>2</sub>S, is not represented in Figure 5.1 since its details are not clear).

These preliminary results have been obtained by anoxic incubation of fecal samples (at the University of Vienna) or with pure cultures of anaerobes (in our group as described above), each with SQ as substrate, however, it is well known that not all environmental or gut-microbiome bacteria can be cultivated or isolated in this way, and also that batch cultivation selects for the fastest-growing organisms (Fuchs, Eitinger *et al.* 2014), which are not necessarily the ones that are most prominently catalyzing these degradation processes in the original habitat (here, in the human gut). Therefore, it is an interesting and important project in the future to determine which microbes and pathways are prevalent in the microbial community of, e.g., the human gut *in vivo*. One way to access a more diverse laboratory system for testing SQ degradation is cultivation in continuous culture, *i.e.*, a chemostat that in a simplified way mimics the conditions in the human gut, such as described in a review by Guzman-Rodriguez *et al.* (Guzman-Rodriguez, McDonald *et al.* 2018). For both types of examinations as well as direct fecal samples, metagenomic and especially metatranscriptomic analysis will give further valuable insights into the SQ degradation processes taking place *in vivo*.

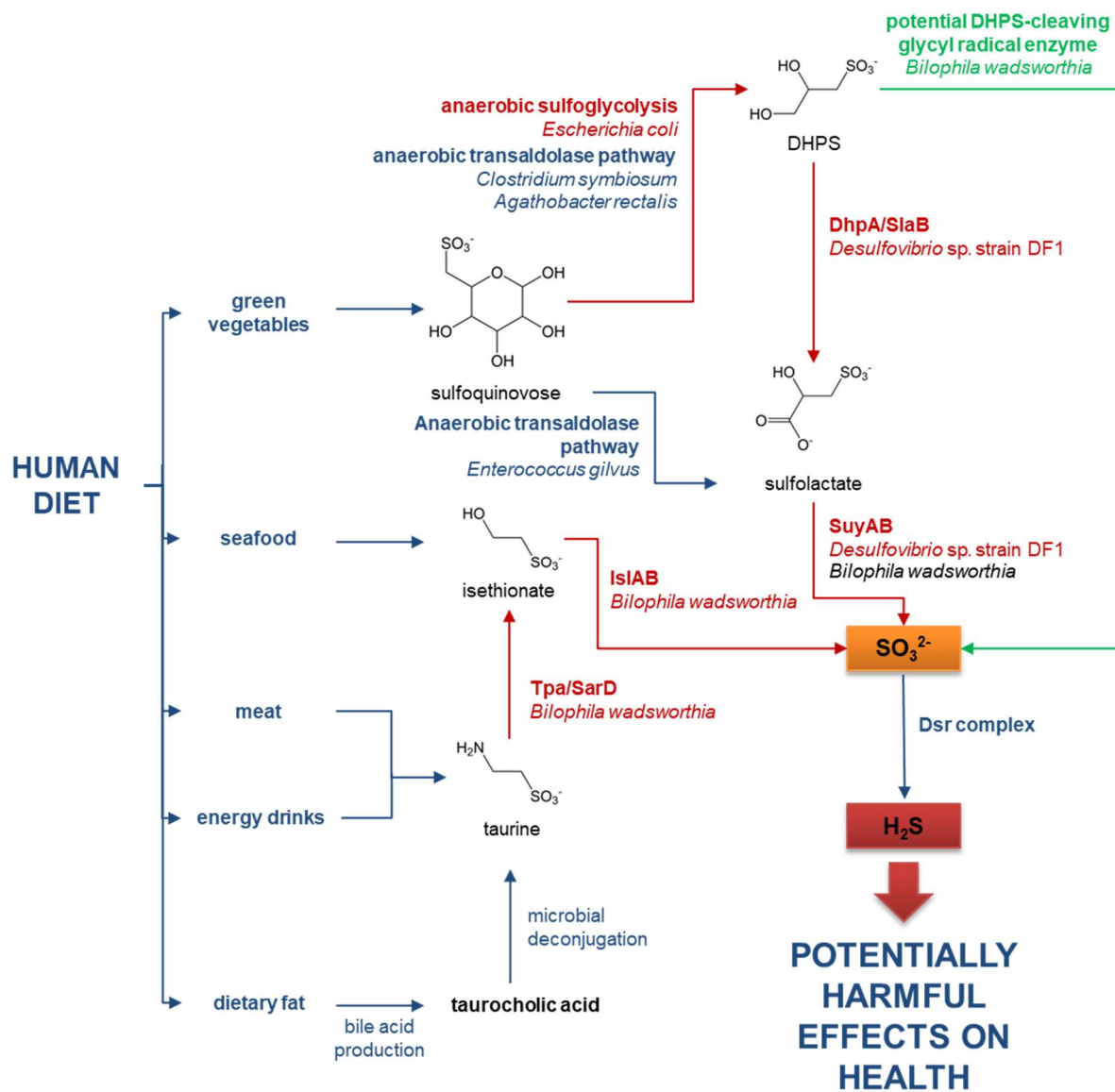


**Figure 5.1. The currently established anaerobic degradation pathways for organosulfonates.** In this work, the catabolic routes with the key enzymes marked in red were discovered or significant contributions to their clarification were made. The potential DHPS-cleaving GRE marked in green is still under examination in our group. DhpA: DHPS dehydrogenase; SlaB: sulfolactaldehyde dehydrogenase; SuyAB: sulfolactate sulfite-lyase; Tpa: taurine:pyruvate aminotransferase; SarD: sulfoacetaldehyde reductase; IsIAB: isethionate sulfite-lyase; Dsr: dissimilatory sulfite reductase

*B. wadsworthia* is known to be an important member of the human gut flora and is implicated in disease development (see Introduction and Chapter 3). It can utilize both DHPS and sulfolactate, which can be formed in the human gut from SQ as described above, as well as other C<sub>3</sub>- and C<sub>2</sub>-organosulfonates, most notably taurine (Figure 5.1). Taurine is a common substrate in the human gut and derives from dietary intake as meat, seafood and energy drinks, as well as being synthesized endogenously as part of taurocholate, one of the bile salts generated for the digestion of fat (for a more detailed description, see Chapter 4).

*B. wadsworthia* can only grow on low amounts of taurocholate and to very low densities. In

growth experiments done by myself and others, a consistently growing culture could never be established. It seems likely that *B. wadsworthia* is not specialized to use the whole molecule and struggles to tolerate the choline moiety. It would be worthwhile to investigate modifications to the culturing practice to potentially improve growth, such as providing surfaces for *B. wadsworthia* to form a protective biofilm, or by co-culture with a choline degrader. In contrast, *B. wadsworthia* grows readily on free taurine and an electron donor such as lactate. In fact, it is so specialized on organosulfonate respiration that it is unable (or has lost the ability) to respire inorganic sulfate. With the present work, we could elucidate important details of the strategies by which *B. wadsworthia* has adapted to this niche. In a collaborative project with Spencer Peck and Emily Balskus at the University of Harvard, the complete taurine degradation pathway was revealed and shown to proceed *via* a glycyl radical enzyme (GRE) that cleaves the carbon-sulfur bond of isethionate, which is the intermediate from taurine degradation (see Chapter 3). This enzyme represents a novel class of GREs, which were previously only known to cleave carbon-carbon, carbon-oxygen, or carbon-nitrogen bonds (Craciun and Balskus 2012). In fact, *B. wadsworthia* can express two of these desulfonating GREs: one that was shown to cleave isethionate into sulfite and acetaldehyde (IslAB) and is involved in isethionate and taurine metabolism (Chapter 3); and another one that is strongly expressed during growth with DHPS, as has been shown in a Bachelor thesis of Sebastian Haiß whom I supervised. Preliminary experiments by Karin Denger indicate that this second GRE cleaves DHPS into sulfite and hydroxyacetone. Further, during growth with sulfolactate, *B. wadsworthia* expresses another desulfonative enzyme, a SuyAB homolog, as has been characterized in *Desulfovibrio* sp. strain DF1 (Fiedler 2018). Finally, it was revealed that specifically during growth with isethionate and taurine, *B. wadsworthia* forms microcompartments (BMCs) in its cytosol, organelle-like substructures that isolate the GRE reaction within. In these compartments, the toxic and volatile acetaldehyde formed by IslAB is enclosed and further metabolized to acetylphosphate. Such microcompartments are not formed during growth with sulfolactate, which produces sulfite and non-toxic pyruvate instead of acetaldehyde. Hence, it is likely that the production of the toxic intermediate acetaldehyde requires isolation in a BMC. These GRE-associated microcompartments are a new and previously undescribed class of BMC.

One of the many intriguing questions that were identified through the results of this work, which are now accessible to future examination, is how the redox balance is maintained within the BMCs of *B. wadsworthia*. Typically, cofactors are internally recycled in a BMC, so as to not have to transport them across the shell, as described extensively in Chapter 4. Other aldehyde-forming microcompartments usually contain an alcohol dehydrogenase that reduces part of the aldehyde pool to its corresponding alcohol to regenerate NAD<sup>+</sup> for the

aldehyde dehydrogenase (Cheng, Fan *et al.* 2012; Huseby and Roth 2013), but the *B. wadsworthia* isethionate utilization gene cluster does not encode such a dehydrogenase. Instead, it contains a set of genes encoding enzymes with iron-sulfur clusters (PduS and PduT) that were demonstrated in two independent studies (Cheng and Bobik 2010; Parsons, Lawrence *et al.* 2010) to recycle the cobalamin cofactor of B<sub>12</sub>-dependent, BMC-encapsulated enzymes by reducing Co<sup>3+</sup> oxidized by side reactions back to Co<sup>+</sup> to form active cobalamin. It also contains a gene encoding a pyruvate:ferredoxin oxidoreductase that is highly expressed and associated with the BMC (Chapter 4). It is tempting to speculate whether these iron-sulfur clusters, including one that might be part of a BMC shell protein, and the flavin cofactors associated with them, may indeed function as a redox link between the inside and the outside of the microcompartment in order to shuttle electrons from NADH out of the BMC. Alternatively, they might be part of a system to recycle the S-adenosylmethionine cofactor that is required by IsIB in order to activate IsIA. Since a function of these iron-sulfur cluster-containing shell-proteins has so far only been described for PduS and PduT in association with the cobalamin of the B<sub>12</sub> cofactor, it is very interesting to overexpress and test these proteins for their ability to accept electrons from NADH (or to regenerate S-adenosylmethionine) in order to elucidate their function in a BMC not containing B<sub>12</sub>-dependent enzymes, and to complete the picture on the functions and roles of the isethionate-cleavage BMCs in *B. wadsworthia*.

In conclusion, in this thesis four bacterial pathways for anaerobic degradation of SQ, DHPS, sulfolactate or taurine, respectively, were revealed and each provided both the fundamental understanding as well as the enzyme and gene identities. On this basis these processes, which may lead to formation of H<sub>2</sub>S in the environment and in the human gut, can be examined in more detail in future. Furthermore, together with collaborators we identified a new class of GREs, cleaving carbon-sulfur bonds in a highly oxygen-sensitive radical reaction. In addition, it was shown that this GRE is contained in a BMC, thereby defining a new class of BMCs involved in the desulfonation of organosulfonates.

## List of abbreviations

Please note that in aqueous solutions, H<sub>2</sub>S, HS<sup>-</sup> and to a small extent S<sup>2-</sup> are in equilibrium at physiological pH, but that H<sub>2</sub>S will be used throughout this study to refer to all three species as well as to H<sub>2</sub>S in the gas phase.

Apart from the units given below, SI (*système international*) units (base and derived) and prefixes are used.

(2D-)PAGE:	(two-dimensional) polyacrylamide gel electrophoresis
(RT-)PCR:	(real-time) polymerase chain reaction, RT-PCR includes a quantitative measurement of DNA amplification
(Vitamine) B <sub>12</sub> :	adenosylcobalamin coenzyme
[M-H] <sup>-</sup> ion:	quasimolecular ion produced in electrospray ionization
<i>A. rectalis</i> :	<i>Agathobacter rectalis</i>
ABC transporter:	ATP-binding cassette transporter
AckA:	acetate kinase
AdhE:	acetylating acetaldehyde dehydrogenase
Ald:	alanine dehydrogenase
AMP/ADP/ATP:	adenosine-5'-mono-/di-/triphosphate
APS:	adenosine-5'-phosphosulfate
<i>B. wadsworthia</i> :	<i>Bilophila wadsworthia</i>
BDPA:	bisdiphenylene-β-phenylallyl), calibration compound for electron paramagnetic resonance spectroscopy
BLAST:	Basic Local Alignment Search Tool
BMC:	bacterial microcompartment
bp:	base pairs (DNA length measurement)
<i>C. freundii</i> :	<i>Citrobacter freundii</i>
<i>C. symbiosum</i> :	<i>Clostridium symbiosum</i>
ccmK, ccmL:	microcompartment shell protein originally identified in carboxysomes (carbon dioxide concentration mechanism)
CoA:	coenzyme A,
COG:	Clusters of Orthologous Groups
CutC:	choline trimethylamine-lyase
<i>D. alaskensis</i> :	<i>Desulfovibrio alaskensis</i>

Da:	Dalton (unified atomic mass unit)
DAD:	diode array detector
DctP:	substrate-binding protein of a TRAP transporter
DHAP:	dihydroxyacetonephosphate
DhpA:	dihydroxypropanesulfonate dehydrogenase (to sulfolactaldehyde)
DHPS:	2,3-dihydroxypropane-1-sulfonate
DNA:	deoxyribonucleic acid
DNPH:	dinitrophenylhydrazine
DSMZ:	German Collection of Microorganisms and Cell Cultures ( <i>Deutsche Sammlung von Mikroorganismen und Zellkulturen</i> )
Dsr:	dissimilatory sulfite reductase
DTT:	dithiothreitol
<i>E. coli</i> :	<i>Escherichia coli</i>
<i>E. gilvus</i> :	<i>Enterococcus gilvus</i>
e.g.:	<i>exempli gratia</i> , for example
EDTA:	ethylenediaminetetraacetic acid
ELSD:	evaporative light scattering detector
EMP (pathway):	Embden-Meyerhof-Parnas pathway (glucose metabolism)
EPR:	electron paramagnetic resonance spectroscopy
ESI:	electrospray ionization
<i>et al.</i> :	<i>et alii</i> , and others
EutN:	microcompartment shell protein originally identified in ethanolamine utilization microcompartments
<i>g</i> :	Earth's gravity, used to denote relative centrifugal forces
G6P:	glucose-6-phosphate
GAP:	glyceraldehyde 3-phosphate
GRE:	glycyl radical enzyme
h:	hour
HEPES:	(2-[4-(2-hydroxyethyl)piperazin-1-yl]ethanesulfonic acid
HILIC:	hydrophilic interaction liquid chromatography
His:	histidine
HPLC:	high performance liquid chromatography
HpsN:	dihydroxypropanesulfonate dehydrogenase (to sulfolactate)
<i>i.e.</i> :	<i>id est</i> , it/that is

IBD:	irritable bowel syndrome
IMG/M:	Integrated Microbial Genomes & Microbiomes
IPTG:	isopropyl $\beta$ -d-1-thiogalactopyranoside
IslAB.	isethionate sulfo-lyase
JGI:	Joint Genome Institute
$K_d$ :	dissociation constant
$K_M^{app}$ :	apparent Michaelis constant (in Michaelis-Menten enzyme kinetics).
LB:	lysogeny broth or Luria-Bertani medium, both referring to the same medium
min:	minute
MOPS:	3-( <i>N</i> -morpholino)propanesulfonic acid
MS:	mass spectrometry
$NAD^+$ /NADH:	nicotinamide adenine dinucleotide, oxidized/reduced form
$NADP^+$ /NADPH: form	nicotinamide adenine dinucleotide phosphate, oxidized/reduced
NAM:	<i>N</i> -(9-acridinyl)-maleimide
NCBI:	National Center for Biotechnology Information
NTA:	nitrilotriacetic acid
$OD_{xnm}$ :	optical density (absorbance) measurement at a wavelength of x nm
PD:	1,2-propanediol dehydratase
PDB:	Protein Data Bank
PduS:	cobalamin reductase originally identified in propanediol utilization microcompartments
PduT:	microcompartment shell protein originally identified in propanediol utilization microcompartments
PEP:	phosphoenolpyruvate;
pfam:	protein family database
PFL:	pyruvate-formate lyase;
PFOR:	pyruvate:ferredoxin oxidoreductase
$P_i$ :	phosphate (inorganic)
Pta:	phosphotransacetylase
R-	organic side chain
RID:	refractive index detector
RNA:	ribonucleic acid

RnfC:	$\text{Na}^+$ -translocating ferredoxin:NAD <sup>+</sup> oxidoreductase, subunit of the Rnf complex
SAM:	S-adenosylmethionine
SarD:	sulfoacetaldehyde reductase
Sat:	sulfate adenylyltransferase
SDS:	sodium dodecyl sulfate
SF:	6-deoxy-6-sulfofructose
SFP:	6-deoxy-6-sulfofructose phosphate;
SL:	3-sulfolactate
SLA:	3-sulfolactaldehyde
SlaB:	sulfolactaldehyde dehydrogenase
SOC:	Super Optimal broth with Catabolite repression
SQ:	sulfoquinovose (6-desoxy-6-sulfoglucose)
SQDG:	sulfoquinovosyl diacylglycerols
SuyAB:	sulfolactate sulfite-lyase
TDP:	thiamine diphosphate
TEM:	transmission electron microscopy
TIC:	total ion count (in mass spectrometry)
Tpa:	taurine:pyruvate aminotransferase
TRAP:	tripartite ATP-independent periplasmic transporter
Tris:	tris(hydroxymethyl)aminomethane
U:	unit for measuring enzyme activity ("Unit"), corresponding to one $\mu\text{mol}$ of substrate turnover per minute
$V_{\max}$ :	maximum reaction rate in Michaelis-Menten enzyme kinetics
v/v:	volume per volume (referring to concentrations given in percent)
w/v:	weight per volume (referring to concentrations given in percent)

## Additional material

**Table S3.1 (Chapter 3). List of predicted isethionate sulfite-lyases or other C–S bond cleaving GREs as retrieved from the non-redundant NCBI database at a threshold of 62% identity.**

No.	Annotation	Taxonomy					Accession
		Phylum	Class	Order	Family	Species / Organism	Genbank
1	Formate acetyltransferase	Actinobacteria	Actinobacteria	Bifidobacteriales	Bifidobacteriaceae	<i>Bifidobacterium callitrichos</i> DSM 23973	WP_043166045.1
2	Formate acetyltransferase	Actinobacteria	Actinobacteria	Bifidobacteriales	Bifidobacteriaceae	<i>Bifidobacterium tissieri</i>	OZG57617.1
3	Formate acetyltransferase	Actinobacteria	Actinobacteria	Bifidobacteriales	Bifidobacteriaceae	<i>Bifidobacterium tissieri</i>	WP_094663811.1
4	Glycyl radical enzyme	Actinobacteria	Coriobacteriia	Eggerthellales	Eggerthellaceae	<i>Gordonibacter</i> sp. An230	WP_087193818.1
5	4-Hydroxyphenylacetate decarboxylase	Bacteroidetes	Bacteroidia	Bacteroidales		<i>Bacteroidales</i> bacterium Barb6XT	OAV69163.1
6	Glycyl radical enzyme	Bacteroidetes	Bacteroidia	Bacteroidales		<i>Bacteroidales</i> bacterium Barb6XT	WP_066178498.1
7	Glycyl radical enzyme	Firmicutes	Bacilli	Bacillales	Paenibacillaceae	<i>Fontibacillus panacisegetis</i>	WP_091226859.1
8	Formate acetyltransferase	Firmicutes	Bacilli	Bacillales	Paenibacillaceae	<i>Paenibacillus borealis</i>	WP_042216496.1
9	Formate acetyltransferase	Firmicutes	Clostridia	Clostridiales	Lachnospiraceae	<i>Anaerostipes hadrus</i>	AQP40533.1
10	Formate acetyltransferase	Firmicutes	Clostridia	Clostridiales	Lachnospiraceae	<i>Anaerostipes hadrus</i> DSM 3319	EKY23466.1
11	Glycyl radical protein	Firmicutes	Clostridia	Clostridiales	Clostridiaceae	<i>Clostridium arbusti</i> SL206	WP_010235418.1
12	Formate acetyltransferase	Firmicutes	Clostridia	Clostridiales	Clostridiaceae	<i>Clostridium butyricum</i>	WP_027636278.1
13	Formate acetyltransferase	Firmicutes	Clostridia	Clostridiales	Clostridiaceae	<i>Clostridium butyricum</i>	WP_043853189.1
14	Glycyl radical enzyme	Firmicutes	Clostridia	Clostridiales	Clostridiaceae	<i>Clostridium butyricum</i>	WP_071982924.1
15	Formate acetyltransferase	Firmicutes	Clostridia	Clostridiales	Clostridiaceae	<i>Clostridium butyricum</i> E4 str. BoNT	WP_003406960.1
16	Benzylsuccinate synthase	Firmicutes	Clostridia	Clostridiales	Clostridiaceae	<i>Clostridium chromiireducens</i>	OPJ59679.1
17	Putative formate acetyltransferase	Firmicutes	Clostridia	Clostridiales	Clostridiaceae	<i>Clostridium cylindrosporum</i> DSM 605	WP_048570467.1
18	Pyruvate formate-lyase	Firmicutes	Clostridia	Clostridiales	Clostridiaceae	<i>Clostridium pasteurianum</i> BC1	WP_015614283.1
19	Glycyl radical protein	Firmicutes	Clostridia	Clostridiales	Peptococcaceae	<i>Dehalobacterium formicoaceticum</i>	WP_089608549.1

20	Glycyl radical enzyme	Firmicutes	Clostridia	Clostridiales	Peptococcaceae	<i>Desulfitibacter</i> sp. BRH_c19	KUO50820.1
21	Pyruvate formate-lyase	Firmicutes	Clostridia	Clostridiales	Peptococcaceae	<i>Desulfitobacterium dehalogenans</i> ATCC 51507	WP_014792329.1
22	Formate acetyltransferase	Firmicutes	Clostridia	Clostridiales	Peptococcaceae	<i>Desulfitobacterium hafniense</i>	WP_011459062.1
23	Formate acetyltransferase	Firmicutes	Clostridia	Clostridiales	Peptococcaceae	<i>Desulfitobacterium hafniense</i> DCB-2	WP_015942724.1
24	Formate acetyltransferase	Firmicutes	Clostridia	Clostridiales	Peptococcaceae	<i>Desulfitobacterium hafniense</i> DP7	WP_005810281.1
25	Pyruvate formate-lyase	Firmicutes	Clostridia	Clostridiales	Peptococcaceae	<i>Desulfitobacterium hafniense</i> Y51	BAE82205.1
26	Pyruvate formate-lyase	Firmicutes	Clostridia	Clostridiales	Peptococcaceae	<i>Desulfosporosinus youngiae</i> DSM 17734	WP_007786432.1
27	Formate acetyltransferase	Firmicutes	Clostridia	Clostridiales	Peptococcaceae	<i>Desulfotomaculum aeronauticum</i> DSM 10349	WP_072912824.1
28	Glycyl radical protein	Firmicutes	Clostridia	Clostridiales	Peptococcaceae	<i>Desulfotomaculum arcticum</i> DSM 17038	WP_092474605.1
29	Glycyl radical enzyme	Firmicutes	Clostridia	Clostridiales	Peptococcaceae	<i>Desulfotomaculum ferrireducens</i>	AQS57885.1
30	Formate acetyltransferase	Firmicutes	Clostridia	Clostridiales	Peptococcaceae	<i>Desulfotomaculum kuznetsovii</i> DSM 6115	AEG16045.1
31	Glycyl radical protein	Firmicutes	Clostridia	Clostridiales	Peptococcaceae	<i>Desulfotomaculum nigrificans</i> DSM 574	WP_003540773.1
32	Formate acetyltransferase	Firmicutes	Clostridia	Clostridiales	Peptococcaceae	<i>Desulfotomaculum reducens</i> MI-1	WP_011879050.1
33	Formate acetyltransferase	Firmicutes	Clostridia	Clostridiales	Peptococcaceae	<i>Desulfotomaculum ruminis</i> DSM 2154	WP_013840536.1
34	Pyruvate formate-lyase	Firmicutes	Clostridia	Clostridiales	Eubacteriaceae	<i>Eubacterium cellulosolvens</i> 6	WP_004602188.1
35	Glycyl radical enzyme	Firmicutes	Clostridia	Clostridiales	Eubacteriaceae	<i>Eubacterium oxidoreducens</i>	WP_090171121.1
36	Glycyl radical enzyme	Firmicutes	Clostridia	Clostridiales	Eubacteriaceae	<i>Pseudobutyrivibrio</i> sp. OR37	WP_090549811.1
37	Glycyl radical enzyme	Firmicutes	Clostridia	Clostridiales		<i>Clostridiales</i> bacterium 36_14	OKZ78447.1
38	Formate acetyltransferase	Firmicutes	Clostridia	Clostridiales	Lachnospiraceae	<i>Lachnospiraceae</i> bacterium	SKB77358.1
39	Pyruvate formate-lyase	Firmicutes	Clostridia	Clostridiales	Lachnospiraceae	<i>Lachnospiraceae</i> bacterium 5_1_63FAA	EFV17604.1
40	Glycyl radical enzyme	Firmicutes	Clostridia	Clostridiales	Peptococcaceae	<i>Peptococcus niger</i>	WP_091791955.1
41	Formate acetyltransferase	Firmicutes	Clostridia	Clostridiales	Lachnospiraceae	<i>Pseudobutyrivibrio ruminis</i>	WP_074791333.1
42	Glycyl radical enzyme	Firmicutes	Clostridia	Clostridiales	Lachnospiraceae	<i>Pseudobutyrivibrio</i> sp. JW11	WP_090481662.1
43	Formate acetyltransferase	Firmicutes	Clostridia	Clostridiales	Peptococcaceae	<i>Peptococcaceae</i> bacterium BICA1-8	KJS86610.1

44	Pyruvate formate-lyase	Firmicutes	Negativicutes	Selenomonadales	Selenomonadaceae	<i>Anaerovibrio</i> sp. JC8	ORT99124.1
45	Formate acetyltransferase	Firmicutes	Negativicutes	Selenomonadales	Selenomonadaceae	<i>Anaerovibrio</i> sp. RM50	WP_027406814.1
46	Glycyl radical protein	Firmicutes	Negativicutes	Selenomonadales	Sporomusaceae	<i>Dendrosporobacter querciculus</i> DSM 1736	WP_092073083.1
47	Glycyl radical protein	Firmicutes	Negativicutes	Selenomonadales	Sporomusaceae	<i>Propionispora vibrioides</i> DSM 13305	WP_091749809.1
48	Pyruvate formate-lyase	Firmicutes	Negativicutes	Selenomonadales	Sporomusaceae		SCM78628.1
49	Pyruvate formate-lyase	Firmicutes	Negativicutes	Selenomonadales	Sporomusaceae		SCM78658.1
50	Glycyl radical enzyme	Firmicutes	Negativicutes	Selenomonadales	Sporomusaceae	<i>Sporomusa silvacetica</i>	WP_094606507.1
51	Benzylsuccinate synthase	Firmicutes	Negativicutes	Selenomonadales	Sporomusaceae	<i>Sporomusa silvacetica</i> DSM 10669	OZC15302.1
52	Glycyl radical protein	Firmicutes	Negativicutes	Selenomonadales	Sporomusaceae	<i>Sporomusa silvacetica</i> DSM 10669	WP_094606471.1
53	Benzylsuccinate synthase	Firmicutes	Negativicutes	Selenomonadales	Sporomusaceae	<i>Sporomusa sphaeroides</i> DSM 2875	WP_075757473.1
54	Benzylsuccinate synthase	Firmicutes	Negativicutes	Selenomonadales	Sporomusaceae	<i>Sporomusa sphaeroides</i> DSM 2875	WP_075757489.1
55	Formate acetyltransferase	Proteobacteria	Deltaproteobacteria	Desulfobacterales	Desulfobulbaceae	<i>Desulfopila aestuariai</i> DSM 18488	WP_073616382.1
56	Glycyl radical protein	Proteobacteria	Deltaproteobacteria	Desulfobacterales	Desulfobacteraceae	<i>Desulfovira joergensenii</i> DSM 10085	WP_033398525.1
57	Formate acetyltransferase	Proteobacteria	Deltaproteobacteria	Desulfobacterales	Desulfobulbaceae	<i>Desulfotalea psychrophila</i> LSv54	WP_011190268.1
58	Uncharacterized protein	Proteobacteria	Deltaproteobacteria	Desulfovibrionales	Desulfovibrionaceae	<i>Bilophila</i> sp. 4_1_30	WP_009368175.1
59	Uncharacterized protein	Proteobacteria	Deltaproteobacteria	Desulfovibrionales	Desulfovibrionaceae	<i>Bilophila</i> sp. 4_1_30	WP_009733371.1
60	Glycyl radical protein	Proteobacteria	Deltaproteobacteria	Desulfovibrionales	Desulfovibrionaceae	<i>Bilophila wadsworthia</i>	WP_029436929.1
61	Glycyl radical enzyme	Proteobacteria	Deltaproteobacteria	Desulfovibrionales	Desulfovibrionaceae	<i>Bilophila wadsworthia</i>	WP_005027953.1
62	Glycyl radical protein	Proteobacteria	Deltaproteobacteria	Desulfovibrionales	Desulfomicrobiaceae	<i>Desulfomicrobium apsheronum</i>	WP_092373161.1
63	Formate acetyltransferase	Proteobacteria	Deltaproteobacteria	Desulfovibrionales	Desulfomicrobiaceae	<i>Desulfomicrobium baculum</i> DSM 4028	WP_015773771.1
64	Formate acetyltransferase	Proteobacteria	Deltaproteobacteria	Desulfovibrionales	Desulfomicrobiaceae	<i>Desulfomicrobium baculum</i> DSM 4028	WP_015774320.1
65	Glycyl radical protein	Proteobacteria	Deltaproteobacteria	Desulfovibrionales	Desulfomicrobiaceae	<i>Desulfomicrobium escambiense</i>	WP_028577862.1
66	Glycyl radical protein	Proteobacteria	Deltaproteobacteria	Desulfovibrionales	Desulfomicrobiaceae	<i>Desulfomicrobium norvegicum</i>	WP_092191323.1
67	Formate acetyltransferase	Proteobacteria	Deltaproteobacteria	Desulfovibrionales	Desulfonatronaceae	<i>Desulfonatronum thioautotrophicum</i>	WP_045218508.1
68	Formate acetyltransferase	Proteobacteria	Deltaproteobacteria	Desulfovibrionales	Desulfomicrobiaceae	<i>Desulfoplanes formicivorans</i>	WP_069857699.1
69	Formate acetyltransferase	Proteobacteria	Deltaproteobacteria	Desulfovibrionales	Desulfomicrobiaceae	<i>Desulfoplanes formicivorans</i>	WP_069858090.1

70	Formate acetyltransferase	Proteobacteria	Deltaproteobacteria	Desulfovibrionales	Desulfovibrionaceae	<i>Desulfovibrio bizertensis</i> DSM 18034	SKA70293.1
71	Glycyl radical protein	Proteobacteria	Deltaproteobacteria	Desulfovibrionales	Desulfovibrionaceae	<i>Desulfovibrio cuneatus</i> DSM 11391	WP_027187538.1
72	Formate acetyltransferase	Proteobacteria	Deltaproteobacteria	Desulfovibrionales	Desulfovibrionaceae	<i>Desulfovibrio desulfuricans</i>	SFW72879.1
73	Formate acetyltransferase	Proteobacteria	Deltaproteobacteria	Desulfovibrionales	Desulfovibrionaceae	<i>Desulfovibrio desulfuricans</i>	WP_020000116.1
74	Glycyl radical protein	Proteobacteria	Deltaproteobacteria	Desulfovibrionales	Desulfovibrionaceae	<i>Desulfovibrio desulfuricans</i>	WP_022658610.1
75	Glycyl radical protein	Proteobacteria	Deltaproteobacteria	Desulfovibrionales	Desulfovibrionaceae	<i>Desulfovibrio desulfuricans</i>	WP_041724859.1
76	Pyruvate formate-lyase	Proteobacteria	Deltaproteobacteria	Desulfovibrionales	Desulfovibrionaceae	<i>Desulfovibrio desulfuricans</i> ND132	WP_014322652.1
77	Formate acetyltransferase	Proteobacteria	Deltaproteobacteria	Desulfovibrionales	Desulfovibrionaceae	<i>Desulfovibrio desulfuricans</i> subsp. <i>desulf.</i> ATCC 27774	ACL49338.1
78	Glycyl radical enzyme	Proteobacteria	Deltaproteobacteria	Desulfovibrionales	Desulfovibrionaceae	<i>Desulfovibrio fairfieldensis</i>	AMD91514.1
79	Glycyl radical protein	Proteobacteria	Deltaproteobacteria	Desulfovibrionales	Desulfovibrionaceae	<i>Desulfovibrio fairfieldensis</i>	WP_083521970.1
80	Formate acetyltransferase	Proteobacteria	Deltaproteobacteria	Desulfovibrionales	Desulfovibrionaceae	<i>Desulfovibrio litoralis</i> DSM 11393	WP_072695368.1
81	Glycyl radical protein	Proteobacteria	Deltaproteobacteria	Desulfovibrionales	Desulfovibrionaceae	<i>Desulfovibrio oxyclinae</i> DSM 11498	WP_018124699.1
82	Formate acetyltransferase	Proteobacteria	Deltaproteobacteria	Desulfovibrionales	Desulfovibrionaceae	<i>Desulfovibrio piezophilus</i> C1TLV30	CCH48387.1
83	Glycyl radical protein	Proteobacteria	Deltaproteobacteria	Desulfovibrionales	Desulfovibrionaceae	<i>Desulfovibrio piezophilus</i> C1TLV30	WP_041720703.1
84	Pyruvate formate-lyase	Proteobacteria	Deltaproteobacteria	Desulfovibrionales	Desulfovibrionaceae	<i>Desulfovibrio piger</i>	WP_072335172.1
85	Formate acetyltransferase	Proteobacteria	Deltaproteobacteria	Desulfovibrionales	Desulfovibrionaceae	<i>Desulfovibrio piger</i> ATCC 29098	WP_006008826.1
86	Uncharacterized protein	Proteobacteria	Deltaproteobacteria	Desulfovibrionales	Desulfovibrionaceae	<i>Desulfovibrio</i> sp. 6_1_46AFAA	EGW52515.1
87	Glycyl radical protein	Proteobacteria	Deltaproteobacteria	Desulfovibrionales	Desulfovibrionaceae	<i>Desulfovibrio</i> sp. A2	EGY24021.1
88	Glycyl radical protein	Proteobacteria	Deltaproteobacteria	Desulfovibrionales	Desulfovibrionaceae	<i>Desulfovibrio</i> sp. A2	WP_007525054.1
89	Glycyl radical protein	Proteobacteria	Deltaproteobacteria	Desulfovibrionales	Desulfovibrionaceae	<i>Desulfovibrio</i> sp. A2	WP_043610275.1
90	Glycyl radical protein	Proteobacteria	Deltaproteobacteria	Desulfovibrionales	Desulfovibrionaceae	<i>Desulfovibrio</i> sp. An276	WP_087349870.1
91	Glycyl radical protein	Proteobacteria	Deltaproteobacteria	Desulfovibrionales	Desulfovibrionaceae	<i>Desulfovibrio</i> sp. An276	WP_087350898.1
92	Glycyl radical protein	Proteobacteria	Deltaproteobacteria	Desulfovibrionales	Desulfovibrionaceae	<i>Desulfovibrio</i> sp. An276	WP_087355015.1
93	Glycyl radical protein	Proteobacteria	Deltaproteobacteria	Desulfovibrionales	Desulfovibrionaceae	<i>Desulfovibrio</i> sp. MES5	OXS28002.1
94	Glycyl radical protein	Proteobacteria	Deltaproteobacteria	Desulfovibrionales	Desulfovibrionaceae	<i>Desulfovibrio termitidis</i>	WP_035067385.1
95	Glycyl radical protein	Proteobacteria	Deltaproteobacteria	Desulfovibrionales	Desulfovibrionaceae	<i>Desulfovibrio termitidis</i> HI1	WP_035063873.1
96	Formate acetyltransferase	Proteobacteria	Deltaproteobacteria	Desulfovibrionales	Desulfovibrionaceae	<i>Desulfovibrio vulgaris</i> DP4	WP_011791647.1
97	Pyruvate formate-lyase	Proteobacteria	Deltaproteobacteria	Desulfovibrionales	Desulfovibrionaceae	<i>Desulfovibrio vulgaris</i> RCH1	ADP87748.1

98	Formate acetyltransferase	Proteobacteria	Deltaproteobacteria	Desulfovibrionales	Desulfovibrionaceae	<i>Desulfovibrio vulgaris</i> str. Hildenborough ATCC 29579	WP_010940090.1
99	Glycyl radical enzyme	Proteobacteria	Deltaproteobacteria	Desulfovibrionales	Desulfovibrionaceae	uncultured <i>Desulfovibrio</i> sp.	SBV92506.1
100	Formate acetyltransferase	Proteobacteria	Deltaproteobacteria	Desulfovibrionales	Desulfovibrionaceae	uncultured <i>Desulfovibrio</i> sp.	SBW01768.1
101	Glycyl radical protein	Proteobacteria	Deltaproteobacteria	Desulfovibrionales	Desulfovibrionaceae	<i>Halodesulfovibrio aestuarii</i>	WP_027361990.1
102	Formate acetyltransferase	Proteobacteria	Deltaproteobacteria	Desulfovibrionales	Desulfovibrionaceae	<i>Halodesulfovibrio marinisediminis</i> DSM 17456	WP_074216573.1
103	Formate acetyltransferase	Proteobacteria	Deltaproteobacteria	Desulfovibrionales	Desulfovibrionaceae	<i>Halodesulfovibrio spirochaetisodalis</i>	WP_066852996.1
104	Glycyl radical enzyme	Proteobacteria	Deltaproteobacteria	Desulfovibrionales	Desulfovibrionaceae	<i>Mailhella massiliensis</i>	WP_077071615.1
105	Glycyl radical enzyme	Proteobacteria	Deltaproteobacteria	Desulfovibrionales	Desulfovibrionaceae	<i>Mailhella massiliensis</i>	WP_077073585.1
106	Glycyl radical protein	Proteobacteria	Deltaproteobacteria	Desulfovibrionales	Desulfovibrionaceae	<i>Mailhella massiliensis</i>	WP_077073949.1
107	Glycyl radical protein	Proteobacteria	Deltaproteobacteria	Desulfovibrionales	Desulfovibrionaceae	<i>Mailhella massiliensis</i>	WP_077073952.1
108	Formate acetyltransferase	Proteobacteria	Deltaproteobacteria	Syntrophobacterales	Syntrophobacteraceae	<i>Desulfacinum hydrothermale</i> DSM 13146	SMC22069.1
109	Formate acetyltransferase	Proteobacteria	Deltaproteobacteria	Syntrophobacterales	Syntrophobacteraceae	<i>Desulfacinum infernum</i> DSM 9756	WP_073041932.1
110	Pyruvate formate-lyase	Proteobacteria	Gammaproteobacteria	Enterobacterales	Pectobacteriaceae	<i>Brenneria goodwinii</i>	WP_048638610.1
111	Formate acetyltransferase	Proteobacteria	Gammaproteobacteria	Enterobacterales	Pectobacteriaceae	<i>Brenneria</i> sp. EniD312	WP_009112175.1
112	Glycyl radical protein	Proteobacteria	Gammaproteobacteria	Enterobacterales	Pectobacteriaceae	<i>Pectobacterium parmentieri</i> CFIA1002	WP_025920032.1
113	Formate acetyltransferase	Proteobacteria	Gammaproteobacteria	Enterobacterales	Pectobacteriaceae	<i>Pectobacterium parmentieri</i> WPP163	WP_015731066.1
114	Pyruvate formate-lyase	Proteobacteria	Gammaproteobacteria	Enterobacterales	Pectobacteriaceae	<i>Pectobacterium</i> sp. SCC3193	WP_014701133.1
115	Glycyl radical enzyme	Proteobacteria	Gammaproteobacteria	Enterobacterales	Pectobacteriaceae	<i>Pectobacterium wasabiae</i> CFBP 3304	WP_005975687.1

## **Record of achievement and list of publications**

**Chapter 2:** I designed and performed all growth experiments on the pure cultures of *E. coli* and its knockout mutants, *Desulfovibrio* sp. DF1, and the coculture of these (not including the isolation and purification of *Desulfovibrio* sp. DF1), for these experiments I also performed all substrate and product analysis as well as sample preparation and analysis of proteomics measurement and 2D-PAGE. I repeated experiments regarding to enzyme activities in cell-free extracts and designed and performed all cloning, expression, purification and activity measurements of heterologous enzymes. Furthermore, I did the phylogenetic analysis and contributed to the text and figures of the manuscript.

**Chapter 3:** I performed all cloning, expression, purification and activity measurements of heterologous taurine:pyruvate aminotransferase and sulfoacetaldehyde reductase and prepared samples for proteomic analysis. I designed figures and wrote method sections relating to these experiments.

**Chapter 4:** I designed and analysed all experiments and performed most replicates of the activity measurements. I supervised the execution of the other enzyme activity assays and proteomic analysis, electron microscopy and transcriptomic analysis in the course of the thesis work by Stefanie Dörr and Sebastian Haiß. I also wrote the manuscript.

### **Chapters of this thesis are published as follows:**

Burrichter, Anna, Denger, Karin, Franchini, Paolo, Huhn, Thomas, Müller, Nicolai, Spiteller, Dieter, Schleheck, David (2018): Anaerobic Degradation of the Plant Sugar Sulfoquinovose Concomitant With H<sub>2</sub>S Production: *Escherichia coli* K-12 and *Desulfovibrio* sp. Strain DF1 as Co-culture Model. *Frontiers in Microbiology* 9(2792).

Peck, Spencer C., Denger, Karin, Burrichter, Anna, Irwin, Stephania M., Balskus, Emily P., Schleheck, David (2019): A glycyl radical enzyme enables hydrogen sulfide production by the human intestinal bacterium *Bilophila wadsworthia*. *Proceedings of the National Academy of Sciences* 116(8):3171.

### **Further publication to be submitted:**

Burrichter, Anna, Bergmann, Paavo, Dörr, Stefanie, Haiß, Sebastian, Schleheck, David (2018): Bacterial microcompartments as part of taurine metabolism in *Bilophila wadsworthia*.

## References

- Abayakoon, P., Lingford, J. P., Jin, Y., Bengt, C., Davies, G. J., Yao, S., Goddard-Borger, E. D. and Williams, S. J. (2017): "Discovery and characterization of a sulfoquinovose mutarotase using kinetic analysis at equilibrium by exchange spectroscopy." *Biochemical Journal* **475**(7): 1371-1383.
- Akasaka, K., Matsuda, H., Ohrui, H., Meguro, H. and Suzuki, T. (1990): "Fluorometric determination of sulfite in wine by *N*-(9-acridinyl)maleimide." *Agricultural and Biological Chemistry* **54**(2): 501-504.
- Akhtar, M. K. and Jones, P. R. (2008): "Deletion of *iscR* stimulates recombinant clostridial Fe-Fe hydrogenase activity and H<sub>2</sub>-accumulation in *Escherichia coli* BL21(DE3)." *Applied Microbiology and Biotechnology* **78**(5): 853-862.
- Anderson, R., Kates, M. and Volcani, B. E. (1978): "Identification of the sulfolipids in the non-photosynthetic diatom *Nitzschia alba*." *Biochimica et Biophysica Acta* **528**(1): 89-106.
- Anderson, T. F. and Pratt, L. M. (1995): Isotopic evidence for the origin of organic sulfur and elemental sulfur in marine sediments. *Geochemical Transformations of Sedimentary Sulfur*. American Chemical Society. **612**: 378-396.
- Arzese, A., Mercuri, F., Trevisan, R., Menozzi, M. G. and Botta, G. A. (1997): "Recovery of *Bilophila wadsworthia* from clinical specimens in Italy." *Anaerobe* **3**(4): 219-224.
- Attene-Ramos, M. S., Nava, G. M., Muellner, M. G., Wagner, E. D., Plewa, M. J. and Gaskins, H. R. (2010): "DNA damage and toxicogenomic analyses of hydrogen sulfide in human intestinal epithelial FHs 74 Int cells." *Environmental and Molecular Mutagenesis* **51**(4): 304-314.
- Attene-Ramos, M. S., Wagner, E. D., Gaskins, H. R. and Plewa, M. J. (2007): "Hydrogen sulfide induces direct radical-associated DNA damage." *Molecular Cancer Research* **5**(5): 455-459.
- Attene-Ramos, M. S., Wagner, E. D., Plewa, M. J. and Gaskins, H. R. (2006): "Evidence that hydrogen sulfide is a genotoxic agent." *Molecular Cancer Research* **4**(1): 9.
- Autry, A. R. and Fitzgerald, J. W. (1990): "Sulfonate S: A major form of forest soil organic sulfur." *Biology and Fertility of Soils* **10**(1): 50-56.
- Axen, S. D., Erbilgin, O. and Kerfeld, C. A. (2014): "A taxonomy of bacterial microcompartment loci constructed by a novel scoring method." *PLoS Computational Biology* **10**(10): e1003898.
- Baba, T., Ara, T., Hasegawa, M., Takai, Y., Okumura, Y., Baba, M., Datsenko, K. A., Tomita, M., Wanner, B. L. and Mori, H. (2006): "Construction of *Escherichia coli* K-12 in-frame, single-gene knockout mutants: the Keio collection." *Molecular Systems Biology* **2**: 2006.0008.
- Backman, L. R. F., Funk, M. A., Dawson, C. D. and Drennan, C. L. (2017): "New tricks for the glycyl radical enzyme family." *Critical Reviews in Biochemistry and Molecular Biology* **52**(6): 674-695.
- Badziong, W. and Thauer, R. K. (1978): "Growth yields and growth rates of *Desulfovibrio vulgaris* (Marburg) growing on hydrogen plus sulfate and hydrogen plus thiosulfate as the sole energy sources." *Archives of Microbiology* **117**(2): 209-214.
- Baron, E. J. (1997): "*Bilophila wadsworthia*: a unique Gram-negative anaerobic rod." *Anaerobe* **3**(2): 83-86.
- Baron, E. J., Curren, M., Henderson, G., Jousimies-Somer, H., Lee, K., Lechowitz, K., Strong, C. A., Summanen, P., Tuner, K. and Finegold, S. M. (1992): "*Bilophila wadsworthia* isolates from clinical specimens." *Journal of Clinical Microbiology* **30**(7): 1882-1884.
- Baron, E. J., Summanen, P., Downes, J., Roberts, M. C., Wexler, H. and Finegold, S. M. (1989): "*Bilophila wadsworthia*, gen. nov. and sp. nov., a unique gram-negative anaerobic rod recovered from appendicitis specimens and human faeces." *Journal of General and Applied Microbiology* **135**(12): 3405-3411.
- Bastiaanssen, T. F. S., Cowan, C. S. M., Claesson, M. J., Dinan, T. G. and Cryan, J. F. (2018): "Making sense of ... the microbiome in psychiatry." *International Journal of Neuropsychopharmacology* **22**(1): 37-52.

- Benson, A. A. (1963): "The plant sulfolipid." *Advances in Lipid Research* **1**: 387-394.
- Benson, A. A., Daniel, H. and Wiser, R. (1959): "A sulfolipid in plants." *Proceedings of the National Academy of Sciences of the United States of America* **45**(11): 1582-1587.
- Benson, A. A. and Shibuya, I. (1961): "Sulfocarbohydrate metabolism." *Federation Proceedings* **20**: 79.
- Bergmeyer, H. U. (1970): Methoden der enzymatischen Analyse. Bd 2. Vlg. Chemie.
- Bianchi, V., Eliasson, R., Fontecave, M., Mulliez, E., Hoover, D. M., Matthews, R. G. and Reichard, P. (1993): "Flavodoxin is required for the activation of the anaerobic ribonucleotide reductase." *Biochemical and Biophysica Research Communications* **197**(2): 792-797.
- Bobik, T. A., Havemann, G. D., Busch, R. J., Williams, D. S. and Aldrich, H. C. (1999): "The propanediol utilization (*pdu*) operon of *Salmonella enterica* serovar Typhimurium LT2 includes genes necessary for formation of polyhedral organelles involved in coenzyme B<sub>12</sub>-dependent 1,2-propanediol degradation." *Journal of Bacteriology* **181**(19): 5967-5975.
- Bodea, S., Funk, M. A., Balskus, E. P. and Drennan, C. L. (2016): "Molecular basis of C-N bond cleavage by the glycyl radical enzyme choline trimethylamine-lyase." *Cell Chemical Biology* **23**(10): 1206-1216.
- Bolger, A. M., Lohse, M. and Usadel, B. (2014): "Trimmomatic: a flexible trimmer for Illumina sequence data." *Bioinformatics* **30**(15): 2114-2120.
- Bonsen, P. P., Spudich, J. A., Nelson, D. L. and Kornberg, A. (1969): "Biochemical studies of bacterial sporulation and germination. XII. A sulfonic acid as a major sulfur compound of *Bacillus subtilis* spores." *Journal of Bacteriology* **98**(1): 62-68.
- Bradford, M. M. (1976): "A rapid and sensitive method for the quantitation of microgram quantities of protein utilizing the principle of protein-dye binding." *Analytical Biochemistry* **72**: 248-254.
- Brand, H. S., Jorning, G. G. and Chamuleau, R. A. (1998): "Changes in urinary taurine and hypotaurine excretion after two-thirds hepatectomy in the rat." *Amino Acids* **15**(4): 373-383.
- Brinsmade, S. R., Paldon, T. and Escalante-Semerena, J. C. (2005): "Minimal functions and physiological conditions required for growth of *Salmonella enterica* on ethanolamine in the absence of the metabolosome." *Journal of Bacteriology* **187**(23): 8039-8046.
- Buckel, W. and Thauer, R. K. (2013): "Energy conservation via electron bifurcating ferredoxin reduction and proton/Na<sup>+</sup> translocating ferredoxin oxidation." *Biochimica et Biophysica Acta - Bioenergetics* **1827**(2): 94-113.
- Buckel, W. and Thauer, R. K. (2018): "Flavin-based electron bifurcation, ferredoxin, flavodoxin, and anaerobic respiration with protons (Ech) or NAD<sup>+</sup> (Rnf) as electron acceptors: A historical review." *Frontiers in Microbiology* **9**(401).
- Burrichter, A., Denger, K., Franchini, P., Huhn, T., Müller, N., Spiteller, D. and Schleheck, D. (2018): "Anaerobic degradation of the plant sugar sulfoquinovose concomitant with H<sub>2</sub>S production: *Escherichia coli* K-12 and *Desulfovibrio* sp. strain DF1 as co-culture model." *Frontiers in Microbiology* **9**(2792).
- Busby, W. F. (1966): "Sulfopropanedial and cysteinolic acid in the diatom." *Biochimica et Biophysica Acta - General Subjects* **121**(1): 160-161.
- Cai, F., Sutter, M., Bernstein, S. L., Kinney, J. N. and Kerfeld, C. A. (2015): "Engineering bacterial microcompartment shells: chimeric shell proteins and chimeric carboxysome shells." *ACS Synthetic Biology* **4**(4): 444-453.
- Cai, W. J., Wang, M. J., Ju, L. H., Wang, C. and Zhu, Y. C. (2010): "Hydrogen sulfide induces human colon cancer cell proliferation: role of Akt, ERK and p21." *Cell Biology International* **34**(6): 565-572.
- Canfield, D. E. and Farquhar, J. (2012): The global sulfur cycle. *Fundamentals of Geobiology*. A. H. Knoll, D. E. Canfield and K. O. Konhauser. Wiley-Blackwell: 49-64.
- Canfield, D. E., Jørgensen, B. B., Fossing, H., Glud, R., Gundersen, J., Ramsing, N. B., Thamdrup, B., Hansen, J. W., Nielsen, L. P. and Hall, P. O. J. (1993): "Pathways of organic carbon oxidation in three continental margin sediments." *Marine Geology* **113**(1): 27-40.
- Cannon, G. C., Bradburne, C. E., Aldrich, H. C., Baker, S. H., Heinhorst, S. and Shively, J. M. (2001): "Microcompartments in prokaryotes: carboxysomes and related polyhedra." *Applied and Environmental Microbiology* **67**(12): 5351-5361.

- Cao, Q., Zhang, L., Yang, G., Xu, C. and Wang, R. (2010): "Butyrate-stimulated H<sub>2</sub>S production in colon cancer cells." *Antioxidants & Redox Signaling* **12**(9): 1101-1109.
- Carbonero, F., Benefiel, A. C., Alizadeh-Ghamsari, A. H. and Gaskins, H. R. (2012): "Microbial pathways in colonic sulfur metabolism and links with health and disease." *Frontiers in Physiology* **3**: 448.
- Chen, Y. R., Zhou, L. Z., Fang, S. T., Long, H. Y., Chen, J. Y. and Zhang, G. X. (2019): "Isolation of *Desulfovibrio* spp. from human gut microbiota using a next-generation sequencing directed culture method." *Letters in Applied Microbiology* **68**(6): 553-561.
- Cheng, S. and Bobik, T. A. (2010): "Characterization of the PduS cobalamin reductase of *Salmonella enterica* and its role in the Pdu microcompartment." *Journal of Bacteriology* **192**(19): 5071-5080.
- Cheng, S., Fan, C., Sinha, S. and Bobik, T. A. (2012): "The PduQ enzyme is an alcohol dehydrogenase used to recycle NAD<sup>+</sup> internally within the Pdu microcompartment of *Salmonella enterica*." *PLoS ONE* **7**(10): e47144.
- Cherepanov, P. P. and Wackernagel, W. (1995): "Gene disruption in *Escherichia coli*: Tc<sup>R</sup> and Km<sup>R</sup> cassettes with the option of Flp-catalyzed excision of the antibiotic-resistance determinant." *Gene* **158**(1): 9-14.
- Chien, C.-C., Leadbetter, E. R. and Godchaux, W., III (1995): "Sulfonate-sulfur can be assimilated for fermentative growth." *FEMS Microbiology Letters* **129**(2-3): 189-193.
- Chowdhury, C., Sinha, S., Chun, S., Yeates, T. O. and Bobik, T. A. (2014): "Diverse bacterial microcompartment organelles." *Microbiology and Molecular Biology Reviews* **78**(3): 438-468.
- Clayden, J., Greeves, N. and Warren, S. (2012): *Organic Chemistry*. Oxford University Press.
- Cline, J. D. (1969): "Spectrophotometric determination of hydrogen sulfide in natural waters." *Limnology and Oceanography* **14**(3): 454-458.
- Codd, G. A. and Marsden, W. J. N. (1984): "The carboxysomes (polyhedral bodies) of autotrophic prokaryotes." *Biological Reviews* **59**(3): 389-422.
- Conway, T. and Cohen, P. S. (2015): "Commensal and pathogenic *Escherichia coli* metabolism in the gut." *Microbiology Spectrum* **3**(3).
- Cook, A. M. and Denger, K. (2002): "Dissimilation of the C<sub>2</sub>-sulfonates." *Archives of Microbiology* **179**(1): 1-6.
- Cook, A. M., Denger, K. and Smits, T. (2006): "Dissimilation of C<sub>3</sub>-sulfonates." *Archives of Microbiology* **185**: 83-90.
- Craciun, S. and Balskus, E. P. (2012): "Microbial conversion of choline to trimethylamine requires a glycol radical enzyme." *Proceedings of the National Academy of Sciences of the United States of America* **109**(52): 21307-21312.
- Craciun, S., Marks, J. A. and Balskus, E. P. (2014): "Characterization of choline trimethylamine-lyase expands the chemistry of glycol radical enzymes." *ACS Chemical Biology* **9**(7): 1408-1413.
- Crowley, C. S., Cascio, D., Sawaya, M. R., Kopstein, J. S., Bobik, T. A. and Yeates, T. O. (2010): "Structural insight into the mechanisms of transport across the *Salmonella enterica* Pdu microcompartment shell." *Journal of Biological Chemistry* **285**(48): 37838-37846.
- da Silva, S. M., Venceslau, S., Fernandes, C. L. V., Valente, F. and Cardoso Pereira, I. (2008): "Hydrogen as an energy source for the human pathogen *Bilophila wadsworthia*." *Antonie Van Leeuwenhoek* **93**: 381-390.
- Dalsgaard, T. and Bak, F. (1994): "Nitrate reduction in a sulfate-reducing bacterium, *Desulfovibrio desulfuricans*, isolated from rice paddy soil: sulfide inhibition, kinetics, and regulation." *Applied and Environmental Microbiology* **60**(1): 291-297.
- Datsenko, K. A. and Wanner, B. L. (2000): "One-step inactivation of chromosomal genes in *Escherichia coli* K-12 using PCR products." *Proceedings of the National Academy of Sciences of the United States of America* **97**(12): 6640-6645.
- David, L. A., Maurice, C. F., Carmody, R. N., Gootenberg, D. B., Button, J. E., Wolfe, B. E., Ling, A. V., Devlin, A. S., Varma, Y., Fischbach, M. A., Biddinger, S. B., Dutton, R. J. and Turnbaugh, P. J. (2014): "Diet rapidly and reproducibly alters the human gut microbiome." *Nature* **505**(7484): 559-563.
- Dawson, P. A. and Karpen, S. J. (2015): "Intestinal transport and metabolism of bile acids." *Journal of Lipid Research* **56**(6): 1085-1099.

- Denger, K. and Cook, A. M. (1997): "Assimilation of sulfur from alkyl- and arylsulfonates by *Clostridium* spp." *Archives of Microbiology* **167**(2-3): 177-181.
- Denger, K. and Cook, A. M. (2010): "Racemase activity effected by two dehydrogenases in sulfolactate degradation by *Chromohalobacter salexigens*: purification of S-sulfolactate dehydrogenase." *Microbiology* **156**(Pt 3): 967-974.
- Denger, K., Huhn, T., Hollemeyer, K., Schleheck, D. and Cook, A. M. (2012): "Sulfoquinovose degraded by pure cultures of bacteria with release of C<sub>3</sub>-organosulfonates: complete degradation in two-member communities." *FEMS Microbiology Letters* **328**(1): 39-45.
- Denger, K., Kertesz, M. A., Vock, E. H., Schon, R., Magli, A. and Cook, A. M. (1996): "Anaerobic desulfonation of 4-tolylsulfonate and 2-(4-sulfophenyl) butyrate by a *Clostridium* sp." *Applied and Environmental Microbiology* **62**(5): 1526-1530.
- Denger, K., Laue, H. and Cook, A. M. (1997a): "Anaerobic taurine oxidation: a novel reaction by a nitrate-reducing *Alcaligenes* sp." *Microbiology* **143**(6): 1919-1924.
- Denger, K., Laue, H. and Cook, A. M. (1997b): "Thiosulfate as a metabolic product: the bacterial fermentation of taurine." *Archives of Microbiology* **168**(4): 297-301.
- Denger, K., Mayer, J., Buhmann, M., Weinitschke, S., Smits, T. H. and Cook, A. M. (2009): "Bifurcated degradative pathway of 3-sulfolactate in *Roseovarius nubinhibens* ISM via sulfoacetaldehyde acetyltransferase and S-cysteate sulfolyase." *Journal of Bacteriology* **191**(18): 5648-5656.
- Denger, K., Ruff, J., Rein, U. and Cook, A. M. (2001): "Sulphoacetaldehyde sulpho-lyase (EC 4.4.1.12) from *Desulfonispora thiosulfatigenes*: purification, properties and primary sequence." *Biochemical Journal* **357**(Pt 2): 581-586.
- Denger, K., Smits, T. H. M. and Cook, A. M. (2006): "L-Cysteate sulpho-lyase, a widespread pyridoxal 5'-phosphate-coupled desulphonative enzyme purified from *Silicibacter pomeroyi* DSS-3<sup>T</sup>." *Biochemical Journal* **394**(3): 657-664.
- Denger, K., Weiss, M., Felux, A. K., Schneider, A., Mayer, C., Spiteller, D., Huhn, T., Cook, A. M. and Schleheck, D. (2014): "Sulphoglycolysis in *Escherichia coli* K-12 closes a gap in the biogeochemical sulphur cycle." *Nature* **507**(7490): 114-117.
- Devkota, S., Wang, Y., Musch, M. W., Leone, V., Fehlner-Peach, H., Nadimpalli, A., Antonopoulos, D. A., Jabri, B. and Chang, E. B. (2012): "Dietary-fat-induced taurocholic acid promotes pathobiont expansion and colitis in IBD mice." *Nature* **487**(7405): 104-108.
- Durham, B. P., Sharma, S., Luo, H., Smith, C. B., Amin, S. A., Bender, S. J., Dearth, S. P., Van Mooy, B. A. S., Campagna, S. R., Kujawinski, E. B., Armbrust, E. V. and Moran, M. A. (2015): "Cryptic carbon and sulfur cycling between surface ocean plankton." *Proceedings of the National Academy of Sciences of the United States of America* **112**(2): 453-457.
- Eckburg, P. B., Bik, E. M., Bernstein, C. N., Purdom, E., Dethlefsen, L., Sargent, M., Gill, S. R., Nelson, K. E. and Relman, D. A. (2005): "Diversity of the human intestinal microbial flora." *Science* **308**(5728): 1635-1638.
- Eichhorn, E., van der Ploeg, J. R., Kertesz, M. A. and Leisinger, T. (1997): "Characterization of  $\alpha$ -ketoglutarate-dependent taurine dioxygenase from *Escherichia coli*." *Journal of Biological Chemistry* **272**(37): 23031-23036.
- Eichhorn, E., van der Ploeg, J. R. and Leisinger, T. (1999): "Characterization of a two-component alkanesulfonate monooxygenase from *Escherichia coli*." *Journal of Biological Chemistry* **274**(38): 26639-26646.
- Erbilgin, O., McDonald, K. L. and Kerfeld, C. A. (2014): "Characterization of a planctomycetal organelle: a novel bacterial microcompartment for the aerobic degradation of plant saccharides." *Applied and Environmental Microbiology* **80**(7): 2193-2205.
- Evans, S. J., Bassis, C. M., Hein, R., Assari, S., Flowers, S. A., Kelly, M. B., Young, V. B., Ellingrod, V. E. and McInnis, M. G. (2017): "The gut microbiome composition associates with bipolar disorder and illness severity." *Journal of Psychiatric Research* **87**: 23-29.
- Fakhraee, M. and Katsev, S. (2019): "Organic sulfur was integral to the Archean sulfur cycle." *Nature Communications* **10**(1): 4556.
- Fakhraee, M., Li, J. and Katsev, S. (2017): "Significant role of organic sulfur in supporting sedimentary sulfate reduction in low-sulfate environments." *Geochimica et Cosmochimica Acta* **213**: 502-516.

- Farag, A. S., Klikarova, J., Ceslova, L., Vytras, K. and Sys, M. (2019): "Voltammetric determination of taurine in energy drinks after o-phthalaldehyde-ethanethiol derivatization." *Talanta* **202**: 486-493.
- Felux, A. K. (2015): Sulfoquinovose degradation in bacteria *Doctoral thesis, University of Konstanz*.
- Felux, A. K., Spitteler, D., Klebensberger, J. and Schleheck, D. (2015): "Entner-Doudoroff pathway for sulfoquinovose degradation in *Pseudomonas putida* SQ1." *Proceedings of the National Academy of Sciences of the United States of America* **112**(31): E4298-4305.
- Feng, Z., Long, W., Hao, B., Ding, D., Ma, X., Zhao, L. and Pang, X. (2017): "A human stool-derived *Bilophila wadsworthia* strain caused systemic inflammation in specific-pathogen-free mice." *Gut Pathogens* **9**: 59.
- Ferlez, B., Sutter, M. and Kerfeld, C. A. (2019): "Glycyl radical enzyme-associated microcompartments: Redox-replete bacterial organelles." *Molecular Biology and Physiology* **10**(1): e02327-02318.
- Fiedler, A. (2018): Characterization of degradation of organosulfonates by gut microbiome-relevant bacteria *Master's thesis, University of Konstanz*.
- Finster, K. (2008): "Microbiological disproportionation of inorganic sulfur compounds." *Journal of Sulfur Chemistry* **29**(3-4): 281-292.
- Flamholz, A., Noor, E., Bar-Even, A., Liebermeister, W. and Milo, R. (2013): "Glycolytic strategy as a tradeoff between energy yield and protein cost." *Proceedings of the National Academy of Sciences of the United States of America* **110**(24): 10039-10044.
- Frank, P., Hedman, B., Carlson, R. M. K., Tyson, T. A., Roe, A. L. and Hodgson, K. O. (1987): "A large reservoir of sulfate and sulfonate resides within plasma cells from *Ascidia ceratodes*, revealed by x-ray absorption near-edge structure spectroscopy." *Biochemistry* **26**(16): 4975-4979.
- Frey, J., Schneider, F., Schink, B. and Huhn, T. (2018): "Synthesis of short-chain hydroxyaldehydes and their 2,4-dinitrophenylhydrazone derivatives, and separation of their isomers by high-performance liquid chromatography." *Journal of Chromatography A* **1531**: 143-150.
- Fuchs, G., Eitinger, T., Heider, J., Kemper, B., Kothe, E., Overmann, J., Schink, B., Schneider, E. and Unden, G. (2014): *Allgemeine Mikrobiologie*. Georg Thieme Verlag, Stuttgart.
- Furne, J., Springfield, J., Koenig, T., DeMaster, E. and Levitt, M. D. (2001): "Oxidation of hydrogen sulfide and methanethiol to thiosulfate by rat tissues: a specialized function of the colonic mucosa." *Biochemical Pharmacology* **62**(2): 255-259.
- Gerlt, J. A., Bouvier, J. T., Davidson, D. B., Imker, H. J., Sadkin, B., Slater, D. R. and Whalen, K. L. (2015): "Enzyme Function Initiative-Enzyme Similarity Tool (EFI-EST): A web tool for generating protein sequence similarity networks." *Biochimica et Biophysica Acta* **1854**(8): 1019-1037.
- Gibson, G. R., Cummings, J. H. and Macfarlane, G. T. (1991): "Growth and activities of sulphate-reducing bacteria in gut contents of healthy subjects and patients with ulcerative colitis." *FEMS Microbiology Letters* **86**(2): 103-111.
- Goddard-Borger, E. D. and Williams, S. J. (2017): "Sulfoquinovose in the biosphere: occurrence, metabolism and functions." *Biochemical Journal* **474**(5): 827-849.
- Goldstein, E. J., Citron, D. M., Peraino, V. A. and Cross, S. A. (2003): "*Desulfovibrio desulfuricans* bacteremia and review of human *Desulfovibrio* infections." *Journal of Clinical Microbiology* **41**(6): 2752-2754.
- Graham, D. E., Xu, H. and White, R. H. (2002): "Identification of coenzyme M biosynthetic phosphosulfolactate synthase: A new family of sulfonate-biosynthesizing enzymes." *Journal of Biological Chemistry* **277**(16): 13421-13429.
- Gregory, J. C., Buffa, J. A., Org, E., Wang, Z., Levison, B. S., Zhu, W., Wagner, M. A., Bennett, B. J., Li, L., DiDonato, J. A., Lusis, A. J. and Hazen, S. L. (2015): "Transmission of atherosclerosis susceptibility with gut microbial transplantation." *Journal of Biological Chemistry* **290**(9): 5647-5660.
- Guo, F.-F., Yu, T.-C., Hong, J. and Fang, J.-Y. (2016): "Emerging roles of hydrogen sulfide in inflammatory and neoplastic colonic diseases." *Frontiers in physiology* **7**: 156-156.

- Guzman-Rodriguez, M., McDonald, J. A. K., Hyde, R., Allen-Vercoe, E., Claud, E. C., Sheth, P. M. and Petrof, E. O. (2018): "Using bioreactors to study the effects of drugs on the human microbiota." *Methods* **149**: 31-41.
- Harwood, J. L. and Nicholls, R. G. (1979): "The plant sulpholipid - a major component of the sulphur cycle." *Biochemical Society Transactions* **7**(2): 440-447.
- Hayashi, H., Sakamoto, M. and Benno, Y. (2002): "Phylogenetic analysis of the human gut microbiota using 16S rDNA clone libraries and strictly anaerobic culture-based methods." *Microbiology and Immunology* **46**(8): 535-548.
- Hensgens, C. M., Hagen, W. R. and Hansen, T. A. (1995): "Purification and characterization of a benzylviologen-linked, tungsten-containing aldehyde oxidoreductase from *Desulfovibrio gigas*." *Journal of Bacteriology* **177**(21): 6195-6200.
- Herring, T. I., Harris, T. N., Chowdhury, C., Mohanty, S. K. and Bobik, T. A. (2018): "A bacterial microcompartment is used for choline fermentation by *Escherichia coli* 536." *Journal of Bacteriology* **200**(10): e00764-00717.
- Hertel, J., Harms, A. C., Heinzen, A., Baldini, F., Thines, C. C., Glaab, E., Vasco, D. A., Pietzner, M., Stewart, I. D., Wareham, N. J., Langenberg, C., Trenkwalder, C., Krüger, R., Hankemeier, T., Fleming, R. M. T., Mollenhauer, B. and Thiele, I. (2019): "Integrated analyses of microbiome and longitudinal metabolome data reveal microbial-host interactions on sulfur metabolism in Parkinson's disease." *Cell Reports* **29**(7): 1767-1777.e1768.
- Heukeshoven, J. and Dernick, R. (1985): "Simplified method for silver staining of proteins in polyacrylamide gels and the mechanism of silver staining." *Electrophoresis* **6**(3): 103-112.
- HMP-Consortium (2012): "A framework for human microbiome research." *Nature* **486**: 215-221.
- Holst, P. B., Nielsen, S. E., Anthoni, U., Bisht, K. S., Christoffersen, C., Gupta, S., Parmar, V. S., Nielsen, P. H., Sahoo, D. B. and Singh, A. (1994): "Isethionate in certain red algae." *Journal of Applied Phycology* **6**(5): 443-446.
- Hosoki, R., Matsuki, N. and Kimura, H. (1997): "The possible role of hydrogen sulfide as an endogenous smooth muscle relaxant in synergy with nitric oxide." *Biochemical and Biophysica Research Communications* **237**(3): 527-531.
- Huber, I. (2017): Establishment of bacterial microcompartments in the industrial production strain *Corynebacterium glutamicum* *Doctoral thesis, Heinrich-Heine-Universität Düsseldorf; Forschungszentrum Jülich*.
- Hubert, C. (2010): Microbial ecology of oil reservoir souring and its control by nitrate injection. *Handbook of Hydrocarbon and Lipid Microbiology*. K. N. Timmis. Springer, Berlin, Heidelberg: 2753-2766.
- Huseby, D. L. and Roth, J. R. (2013): "Evidence that a metabolic microcompartment contains and recycles private cofactor pools." *Journal of Bacteriology* **195**(12): 2864.
- Huxtable, R. J. (1992): "Physiological actions of taurine." *Physiological Reviews* **72**(1): 101-163.
- Ijssennagger, N., Belzer, C., Hooiveld, G. J., Dekker, J., van Mil, S. W., Muller, M., Kleerebezem, M. and van der Meer, R. (2015): "Gut microbiota facilitates dietary heme-induced epithelial hyperproliferation by opening the mucus barrier in colon." *Proceedings of the National Academy of Sciences of the United States of America* **112**(32): 10038-10043.
- Ijssennagger, N., van der Meer, R. and van Mil, S. W. C. (2016): "Sulfide as a mucus barrier-breaker in inflammatory bowel disease?" *Trends in Molecular Medicine* **22**(3): 190-199.
- Jacobsen, J. G., Collins, L. L. and Smith, L. H. (1967): "Urinary excretion of isethionic acid in man." *Nature* **214**(5094): 1247-1248.
- Jacobsen, J. G. and Smith, L. H. (1968): "Biochemistry and physiology of taurine and taurine derivatives." *Physiological Reviews* **48**(2): 424-511.
- Jiang, H., Ling, Z., Zhang, Y., Mao, H., Ma, Z., Yin, Y., Wang, W., Tang, W., Tan, Z., Shi, J., Li, L. and Ruan, B. (2015): "Altered fecal microbiota composition in patients with major depressive disorder." *Brain, Behavior, and Immunity* **48**: 186-194.
- Jie, Z., Xia, H., Zhong, S.-L., Feng, Q., Li, S., Liang, S., Zhong, H., Liu, Z., Gao, Y., Zhao, H., Zhang, D., Su, Z., Fang, Z., Lan, Z., Li, J., Xiao, L., Li, J., Li, R., Li, X., Li, F., Ren, H., Huang, Y., Peng, Y., Li, G., Wen, B., Dong, B., Chen, J.-Y., Geng, Q.-S., Zhang, Z.-W., Yang, H., Wang, J., Wang, J., Zhang, X., Madsen, L., Brix, S., Ning, G., Xu, X., Liu, X., Hou, Y., Jia, H.,

- He, K. and Kristiansen, K. (2017): "The gut microbiome in atherosclerotic cardiovascular disease." *Nature Communications* **8**(1): 845-845.
- Kabil, O., Vitvitsky, V. and Banerjee, R. (2014): "Sulfur as a signaling nutrient through hydrogen sulfide." *Annual Review of Nutrition* **34**: 171-205.
- Keith, S. M. and Herbert, R. A. (1983): "Dissimilatory nitrate reduction by a strain of *Desulfovibrio desulfuricans*." *FEMS Microbiology Letters* **18**(1): 55-59.
- Kennedy, S. I. T. and Fewson, C. A. (1968): "Enzymes of the mandelate pathway in bacterium N.C.I.B. 8250." *Biochemical Journal* **107**(4): 497.
- Kerfeld, C. A., Aussignargues, C., Zarzycki, J., Cai, F. and Sutter, M. (2018): "Bacterial microcompartments." *Nature Reviews Microbiology* **16**(5): 277-290.
- Kerfeld, C. A., Heinhorst, S. and Cannon, G. C. (2010): "Bacterial microcompartments." *Annual Review of Microbiology* **64**(1): 391-408.
- Kertesz, M. A. (2000): "Riding the sulfur cycle - metabolism of sulfonates and sulfate esters in Gram-negative bacteria." *FEMS Microbiology Reviews* **24**(2): 135-175.
- Kimura, H. (2011): "Hydrogen sulfide: its production, release and functions." *Amino Acids* **41**(1): 113-121.
- Knappe, J. and Sawer, G. (1990): "A radical-chemical route to acetyl-CoA: the anaerobically induced pyruvate formate-lyase system of *Escherichia coli*." *FEMS Microbiology Letters* **75**(4): 383-398.
- Koechlin, B. A. (1954): "The isolation and identification of the major anion fraction of the axoplasm of squid giant nerve fibers." *Proceedings of the National Academy of Sciences of the United States of America* **40**(2): 60-62.
- Kofoid, E., Rappleye, C., Stojiljkovic, I. and Roth, J. (1999): "The 17-gene ethanolamine (*eut*) operon of *Salmonella typhimurium* encodes five homologues of carboxysome shell proteins." *Journal of Bacteriology* **181**(17): 5317-5329.
- Koivusalmi, E., Haatainen, E. and Root, A. (1999): "Quantitative RP-HPLC determination of some aldehydes and hydroxyaldehydes as their 2,4-dinitrophenylhydrazone derivatives." *Analytical Chemistry* **71**(1): 86-91.
- Kolmogorov, M., Raney, B., Paten, B. and Pham, S. (2014): "Ragout - a reference-assisted assembly tool for bacterial genomes." *Bioinformatics* **30**(12): i302-i309.
- Kootte, R. S., Levin, E., Salojarvi, J., Smits, L. P., Hartstra, A. V., Udayappan, S. D., Hermes, G., Bouter, K. E., Koopen, A. M., Holst, J. J., Knop, F. K., Blaak, E. E., Zhao, J., Smidt, H., Harms, A. C., Hankemeijer, T., Bergman, J., Romijn, H. A., Schaap, F. G., Olde Damink, S. W. M., Ackermans, M. T., Dallinga-Thie, G. M., Zoetendal, E., de Vos, W. M., Serlie, M. J., Stroes, E. S. G., Groen, A. K. and Nieuwdorp, M. (2017): "Improvement of insulin sensitivity after lean donor feces in metabolic syndrome is driven by baseline intestinal microbiota composition." *Cell Metabolism* **26**(4): 611-619.e616.
- Kronberg, B., Holmberg, K. and Lindman, B. (2014): Surface chemistry of surfactants and polymers. Wiley.
- Kuehl, J. V., Price, M. N., Ray, J., Wetmore, K. M., Esquivel, Z., Kazakov, A. E., Nguyen, M., Kuehn, R., Davis, R. W., Hazen, T. C., Arkin, A. P. and Deutschnauer, A. (2014): "Functional genomics with a comprehensive library of transposon mutants for the sulfate-reducing bacterium *Desulfovibrio alaskensis* G20." *mBio* **5**(3): e01041-01014.
- Kuriyama, I., Musumi, K., Yonezawa, Y., Takemura, M., Maeda, N., Iijima, H., Hada, T., Yoshida, H. and Mizushina, Y. (2005): "Inhibitory effects of glycolipids fraction from spinach on mammalian DNA polymerase activity and human cancer cell proliferation." *The Journal of Nutritional Biochemistry* **16**(10): 594-601.
- Laemmli, U. K. (1970): "Cleavage of structural proteins during the assembly of the head of bacteriophage T4." *Nature* **227**(5259): 680-685.
- LaMattina, J. W., Keul, N. D., Reitzer, P., Kapoor, S., Galzerani, F., Koch, D. J., Gouvea, I. E. and Lanzilotta, W. N. (2016): "1,2-Propanediol dehydration in *Roseburia inulinivorans*: structural basis for substrate and enantiomer selectivity." *Journal of Biological Chemistry* **291**(30): 15515-15526.
- Landa, M., Burns, A. S., Roth, S. J. and Moran, M. A. (2017): "Bacterial transcriptome remodeling during sequential co-culture with a marine dinoflagellate and diatom." *ISME Journal*.

- Langmead, B. and Salzberg, S. L. (2012): "Fast gapped-read alignment with Bowtie 2." *Nature Methods* **9**(4): 357-359.
- Laue, H. (2000): Biochemical and molecular characterization of taurine metabolism in the anaerobic bacterium *Bilophila wadsworthia* *Doctoral thesis, University of Konstanz*.
- Laue, H. and Cook, A. M. (2000a): "Biochemical and molecular characterization of taurine:pyruvate aminotransferase from the anaerobe *Bilophila wadsworthia*." *European Journal of Biochemistry* **267**(23): 6841-6848.
- Laue, H. and Cook, A. M. (2000b): "Purification, properties and primary structure of alanine dehydrogenase involved in taurine metabolism in *Bilophila wadsworthia*." *Archives of Microbiology* **174**: 162-167.
- Laue, H., Denger, K. and Cook, A. M. (1997): "Taurine reduction in anaerobic respiration of *Bilophila wadsworthia* RZATAU." *Applied and Environmental Microbiology* **63**(5): 2016-2021.
- Lee, R. F. and Benson, A. A. (1972): "The metabolism of glyceryl [<sup>35</sup>S] sulfoquinovoside by the coral tree, *Erythrina crista-galli*, and alfalfa, *Medicago sativa*." *Biochimica et Biophysica Acta - General Subjects* **261**(1): 35-37.
- Letunic, I. and Bork, P. (2016): "Interactive tree of life (iTOL) v3: an online tool for the display and annotation of phylogenetic and other trees." *Nucleic Acids Research* **44**(W1): W242-245.
- Levin, B. J. and Balskus, E. P. (2018): "Characterization of 1,2-propanediol dehydratase reveals distinct mechanisms for B<sub>12</sub>-dependent and glycyl radical enzymes." *Biochemistry* **57**: 3222-3226.
- Levin, B. J., Huang, Y. Y., Peck, S. C., Wei, Y., Martinez-Del Campo, A., Marks, J. A., Franzosa, E. A., Huttenhower, C. and Balskus, E. P. (2017): "A prominent glycyl radical enzyme in human gut microbiomes metabolizes trans-4-hydroxy-l-proline." *Science* **355**(6325).
- Levine, J., Ellis, C. J., Furne, J. K., Springfield, J. and Levitt, M. D. (1998): "Fecal hydrogen sulfide production in ulcerative colitis." *American Journal of Gastroenterology* **93**(1): 83-87.
- Li, H., Handsaker, B., Wysoker, A., Fennell, T., Ruan, J., Homer, N., Marth, G., Abecasis, G. and Durbin, R. (2009): "The Sequence Alignment/Map format and SAMtools." *Bioinformatics* **25**(16): 2078-2079.
- Liberton, M., Austin, J. R., Berg, R. H. and Pakrasi, H. B. (2011): "Unique thylakoid membrane architecture of a unicellular N<sub>2</sub>-fixing cyanobacterium revealed by electron tomography." *Plant Physiology* **155**(4): 1656.
- Lie, T. J., Godchaux, W. and Leadbetter, E. R. (1999): "Sulfonates as terminal electron acceptors for growth of sulfite-reducing bacteria (*Desulfitobacterium* spp.) and sulfate-reducing bacteria: effects of inhibitors of sulfidogenesis." *Applied and Environmental Microbiology* **65**(10): 4611-4617.
- Lie, T. J., Pitta, T., Leadbetter, E. R., Godchaux, W., 3rd and Leadbetter, J. R. (1996): "Sulfonates: novel electron acceptors in anaerobic respiration." *Archives of Microbiology* **166**(3): 204-210.
- Lin, X., Handley, K. M., Gilbert, J. A. and Kostka, J. E. (2015): "Metabolic potential of fatty acid oxidation and anaerobic respiration by abundant members of *Thaumarchaeota* and *Thermoplasmata* in deep anoxic peat." *ISME Journal* **9**(12): 2740-2744.
- Little, B. J., Lee, J. S. and Ray, R. I. (2008): "The influence of marine biofilms on corrosion: A concise review." *Electrochimica Acta* **54**(1): 2-7.
- Longnecker, K., Sievert, S. M., Sylva, S. P., Seewald, J. S. and Kujawinski, E. B. (2018): "Dissolved organic carbon compounds in deep-sea hydrothermal vent fluids from the East Pacific Rise at 9°50'N." *Organic Geochemistry* **125**: 41-49.
- Loubinoux, J., Bronowicki, J.-P., Pereira, I. A. C., Mougenel, J.-L. and Le Faou, A. E. (2002): "Sulfate-reducing bacteria in human feces and their association with inflammatory bowel diseases." *FEMS Microbiology Ecology* **40**(2): 107-112.
- Love, M. I., Huber, W. and Anders, S. (2014): "Moderated estimation of fold change and dispersion for RNA-seq data with DESeq2." *Genome Biology* **15**(12): 550.
- Lovley, D. R., Roden, E. E., Phillips, E. J. P. and Woodward, J. C. (1993): "Enzymatic iron and uranium reduction by sulfate-reducing bacteria." *Marine Geology* **113**(1): 41-53.
- Luo, R., Liu, B., Xie, Y., Li, Z., Huang, W., Yuan, J., He, G., Chen, Y., Pan, Q., Liu, Y., Tang, J., Wu, G., Zhang, H., Shi, Y., Liu, Y., Yu, C., Wang, B., Lu, Y., Han, C., Cheung, D. W., Yiu,

- S. M., Peng, S., Xiaoqian, Z., Liu, G., Liao, X., Li, Y., Yang, H., Wang, J., Lam, T. W. and Wang, J. (2012): "SOAPdenovo2: an empirically improved memory-efficient short-read *de novo* assembler." *Gigascience* **1**(1): 18.
- Magee, E. A., Richardson, C. J., Hughes, R. and Cummings, J. H. (2000): "Contribution of dietary protein to sulfide production in the large intestine: an *in vitro* and a controlled feeding study in humans." *American Journal of Clinical Nutrition* **72**(6): 1488-1494.
- Mayer, J., Huhn, T., Habeck, M., Denger, K., Hollemeyer, K. and Cook, A. M. (2010): "2,3-Dihydroxypropane-1-sulfonate degraded by *Cupriavidus pinatubonensis* JMP134: purification of dihydroxypropanesulfonate 3-dehydrogenase." *Microbiology* **156**(Pt 5): 1556-1564.
- Meyer, T. S. and Lamberts, B. L. (1965): "Use of Coomassie brilliant blue R250 for the electrophoresis of microgram quantities of parotid saliva proteins on acrylamide-gel strips." *Biochimica et Biophysica Acta* **107**: 144-145.
- Moench, T. T. and Zeikus, J. G. (1983): "An improved preparation method for a titanium (III) media reductant." *Journal of Microbiological Methods* **1**(4): 199-202.
- Montella, C., Bellsolell, L., Perez-Luque, R., Badia, J., Baldoma, L., Coll, M. and Aguilar, J. (2005): "Crystal structure of an iron-dependent group III dehydrogenase that interconverts *L*-lactaldehyde and *L*-1,2-propanediol in *Escherichia coli*." *Journal of Bacteriology* **187**(14): 4957-4966.
- Moore, T. C. and Escalante-Semerena, J. C. (2016): "The EutQ and EutP proteins are novel acetate kinases involved in ethanolamine catabolism: physiological implications for the function of the ethanolamine metabolosome in *Salmonella enterica*." *Molecular Microbiology* **99**(3): 497-511.
- Morris, A. W. and Riley, J. P. (1966): "The bromide/chlorinity and sulphate/chlorinity ratio in sea water." *Deep Sea Research and Oceanographic Abstracts* **13**(4): 699-705.
- Moura, I., Bursakov, S., Costa, C. and Moura, J. J. G. (1997): "Nitrate and nitrite utilization in sulfate-reducing bacteria." *Anaerobe* **3**(5): 279-290.
- Müller, N., Griffin, B. M., Stingl, U. and Schink, B. (2008): "Dominant sugar utilizers in sediment of Lake Constance depend on syntrophic cooperation with methanogenic partner organisms." *Environmental Microbiology* **10**(6): 1501-1511.
- Muyzer, G. and Stams, A. J. M. (2008): "The ecology and biotechnology of sulphate-reducing bacteria." *Nature Reviews Microbiology* **6**(6): 441-454.
- Naseribafrouei, A., Hestad, K., Avershina, E., Sekelja, M., Linlokken, A., Wilson, R. and Rudi, K. (2014): "Correlation between the human fecal microbiota and depression." *Neurogastroenterology & Motility* **26**(8): 1155-1162.
- Nava, G. M., Carbonero, F., Croix, J. A., Greenberg, E. and Gaskins, H. R. (2012): "Abundance and diversity of mucosa-associated hydrogenotrophic microbes in the healthy human colon." *ISME Journal* **6**(1): 57-70.
- Nishimura, J. S. and Griffith, M. J. (1981): Acetate kinase from *Veillonella alcalescens*: EC 2.7.2.1 ATP:acetate phosphotransferase. *Methods in Enzymology*. Academic Press. **71**: 311-316.
- O'Brien, J. R., Raynaud, C., Croux, C., Girbal, L., Soucaille, P. and Lanzilotta, W. N. (2004): "Insight into the mechanism of the B<sub>12</sub>-independent glycerol dehydratase from *Clostridium butyricum*: preliminary biochemical and structural characterization." *Biochemistry* **43**(16): 4635-4645.
- Obadors, N., Cabiscol, E., Aguilar, J. and Ros, J. (1998): "Site-directed mutagenesis studies of the metal-binding center of the iron-dependent propanediol oxidoreductase from *Escherichia coli*." *European Journal of Biochemistry* **258**(1): 207-213.
- Palmieri, G., Balestrieri, M., Peter-Katalinić, J., Pohlentz, G., Rossi, M., Fiume, I. and Pocsfalvi, G. (2013): "Surface-exposed glycoproteins of hyperthermophilic *Sulfolobus solfataricus* P2 show a common N-glycosylation profile." *Journal of Proteome Research* **12**(6): 2779-2790.
- Pang, A., Warren, M. J. and Pickersgill, R. W. (2011): "Structure of PduT, a trimeric bacterial microcompartment protein with a 4Fe-4S cluster-binding site." *Acta Crystallographica Section D Biological Crystallography* **67**(Pt 2): 91-96.

- Park, H. S., Lin, S. and Voordouw, G. (2008): "Ferric iron reduction by *Desulfovibrio vulgaris* Hildenborough wild type and energy metabolism mutants." *Antonie Van Leeuwenhoek* **93**(1-2): 79-85.
- Parsons, J. B., Dinesh, S. D., Deery, E., Leech, H. K., Brindley, A. A., Heldt, D., Frank, S., Smales, C. M., Lunsdorf, H., Rambach, A., Gass, M. H., Bleloch, A., McClean, K. J., Munro, A. W., Rigby, S. E., Warren, M. J. and Prentice, M. B. (2008): "Biochemical and structural insights into bacterial organelle form and biogenesis." *Journal of Biological Chemistry* **283**(21): 14366-14375.
- Parsons, J. B., Lawrence, A. D., McLean, K. J., Munro, A. W., Rigby, S. E. J. and Warren, M. J. (2010): "Characterisation of PduS, the pdu metabolosome corrin reductase, and evidence of substructural organisation within the bacterial microcompartment." *PLoS ONE* **5**(11): e14009-e14009.
- Peck, S. C., Denger, K., Burrichter, A., Irwin, S. M., Balskus, E. P. and Schleheck, D. (2019): "A glycyl radical enzyme enables hydrogen sulfide production by the human intestinal bacterium *Bilophila wadsworthia*." *Proceedings of the National Academy of Sciences of the United States of America* **116**(8): 3171.
- Pertea, M., Pertea, G. M., Antonescu, C. M., Chang, T.-C., Mendell, J. T. and Salzberg, S. L. (2015): "StringTie enables improved reconstruction of a transcriptome from RNA-seq reads." *Nature Biotechnology* **33**: 290.
- Petit, E., LaTouf, W. G., Coppi, M. V., Warnick, T. A., Currie, D., Romashko, I., Deshpande, S., Haas, K., Alvelo-Maurosa, J. G., Wardman, C., Schnell, D. J., Leschine, S. B. and Blanchard, J. L. (2013): "Involvement of a bacterial microcompartment in the metabolism of fucose and rhamnose by *Clostridium phytofermentans*." *PLoS ONE* **8**(1): e54337-e54337.
- Pfennig, N. (1978): "Rhodocyclus purpureus gen. nov. and sp. nov., a ring-shaped, vitamin B<sub>12</sub>-requiring member of the family Rhodospirillaceae." *International Journal of Systematic and Evolutionary Microbiology* **28**(2): 283-288.
- Price, G. D., Howitt, S. M., Harrison, K. and Badger, M. R. (1993): "Analysis of a genomic DNA region from the cyanobacterium *Synechococcus* sp. strain PCC7942 involved in carboxysome assembly and function." *Journal of Bacteriology* **175**(10): 2871-2879.
- Ramasamy, S., Singh, S., Taniere, P., Langman, M. J. and Eggo, M. C. (2006): "Sulfide-detoxifying enzymes in the human colon are decreased in cancer and upregulated in differentiation." *American Journal of Physiology Gastrointestinal and Liver Physiology* **291**(2): G288-296.
- Raynaud, C., Sarçabal, P., Meynil-Salles, I., Croux, C. and Soucaille, P. (2003): "Molecular characterization of the 1,3-propanediol (1,3-PD) operon of *Clostridium butyricum*." *Proceedings of the National Academy of Sciences of the United States of America* **100**(9): 5010-5015.
- Rein, U., Gueta, R., Denger, K., Ruff, J., Hollemeyer, K. and Cook, A. M. (2005): "Dissimilation of cysteate via 3-sulfolactate sulfo-lyase and a sulfate exporter in *Paracoccus pantotrophus* NKNCYSA." *Microbiology* **151**(Pt 3): 737-747.
- Rey, F. E., Gonzalez, M. D., Cheng, J., Wu, M., Ahern, P. P. and Gordon, J. I. (2013): "Metabolic niche of a prominent sulfate-reducing human gut bacterium." *Proceedings of the National Academy of Sciences of the United States of America* **110**(33): 13582-13587.
- Ridlon, J. M., Wolf, P. G. and Gaskins, H. R. (2016): "Taurocholic acid metabolism by gut microbes and colon cancer." *Gut Microbes* **7**(3): 201-215.
- Ripps, H. and Shen, W. (2012): "Review: Taurine: A "very essential" amino acid." *Molecular Vision* **18**: 2673-2686.
- Roediger, W. E., Moore, J. and Babidge, W. (1997): "Colonic sulfide in pathogenesis and treatment of ulcerative colitis." *Digestive Diseases and Sciences* **42**(8): 1571-1579.
- Rogers, G. B., Keating, D. J., Young, R. L., Wong, M. L., Licinio, J. and Wesselingh, S. (2016): "From gut dysbiosis to altered brain function and mental illness: mechanisms and pathways." *Molecular Psychiatry* **21**(6): 738-748.
- Rowan, F., Docherty, N. G., Murphy, M., Murphy, B., Calvin Coffey, J. and O'Connell, P. R. (2010): "Desulfovibrio bacterial species are increased in ulcerative colitis." *Diseases of the Colon & Rectum* **53**(11): 1530-1536.

- Roy, A. B., Hewlins, M. J. E., Ellis, A. J., Harwood, J. L. and White, G. F. (2003): "Glycolytic breakdown of sulfoquinovose in bacteria: a missing link in the sulfur cycle." Applied and Environmental Microbiology **69**(11): 6434-6441.
- Ruff, J., Denger, K. and Cook, A. M. (2003): "Sulphoacetaldehyde acetyltransferase yields acetyl phosphate: purification from *Alcaligenes defragrans* and gene clusters in taurine degradation." Biochemical Journal **369**(Pt 2): 275-285.
- Sampson, T. R., Debelius, J. W., Thron, T., Janssen, S., Shastri, G. G., Ilhan, Z. E., Challis, C., Schretter, C. E., Rocha, S., Grdinaru, V., Chesselet, M. F., Keshavarzian, A., Shannon, K. M., Krajmalnik-Brown, R., Wittung-Stafshede, P., Knight, R. and Mazmanian, S. K. (2016): "Gut microbiota regulate motor deficits and neuroinflammation in a model of Parkinson's disease." Cell **167**(6): 1469-1480.e1412.
- Sawyer, C. N. and Ryckman, D. W. (1957): "Anionic synthetic detergents and water supply problems." Journal - American Water Works Association **49**(4): 480-490.
- Schaus, S. E., Brandes, B. D., Larow, J. F., Tokunaga, M., Hansen, K. B., Gould, A. E., Furrow, M. E. and Jacobsen, E. N. (2002): "Highly selective hydrolytic kinetic resolution of terminal epoxides catalyzed by chiral (salen)Co<sup>III</sup> complexes. Practical synthesis of enantioenriched terminal epoxides and 1,2-diols." Journal of the American Chemical Society **124**: 1307-1315.
- Schindel, H. S., Karty, J. A., McKinlay, J. B. and Bauer, C. E. (2018): "Characterization of a glycyl-radical enzyme bacterial microcompartment pathway in *Rhodobacter capsulatus*." Journal of Bacteriology: JB.00343-00318.
- Schleheck, D. (2003): Biodegradation of synthetic surfactants: linear alkylbenzenesulfonates (LAS) and related compounds Doctoral thesis, University of Konstanz.
- Schmidt, A., Müller, N., Schink, B. and Schleheck, D. (2013): "A proteomic view at the biochemistry of syntrophic butyrate oxidation in *Syntrophomonas wolfei*." PLoS One **8**(2): e56905.
- Seitz, A. P., Leadbetter, E. R. and Godchaux, W. (1993): "Utilization of sulfonates as sole sulfur source by soil bacteria including *Comamonas acidovorans*." Archives of Microbiology **159**(5): 440-444.
- Sen, N., Paul, B. D., Gadalla, M. M., Mustafa, A. K., Sen, T., Xu, R., Kim, S. and Snyder, S. H. (2012): "Hydrogen sulfide-linked sulfhydration of NF-κB mediates its antiapoptotic actions." Molecular Cell **45**(1): 13-24.
- Shatalin, K., Shatalina, E., Mironov, A. and Nudler, E. (2011): "H<sub>2</sub>S: A universal defense against antibiotics in bacteria." Science **334**(6058): 986.
- Shimada, T., Yamamoto, K., Nakano, M., Watanabe, H., Schleheck, D. and Ishihama, A. (2018): "Regulatory role of CsQR (YihW) in transcription of the genes for catabolism of the anionic sugar sulfoquinovose (SQ) in *Escherichia coli* K-12." Microbiology [in revision].
- Shisler, K. A. and Broderick, J. B. (2014): "Glycyl radical activating enzymes: Structure, mechanism, and substrate interactions." Archives of Biochemistry and Biophysics **546**: 64-71.
- Shively, J. M., Ball, F., Brown, D. H. and Saunders, R. E. (1973): "Functional organelles in prokaryotes: polyhedral inclusions (carboxysomes) of *Thiobacillus neapolitanus*." Science **182**(4112): 584-586.
- Singh, S. B. and Lin, H. C. (2015): "Hydrogen sulfide in physiology and diseases of the digestive tract." Microorganisms **3**(4): 866-889.
- Spaeth, D. G. and Schneider, D. L. (1974): "Taurine synthesis, concentration, and bile salt conjugation in rat, guinea pig, and rabbit." Proceedings of the Society for Experimental Biology and Medicine **147**(3): 855-858.
- Speciale, G., Jin, Y., Davies, G. J., Williams, S. J. and Goddard-Borger, E. D. (2016): "YihQ is a sulfoquinovosidase that cleaves sulfoquinovosyl diacylglyceride sulfolipids." Nature Chemical Biology **12**(4): 215-217.
- Stefanie, J. W. H. O. E., Visser, A., Pol, L. W. H. and Stams, A. J. M. (1994): "Sulfate reduction in methanogenic bioreactors." FEMS Microbiology Reviews **15**(2-3): 119-136.
- Stettner, A. I. and Segre, D. (2013): "The cost of efficiency in energy metabolism." Proceedings of the National Academy of Sciences of the United States of America **110**(24): 9629-9630.

- Stojiljkovic, I., Bäumler, A. J. and Heffron, F. (1995): "Ethanolamine utilization in *Salmonella typhimurium*: nucleotide sequence, protein expression, and mutational analysis of the *cchA cchB eutE eutJ eutG eutH* gene cluster." *Journal of Bacteriology* **177**(5): 1357.
- Suarez, F., Furne, J., Springfield, J. and Levitt, M. (1998): "Production and elimination of sulfur-containing gases in the rat colon." *American Journal of Physiology* **274**(4): G727-733.
- Szabo, C., Coletta, C., Chao, C., Modis, K., Szczesny, B., Papapetropoulos, A. and Hellmich, M. R. (2013): "Tumor-derived hydrogen sulfide, produced by cystathionine- $\beta$ -synthase, stimulates bioenergetics, cell proliferation, and angiogenesis in colon cancer." *Proceedings of the National Academy of Sciences of the United States of America* **110**(30): 12474-12479.
- Tabita, F. R. (1999): "Microbial ribulose 1,5-bisphosphate carboxylase/oxygenase: A different perspective." *Photosynthesis Research* **60**(1): 1-28.
- Tanaka, S., Kerfeld, C. A., Sawaya, M. R., Cai, F., Heinhorst, S., Cannon, G. C. and Yeates, T. O. (2008): "Atomic-level models of the bacterial carboxysome shell." *Science* **319**(5866): 1083.
- Thomason, L. C., Costantino, N. and Court, D. L. (2007): "*E. coli* genome manipulation by P1 transduction." *Current Protocols in Molecular Biology* **1**: Unit 1.17.
- Thompson, T. G., Lang, J. W. and Anderson, L. (1927): The sulphate-chloride ratio of the waters of the north Pacific. University of Washington.
- Tomasova, L., Konopelski, P. and Ufnal, M. (2016): "Gut bacteria and hydrogen sulfide: the new old players in circulatory system homeostasis." *Molecules* **21**(11): e1158.
- Tong, Y., Wei, Y., Hu, Y., Ang, E. L., Zhao, H. and Zhang, Y. (2019): "A pathway for isethionate dissimilation in *Bacillus kruvlichiae*." *Applied and Environmental Microbiology* **85**(15): e00793-00719.
- Tschech, A. and Pfennig, N. (1984): "Growth yield increase linked to caffeoate reduction in *Acetobacterium woodii*." *Archives of Microbiology* **137**(2): 163-167.
- Turnbaugh, P. J., Ley, R. E., Mahowald, M. A., Magrini, V., Mardis, E. R. and Gordon, J. I. (2006): "An obesity-associated gut microbiome with increased capacity for energy harvest." *Nature* **444**(7122): 1027-1031.
- Uria-Nickelsen, M. R., Leadbetter, E. R. and Godchaux, W., III (1994): "Sulfonate-sulfur utilization involves a portion of the assimilatory sulfate reduction pathway in *Escherichia coli*." *FEMS Microbiology Letters* **123**(1-2): 43-48.
- Vairavamurthy, A., Manowitz, B., Luther, G. W. and Jeon, Y. (1993): "Oxidation state of sulfur in thiosulfate and implications for anaerobic energy metabolism." *Geochimica et Cosmochimica Acta* **57**(7): 1619-1623.
- Vairavamurthy, A., Zhou, W., Eglinton, T. and Manowitz, B. (1994): "Sulfonates: A novel class of organic sulfur compounds in marine sediments." *Geochimica et Cosmochimica Acta* **58**(21): 4681-4687.
- van der Ploeg, J. R., Weiss, M. A., Saller, E., Nashimoto, H., Saito, N., Kertesz, M. A. and Leisinger, T. (1996): "Identification of sulfate starvation-regulated genes in *Escherichia coli*: a gene cluster involved in the utilization of taurine as a sulfur source." *Journal of Bacteriology* **178**(18): 5438.
- van Elsas, J. D., Semenov, A. V., Costa, R. and Trevors, J. T. (2011): "Survival of *Escherichia coli* in the environment: fundamental and public health aspects." *ISME Journal* **5**(2): 173-183.
- Venable, J. H. and Coggeshall, R. (1965): "A simplified lead citrate stain for use in electron microscopy." *Journal of Cell Biology* **25**(2): 407.
- Vollrath, F., Fairbrother, W. J., Williams, R. J. P., Tillinghast, E. K., Bernstein, D. T., Gallagher, K. S. and Townley, M. A. (1990): "Compounds in the droplets of the orb spider's viscous spiral." *Nature* **345**(6275): 526-528.
- Vrieze, A., Van Nood, E., Holleman, F., Salojarvi, J., Kootte, R. S., Bartelsman, J. F., Dallinga-Thie, G. M., Ackermans, M. T., Serlie, M. J., Oozeer, R., Derrien, M., Druesne, A., Van Hylckama Vlieg, J. E., Bloks, V. W., Groen, A. K., Heilig, H. G., Zoetendal, E. G., Stroes, E. S., de Vos, W. M., Hoekstra, J. B. and Nieuwdorp, M. (2012): "Transfer of intestinal microbiota from lean donors increases insulin sensitivity in individuals with metabolic syndrome." *Gastroenterology* **143**(4): 913-916.e917.

- Waldo, G. S., Carlson, R. M. K., Moldowan, J. M., Peters, K. E. and Penner-Hahn, J. E. (1991): "Sulfur speciation in heavy petroleums: Information from X-ray absorption near-edge structure." *Geochimica et Cosmochimica Acta* **55**(3): 801-814.
- Wallace, J. L. (2010): "Physiological and pathophysiological roles of hydrogen sulfide in the gastrointestinal tract." *Antioxidants & Redox Signaling* **12**(9): 1125-1133.
- Wallace, J. L., Motta, P. and Buret, A. G. (2018): "Hydrogen sulfide: an agent of stability at the microbiome-mucosa interface." *Gastrointestinal and Liver Physiology* **314**: G143-G149.
- Wang, X., Heazlewood, S. P., Krause, D. O. and Florin, T. H. J. (2003): "Molecular characterization of the microbial species that colonize human ileal and colonic mucosa by using 16S rDNA sequence analysis." *Journal of Applied Microbiology* **95**(3): 508-520.
- Wasmund, K., Mussmann, M. and Loy, A. (2017): "The life sulfuric: microbial ecology of sulfur cycling in marine sediments." *Environmental Microbiology Reports* **9**(4): 323-344.
- Weijma, J., Gubbels, F., Hulshoff Pol, L. W., Stams, A. J. M., Lens, P. and Lettinga, G. (2002): "Competition for H<sub>2</sub> between sulfate reducers, methanogens and homoacetogens in a gas-lift reactor." *Water Science and Technology* **45**(10): 75-80.
- Weinitschke, S., Sharma, P. I., Stingl, U., Cook, A. M. and Smits, T. H. (2010): "Gene clusters involved in isethionate degradation by terrestrial and marine bacteria." *Applied and Environmental Microbiology* **76**(2): 618-621.
- Welty, J. D., Read, W. O. and Shaw, E. H. (1962): "Isolation of 2-hydroxyethanesulfonic acid (isethionic acid) from dog heart." *Journal of Biological Chemistry* **237**(4): 1160-1161.
- Werne, J. P. and Hollander, D. J. (2004): "Organic sulfur biogeochemistry: recent advances and future research directions." *Special Paper of the Geological Society of America* (379): 135-150.
- Widdel, F., Kohring, G.-W. and Mayer, F. (1983): "Studies on dissimilatory sulfate-reducing bacteria that decompose fatty acids III. Characterization of the filamentous gliding *Desulfonema limicola* gen. nov. sp. nov., and *Desulfonema magnum* sp. nov." *Archives of Microbiology* **134**(4): 286-294.
- Widdel, F. and Pfennig, N. (1981): "Studies on dissimilatory sulfate-reducing bacteria that decompose fatty acids. I. Isolation of new sulfate-reducing bacteria enriched with acetate from saline environments. Description of *Desulfovobacter postgatei* gen. nov., sp. nov." *Archives of Microbiology* **129**(5): 395-400.
- Wood, D. A. (1971): "Sporulation in *Bacillus subtilis*. The appearance of sulpholactic acid as a marker event for sporulation." *Biochemical Journal* **123**(4): 601-605.
- Wu, Y. C., Wang, X. J., Yu, L., Chan, F. K., Cheng, A. S., Yu, J., Sung, J. J., Wu, W. K. and Cho, C. H. (2012): "Hydrogen sulfide lowers proliferation and induces protective autophagy in colon epithelial cells." *PLoS ONE* **7**(5): e37572.
- Xing, M., Wei, Y., Zhou, Y., Zhang, J., Lin, L., Hu, Y., Hua, G., N. Nanjaraj Urs, A., Liu, D., Wang, F., Guo, C., Tong, Y., Li, M., Liu, Y., Ang, E. L., Zhao, H., Yuchi, Z. and Zhang, Y. (2019): "Radical-mediated C-S bond cleavage in C<sub>2</sub>-sulfonate degradation by anaerobic bacteria." *Nature Communications* **10**(1): 1609.
- Yazici, C., Wolf, P. G., Kim, H., Cross, T. L., Vermillion, K., Carroll, T., Augustus, G. J., Mutlu, E., Tussing-Humphreys, L., Braunschweig, C., Xicola, R. M., Jung, B., Llor, X., Ellis, N. A. and Gaskins, H. R. (2017): "Race-dependent association of sulfidogenic bacteria with colorectal cancer." *Gut* **66**(11): 1983-1994.
- Zarzycki, J., Erbilgin, O. and Kerfeld, C. A. (2015): "Bioinformatic characterization of glycol radical enzyme-associated bacterial microcompartments." *Applied and Environmental Microbiology* **81**(24): 8315-8329.
- Zhang, X., Deike, S. A., Ning, Z., Starr, A. E., Butcher, J., Li, J., Mayne, J., Cheng, K., Liao, B., Li, L., R., S., Mack, D., Stintzi, A. and Figeys, D. (2018): "Metaproteomics reveals associations between microbiome and intestinal extracellular vesicle proteins in pediatric inflammatory bowel disease." *Nature Communications* **9**: 2873.
- Zhao, W., Zhang, J., Lu, Y. and Wang, R. (2001): "The vasorelaxant effect of H<sub>2</sub>S as a novel endogenous gaseous K<sub>ATP</sub> channel opener." *EMBO Journal* **20**(21): 6008-6016.
- Zhu, M.-X., Chen, L.-J., Yang, G.-P., Huang, X.-L. and Zhao, Y.-D. (2016): "Composition of organic sulfur in riverine and marine sediments: Insights from sulfur stable isotopes and XANES spectroscopy." *Organic Geochemistry* **99**: 102-112.